ORNL-3480
UC-34 – Physics

SOLID STATE DIVISION

ANNUAL PROGRESS REPORT

FOR PERIOD ENDING MAY 31, 1963

MASTER
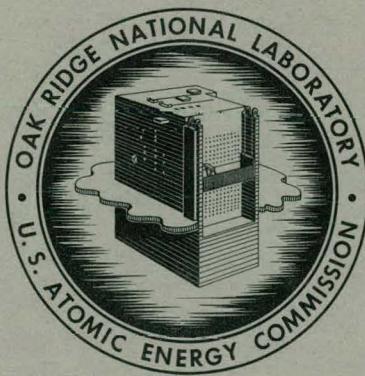
OAK RIDGE NATIONAL LABORATORY
operated by
UNION CARBIDE CORPORATION
for the
U.S. ATOMIC ENERGY COMMISSION

DISCLAIMER

This report was prepared as an account of work sponsored by an agency of the United States Government. Neither the United States Government nor any agency Thereof, nor any of their employees, makes any warranty, express or implied, or assumes any legal liability or responsibility for the accuracy, completeness, or usefulness of any information, apparatus, product, or process disclosed, or represents that its use would not infringe privately owned rights. Reference herein to any specific commercial product, process, or service by trade name, trademark, manufacturer, or otherwise does not necessarily constitute or imply its endorsement, recommendation, or favoring by the United States Government or any agency thereof. The views and opinions of authors expressed herein do not necessarily state or reflect those of the United States Government or any agency thereof.

DISCLAIMER

Portions of this document may be illegible in electronic image products. Images are produced from the best available original document.

Contract No. W-7405-eng-26

SOLID STATE DIVISION

ANNUAL PROGRESS REPORT

For Period Ending May 31, 1963

D. S. Billington, Director
J. H. Crawford, Jr., Associate Director

DATE ISSUED

AUG 23 1963

THIS PAGE

WAS INTENTIONALLY

LEFT BLANK

Table of Contents and Summary

PART I. THEORY

1. STUDIES ASSOCIATED WITH THE THEORY OF RADIATION DAMAGE

Computer studies of the slowing down of energetic atoms in crystals have predicted that penetrations will depend on the crystallographic orientation of the incident particles, an effect which has recently been confirmed experimentally. Calculations for fcc, bcc, and diamond structures all show the importance of channeling in the slowing down of energetic primaries.

A Thomas-Fermi potential has been used to calculate the ranges of atoms having energies from 1 to 100 kev slowing down in a random solid. The calculated ranges are shorter than those found for a Bohr screened Coulomb potential. The Thomas-Fermi results give a somewhat closer fit to experimental data although most data lie between the calculated range curves for these two potentials.

The fraction of defects in a cascade which anneal because of mechanical instability is calculated as a function of increasing defect density, assuming a fixed size for the annealing volume.

Abstract of published paper: *Appl. Phys. Letters* 2, 83 (1963). Channeling of energetic atoms in crystal lattices reduces the number of displaced atoms in a cascade, since channeled atoms tend to dissipate their energy in subthreshold collisions.

Abstract of paper to be published in the *Journal of Applied Physics*. The range distribution of energetic atoms traveling along channels between atomic chains in crystals is calculated analytically. Numerical results are given for copper atoms in copper. From an adequate analysis of experimental data on long ranges of primaries, shot onto crystals in low-indexed directions, information can be obtained about the interatomic potential at distances of about half the lattice spacing.

HIGHER-ORDER MOMENTUM APPROXIMATION IN CLASSICAL COLLISION THEORY

Abstract of published paper: *Z. Physik* 172, 465 (1963). The classical small-angle scattering for repulsive central potentials is treated as a perturbation problem. Higher-order approximations give criteria for convergence and an estimate of the accuracy. Power potentials, the exponentially screened Coulomb potential, a purely exponential potential, and cutoff potentials are discussed. The quantum mechanical limits of this classical treatment are investigated.

2. THEORY OF ELECTRON STATES

EFFECT OF A LARGE MAGNETIC FIELD ON THE FERMI LEVEL OF A METAL

A calculation has been made of the shift of the Fermi level by a large magnetic field and the change this causes in the magnetic susceptibility. It is shown that the effect is likely to be observable for bismuth in a 100-kilogauss field.

BOUNDARY DEGENERACIES IN BRILLOUIN ZONES

When several points of the boundary of an extended Brillouin zone are (a) congruent (in respect to the lattice translations) to the same point of the reduced zone, (b) on the same sphere about the origin, but (c) not related to one another by the rotations of the point group, a new type of degeneracy of energy surfaces arises.

EFFECT OF CORRELATION ON THE HYPERFINE INTERACTION IN LITHIUM

Abstract of published paper: *Phys. Rev.* 130, 198 (1963). It is shown that a well-correlated wave function can give a very good value of the hyperfine interaction in atomic lithium. It is shown that the usual interpretation of the results obtained for lithium with the unrestricted Hartree-Fock method is not entirely acceptable.

3. STUDIES ON DEFECTS IN IONIC CRYSTALS

EXCITED STATES OF THE F-CENTER

The F-center electronic wave function is expressed in the linear combination of atomic orbitals approximation. The atomic orbitals used are those usually associated with the conduction band of the perfect crystal (e.g., the 2s and 2p lithium orbitals in the case of LiCl). Excited states of symmetries other than that usually associated with optical transitions are found. The K-band has not been found thus far.

ELECTRONIC STRUCTURE OF THE M-CENTER

Electronic properties of the M-center in LiCl are calculated in the Heitler-London approximation. The assumptions of the calculations are discussed, and results are presented and compared with experiment.

PART II. CRYSTAL PHYSICS

4. X-RAY DIFFRACTION

Published in *Appl. Phys. Letters* **2**, 127 (1963). X rays were anomalously transmitted in nearly perfect copper crystals up to 1.3 mm thick. Photographs taken of this phenomenon apparently reveal individual imperfections.

Summary of a paper to be presented at the 13th Annual Conference on Applications of X-Ray Analysis, Denver, Colorado, August 8, 1963. A versatile instrument used in x-ray line-width measurements in tenths of seconds has been developed. It is also useful for Borrmann studies.

Submitted for publication. By means of the double-crystal technique, x-ray line half-widths as small as 3.0 sec have been measured in copper. This is in close agreement with the predicted value for a perfect crystal using the Darwin theory.

The results of the 1962 annealing operation of the ORNL Graphite Reactor are shown and compared with the two previous annealing programs.

5. ELECTRON MICROSCOPY

Summary of a paper to be presented at 21st Annual Meeting of the Electron Microscope Society of America, Denver, Colorado, August 28–31, 1963. The observation of fission tracks in single crystals of UO$_2$ results from diffraction contrast effects and occurs only in the surface region of the crystals.

Studies to evaluate the parameters affecting fission-track registration in thin films and preliminary studies of thin foils of Cu–15 at. % Al and of Cu are described. Examples of high-resolution micrographs obtained with a new electron microscope are given.

Abstract of a paper to be submitted for publication. Expressions are derived for the number of particles of deposit formed during condensation of a vapor onto an inert substrate.

Submitted for publication in the *Journal of Applied Physics*. A theoretical expression for the epitaxial temperature is shown to be in reasonable agreement with experimental data.

6. SPIN RESONANCE

Abstract of published paper: *Phys. Rev.* **130**, 577 (1963). The temperature dependence of the spin-lattice relaxation time of the E_1' and E_2' centers was measured from 250 to $1.3°K$. The dominant feature of the Raman relaxation is a temperature variation of about T^3, which is much slower than expected by standard theory.

The observation of a hyperfine interaction with a paramagnetic center in Co^{60} gamma-ray-irradiated synthetic quartz has been found to be the case in which the quantizing field at the nucleus, from which the interaction arises, is the laboratory field and not the field due to the paramagnetic center.

Additional support for the hypothesis that the polarization currents in several glasses are ohmic in character has been adduced. The peak in the enhancement of the polarization currents as a function of Co^{60} gamma-ray dose has been verified. The data are interpreted as an indication that the peak is primarily attributable to those polarization processes with the largest characteristic times.

7. SUPERCONDUCTIVITY

Abstract of published paper: *Appl. Phys. Letters* **2**, 102 (1963). Anomalous longitudinal critical currents were observed in several cold-drawn superconducting samples. A single-layer force-free toroid was constructed in light of these data, but the result was inconclusive. Helical current flow is suggested as an explanation of the critical-current behavior.

A uniform-field superconducting solenoid has been constructed for use in low-temperature magnetic measurements. The maximum field attainable is 11 kilo-oersteds, and axial field measurements indicate agreement with design calculations.

MAGNETIZATION STUDIES OF SUPERCONDUCTORS

Magnetization curves for superconducting alloys are now being obtained. Hysteretic effects and a long superconducting tail are prominent features of the cold-drawn materials. Critical-current behavior is to be examined for correlation with the magnetic transition.

CRITICAL CURRENTS IN Nb-Zr ALLOYS

Abstract of a paper submitted for publication. Results of tests on Nb-Zr alloys in high magnetic fields are presented. The behavior of test solenoids in external fields is also given, and several inferences are discussed.

PART III. METALS

8. INVESTIGATIONS OF METAL SURFACES

F. W. Young, Jr., L. D. Hulett, Ugo Bertocci, L. H. Jenkins, and J. R. Savage

GROWTH OF COPPER CRYSTALS OF LOW DISLOCATION DENSITY

The growth direction of crystals grown by the Bridgman technique was random for identical growth conditions, but the dislocation density was an inverse function of the angular deviation of the growth direction from the (111) zone. Effects of thermal stresses during both seeded and unseeded growth are also discussed.

Methods of crystal preparation and handling are discussed, and the results obtained as well as the conclusions which can be drawn concerning dislocations and other structural features are pointed out in some detail.

Abstract of paper to be published in the *Proceedings of the ASM-AIME Symposium, Oct. 27–28, 1962, New York*. The possible role of crystal imperfections, particularly dislocations, in the nucleation of steps is reviewed, and the kinetics of the growth of etch pits at dislocations on (111) surfaces is presented. Results are interpreted in terms of kinematic dissolution theory.

Effects of crystal geometry on the formation and motion of ledges on copper surfaces 0 to 2° removed from the (111) are reported. Preliminary results on the effects of solution composition and dissolution rate are included.

Abstract of paper submitted to the *Journal of the Electrochemical Society*. The influence of current density, solution composition, and slight misorientations of the surface from the (111) on the formation of etch pits at dislocations have been studied.

To explain the development of facets on only a portion of a spherical crystal exposed to copper-containing solutions, equilibration experiments were conducted. Results are discussed in terms of relative stability of orientations and differences in exchange current density.

Current and potential relations are used to explain the roles of iodide and bromide in the formation of etch pits on the (111) and also to determine exchange current densities on various orientations.

9. LOW-TEMPERATURE IRRADIATION STUDIES

R. R. Coltman, C. E. Klabunde, D. L. McDonald, J. K. Redman, and G. F. Fielder

Construction of a new low-temperature irradiation facility located at the Bulk Shielding Reactor is near completion. The thermal-neutron flux is 2.5×10^{12} neutrons $cm^{-2} sec^{-1}$. The heat capacity of the new refrigeration system is at least 20 w at $3.6°K$. Tests on a mockup of a proposed converter tube, which produces a fission neutron flux of 6×10^{10} neutrons $cm^{-2} sec^{-1}$ and needs no external cooling, are satisfactory.

Published paper by D. L. McDonald: *Appl. Phys. Letters* **2**, 175 (May 1, 1963). By the use of thermal conductivity measurements, considerable recovery below room temperature is seen in BeO after neutron irradiation at $100°K$.

10. ELASTICITY AND ANELASTICITY STUDIES

Measurements of amplitude dependence of internal friction in irradiated copper were made in order to obtain information on the stress necessary to break dislocations away from radiation-defect pinning points. The dose dependence of the breakaway stress was found to be similar to the dose dependence of radiation hardening.

A technique has been developed for observing third-order elasticity in solids. A large-amplitude ultrasonic wave is propagated in the sample. Because of the non-Hooke's-law nature of the medium at finite amplitudes, harmonics of this wave are generated as the wave progresses. Measurement of the fundamental and the second harmonic component have been made in polycrystalline aluminum. A theoretical analysis of the problem should give quantitative information about the third-order elastic constants of the solid.

11. Ar⁺ ION BOMBARDMENT OF METAL SURFACES

Yield measurements were made on additional orientations of monocrystalline copper. Atom-ejection patterns were obtained for the three low-index planes of Cu_3Au. Patterns obtained from either cadmium or magnesium did not show structure.

A dual-beam mass spectrometer was received and installed. Mass and energy analyses are reported on the positive ions ejected from two copper monocrystals.

PART IV. NONMETALS

12. SEMICONDUCTOR STUDIES

Studies of radiation-induced trapping levels in germanium by low-temperature photoconductivity measurements indicate that the phenomenon is a two-step process: the traps first "grow" in at low temperatures ($<130^{\circ}$C) and are then annealed out at higher temperatures. These efforts are now being carried out in two parts: (1) a study of trap growth as a function of annealing and (2) annealing out of traps at higher temperatures.

An abstract of a published paper describing radiation-produced net acceptor levels in the upper half of the forbidden gap of silicon is reproduced. Partial results of a study of the lower half of the gap are also presented and discussed.

13. INSULATING CRYSTALS

The study of the intensity dependence of F-center production by accelerator electrons has yielded evidence that a dynamic equilibrium exists between F- and M-centers in KCl and that this equilibrium is established rapidly with reference to the time scale of actual production of color centers.

Studies at the Laboratory on F- and M-band introduction in KCl by ionizing radiation have shown that late-stage coloring properties vary greatly among crystals obtained from various sources. As a result of this finding, the authors felt it necessary to point out in the literature just how great the variations in F-coloration rates are among crystals even from one supplier. To further emphasize the variability of physical properties of commercial KCl crystals, data on ultraviolet-excited luminescence and light scattering were added to that on F-coloration rates.

Abstract of paper to be published in the June 1963 issue of the *Journal of Applied Physics*. The effect of heat treatment and irradiation on the mechanical properties of potassium chloride single crystals of varying impurity concentrations is investigated.

Abstract of paper to be published in the August 1963 issue of the *Journal of Applied Physics*. Measurements of the flow stress and of F-band coloration have been made at room temperature on a number of different samples of KCl as a function of gamma and electron irradiation.

Light-scattering techniques have been used to determine the character of the dominant scattering units in KCl and their size, shape, and concentration. It is found that for Harshaw and Isomet KCl the scattering is from impurity clouds surrounding edge dislocations and that these cylindrical scattering units have a length of about 3×10^{-4} cm and a radius of less than 2.5×10^{-6} cm.

14. PURE MATERIALS PROGRAM

This program is concerned with the development of improved techniques of initial purification, crystal growth, and final assay as required for the production of research-quality specimens of immediate and long-range interest.

This report very briefly describes the purpose and present status of the Research Materials Information Center. It also includes a short description of the first aperiodic bulletin of available and desired materials.

Crystal growth from the melt under He pressure has been explored. Polycrystalline masses have been obtained by this technique.

Abstract of paper submitted for publication in the *Journal of Applied Physics*. Extended exposures of Bi_2Te_3 to Co^{60} gamma radiation apparently result in the production of tellurium vacancies and interlaminar clusters of tellurium interstitials. Evidence of an effect on impurity-band conduction at low temperature is observed.

Published paper: *Appl. Phys. Letters* 1, 79 (1962). Vapor-crystalline equilibrium studies indicate that the nonstoichiometric doping mechanism in Bi_2Se_3 is subtractive in nature (i.e., selenium atoms occupy normal selenium sites, but some bismuth sites are vacant).

A procedure is being developed which employs magnetic susceptibility measurements to assay the excess oxygen content in Cu_2O. Preliminary measurements indicate that the technique has merit. An attempt is being made to correlate excess oxygen concentrations with electrical properties.

The ultimate aim of the pure KCl program is to produce very pure single crystals of KCl having also a low concentration of physical imperfections. The more immediate aim of the program this past year has been to further improve the growing apparatus and to learn by chemical analysis of many different crystals just which impurities are reduced (or increased) in concentration by a particular treatment.

PART V. RADIATION METALLURGY

15. RADIATION METALLURGY

Abstract of published paper: *Nucl. Safety* 4(1), 42 (1962). A review is given of low-temperature brittleness, neutron-irradiation effects on pressure-vessel steels, fundamentals of radiation damage as applied to the calculation of displacement production rates in reactor environments, and radiation enhancement of metallurgical reactions.

Sheet tensile samples of type 330 nickel alloy were irradiated in a partial fuel element in the ORR. Measurements after irradiation indicated an increase in the yield stress and ultimate tensile stress and a decrease in the elongation. Also, a yield point was induced, and the rate of work hardening was decreased.

Abstract of paper presented at the *ASTM Symposium on Radiation Effects on Metals and Neutron Dosimetry, Los Angeles, Oct. 1–5, 1962* (to be published). The results of in-pile stress-rupture tests in the ORR on Inconel 600, 304 stainless steel, Zircaloy-2, and an Nb–1% Zr alloy are described.

A description is given of in-pile stress-rupture experiments on tube-burst samples of Zircaloy-2 and ASTM A212B pressure-vessel steel.

A brief review is given of the effect of neutron irradiation on the mechanical properties of iron and iron-base alloys. An irradiation experiment on Armco iron tensile samples is described, and future plans are outlined.

Apparatus has been developed for the in-pile measurement of low-frequency internal friction. Preliminary measurements have been made in the ORNL Graphite Reactor on an iron-nitrogen alloy.

Previous work has indicated that neutron irradiation promotes a clustering reaction in copper-nickel alloys. The possible role of interstitial migration is discussed, and a presently operating experiment in the ORNL Graphite Reactor is described.

The flux and temperature dependence of the radiation-enhanced ordering in Cu-Al has been measured for freshly prepared samples and for samples given a thermal cycling treatment in the reactor. The results are analyzed in terms of the theory of radiation-enhanced diffusion.

FUNDAMENTAL ASPECTS OF RADIATION EFFECTS ON DIFFUSION-CONTROLLED REACTIONS
IN ALLOYS

Abstract of paper presented at the *ASTM Symposium on Radiation Effects on Metals and Neutron Dosimetry, Los Angeles, Oct. 1–5, 1962* (to be published). A review is given of the theory of diffusion, with special emphasis on the freezing-in problem and on radiation-enhanced diffusion. The theory is compared with recent experimental work on the effect of radiation on ordering reactions in alloys.

PUBLICATIONS, PAPERS, AND SEMINARS

Part I. Theory

D. K. Holmes

THIS PAGE

WAS INTENTIONALLY

LEFT BLANK

1. Studies Associated with the Theory of Radiation Damage

COMPUTER STUDIES OF THE SLOWING DOWN OF ENERGETIC ATOMS IN CRYSTALS

M. T. Robinson   O. S. Oen

Our studies of the slowing down of energetic atoms in crystals with the IBM 7090 computer program RANGE II (ref 1) have been continued. The incidence of channeling[1] was so great when the Bohr exponentially screened Coulomb potential was employed that its use was discontinued. Instead, a Born-Mayer (purely exponential) potential was used, with parameters suggested by Gibson et al.[2] to describe the interactions of copper atoms. With this potential, which is reasonably realistic for the most important interatomic separations (around half the crystal nearest-neighbor distance), it was possible to compute penetrations, of 1- to 10-kev copper atoms into copper monocrystals, which are of plausible magnitude. These results provided two immediate conclusions:[3]

1. The penetrating component observed by Davies et al.[4] in the slowing down of several ions in aluminum monocrystals can be attributed to the influence of channeling on the trajectories of the primaries.

2. The penetrations of ions into monocrystals should be sensitive functions of the initial crystallographic direction of the incident particles,

the penetrations in fcc crystals decreasing in the order <011>, <001>, <112>, <013>, <111>.

Figure 1.1 displays our calculated integral penetration distributions for 5-kev copper atoms slowing down to 25 ev in copper. The prediction of crystallographic sensitivity of the penetration, shown by this figure, has recently been verified experimentally for 40-kev $^{85}Kr^+$ ions slowing down in aluminum.[5] Some of the experimental data are shown in Fig. 1.2. The striking similarities between Figs. 1.1 and 1.2 give us considerable confidence in the essential correctness of our model.

---

[1] M. T. Robinson and O. S. Oen, *Solid State Div. Ann. Progr. Rept. Aug. 31, 1962*, ORNL-3364, pp 5—11.

[2] J. B. Gibson, A. N. Goland, M. Milgram, and G. H. Vineyard, *Phys. Rev.* **120**, 1229 (1960).

[3] For details see M. T. Robinson and O. S. Oen, *Appl. Phys. Letters* **2**, 30 (1963).

[4] J. A. Davies, B. Domeij, and J. Uhler, *Arkiv Fysik* **24**, 377 (1963), and earlier references there cited.

[5] G. R. Piercy, F. Brown, J. A. Davies, and M. McCargo, *Phys. Rev. Letters* **10**, 399 (1963).
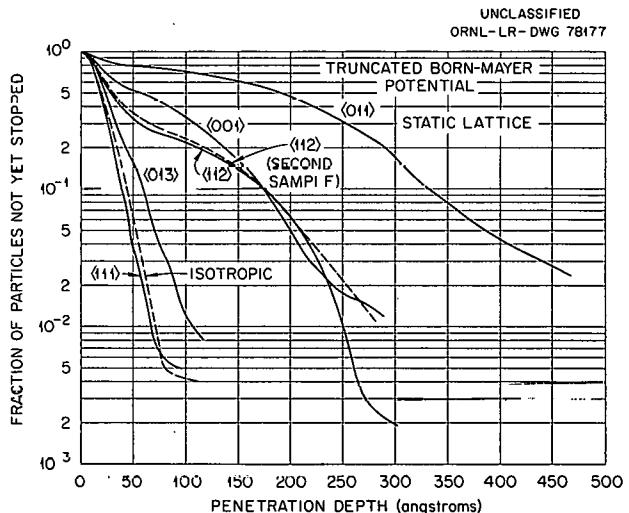
Fig. 1.1. Integral Penetration Distributions Calculated for 5-kev Copper Atoms Slowing Down to 25 ev in Copper, According to a Truncated Born-Mayer Potential. The initial directions of the primaries are shown on the curves.
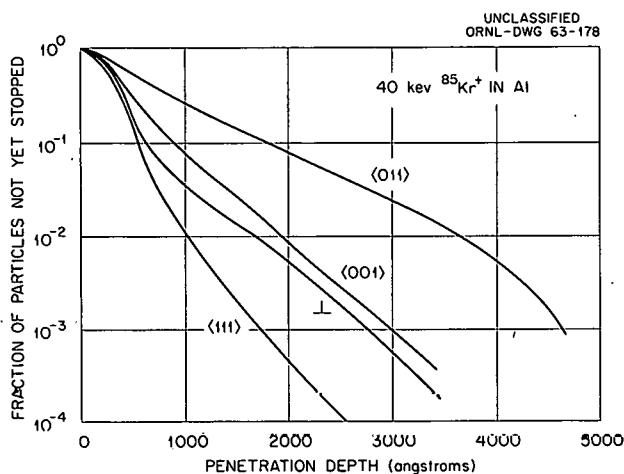
Fig. 1.2. Integral Penetrations Observed [*Phys. Rev. Letters* **10**, 399 (1963)] for 40-kev $^{85}Kr^{+}$ Ions Slowing Down in Monocrystalline Aluminum. The three principal directions all make angles of 28° with the crystal surface normal (marked ⊥). The penetration depth scale has been corrected for angle of incidence.

In order to study the effects of crystal symmetry on the slowing-down problem, independently of changes in the interatomic potential, calculations were performed for copper atoms slowing down not only in fcc copper but also in hypothetical bcc and diamond-structure "copper." All three structures have the same nearest-neighbor distance; some other properties are listed in Table 1.1. Figure 1.3 displays the median penetrations for 1- to 10-kev copper atoms, starting isotropically from lattice sites, in each of the three structures. The differences are determined primarily by the differences in densities of the three solids, although small structural effects are also evident. In Fig. 1.4 are shown median penetrations calculated for copper atoms incident upon low-index surfaces of monocrystalline targets of each of the three structures. The effects of density are largely overridden by those of channeling. Study of this figure and its comparison with Fig. 1.3 shows the following points:

1. Channeling leads to a crystallographic sensitivity of the penetration in all three crystals.
2. The effects of channeling are the greatest in the diamond structure, but are nearly as great in the other cases.

3. The order of the median penetrations is the same as that which is predicted from the "transparency"[6] of the various crystallographic directions.

[6]A. L. Southern, W. R. Willis, and M. T. Robinson, *J. Appl. Phys.* **34**, 153 (1963).

Table 1.1. Some Crystallographic Properties of the "Copper" Targets

Nearest-neighbor distance: 2.5562 A

	FCC	BCC	Diamond
Coordination number	12	8	4
Lattice constant, A	3.6150	2.9516	5.9032
Relative density	1.0000	0.9186	0.4593
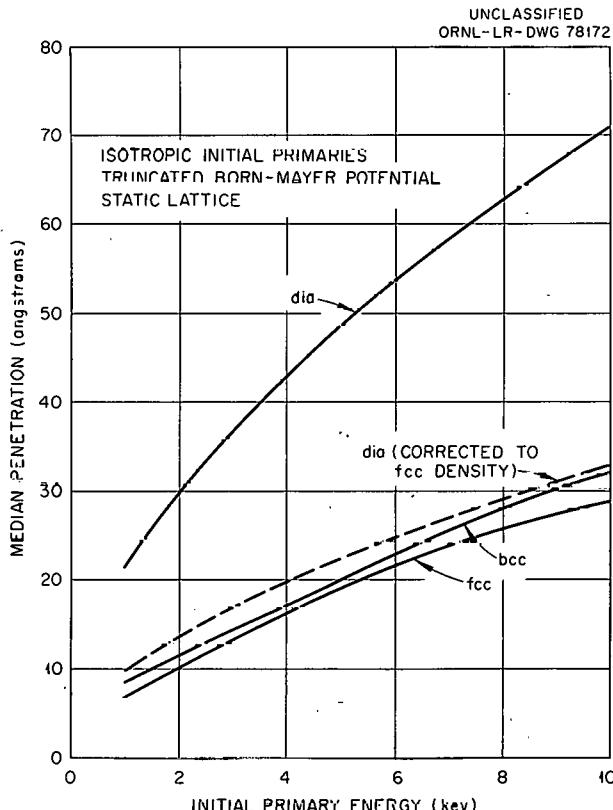
Fig. 1.3. Median Penetrations Calculated for Initially Isotropic Copper Atoms Slowing Down to 25 ev in "Copper" According to a Truncated Born-Mayer Potential.
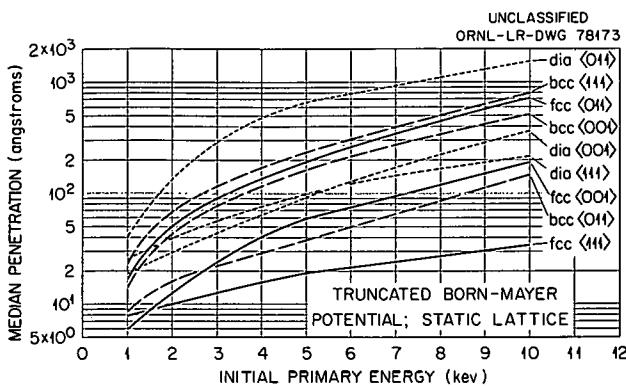
Fig. 1.4. Median Penetrations Calculated for Copper Atoms Incident upon the Principal Planes of "Copper" Targets. Truncated Born-Mayer potential.

A full account of the RANGE II calculations is being prepared for publication.

RANGES OF ENERGETIC ATOMS IN SOLIDS FOR A THOMAS-FERMI POTENTIAL

O. S. Oen   M. T. Robinson

Our earlier calculations[7] of the ranges of atoms having energies from 1 to 100 kev, slowing down through binary elastic collisions in a random solid, have been extended by using a Thomas-Fermi potential. The screening radius of the potential of the two colliding atoms is chosen by the method suggested by Firsov.[8] A comparison of the Thomas-Fermi potential and the Bohr potential ($k = 1.0$), which was used in our previous work, is shown in Fig. 1.5. It is seen that the Thomas-Fermi potential predicts a greater interaction energy except for very small separation distances. Calculations have been made for several ratios of the mass of the slowing-down atom to the lattice atom. The calculated ranges are considerably shorter than those found previously using the Bohr potential except for very high energies. Most of the experimental range data lies between the

---

[7]M. T. Robinson, D. K. Holmes, and O. S. Oen, pp 105–17 in *Le Bombardement Ionique: Theories et Applications, Colloques Internationaux du Centre National de la Recherche Scientifique No. 113, Bellevue, Dec. 4–8, 1961*, Editions du C.N.R.S., Paris, 1962; O. S. Oen, D. K. Holmes, and M. T. Robinson, *J. Appl. Phys.* **34**, 302 (1963).

[8]O. B. Firsov, *Soviet Phys. JETP* **6**, 534 (1958).

calculated range curves for these two potentials although the Thomas-Fermi potential gives somewhat better overall agreement. Figure 1.6 shows a typical comparison of experiment[9] and theory for the median penetration of xenon ions in aluminum.

---

[9]J. A. Davies (private communication).
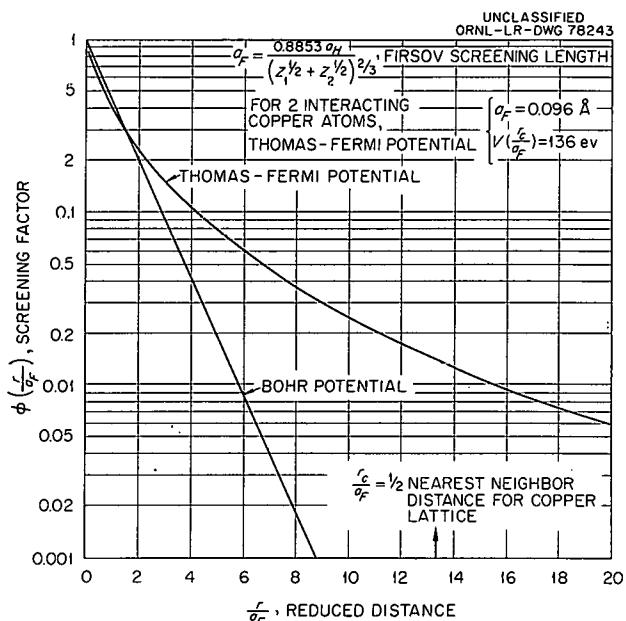
Fig. 1.5. Comparison of Bohr and Thomas-Fermi Potentials.
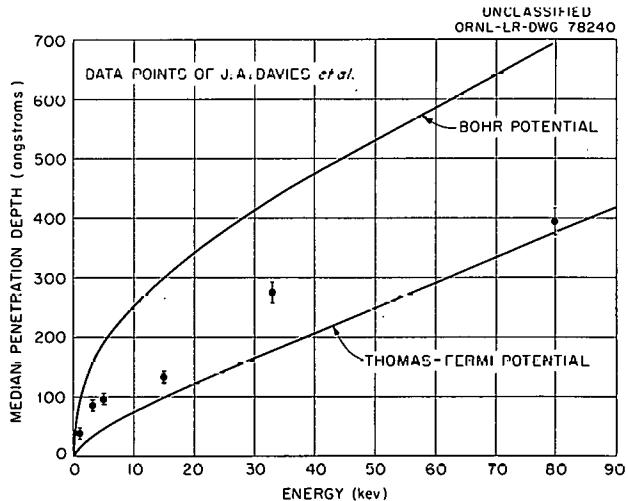
Fig. 1.6. Median Penetration Depths of Xe[133] Ions in Aluminum.

Ranges calculated[10] by integrating the reciprocal of the stopping power agree fairly well with our Monte Carlo calculations, especially when the mass of the slowing-down atom is large compared with a lattice atom.

SELF-ANNEAL OF FRENKEL PAIRS IN LARGE RADIATION-INDUCED DISPLACEMENT CASCADES

G. Leibfried   D. K. Holmes

Primary displaced atoms of high energy in solids produce displacement cascades containing a large number of Frenkel pairs in a relatively small volume. The density of vacancies and interstitials can be so large that annihilation occurs from purely static effects without diffusive motion. Frenkel pairs (vacancy-interstitial pairs) whose separation is such that the two defects are included in an annihilation volume (v_a) annihilate each other eventually under the action of forces between the defects, that is, they are mechanically unstable. Recent investigation[11] has shown that, at least in copper, v_a may be large, including from 50 to 100 atomic volumes. It is thus of interest to examine the extent of such self-annealing on a general basis.

The model investigated to date is a purely statistical one in which N vacancies and N interstitial atoms are allowed to fall randomly into a volume V. All pairs falling within a volume V_a are progressively annihilated, starting with the pairs of closest separation and ending with those pairs of maximum possible separation. A convenient parameter measuring the density of defects is

$$\alpha \equiv \left(\frac{N}{V}\right) v_a , \qquad (1)$$

where α is the average number of defects (of one kind) falling into a volume v_a. Several approaches have been attempted in an effort to obtain a tractable analytical expression for the expected fraction of defects which will be annihilated. While a final solution is yet to be achieved, one

fairly simple model seems to give good results when compared with Monte Carlo calculations (which are supposed to give the accurate result). This simple model gives the result for the fraction of pairs annealed:

$$f_A = \frac{1}{1 + 1/\alpha} . \qquad (2)$$

As a somewhat extreme example of the use of this result, suppose that in a fast-neutron-produced damaged region in copper there are 2 at. % defect pairs, and that the annihilation volume includes 100 lattice atoms. Then

$$\alpha = \frac{N}{V} v_a = \left(\frac{N}{V} v_{at.}\right)\left(\frac{v_a}{v_{at.}}\right) = (0.02)(100) = 2$$

and

$$f_A = \frac{1}{1 + 1/2} \cong 0.67 ,$$

so two-thirds of the defects are annihilated, simply by mechanical instability.

EFFECT OF CHANNELING ON DISPLACEMENT-CASCADE THEORY[12]

O. S. Oen   M. T. Robinson

Energetic atoms moving in channels of the crystal lattice lose their energy in very small increments. The implication of this in radiation damage is that the number of displaced atoms in a cascade will be reduced because atoms which become channeled while slowing down tend to dissipate their energy in subthreshold collisions. By assuming that an atom, following a collision, has a probability P of being channeled and that it subsequently produces no more displacements, it is shown that the Kinchin and Pease displacement model becomes

$$\nu = \frac{1}{1 - 2P}\left[(1 - P)\left(\frac{E_0}{2E_d}\right)^{1-2P} - P\right] ,$$

$$E_0 > 2E_d , \qquad (1)$$

[10] J. Lindhard and M. Scharff, *Phys. Rev.* **124,** 128 (1961).

[11] J. B. Gibson, A. N. Goland, M. Milgram, and G. H. Vineyard, *Phys. Rev.* **120,** 1229 (1960).

[12] Abstract of published paper: *Appl. Phys. Letters* **2,** 83 (1963).

where ν is the total number of displaced atoms in a cascade initiated by a primary of energy E_0 and E_d is the displacement threshold energy. Expression (1) predicts that the number of displacements depends on E_0 to some power less than unity. This is in the right direction to remove the disagreement between experiment and theory.

LONG-RANGE CHANNELING EFFECTS IN IRRADIATED CRYSTALS[13,14]

C. Lehmann   G. Leibfried

If an energetic atom, a primary, slows down in a lattice, it has the possibility of traveling long distances without essential interaction along almost force-free channels bordered by close-packed atomic chains. This effect has not been considered until recently, because for the sake of simplicity the lattice mostly has been replaced by a corresponding random arrangement. This "channeling" behavior has been found in machine calculations by Robinson, Holmes, and Oen[15] which take the lattice structure into account. In this paper the behavior of a primary moving along a channel bordered by the most densely packed directions is investigated analytically. Numerical results are given for a copper primary moving in a copper crystal, but the results can be easily extended to other cases. Two potentials are used: an exponentially screened Coulomb potential after Bohr, used also in the machine calculations and

[13]To be published in *Journal of Applied Physics*.

[14]The paper mentioned in the last progress report (*Solid State Div. Ann. Progr. Rept. Aug. 31, 1962*, ORNL-3364, p 13) has been completely rewritten. In the meantime long-range channeling in single crystals has been shown experimentally [G. R. Piercy, F. Brown, J. A. Davies, and M. McCargo, *Phys. Rev. Letters* 10, 399 (1963)], and hence the first version of the paper has lost its hypothetical character. The experimental feasibility has now been taken into account, and an analysis is given of how to obtain, from experimental data on long ranges, information about the atomic interaction potential at distances of about half the lattice spacing. The mathematical treatment is more concise, and more results of numerical calculations are added.

[15]M. T. Robinson, D. K. Holmes, and O. S. Oen, *Bull. Am. Phys. Soc.* 7(3), 171 (1962); M. T. Robinson and O. S. Oen, *Appl. Phys. Letters* 2, 30 (1963).

thought to give an adequate description for relatively high energies and small interatomic distances; and a purely exponential potential after Born-Mayer, better suited for relatively low energies and large atomic distances. The maximum ranges are very large: for 10 kev in the order of 10^3 lattice parameters for the Born-Mayer potential and up to 10^7 for the Bohr potential. Presumably, the Born-Mayer potential is a better description for these events. The investigation is confined to motions near the channel axis. Therefore, we only obtain the range distribution near the maximum range. From an adequate analysis of experimental data on long ranges of primaries, shot onto crystals in low-indexed directions, one can obtain information about the potential at distances of about half the lattice spacing.

HIGHER-ORDER MOMENTUM APPROXIMATION IN CLASSICAL COLLISION THEORY[16]

C. Lehmann   G. Leibfried

The classical scattering of two particles with repulsive central forces is calculated for small scattering angles using perturbation theory. The potential is considered as a perturbation. The first approximation is the well-known "momentum approximation." Higher-order approximations provide criteria for convergence and allow estimation of the accuracy of the approximation. Furthermore, the conditions of validity of the momentum approximation are discussed for cut-off potentials. Power potentials, the exponentially screened Coulomb potential, and a purely exponential potential are investigated in detail, especially the latter two. The method is demonstrated numerically by an example which corresponds to the interaction of copper atoms. Also, the quantum mechanical limits of this classical treatment are investigated.

[16]Abstract of published paper: *Z. Physik* 172, 465 (1963).

2. Theory of Electron States

EFFECT OF A LARGE MAGNETIC FIELD ON THE FERMI LEVEL OF A METAL

J. H. Barrett

Electron orbits in a metal are quantized in the presence of a magnetic field. The effects of such quantization appear in the magnetic susceptibility, magnetoresistance, Hall effect, and other phenomena. As one aspect of the theory of such

There will be two relatively simple cases to consider. Case I is that in which the (a) and (b) ellipsoids contain all of the carriers; case II is that in which there are enough other carriers present to hold the Fermi level constant regardless of the effect of the magnetic field on the (a) electrons. In any case the Fermi level is determined by the condition $n_e = n_h$. The number of electrons or holes enclosed by an ellipsoid at absolute zero is given by

$$n = \frac{1}{4\pi^2}\left(\frac{2m_d}{\hbar^2}\right)^{3/2}\hbar\omega_c\left[\sum_{n=0}^{n_{max}}\sqrt{E_F - \left(n + \frac{1}{2} - \Delta\right)\hbar\omega_c} + \sum_{n=0}^{n_{max}}\sqrt{E_F - \left(n + \frac{1}{2} + \Delta\right)\hbar\omega_c}\right], \quad (1)$$

phenomena, some consideration has been given to the secondary effect of the magnetic field on these phenomena through its effect on the Fermi level.[1] It has been shown that this latter effect is small if $\hbar\omega_c \ll E_F$, where $\omega_c = eB/m_c c$ is the cyclotron frequency and m_c the cyclotron effective mass. Hence the effect of the field on the Fermi level is usually neglected. However, this effect will be large if $\hbar\omega_c \gg E_F$ for a large fraction of the electrons and holes in the metal. Fulfillment of the condition $\hbar\omega_c \gg E_F$ is aided by having m_c and E_F small.

A metal that seems likely to fulfill these conditions is bismuth. Its Fermi surface is known to include (a) three nearly ellipsoidal electron surfaces and (b) one ellipsoidal hole surface.[2] In addition there is evidence for one or more additional portions of the Fermi surface.[3] For a 100-kilogauss field directed along a bisectrix direction, $\hbar\omega_c/E_F \approx 4$ for two of the three (a) ellipsoids and ≈ 8 for the third one.

where

m_d = density of states effective mass,

$\Delta = \frac{1}{2}$ (spin-orbit splitting)/(cyclotron splitting),

n_{max} = maximum n for which the quantity under the square root is positive.

For $\hbar\omega_c \ll E_F$, Eq. (1) becomes

$$n = \frac{1}{3\pi^2}\left(\frac{2m_d}{\hbar^2}\right)^{3/2}E_F^{3/2}. \quad (1')$$

For case I, Eq. (1) can be used to calculate the effect of a magnetic field on the Fermi level. The simplest way to detect this effect is by measuring the magnetic susceptibility. The contribution of

[1] R. B. Dingle, *Proc. Roy. Soc.* **A211**, 500 (1952); P. N. Argyres, *J. Phys. Chem. Solids* **4**, 19 (1958).

[2] Yi-Han Kao, *Phys. Rev.* **129**, 1122 (1963).

[3] L. S. Lerner, *Phys. Rev.* **130**, 605 (1963).

an ellipsoid to the susceptibility at absolute zero is

$$\chi = \frac{1}{3\pi^2}\left(\frac{2m_d}{\hbar^2}\right)^{3/2}\left(\frac{e\hbar}{m_c c}\right)^2\left\{\sum_{n=0}^{n_{max}}\left[\frac{5}{2}\left(n+\frac{1}{2}-\Delta\right)\hbar\omega_c - E_F\right]\left[E_F - \left(n+\frac{1}{2}-\Delta\right)\hbar\omega_c\right]^{1/2}\right.$$

$$\left. + \sum_{n=0}^{n_{max}}\left[\frac{5}{2}\left(n+\frac{1}{2}+\Delta\right)\hbar\omega_c - E_F\right]\left[E_F - \left(n+\frac{1}{2}+\Delta\right)\hbar\omega_c\right]^{1/2}\right\}. \quad (2)$$

Equations (1) and (2) have been used to calculate χ for case I. The results are plotted in Fig. 2.1. For case II the Fermi level will remain constant, and Eq. (2) suffices to calculate χ. These results are also plotted in Fig. 2.1.

The plotted curves were calculated for the absolute zero of temperature, and collision broadening was neglected. The effects of a non-zero temperature and of collision broadening will be to smooth out the oscillations in the curves. Their effects will be pronounced in the vicinity of 25 kilogauss ($10^5/B = 4$) but will not change the nature of the curves at fields approaching 100 kilogauss.
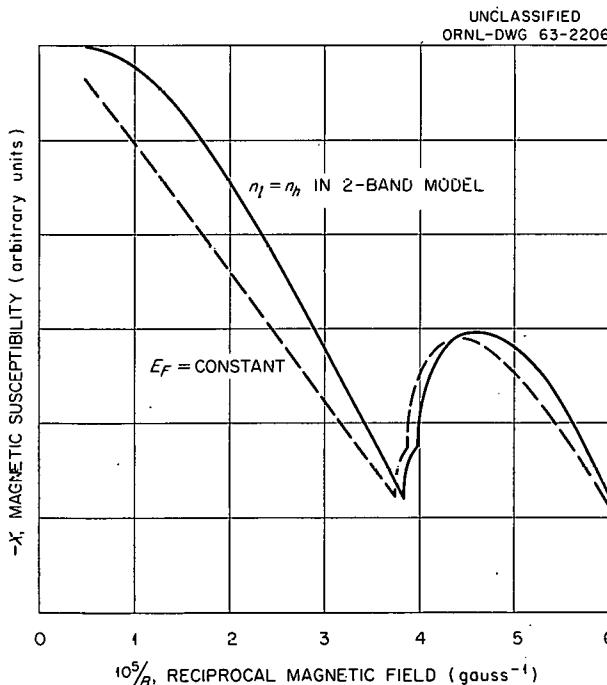
Fig. 2.1. Plot of the Magnetic Susceptibility vs the Reciprocal of the Magnetic Field.

In collaboration with the Superconductivity Group an experiment is being planned to study the high-field dependence of the susceptibility of bismuth utilizing the 100-kilogauss facility of the Oak Ridge Magnet Laboratory.

BOUNDARY DEGENERACIES IN BRILLOUIN ZONES

H. C. Schweinler

Associated with a lattice of points $\vec{a}_j n^j$ in real space (n^j integral; $\vec{a}_1 \cdot [\vec{a}_2 \times \vec{a}_3] \neq 0$) is a reciprocal lattice of points $b_i \vec{b}^i$ (b_i integral; $\vec{b}^i \cdot \vec{a}_j = \delta^i{}_j$). The set of planes which are the perpendicular bisectors of the line segments from the origin to each other lattice point of reciprocal space partitions this space into polyhedral regions. The interior points of these polyhedral regions form three-dimensional open sets of points representing general propagation vectors. The boundary of each such polyhedron is composed of (a) two-dimensional open sets (the faces, excluding edges and vertices), (b) one-dimensional open sets (the edges, excluding vertices), and (c) zero-dimensional sets (the vertices). The points which can be joined to the origin by a straight-line segment which intersects l perpendicular-bisecting planes form the interior of the $(l + 1)$th Brillouin zone. These points can be mapped by reciprocal lattice translations onto the interior of the first Brillouin zone.

We shall be primarily concerned with the image of the boundaries of the higher Brillouin zones in the first zone or its boundary. Thus, for each extended zone after the first, there is induced a partition of the first zone by the translational images of the boundaries of the extended zone. Special interest is attached to points in the reduced zone from a given extended zone whose inverse images lie on a sphere about the origin

and, accordingly, are degenerate in the limiting case of vanishing periodic potential. Bouckaert, Smoluchowski, and Wigner[4] have treated the case in which the inverse images are related by the point symmetry of the lattice; accordingly, we concentrate on the case in which the inverse images are related by lattice translations only, or by lattice translations and the operations of the point group. Several examples have been given[5] for the two-dimensional square lattice.

Secular equations have been set up for the prototype case of the motion of a quantum mechanical particle in a periodic potential. The energy is considered as a function of the (small) deviation vector of the propagation vector from a boundary value. Separate cases arise for boundaries of types (a), (b), and (c) listed in the first paragraph, requiring individual treatment.

EFFECT OF CORRELATION ON THE HYPERFINE INTERACTION IN LITHIUM[6]

K. F. Berggren[7]   R. F. Wood

The results of calculations of the hyperfine interaction in the ground state of lithium, made with the use of well-correlated wave functions, are reported. An analysis of the wave functions is made in terms of operators which resolve the general doublet function into two components, one of which is characterized by a spatially symmetric core function. The calculations show that this component with the spatially symmetric core can give very good values for both the energy (-7.47630 atomic units) and the hyperfine interaction (98.8% of exptl). The inclusion of the second doublet component and some quarter component in the wave function has very little effect on either the energy or the hyperfine interaction. These results are discussed and compared with those obtained with the unrestricted Hartree-Fock (UHF) method. The conclusion is reached that the usual interpretation of the results obtained for lithium with the UHF method is not entirely acceptable.

[4]L. P. Bouckaert, R. Smoluchowski, and E. P. Wigner, *Phys. Rev.* **50**, 58 (1936).

[5] *Solid State Div. Ann. Progr. Rept. Aug. 31, 1962,* ORNL-3364, p 22.

[6]Abstract of published paper: *Phys. Rev.* **130**, 198 (1963).

[7] Uppsala University, Uppsala, Sweden.

3. Studies on Defects in Ionic Crystals

EXCITED STATES OF THE F-CENTER

R. F. Wood

Calculations are being carried out on the electronic structure of the F-center in an effort to determine whether or not there are bound states other than the two responsible for the main F-band.

The Hamiltonian of the F-electron in the crystal is written as

$$\mathcal{H} = -\frac{1}{2} \nabla^2 + \sum_{g=1}^{N} V(\vec{r} - \vec{R}_g) ,$$

where $V(\vec{r} - \vec{R}_g)$ is the potential due to the gth ion. The vacancy is located at the lattice site, denoted by $g = 0$.

The wave function is expanded as a linear combination of atomic orbitals (LCAO) of the alkali ions. Only the lowest unoccupied orbitals, that is, those usually associated with the conduction band in the perfect crystal, have been chosen. For example, the $2s$ and $2p$ lithium functions are used in the lithium halides. The wave function is written as

$$\Psi_F(\vec{r}) = \sum_{g,\mu} a_{g\mu} \phi_{g\mu}(\vec{r} - \vec{R}_g) ,$$

where g again runs over the ions and μ runs over the atomic orbitals on any one ion.

In the first approximation, the sum over g includes only the first-nearest-neighbor ($1nn$) ions of the vacancy. In the second approximation, second-nearest-neighbor alkali ions ($2nn$) are included in the wave function; in the third approximation $3nn$ alkalis are included, etc. Group theoretical considerations give a great simplification of the secular determinant which results from the usual variation problem. The symmetry

of the F-center in an alkali halide is octahedral, and so the eigenvectors of our problem will belong to one of the five irreducible representations (ten if the inversion operation is included in the group) of the octahedral group. The multiplication table of the octahedral group then shows that optical transitions are allowed from the ground state (Γ_1^+ symmetry) to the excited states of Γ_4^- symmetry. All other optical transitions *from* the ground state are forbidden.

In the first approximation, for LiCl, there are only two bound states of the problem — one going with Γ_1^+ and one going with Γ_4^- — and the transition between these two states accounts very well for the main F-band. No other levels of any symmetry are bound (have negative energy) at this stage of approximation, although there are two which are very nearly bound.

In the second stage of approximation, that is, including $2nn$ lithium ions, two additional levels become bound, one of Γ_1^+ symmetry and one of Γ_5^+ symmetry, corresponding to the two roots which are almost bound in the first approximation. No additional level of 1_4^-, which might correspond to a second excited state accessible to the ground state by a purely optical transition, appears.

These additional bound levels might have some rather important consequences since they could presumably act as electron traps. Such states might account for the long lifetime of the principal excited state. The nonappearance of a second excited state of Γ_4^- symmetry is somewhat puzzling. Experimentally, it is always found that a band of low height occurs just to the high-energy side of the main F-band. This is the K-band, and it has almost always been attributed to a second excited state of the F-center. Since it is an optical band, it should have Γ_4^- symmetry. We are extending our calculations to $3nn$ lithium ion sites in a search for such a band.

The accuracy of these calculations is not great. The occurrence of many three-center integrals which we have calculated only approximately degrades the accuracy somewhat. Also, we have neglected many factors which would have to be included in a more accurate calculation, for example, distortions, exchange effects, which are only partially included here, polarization, etc. On the other hand, we are probably justified in being optimistic because the calculations do give the main F-band with considerable accuracy and the two levels involved in this band seem to lie at about the right place on an energy scale.

ELECTRONIC STRUCTURE OF THE M-CENTER

A. Meyer   R. F. Wood

The color center responsible for the M absorption and emission bands is now considered to consist of two F-centers bound together at nearest-neighbor halide sites. Thus, if the F-center is considered as the lattice analogue of the hydrogen atom in free space, the M-center can be considered as the lattice analogue of a hydrogen molecule, an F-center molecule.

We are carrying out calculations of the electronic structure of the M-center based on this model. We are using the Heitler-London method in which the spatial part of the singlet ground-state wave function can be written as

$$\Psi_M(12) = N[\psi_a(1)\,\psi_b(2) + \psi_a(2)\,\psi_b(1)] .$$

Here ψ_a and ψ_b are the F-center wave functions at sites a and b respectively. The excited-state functions are similar in form but modified to conform to the symmetry of the excited states. We are using F-center functions of the vacancy-centered type, that is,

$$\psi(\vec{r}) = N_F[\phi_0(\vec{r}) + \sum_{i=1} c_i \phi_i(\vec{r} - \vec{R}_i)] ,$$

where ϕ_0 is a function, centered at the vacancy, which describes the major portion of the charge density. The ϕ_i's are orbitals on the neighboring ions and the c_i's are determined by orthogonality conditions. For simplicity, we have taken a simple hydrogenic-like form for ϕ_0, after Wood and Korringa,[1] although the form used by Kojima[2] and Gourary and Adrian[3] would be slighty more accurate.

For the Hamiltonian we have taken

$$\mathcal{H} = -\frac{1}{2}\nabla_1^2 - \frac{1}{2}\nabla_2^2 + \sum_{g=1}^{N} V(\vec{r}_1 - \vec{R}_g)$$

$$+ \sum_{g=1}^{N} V(\vec{r}_2 - \vec{R}_g) - V(\vec{r}_1 - \vec{R}_a) - V(\vec{r}_1 - \vec{R}_b)$$

$$- V(\vec{r}_2 - \vec{R}_a) - V(\vec{r}_2 - \vec{R}_b) + r_{12}^{-1} + R_{ab}^{-1} ,$$

where R_{ab} is the interaction energy of the two vacancies and the form of V is generally assumed to be simple Coulombic.

Thus far, we have carried out calculations for LiCl with results which are rather encouraging. Experimentally, it is found that there are a number of different M absorption lines associated with each F line. Group theoretical considerations show that, on the basis of the model we are using, one can expect an excited state of Σ_u symmetry (we use the homonuclear diatomic molecule notation here for convenience) and two excited states of Π_u symmetry with a small splitting between the last two. In Table 3.1 we show our results for the transition energies compared with the experimental work on KCl extrapolated to LiCl.

[1] R. F. Wood and J. Korringa, Phys. Rev. 123, 1138 (1961).

[2] T. Kojima, J. Phys. Soc. Japan 12, 908 (1957).

[3] B. S. Gourary and F. J. Adrian, Phys. Rev. 105, 1180 (1957).

Table 3.1. Energies of the F- and M-Bands in LiCl

Band Designation	Symmetry of Excited State[a]	Energy (ev)	
		Experimental	Theoretical
F		3.1	3.3
M_1	Σ_u	~2.0	2.5
M_2	Π_u	~3.0	~3.8
Uncertain	Π_u	~3.0 + Δ_e[b]	~3.8 ± Δ_t

[a] The symmetry notation is that for a homonuclear diatomic molecule and is not strictly applicable here, but we use it for convenience.

[b] The splitting Δ_e is small — of the order of a few hundredths to a few tenths of an electron volt. Its sign has not been established for LiCl.

The discrepancy between theory and experiment for the F-band arises primarily from the use of a $2p$ function for the excited state instead of the $3p$ function indicated by Wood and Korringa. The table indicates that the relative distances between the bands are given quite well by our calculations. This seems to be a theoretical verification of the assumed model. We have not yet calculated the splitting, Δ_l, of the two Π states, but indications are that it is very small. The splitting is brought about directly by the inclusion of the ion orbitals in the F-center wave function. In a purely continuum model this splitting would be absent.

Our calculations also indicate that the "binding energy" is greater in the Σ excited state (~ 1.13 ev) than in the ground state (~ 0.34 ev). We interpret this to mean that it should be easier to form M-centers from F-centers when one or both of the F-centers is in an excited state than when both F-centers are in their ground states.

We intend to continue our calculations by turning now to LiF, which is a crystal of more experimental interest than is LiCl.

Part II. Crystal Physics

M. K. Wilkinson

PAGES __15__ to __16__

WERE INTENTIONALLY

LEFT BLANK

4. X-Ray Diffraction

ANOMALOUS TRANSMISSION OF X RAYS IN COPPER CRYSTALS[1]

M. C. Wittels   F. A. Sherrill
F. W. Young, Jr.

The anomalous transmission of x rays is the phenomenon in perfect or nearly perfect crystals for which the apparent absorption coefficient of x rays becomes abnormally small when an incident beam undergoes a Bragg reflection during passage through the crystal. This effect was first observed on quartz;[2] in later experiments it was observed on calcite,[3-5] germanium,[6] and silicon.[7] The possibility of observing and measuring anomalously transmitted x rays in copper became apparent during earlier studies[8] in which Lang[9] topographs were used. This effect has not previously been reported in a metal, to our knowledge; this report presents our initial findings concerning this phenomenon in nearly perfect crystals of copper.[8,10]

Several crystals 1 cm × 1 cm × Z (Z varying from 0.05 mm to 1.3 mm), with the 1-cm^2 face

(110), were prepared by acid sawing and polishing;[11] and from a set of (111) planes normal to this (110) surface, the Bragg conditions were adjusted for simultaneous observation of the anomalous transmitted and reflected beams. The incident radiation was Cu $K\alpha_1$ monochromated by (111) reflection from a perfect silicon crystal; and, although second-order short-wavelength x rays were not eliminated during the recording of the anomalous transmissions, measurable intensities were still easily observed when the potential on the x-ray tube was dropped to 12 kv. This was true for all except the thickest crystal examined, which was 1.3 mm thick.

The anomalous x-ray transmissions were observed by two techniques. In one method crystals were slowly rocked through the (111) reflecting position, and the Geiger counter intensities of the transmitted and reflected beams were recorded as a function of rocking angle. In the second method the two beams were recorded simultaneously on emulsions when the crystals were fixed at the peak (111) reflecting positions. It was observed that the anomalous transmitted and reflected beams were always approximately equal in intensity, in agreement with previous[3] findings. Also, as expected, the intensities decreased with increasing crystal thickness; but a detailed study of this property has not yet been completed.

One crystal, 0.15 mm thick, gave a peak count rate of the anomalous transmitted beam of 1100 quanta/sec, while the 1.3-mm crystal gave a similar peak count rate of only 30 quanta/sec. The narrow width of the transmitted and reflected beams in a 1-mm-thick crystal is demonstrated in the rocking curves shown in Fig. 4.1, where the somewhat enhanced background in the case

---

[1]Published in *Appl. Phys. Letters* 2, 127 (1963).

[2]G. Borrmann, *Physik. Z.* 42, 157–62 (1941).

[3]H. N. Campbell, *J. Appl. Phys.* 22, 1139–42 (1951).

[4]G. L. Rogosa and G. Schwartz, *Phys. Rev.* 87, 995–98 (1952).

[5]G. Brogren and O. Adell, *Arkiv Fysik* 8, 97–112, 401–26 (1945).

[6]L. P. Hunter, *Koninkl. Ned. Akad. Wetenschap., Proc., Ser. B* 61, 214–19 (1958).

[7]B. Okkerse, Philips Research Laboratory, Eindhoven, Netherlands, personal communication, 1961.

[8]M. C. Wittels, F. A. Sherrill, and F. W. Young, Jr., *Appl. Phys. Letters* 1, 22 (1962).

[9]A. R. Lang, *Acta Met.* 5, 358 (1957).

[10]F. W. Young, Jr., *Bull. Am. Phys. Soc.* 7, 215 (1962).

[11]F. W. Young, Jr., and T. R. Wilson, *Rev. Sci. Instr.* 32, 559 (1961).

17
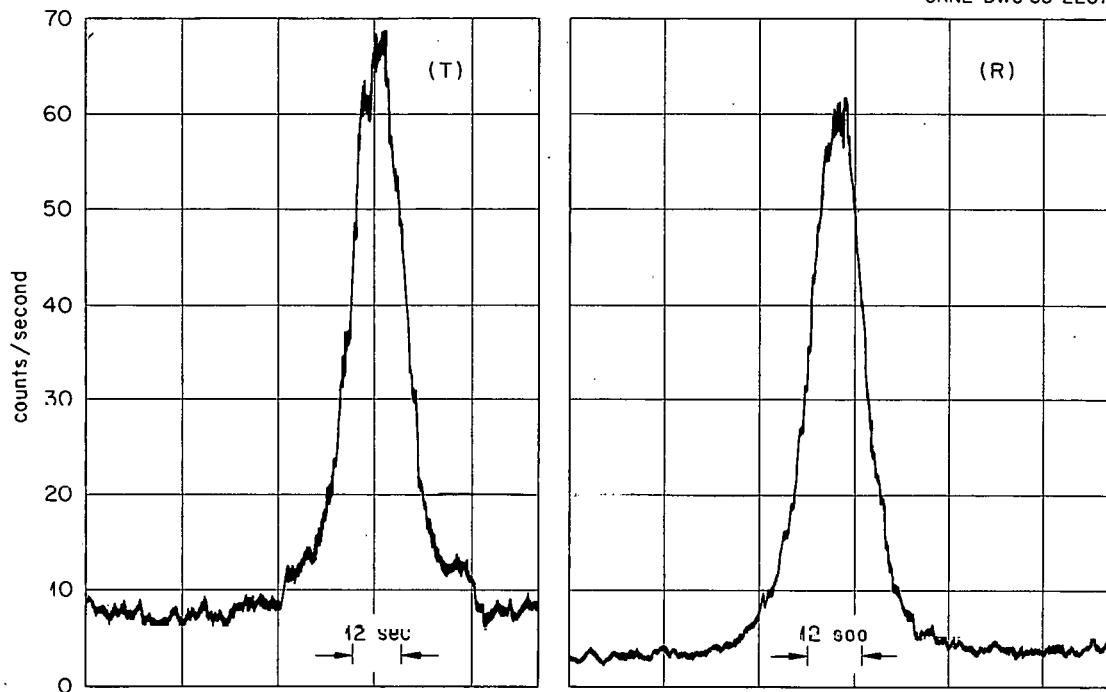
Fig. 4.1. Rocking Curves. Anomalous transmitted (T) and reflected beams (R) for a 1-mm-thick copper crystal; $\lambda = 1.54$ A.

of the anomalous transmitted beam is due to the weak normal transmitted beam in the region near 0°. The anomalous effect for this same crystal is recorded in Fig. 4.2, which shows the images of the transmitted and reflected beams that were obtained simultaneously. The long thin line at the bottom of the figure is the direct beam image taken with the crystal and collimation removed from the path. Some distortion in the reflected beam image is due to both the emulsion thickness and the fact that the flat plate was set at right angles only with respect to the transmitted beam. The gradual variation in intensity along the length of the transmitted beam image is due to a substantial change of imperfection concentration along the length of the crystal traversed by the transmitted beam. Apparent individual imperfections are revealed as light images in Fig. 4.3, which represents a magnification of a portion of the anomalous transmitted beam image shown in Fig. 4.2.

The reflected (111) beam associated with the anomalous transmission of Ag $K\alpha_1$ radiation on the same 1-mm-thick crystal was used in making a Lang topograph of the entire crystal (shown in Fig. 4.4). The light streaks and areas correspond to imperfections in this crystal, but a detailed understanding of these defects is not presently at hand. The large white area in the lower portion of the photograph corresponds to a region of imperfections so dense that they were not resolved. The section of the crystal from which Fig. 4.2 was obtained is indicated by the short arrows in Fig. 4.4; it confirms the existence of a variable density of imperfection in this crystal. It is clearly seen that many defects are present in this 1-mm-thick copper crystal which exhibits anomalous x-ray transmission. The correlations of defects observed by these and other techniques are being investigated further.

19

UNCLASSIFIED
PHOTO 62004
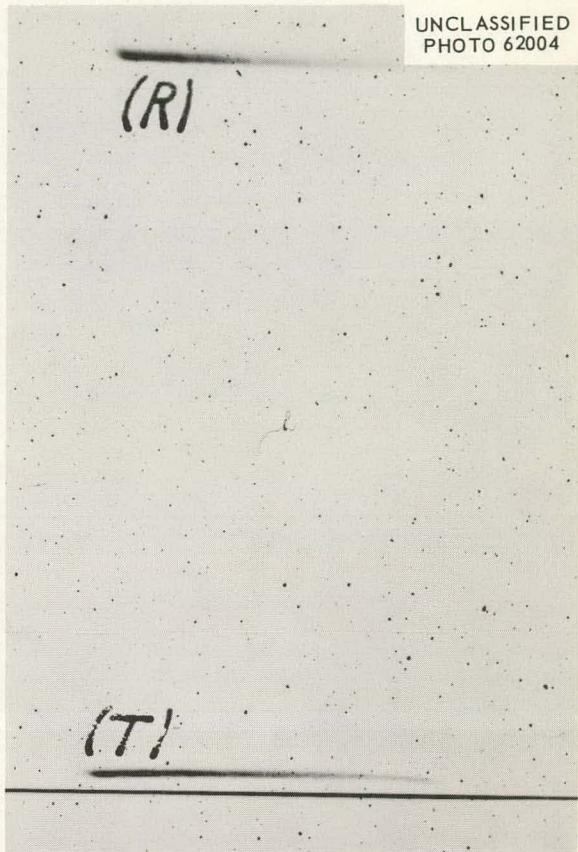
Fig. 4.2. A 16-hr Exposure to Both Beams from Same Crystal as in Fig. 4.1. Upper line, anomalous reflected beam (R); middle line, anomalous transmitted beam (T); and lower line, direct beam with crystal removed. Ilford L-4 nuclear plate, 100-μ emulsion; $\lambda = 1.54$ A. 3X.

UNCLASSIFIED
PHOTO 62005
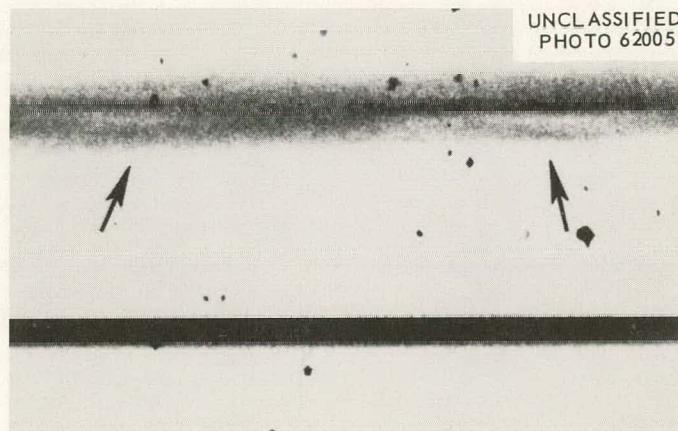
Fig. 4.3. Portion of Anomalous Transmitted Beam (T) and Direct Beam Shown in Fig. 4.2. 30X.
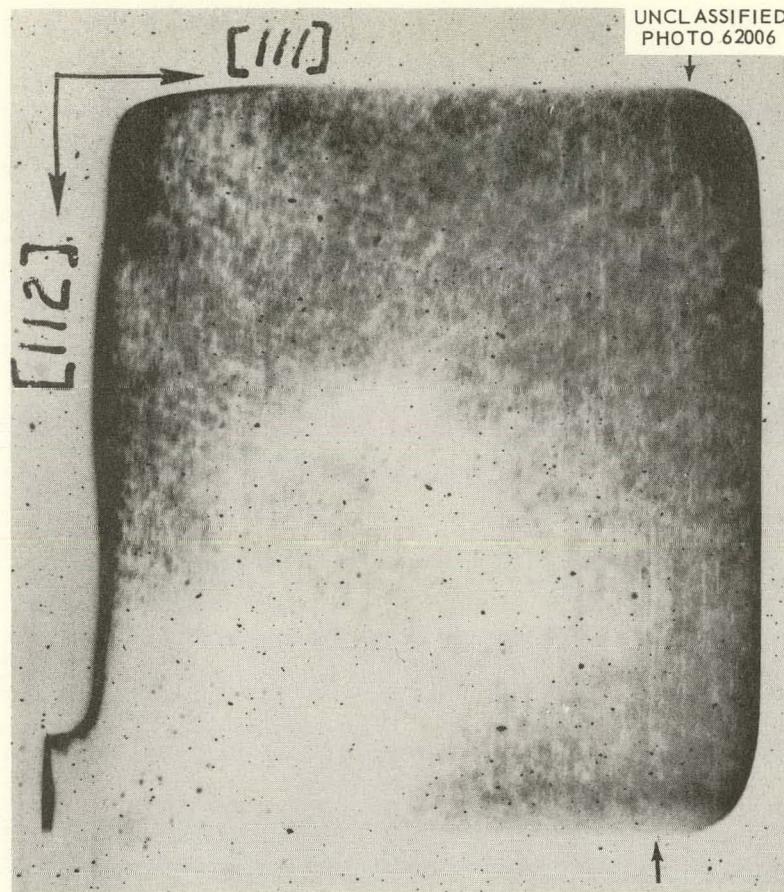
Fig. 4.4. Lang Topograph of Same 1-mm-thick Crystal. Positive photograph, 168 hr exposure. Ilford L-4 nuclear plate, 100-μ emulsion. Ag Ka_1. 9X.

VERTICALLY ROTATING DOUBLE-CRYSTAL X-RAY SPECTROMETER[12]

M. C. Wittels   F. A. Sherrill
A. C. Kimbrough

A versatile double-crystal x-ray spectrometer has been developed for the precise measurement of x-ray diffraction line widths to tenths of a second. The device can be employed in either the parallel or the antiparallel arrangement for rocking curve studies and can also be used in anomalous x-ray transmission experiments with nearly perfect crystals.

Although it is not strictly necessary, a Norelco wide-angle diffractometer is used to hold the first crystal and to provide a fixed axis of rotation for setting successive orders of reflection. A special worm gear drive is adapted to the unit for this purpose. The second crystal arrangement, which is the crux of the instrument, allows vertical rotation of the crystal from $-6°$ to $+165°$ about the fixed rotation axis of the first crystal; and this range covers nearly all possible reflections. A rocking axis for the second crystal is located approximately $3\frac{1}{2}$ in. from the fixed axis of rotation of the first crystal. Since nearly perfect crystals exhibit x-ray diffraction line widths as small as tenths of a second, a sufficiently slow, but synchronous, drive must be applied to rock the second crystal through the

---

[12]Summary of a paper to be presented at the 13th Annual Conference on Applications of X-Ray Analysis, Denver, Colo., Aug. 8, 1963.

total range of reflection. This is accomplished with a worm gear, a gear reducer, and a synchronous motor which are interconnected through sliding couplings. The couplings permit rapid, coarse adjustment of the second crystal into the reflecting range; they also permit the fast,

easy replacement of reducing gears and motors if a change in rocking speed is desired. A view of the second crystal mechanism is shown in Fig. 4.5, and the parallel double-crystal arrangement with shielding removed is indicated in Fig. 4.6.

UNCLASSIFIED
PHOTO 60537
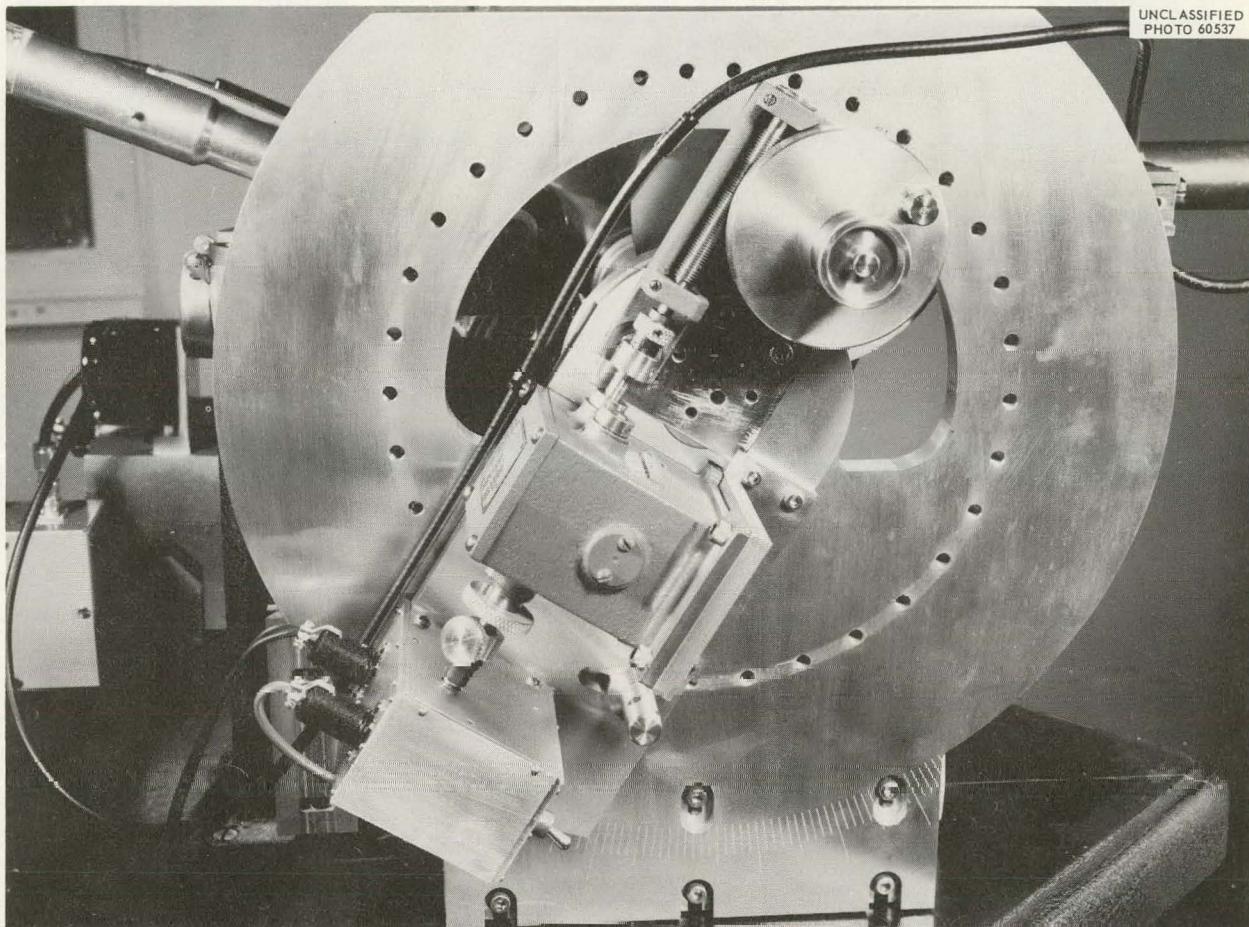
Fig. 4.5. Double-Crystal X-Ray Spectrometer, Outer View.
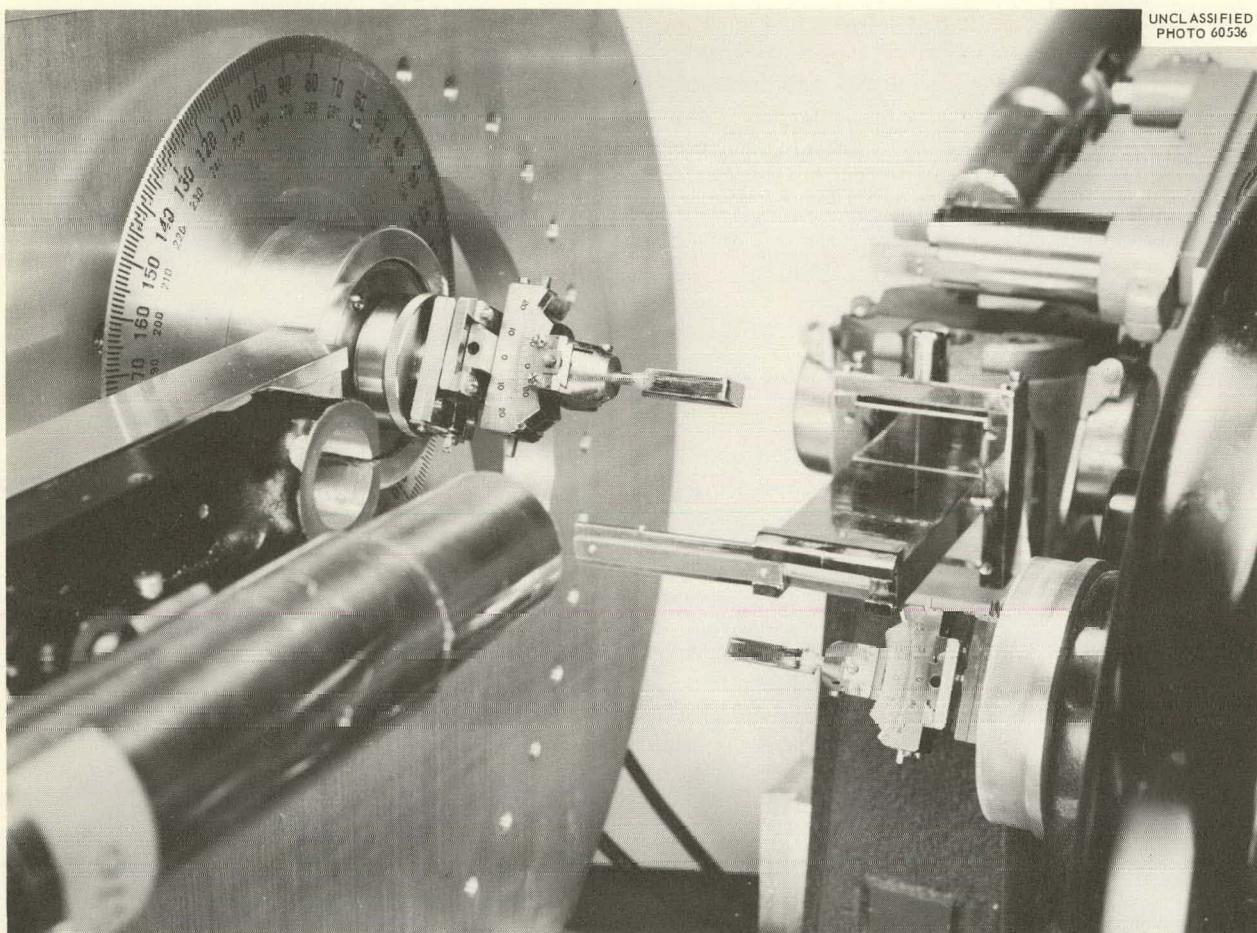
Fig. 4.6. Double-Crystal X-Ray Spectrometer with Shielding Removed and with Two Copper Crystals in the Parallel Arrangement.

X-RAY LINE WIDTHS OF NEARLY PERFECT COPPER CRYSTALS[13]

M. C. Wittels   F. A. Sherrill
F. W. Young, Jr.

It has previously been demonstrated[14] that large, nearly perfect copper crystals could be grown and that the dislocation densities determined both by etch-pit counting and by Lang topographs were in substantial agreement. More recently, it has also been shown that anomalous

x-ray transmission[15] could be observed in crystals up to 1.3 mm thick. In the present investigation, the double-crystal spectrometer was employed to determine the half-widths of reflections from successive orders of (111) in copper so that comparisons could be made with the theoretical predictions of Darwin[16] for perfect crystals.

Crystals with (111) faces were prepared by acid sawing[17] and electropolishing, and the double-crystal spectrometer was arranged in the parallel

[13]To be published in *Applied Physics Letters* (July 1963).

[14]M. C. Wittels, F. A. Sherrill, and F. W. Young, Jr., *Appl. Phys. Letters* 1, 22 (1962).

[15]M. C. Wittels, F. A. Sherrill, and F. W. Young, Jr., *Appl. Phys. Letters* 2, 127 (1963).

[16]C. G. Darwin, *Phil. Mag.* 27, 325, 675 (1914).

[17]F. W. Young, Jr., and T. R. Wilson, *Rev. Sci. Instr.* 32, 559 (1961).

position with crystal pairs adjusted as closely as possible to the parallel condition. For each reflection several runs were made as the crystals were removed and reset to ensure that nonsynchronous motion, counter dead time, and noisy electronics were in no instance influencing the measurements. In addition, the second crystal was translated in 2-mm increments across the reflected beam from the first crystal so that the uniformity of perfection over lengths up to 1 cm could be determined.

Two kinds of rocking curve measurements were made. One kind involved pairs of copper crystals with the parallel arrangement; the other involved

the use of the (333) reflection from a perfect silicon crystal in the first crystal position together with (222) reflections from copper crystals in the second crystal position. Fortuitously, this latter condition results in an arrangement closer to parallel than even crystal cutting errors allow, namely <0.5°. It also allowed for a more accurate determination of a true half-width of the (222) for copper by eliminating the contribution of the broadening inherent in a slightly imperfect first copper crystal.

The results for the paired copper crystal studies are given in Table 4.1, together with the values calculated from the Darwin theory[16] for perfect

Table 4.1. Half-Widths for Copper Crystals Using Mo $K\alpha_1$

Crystal Position 1	Crystal Position 2	Reflection	Measured Half-Widths (sec)	Calculated Half-Widths $\times \sqrt{2}$[a] (sec)	β-Calculated Half-Widths $\left(\beta = \sqrt{Y^2 + \Phi^2}\right)$[b]
Cu(B); dislocation density, $\sim 4 \times 10^3/cm^2$	Cu(A); dislocation density, $\sim 2 \times 10^2/cm^2$	Cu(A)			
		(111)	14.4	13.8	
		(222)	7.9	5.0	
		(333)	5.4	2.6	
		(444)	4.5	1.8	
		(555)	3.9	1.6	
Si(333); dislocation-free; measured half-width = 0.9 sec	Cu(A); dislocation density, $\sim 2 \times 10^2/cm^2$	Cu(A)			
		(222)	3.0		3.6
	Cu(B); dislocation density, $\sim 4 \times 10^3/cm^2$	Cu(B)			
		(222)	3.2		3.6
	Cu(C); dislocation density, $\sim 10^4/cm^2$	Cu(C)			
		(222)	5.0		3.6
	Cu(D); dislocation density, $\sim 3 \times 10^4/cm^2$	Cu(D)			
		(222)	5.2		3.6

[a]Darwin's formula was used in making these calculations.
[b]According to Darwin, $Y = 3.6$ sec for Cu(222).

crystals. His theoretical predictions give a range of total reflection whose width

$$Y = \frac{2N\lambda^2(e^2/mc^2)|F|K}{\sin 2\theta} , \qquad (1)$$

where N is the number of unit cells per cm^3; λ is the x-ray wavelength; F is the structure factor; θ is the angle of reflection; K is the polarization factor (1 or cos 2θ, depending on the polarization of the incident beam); and e, m, and c are the well-known physical constants. We have utilized the Fermi-Thomas-Dirac statistical model[18] for the atomic scattering factors used in these calculations. The value Y in Darwin's expression is termed half-width in the usage here.

In the paired copper measurements an x-ray beam of cross section approximately 6 mm × 0.5 mm impinged on the second crystal; the radiation was Mo $K\alpha_1$; and a krypton-filled Geiger tube was employed for counting purposes. The dislocation densities shown were determined by etch-pit counts. Also indicated in the table are the results for the measurements with the perfect silicon (333) in the first crystal position. In this case the x-ray beam cross section was reduced to 2 mm × 0.5 mm so that the number of dislocations seen by the x rays was reduced or eliminated, depending on the dislocation density of the specific crystal examined. The perfection of this silicon crystal had been previously determined by the double-crystal technique; and its half-width had been found to agree with the value recently reported,[19] namely, a measured value of 0.9 sec for (333) with Mo $K\alpha_1$.

In the calculations using the Darwin[16] theory, we have assumed the polarization vector to be in the plane of incidence of the primary beam and have neglected temperature and absorption corrections. The calculated values for copper pairs in the table also include a multiplying factor $\sqrt{2}$ which results from the assumption that the reflection curve for each crystal is Gaussian with full width at half maximum Y, giving a measured convoluted[20] width $\sqrt{2}Y$ for the single-

crystal reflection curve. The true half-width (Y) can be determined using the expression[21]

$$Y = (\beta^2 - \Phi^2)^{1/2} , \qquad (2)$$

where

Y = true half-width of the second crystal,

β = measured half-width of the second crystal,

Φ = true half-width of the first crystal.

Since the half-width for perfect silicon (333) is considerably smaller than those half-widths measured for copper (222), the measured values shown are very near the true values.

Some typical rocking curves are shown in Figs. 4.7 and 4.8. Several independent sets of measurements revealed that a region of uniform perfection extended at least 1 cm across the (111) surfaces of Cu(A) and Cu(B). The data shown

[20]R. W. James, *The Optical Principles of the Diffraction of X-Rays,* p 318, Bell and Sons, London, 1950.

[21]A. D. Kurtz, S. A. Kulin, and B. L. Averbach, *Phys. Rev.* 101, 1285 (1956).
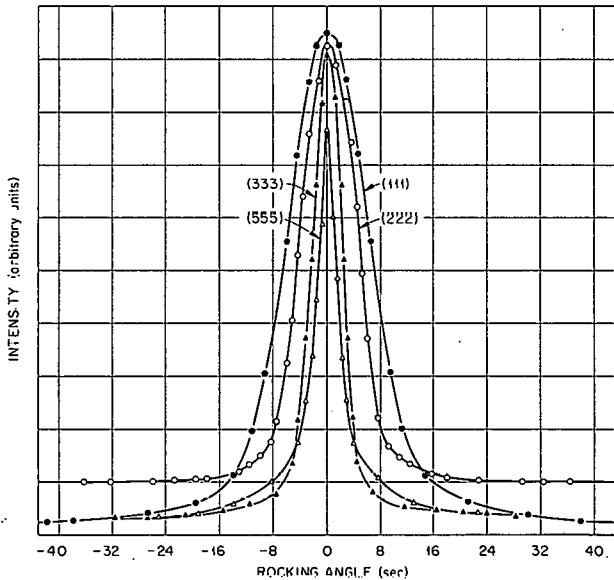
Fig. 4.7. Reflection Curves for Cu(A), Which Show the Effects in Increasing Orders of Reflection. The radiation was Mo $K\alpha_1$, and Cu(B) was used as first crystal.

[18]*International Tables for X-Ray Crystallography,* vol III.

[19]J. R. Patel, R. S. Wagner, and S. Moss, *Acta Met.* 10, 759 (1962).

measurements, had $\sim 4 \times 10^3$ dislocations/cm^2 present was probably an overriding feature in the failure to achieve even closer agreement with the Darwin predictions. By employing the silicon (333) reflection from perfect silicon for the first crystal and copper (222) reflections in the parallel second crystal arrangement, we found a marked narrowing in the (222) rocking curves as indicated in Table 4.1 and Fig. 4.8. In fact, for Cu(A) and Cu(B) the half-widths are somewhat smaller than those predicted by Darwin for perfect copper crystals. It should be emphasized that the copper-pair and silicon-copper measurements are not strictly comparable, however, because x-ray beams of different cross sections were employed and more imperfections were seen in the former case. In addition, the measurements would be somewhat altered with polarization conditions different from those we have assumed. If $|F|$ in Eq. (1) were replaced by $F_0 e^{-M}$, some thermal narrowing might occur even at room temperature because Θ_D, the Debye characteristic temperature for copper, is only 315°K. Simple estimates show that this effect would not be large enough to produce the narrowing noted, however; and additional thermal studies are certainly indicated.

Although there is some evidence indicating a finite half-width increase corresponding to a dislocation density increase in copper, the data are only qualitative. The validity of the Darwin theory on crystal perfection seems to be applicable to metals, semiconductors, and insulators. The correlation of imperfections and thermal effects with x-ray line widths in copper crystals is being investigated further.

Fig. 4.8. (222) Reflection Curves for Cu(A) and Cu(C). The radiation was Mo $K\alpha_1$, and silicon (333) from a perfect crystal was used as first crystal.

for copper crystal pairs are in reasonably good agreement with the data predicted by Darwin for perfect crystals. As expected, the measured values are somewhat larger than the Darwin values, roughly to the same extent as those recently reported for silicon[19] crystals with similar imperfection concentrations. The fact that Cu(B), used as the first crystal in these

GRAPHITE-STORED ENERGY IN THE OGR

M. C. Wittels

The ORNL Graphite Reactor was annealed in October 1962 by the usual reversed-air-flow process. The addition of channel orifice devices in the outer perimeter of the reactor core allowed annealing temperatures to be reached in the outermost fuel channels. Stored-energy measurements in graphite samples removed before and after the annealing program revealed a substantial degree of success in the removal of spontaneously releasable stored energy. This was strikingly evident in the

corner fuel channels, where significant amounts of stored energy existed prior to the annealing operation.

The stored energy in four of these channels is shown in Fig. 4.9. Table 4.2 lists the post-annealing results of stored energy; and to indi- cate the effect of peripheral channel orificing, the extent of all three cycles is shown in Fig. 4.10. Except for very minor unannealed fringes in the northern corners and a pocket on the north lateral side, it is evident that this last annealing program was highly successful.
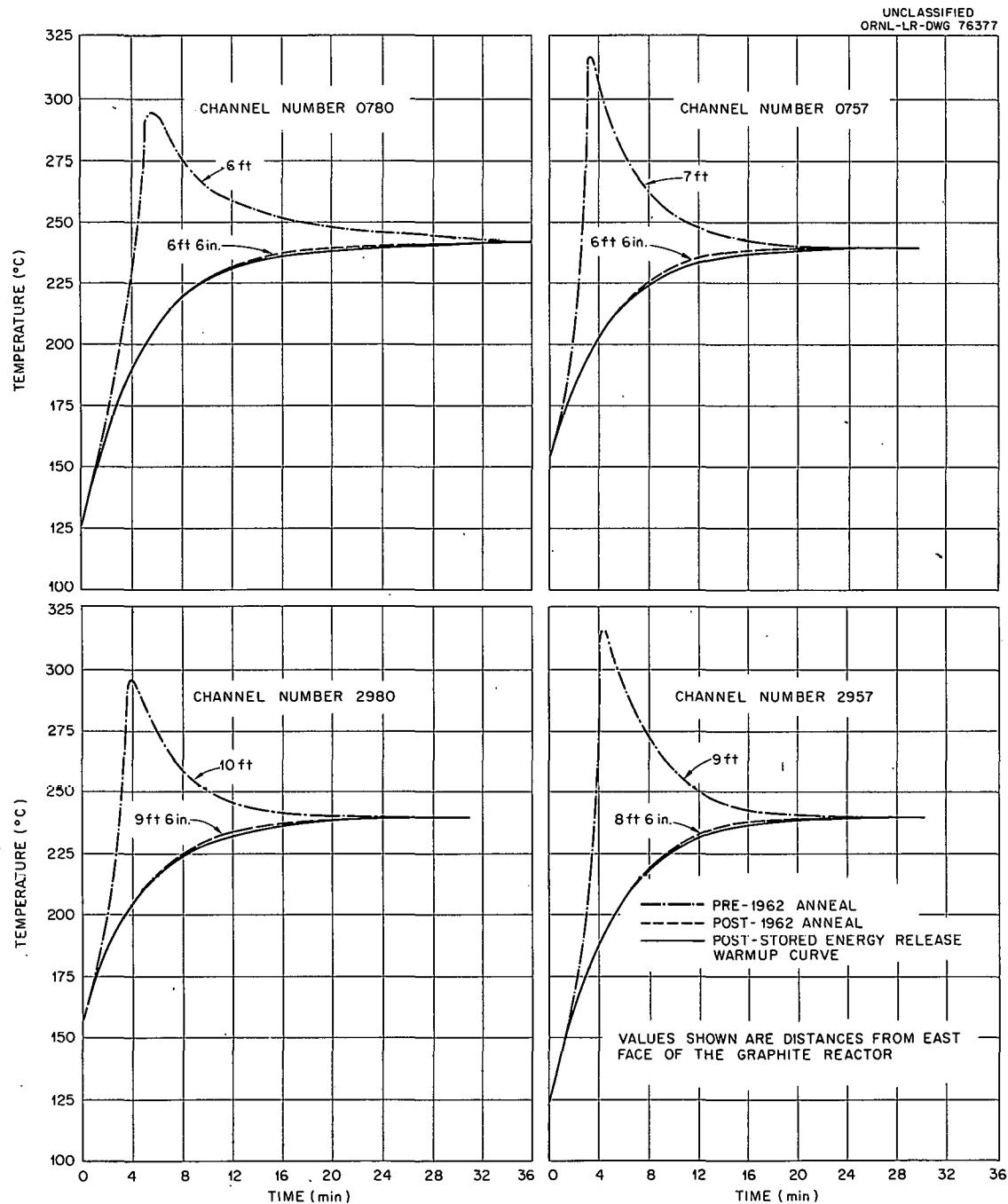
Fig. 4.9. Stored-Energy Release Data.

Table 4.2. Stored-Energy Data — December 1962

Channel	Distance from East Edge (ft)	Energy (cal/g)	Maximum Temperature (°C)	Channel	Distance from East Edge (ft)	Energy (cal/g)	Maximum Temperature (°C)
Corner Fuel Channels				**Lateral Fuel Channels (continued)**			
2980	2.5	4.6	237	0569	6.5	4.3	238
2980	5.5	2.8	238	0569	9.5	2.7	237
2980	9.5	2.2	237	1982	3.5	6.4	238
2980	13.5	5.8	239	1982	6.5	1.2	237
2957	4.5	7.7	239	1982	9.5	2.6	237
2957	8.5	3.2	237				
2957	11	16.8	241	**Reflector Channels**			
0757	3.5	9.7	240	3467	4.5	1.8	237
0757	6.5	3.4	238	3467	6.5	6.8	238
0757	11	6.7	239	3467	11	2.1	237
0780	3.5	4.2	238	3567	3.5	0	237
0780	6.5	2.2	238	3567	6.5	0	237
0780	8.5	2.1	237	3567	11	0	237
				3055	4.5	8.3	238
Lateral Fuel Channels				3055	7.5	13.8	238
3167	3.5	29.3	258	3055	11	15.8	238
3167	8.5	45.1	262	3255	4.5	0	237
3167	11	37.4	259	3255	7.5	0	237
2055	3.5	15.2	241	3255	11	0	237
2055	6.5	3.6	237	3453	3.5	0	237
2055	9.5	10.8	240	3453	6.5	0	237
0569	3.5	6.6	240	3453	11	0	237

Fig. 4.10. Front-Face View of Stored-Energy Status $7\frac{1}{2}$ ft from East Graphite Face.

5. Electron Microscopy

FISSION TRACKS IN SINGLE CRYSTALS OF UO$_2$[1]

T. S. Noggle

Fission-fragment tracks are observed in pre-thinned and irradiated UO$_2$ single crystals as a result of the diffraction contrast arising from strain fields associated with material disturbed by the passage of the fission fragment. Figures 5.1a and 5.1b show typical track structures in this material and illustrate the effect on track contrast of varying the diffraction conditions by tilting the specimen. For comparison, typical track structures observed in evaporated polycrystalline films of UO$_2$ are shown in Fig. 5.2.[2,3] In this latter case the appearance of the tracks is not affected by tilting, because it arises as a result of the displacement of material out of the track volume, which leaves a locally thinner region that is more transparent than the original film.

Replica studies of the free surfaces of the single crystals show that surface disturbances are also generated by the fission fragments. Figure 5.3 shows the surface disturbance observed with replicas on the single crystals, while Fig. 5.4 shows typical results for the evaporated films. It may be noted that surface disturbance in the single crystals is much less than that in the evaporated films. The surface disturbance on the single crystals by passage of fission fragments through the surface is so slight that little information can be deduced concerning the detailed nature of the disturbance.

Track statistics from both transmission and replica studies give lower densities and lengths than expected, and these can be reconciled to the theoretically expected results by assuming that
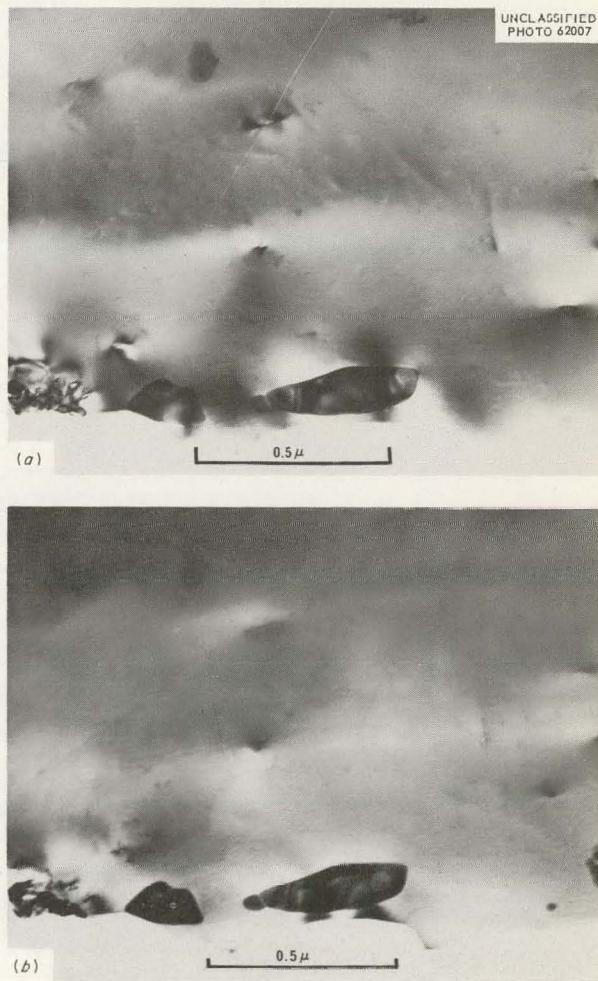
Fig. 5.1. UO$_2$ Single Crystal Irradiated to a Dose of 5×10^{14} fissions/cm^3. Sections a and b illustrate effect of tilting on track contrast. 80,000X. Reduced 38%.

---

[1]Summary of a paper to be presented at the *21st Annual Meeting of the Electron Microscope Society of America*, Denver, Colo., Aug. 28–31, 1963.

[2]T. S. Noggle and J. O. Stiegler, *J. Appl. Phys.* **31**, 2199 (1960).

[3]T. K. Bierlein and B. Mastel, *J. Appl. Phys.* **31**, 2314 (1960).

UNCLASSIFIED
PHOTO 62008

0.5μ
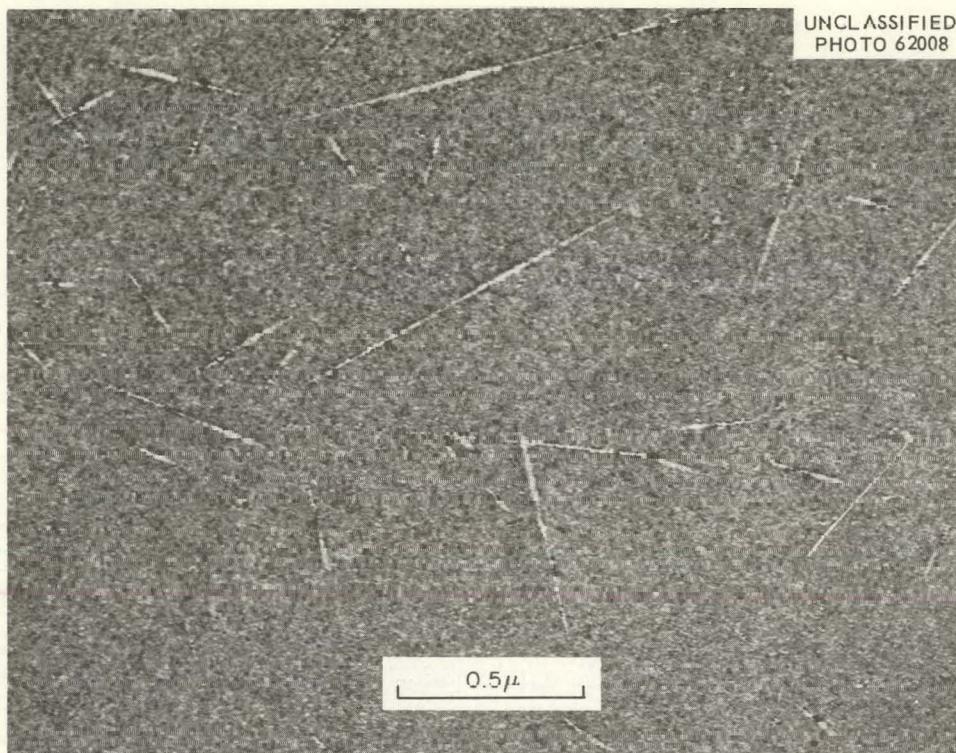
Fig. 5.2. 100-A-thick Film of UO_2. 50,000X.

UNCLASSIFIED
PHOTO 62009

0.5μ
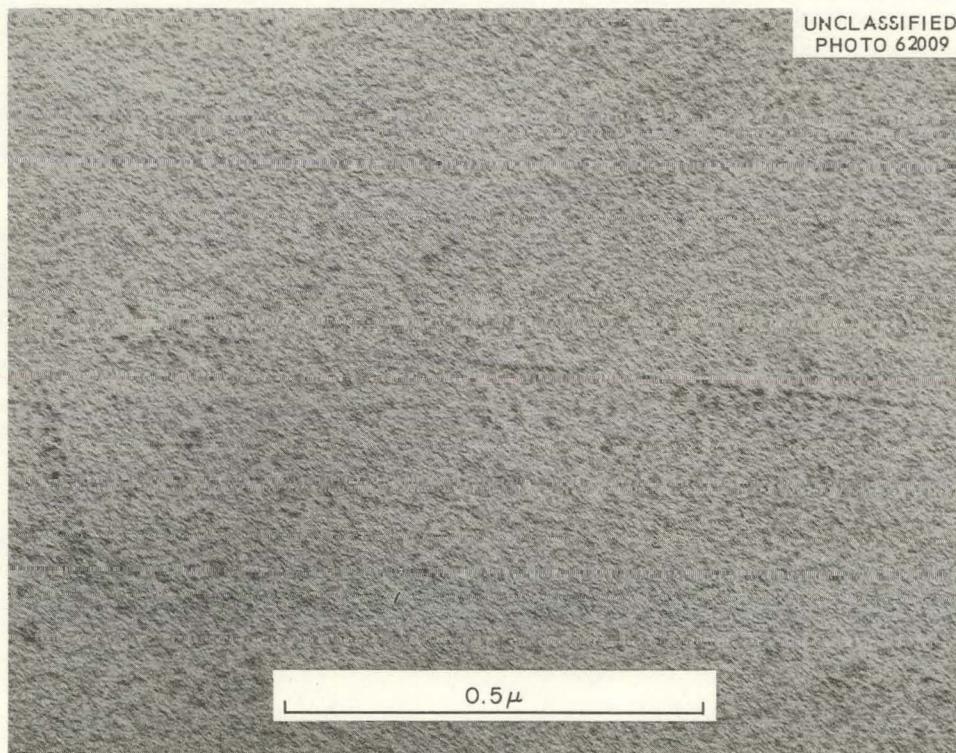
Fig. 5.3. Platinum-Preshadowed Carbon Replica of UO_2 Crystal Irradiated to a Dose of 5×10^{14} fissions/cm^3. 110,000X.
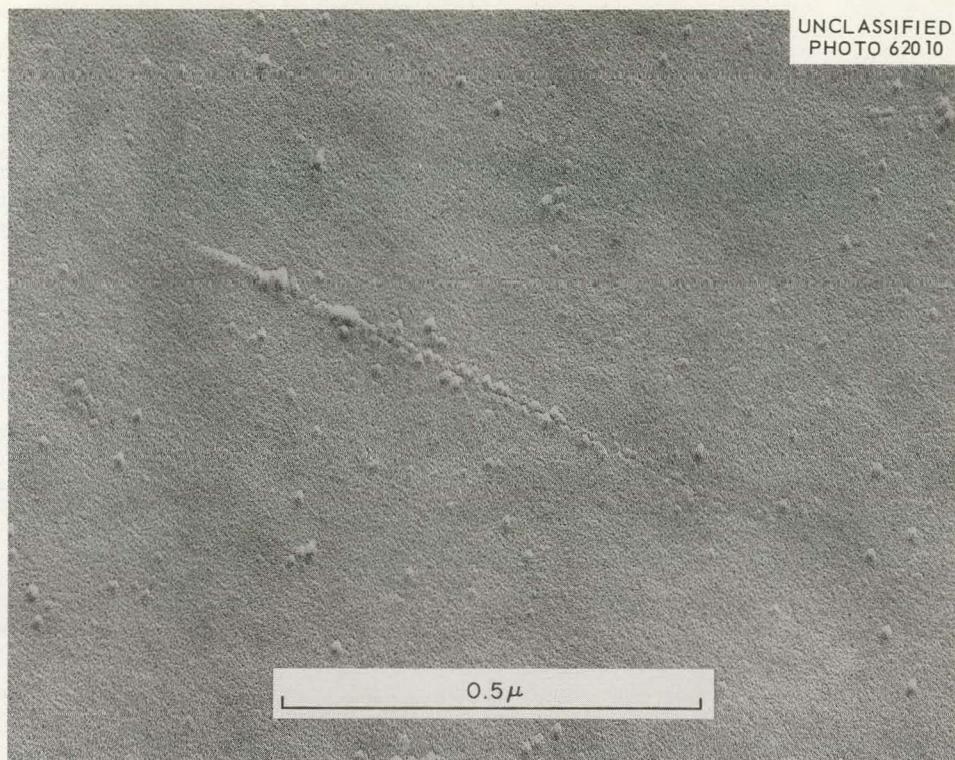
Fig. 5.4. Platinum-Preshadowed Carbon Replica of Evaporated Thin Film of UO_2. 110,000 X.

tracks are registered only for that part of the path near the surface of the crystal. Interpretation of the statistics with this assumption leads to the result that for replica studies detectable surface disturbances are associated with depths no greater than 20 to 40 A, while transmission studies indicate an effective thickness of 100 to 300 A for crystals 500 to 1000 A thick.

To date, no tracks have been observed in crystals thinned subsequent to irradiation, and this fact is in line with the result deduced from the track statistics that the registration of the tracks occurs only near the free surface of the crystals. In addition, no unusual etching behavior has been noted in the irradiated crystals as might be expected from the observation of etching of fission-fragment tracks in mica.[4]

All the results obtained to date suggest that the registration of continuous fission tracks in UO_2 single crystals is associated with the surface regions and presumably arises from the reduced restraint to the displacement of material by the fission spike at and near the free surface.

THIN FILMS AND FOILS

T. S. Noggle

Electron microscope studies of fission-fragment irradiation of thin films has continued with emphasis placed on the more exact evaluation and control of the specimen parameters, which are believed to affect the detailed nature of the track structures.[5] Extension of the observations on the effect of film thickness on the track structures has been made with films of gold and platinum. It has been established that track registration does not occur in these materials at thicknesses greater than approximately 100 A, indicating that the

---

[4]P. B. Price and R. M. Walker, *J. Appl. Phys.* **33**, 3407 (1962).

[5]T. S. Noggle and J. O. Stiegler, *J. Appl. Phys.* **33**, 1726 (1962).

range of thicknesses, over which the different thermal mechanisms contribute to track registration, is less than that found previously for palladium.[5] It is now thought that the grain size of these polycrystalline films plays an important role in the energy transport mechanism believed to determine the details of track registration. Experiments are in progress to vary the grain size in films of constant thickness in order to establish the contribution of this parameter to track registration.

Thin-foil studies on radiation effects in alloys are being made in cooperation with the Radiation Metallurgy Section. Preliminary studies of Cu-15 at. % Al, irradiated to give minimum resistance,[6] revealed no detectable structures which could be attributed to radiation effects in this material. These observations are being extended to higher irradiation doses for which the mechanical properties are changed by the irradiation.[7]

Similar studies are being made on low-dislocation-density copper specimens with the purpose of establishing whether structures not detectable by etch-pit or x-ray techniques[8] are present in this material. Difficulties have arisen in specimen preparation, due to the introduction of dislocations in this extremely soft material; and refinement of techniques has reduced, but not eliminated, these difficulties.

The recent acquisition and installation of a Hitachi HU-11A electron microscope with accessory stages providing tilting, heating, and cooling is expected to facilitate the study of thin foils and permit manipulation of specimens in ways heretofore not possible. This instrument will also permit electron microscope studies under high resolution conditions. Examples of results obtained during preliminary studies are shown in Figs. 5.5–5.8.

[6]J. M. Williams et al., Solid State Div. Ann. Progr. Rept. Aug. 31, 1962, ORNL-3364, pp 129–34.

[7]T. S. Koppenaal, Bull. Am. Phys. Soc., Ser. II 8(3), 197 (1963).

[8]M. C. Wittels et al., Solid State Div. Ann. Progr. Rept. Aug. 31, 1962, ORNL-3364, pp 35–37.

Fig. 5.5. Electron Micrograph of K_2PtCl_4 Crystal Showing (010) Planes Resolved, $d = 4.13$ A. 2,000,000X. Reduced 13%.
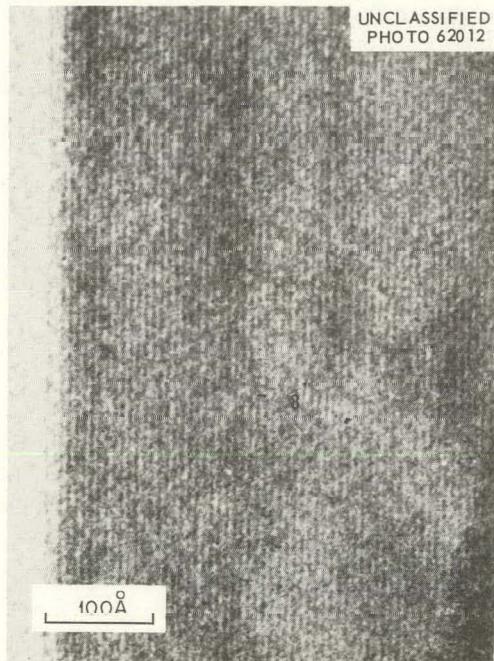
Fig. 5.6. Electron Micrograph of MoO_3 Crystal Showing (020) Planes Resolved, $d = 6.93$ A. 1,500,000X. Reduced 13%.

Fig. 5.7. Electron Micrograph of Copper Phthalocyanine Crystal Showing (210) Spacing Resolved, $d = 9.6$ A. 1,500,000X. Reduced 19%.
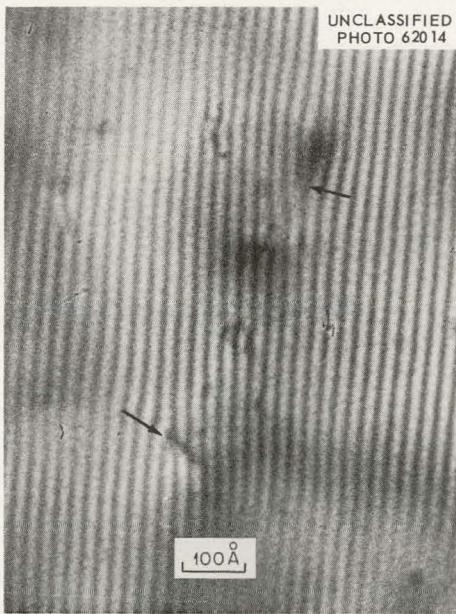
Fig. 5.8. Moiré Pattern of Superimposed (100) Oriented Gold Films. Rotational misorientation 4.7°, Moiré magnification 12X. Arrows show dislocations in Moiré pattern due to dislocations in the films. Moiré pattern of 24 A spacing arises from double diffraction from (200) planes in the gold. Reduced 19%.

STRUCTURE OF VAPOR DEPOSITS[9]

Derek Walton

Expressions are derived for the number of particles of deposit formed during condensation of a vapor onto an inert substrate as a function of time, substrate temperature, and incidence rate. It is assumed that the reevaporation of material from the particles is negligible, that the particles are small compared with their separation, and that the rate of incidence is always much greater than the nucleation rate. It is found that the number of particles is initially proportional to the cube of the time of exposure. This is followed by a period in which the number increases directly with the time, after which the number of particles increases as the time to a fractional power $1/n^* + 2$, where n^* is the number of atoms in the critical nucleus. In the first time interval the number of particles varies as the square of the rate of incidence; in the second, it varies as the rate of incidence to a power $n^* + 1$; and in the last interval, as the rate of incidence to a power $(n^* + 1)/(n^* + 2)$. In all intervals the number of particles varies exponentially with the reciprocal of the temperature.

It has been possible to compare some of these results with experiment, and the agreement is generally good.

COMMENT ON "FORMATION CONDITIONS OF THIN EPITAXIAL GERMANIUM FILMS ON SINGLE CRYSTAL SUBSTRATES" BY B. W. SLOOPE AND C. O. TILLER[10]

Derek Walton

In their paper, Sloope and Tiller[11] present a graph showing the relationship between epitaxial temperature and the incidence rate of metal atoms from the vapor. In a recent publication[12] an expression has been derived relating these two

---

[9]Abstract of a paper to be submitted for publication.

[10]Submitted for publication in the *Journal of Applied Physics*.

[11]B. W. Sloope and C. O. Tiller, *J. Appl. Phys.* **33**, 3461 (1962).

[12]Derek Walton, *Phil. Mag.* **7**, 1673 (1962).

variables. Thus, it is the purpose of this communication to briefly investigate the applicability of the expression to the results obtained by Sloope and Tiller.

If it is assumed that for the deposit to be oriented, it is necessary for an atom joining a growing cluster to be bonded to it with more than a single bond, the epitaxial temperature should be the temperature at which a single bond becomes unstable. Thus the epitaxial temperature should be given by[12]

$$T_e = - \frac{U_1 + Q_{ad}}{k \ln (Ra^2/\nu)} , \qquad (1)$$

where U_1 is the energy of a single bond, Q_{ad} is the binding energy of a single atom to the surface, R is the incidence rate from the vapor, a is the separation between adsorption sites, and ν is a frequency of vibration of the order of 10^{12}.

Sloope and Tiller find that the onset of polycrystallinity in the film occurs at a fixed incidence rate for a given substrate temperature. Consider that this temperature is the epitaxial temperature corresponding to the incidence rate at which the monocrystalline to polycrystalline transition occurs. If the reciprocal of the epitaxial temperature is plotted against the logarithm of the incidence rate, a straight line is obtained as expected from Eq. (1). The slope of this line corresponds to an energy of 1.36 ev, and thus the experimental value for the term (Ra^2/ν) would be 5×10^{-9} at 823°K. Since R is of the order of 10^{16} atoms cm^{-2} sec^{-1}, $a^2 \sim 10^{-15}$ cm^2, and $\nu \sim 10^{12}$ sec^{-1}, the calculated value for this quantity would be of the order of 10^{-11}. Considering the assumptions made in the theory and the uncertainty imposed by the experimental conditions, the agreement is reasonable. Thus it can be concluded that the simple theory, which leads to Eq. (1), appears to be applicable in this case.

√6. Spin Resonance

ELECTRON SPIN-LATTICE RELAXATION AT DEFECT SITES: E' CENTERS IN SYNTHETIC QUARTZ AT 3 KILO-OERSTEDS[1,2]

J. G. Castle, Jr.   D. W. Feldman
R. A. Weeks   P. G. Klemens[3]

Measurements of the spin-lattice relaxation time T_1 by the inversion-recovery technique are reported for two paramagnetic centers in quartz over a wide temperature range: from 1.3 to 250°K for the E_1' center, and from 2 to 80°K for the E_2' center. The data, extending over several orders of magnitude in T_1, are interpreted in terms of cross relaxation, direct processes, and Raman processes. The dominant feature of the Raman relaxation is a temperature variation of about T^3, which is much slower than expected by standard theory.

The theory of spin-lattice relaxation is extended to account for the modification at a defect site of the strain due to a lattice wave. Each defect has at least one characteristic frequency, and the local strain due to a wave of higher frequency is enhanced, being essentially given by the displacement due to the wave, rather than its spatial derivative. If the characteristic frequency is sufficiently low compared to the Debye frequency, the Raman relaxation rate should vary as T^3 (or T^5) over a wide range of temperatures, instead of the usual T^7 (or T^9) variation.

A detailed comparison of the relaxation rates observed for the two E' centers with the above theory suggests that each center has two characteristic frequencies or temperatures θ_i. For the

E_2' center one of these ($\theta_i = 45°K$) is ascribed to the vibration of a neighboring impurity ion, probably a proton. The other temperature ($\cong 5°K$) may arise from the motion of oxygen ions at the defect. The E_1' center has the two characteristic temperatures of 140°K and 14°K.

A model for the E_1' center is proposed: An electron is trapped at a silicon ion located in an oxygen divacancy. This model leads to the likelihood of low characteristic frequencies through a nonrigid SiO_2 group and also through a net negative charge, which should attract one or more interstitial impurity ions.

DIRECT FIELD EFFECTS IN THE HYPERFINE SPECTRA OF A PARAMAGNETIC DEFECT IN QUARTZ: THE E'₂ CENTER

R. A. Weeks

One of the principal features of the spectra of the E_2' center in synthetic quartz[4] is determined by an interaction with a nearby proton. The presence of the nearby proton is confirmed by comparing the spectra in a crystal grown in D_2O with crystals grown by the usual hydrothermal technique. For the interaction with the proton, $|\gamma(H)\,\beta_n H|$ is greater than both $|A|$ and $|B|$, where $\gamma(H)$ is the nuclear g factor of the proton, β_n is the nuclear magneton, H is the applied field, and A and B are the principal values of the hyperfine interaction tensor. It has been shown[5] that for this case the energy of the transition for an $S = 1/2$ state is

$$h\nu = g\beta H + m\left(\frac{g_{||}}{g}A\cos^2\theta + \frac{g_\perp}{g}B\sin^2\theta\right), \quad (1)$$

[1]Abstract of published paper: *Phys. Rev.* **130**, 577 (1963).

[2]Supported in part by the U.S. Air Force through the Air Force Cambridge Research Laboratories.

[3]Westinghouse Research Laboratories, Pittsburgh, Pa.

[4]R. A. Weeks, *Phys. Rev.* **130**, 570 (1963).

[5]J. A. Weil and J. H. Anderson, *J. Chem. Phys.* **35**, 1410 (1961); H. H. Woodbury and G. W. Ludwig, *Phys. Rev.* **124**, 1083 (1961).

where the symbols have their usual meaning and θ is the angle between the axis of symmetry and the applied field.

In Fig. 6.1 the orientation dependence of the spectra of the E_2' center is shown. There are five significant features of this orientation dependence. (1) The observed anisotropy is small, that is, $g_\perp \cong g_{||} \cong 2.00$. (2) The number of lines observed for the rotation about a twofold axis with H, the laboratory field, perpendicular to the twofold axis, may be interpreted as arising from a hyperfine interaction with a nucleus whose spin, I, is $1/2$, and whose isotopic abundance is ~100%. (3) If the lines are assumed to be doublets, arising from a hyperfine interaction with a nucleus of $I = 1/2$, then the hyperfine interaction goes to zero twice within a rotation angle of π. (4) The hyperfine interaction is very small compared to the interaction of the paramagnetic electron with the laboratory field. (5) Measurements at a field of 8700 gauss showed that the doublet splitting was independent of field and thus due to a hyperfine interaction in which $\Delta M_I = 0$, where ΔM_I is the change in the nuclear quantum state.

If this hyperfine interaction is due to an interaction of the paramagnetic center with a nearby proton, then the substitution of a deuteron for the proton should produce the following results: (1) Since the moment of the deuteron is less than the moment of the proton, the observed splitting should be proportionately less. (2) The spin of the deuteron is $I = 1$, which would form a triplet instead of the doublet formed by the proton with $I = 1/2$. (3) Because of field inhomogeneity, the triplet due to the deuteron should not be resolved and only a broad line should be observed. (4) There should be no change in the spin-orbit interaction of the paramagnetic center.

The spin resonance of a deuterated specimen of synthetic quartz is shown in Fig. 6.2c, and that of a crystal grown from a normal solution is shown in Fig. 6.2a. In Fig. 6.2b both crystals were placed in the cavity at the same time. The results are in agreement with the predictions made above and confirm the hypothesis that the observed spectrum is due to an interaction of the paramagnetic center with a nearby proton.
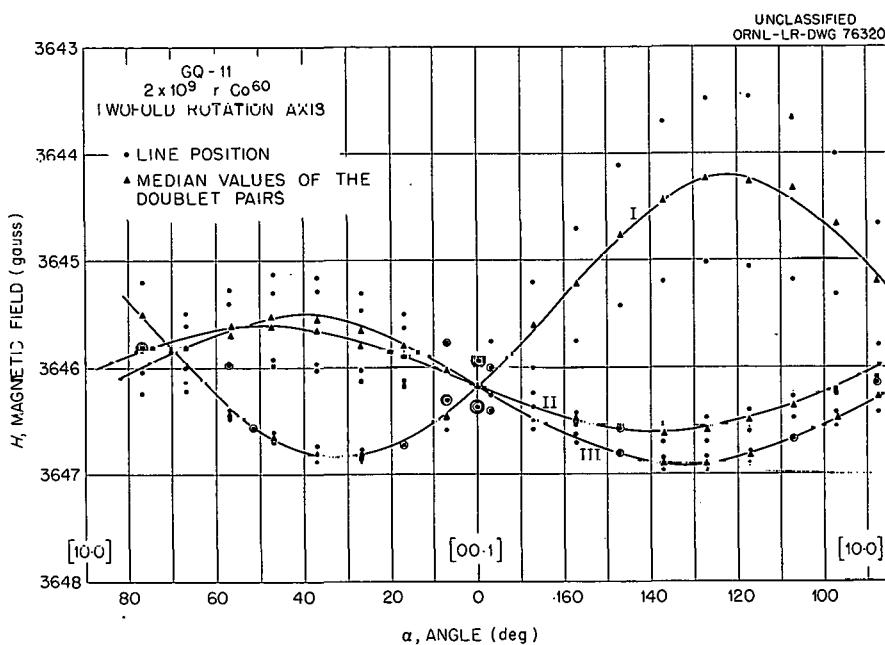
Fig. 6.1. Spectra of the E_2' Center for a Rotation About a Twofold Axis. Each solid circle is a line position, and the relative line intensities are shown by the number of circles around each point. The triangles are the median values of each pair of doublets. The curves were calculated from the g tensor.
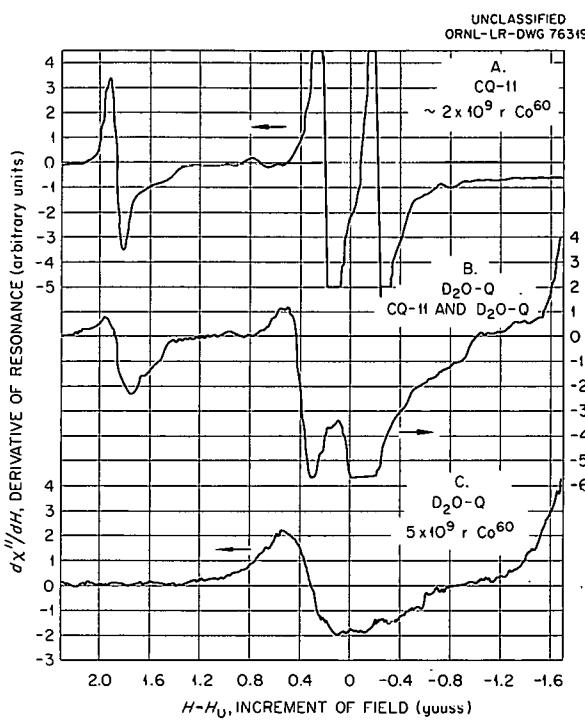
Fig. 6.2. The Spectra in the Vicinity of the E_2' Center in the Synthetic Crystals and in the Deuterated Crystals. The values for the magnetic field were determined by a proton resonance probe, and the relative error in the three measurements was ±0.1 gauss. The modulation field was ~0.07 gauss, peak to peak.

Along an axis of symmetry for one set of the doublets, the splitting of the doublets was found to be ~1.5 gauss, while in a direction perpendicular to this symmetry axis the separation was ~0.2 gauss. These two quantities comprise the A and B terms of Eq. (1), in which $A \cong \pm 1.3$ gauss and $B \cong \pm 0.2$ gauss. Since the magnitude of the direct field interaction term with the proton is $|\gamma \beta_n H| \cong 5$ gauss for the field of ~3600 gauss used in these measurements, it is evident that the transition energies are given by this equation. Curve I in Fig. 6.3 was calculated with the values of A and B, and the data points were taken from Fig. 6.1 for one set of doublets. Applying the symmetry operations appropriate for a quartz crystal to the equation, that is, a rotation by 120° and 240°, curves II and III, respectively, were calculated. The data points were taken from the remaining two sets of doublets, and it is seen that the agreement of the data with the calculated curves is quite good.

For this paramagnetic center the source of the principal hyperfine interaction is a nearby proton, that is, a hydrogen ion. It is presumed to be incorporated in the quartz structure by a bond to an oxygen ion. The laboratory field at the proton is larger than the field due to the paramagnetic center; hence, the quantizing field is the laboratory field. In this case the usual orientation dependence of the hyperfine interaction should not be
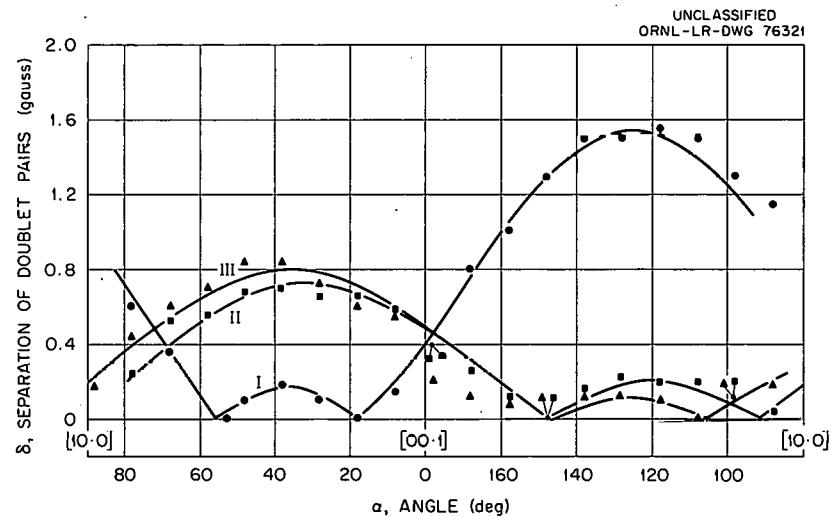
Fig. 6.3. The Separation of the Three Sets of Doublets Is Shown for a Twofold Rotation Axis Perpendicular to the Applied Field. The data points were taken from Fig. 6.1, and the curves were calculated by a method described in the text.

observed. The agreement of the observed orientation dependence of the interaction with that which was calculated from a solution of the secular equation appropriate to this approximation is confirmation that the field of the paramagnetic electron at the proton is less than the laboratory field.

EFFECTS OF IRRADIATION ON POLARIZATION CURRENTS IN GLASS

R. A. Weeks

In the last report on this subject[6] it was shown that the polarization current in the lead silicate glass could be resolved into four distinct components each characterized by a time constant τ. It was also shown that the strengths of these polarization processes were enhanced by gamma-ray irradiation up to a dose of $\sim10^7$ r. For higher doses an apparent decrease in the strengths of some of these processes took place, but the data showing this decrease had a considerable scatter.

It has now been found that such a decrease does take place, although the particular polarization processes associated with the decrease have not been resolved. In addition to the enhancement, which is stable at room temperature for long periods of time (~4 weeks), there is a large increase in the polarization current observed immediately after irradiation, which disappears in ~24 hr. Additional measurements have also been made on the polarization currents as a function of voltage. These have supported the hypothesis that the conductivity is ohmic.

The polarization P is defined as the electric dipole moment per unit volume and is given by the relation

$$P = D - \epsilon_o E , \qquad (1)$$

where D is the displacement field, E is the laboratory field, and ϵ_o is the dielectric constant. The current for a constant laboratory field is $J = \partial D/\partial t$, and from Eq. (1), $-J = \partial P/\partial t$.

The polarization P' at a microscopic point in the material being polarized can also be written

$$P' = N\alpha E' , \qquad (2)$$

where N is the number of polarizable units, α is the polarizability, and E' is the local field acting on the polarizable units. Thus, the current due to these units is

$$J' = \frac{\partial}{\partial t} (N\alpha E') . \qquad (3)$$

The polarizing entities have been represented by only one term in Eq. (3), but in a real material, it is certainly probable that several such terms may be required. Therefore, a better approximation would be to write the polarizability term as a summation, for example, $\alpha = \sum_{i=1}^{n} N_i \alpha_i$.

One of the terms in this summation originates from space-charge effects. The space-charge term is due to an accumulation of charges at the electrodes and also at internal surfaces. With respect to the glasses the experimental results shown in Fig. 6.4 and other results[6] indicate that there is no electrode space-charge term. Considering the known properties of glass, it also appears reasonable to eliminate a space-charge term on internal surfaces. With the elimination of the space-charge terms, only the dipole and orientation terms are left, and Eq. (3) can be written

$$J' = [E + E'(t)] \frac{\partial}{\partial t} \left(\sum_{i=1}^{n} N_i \alpha_i \right)$$

$$+ \left(\sum_{i=1}^{n} N_i \alpha_i \right) \frac{\partial E'(t)}{\partial t} . \qquad (4)$$
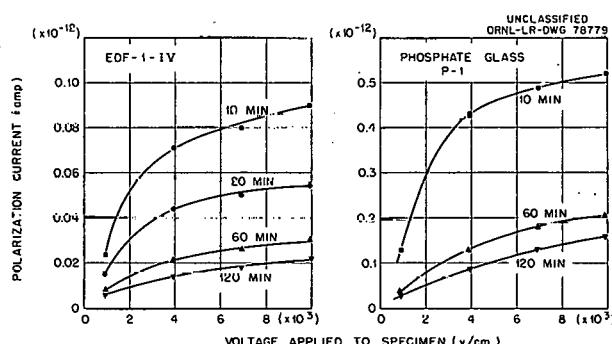
Fig. 6.4. The Polarization Current in a Lead Silicate Glass Is Given as a Function of Voltage for Various Times After Application of the Polarizing Voltage. Before each increase in the voltage the specimen was depolarized by shorting the electrodes.

[6]R. A. Weeks and E. Lell, *Solid State Div. Ann. Progr. Rept, Aug. 31, 1962,* ORNL-3364, p 47.

The relation between the observed current and the current at a microscopic point must now be considered, and there are several experimental facts which have a bearing on this problem. These experimental results are: (1) The observed currents are proportional to applied voltage for voltages >3900 v/cm or to duration of applied voltages for times ≦120 min. (2) The observed polarization currents and final conductivity (at times >30 hr) are inversely proportional to the thickness of specimen. (3) The principle of superposition is obeyed. On the basis of these facts, it is assumed that the observed current and the sum of microscopic currents are identical, that is, $J = J'$.

The experimental observations, which have been reported, have been fitted to a sum of exponential terms.[6] The number of such terms required to fit the data is 4 plus a constant term, and the characteristic times of these four terms are not altered by irradiation. These four terms may be related to the dipole and orientation polarizability terms. Although it is not possible from these data to distinguish the terms, the summation terms in Eq. (4) may be reduced to four terms. Since these data showed that only the strengths of the terms were altered by irradiation, and that the polarizability terms, as defined by the characteristic times, were constant, Eq. (4) becomes

$$J = [E + E'(t)] \left(\alpha_1 \frac{\partial N_1}{\partial t} + \alpha_2 \frac{\partial N_2}{\partial t} \right.$$
$$\left. + \alpha_3 \frac{\partial N_3}{\partial t} + \alpha_4 \frac{\partial N_4}{\partial t} \right)$$
$$+ \left(\alpha_1 N_1 + \alpha_2 N_2 + \alpha_3 N_3 + \alpha_4 N_4 \right) \frac{\partial E'(t)}{\partial t}. \quad (5)$$

This equation has the implied assumption in it that $\partial E'(t)/\partial t$ is small relative to the $\partial N_i/\partial t$ terms. However, since information on this term is lacking, it has not been omitted.

Experimental Results

It has been noted that the polarization currents observed in the lead silicate glass were ohmic. Additional experimental verification of the ohmic character of the polarization current is shown in Fig. 6.4. In these measurements the polarization currents were obtained as a function of voltage.

A given voltage was applied for a period of ~125 min, and the specimen was then depolarized completely before the next voltage was applied. The data points were obtained for varying periods of time after the application of the voltage. For the shorter periods of time (10 min and 20 min) the current is not a linear function of voltage below ~4000 v/cm. At 120 min after application of the voltage the current is approximately proportional to voltage for both of the glasses shown in Fig. 6.4. Although not shown, observations on a pure silica glass have indicated a linear relation between current and voltage from 10 to 120 min. It is evident from Fig. 6.4 that above 4000 v/cm the polarization current is proportional to the applied voltage in the three glasses which have been investigated.

The strengths of the four polarization processes were reported to vary with gamma-ray dose.[6] Some data were given that seem to indicate a peak in the strengths of some of those processes as a function of dose. This peak has been verified although the particular processes (identified by their characteristic times), which are involved, have not been identified. This effect is shown in Figs. 6.5 and 6.6. In Fig. 6.5 the polarization currents at two times after application of a voltage (3900 v/cm) are shown as a function of Co^{60} gamma-ray dose. The peak in the enhancement of the strength of the polarization current by irradiation is clearly evident in both curves. There are differences between the two curves, which indicate that those processes with large characteristic times are primarily affected by the irradiation. This is evident in the ratio between the peak value and initial value for the 10-min curve (~3) and that for the 120-min curve (~5.6) and also in the ratios of peak value to the value at maximum dose (1.3 for the 10-min curve and 1.7 for the 120-min curve). There are also some differences in the shapes of the curves.

In Fig. 6.6 the polarization currents as a function of duration of applied voltage are shown for various Co^{60} gamma-ray doses. The odd-numbered curves were obtained 24 hr after irradiation and the even-numbered curves were measured immediately after irradiation. A comparison of curves XIII and XV with curve VII shows that the largest changes in the polarization occur in those processes with the longest characteristic times.

The even-numbered curves in Fig. 6.6, taken immediately after irradiation, show that there is an enhancement of the polarization, which disappears in ~24 hr. This enhancement is apparently independent of gamma-ray dose for doses greater than 10 min. It may also be independent of dose for those of shorter duration, but experimental evidence is lacking. An investigation of the decay of this short-lifetime enhancement has indicated that at least two processes may be involved.
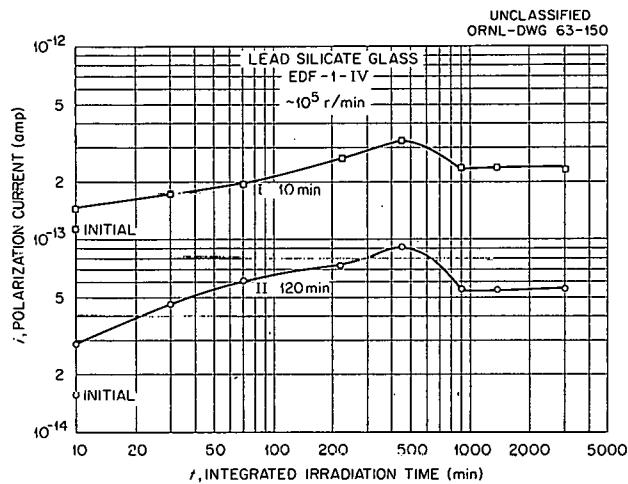
Fig. 6.5. The Polarization Current in a Lead Silicate Glass at Various Times After Application of the Polarizing Voltage Is Shown as a Function of Co[60] Gamma-Ray Dose. The specimen was depolarized between each irradiation.
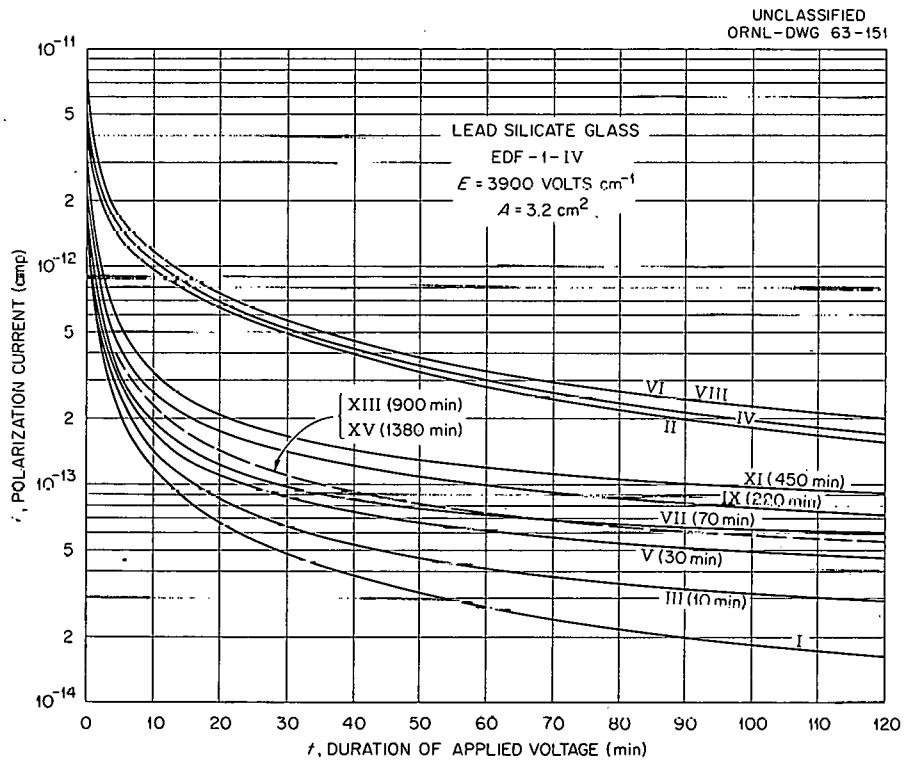
Fig. 6.6. The Polarization Current in a Lead Silicate Glass Is Given for a Period of 120 min as a Function of Co[60] Gamma-Ray Dose. The even-numbered curves were recorded immediately after irradiation, and the odd-numbered curves were recorded 24 hr later. The specimen was depolarized after each measurement.

LONGITUDINAL CRITICAL CURRENTS IN COLD-DRAWN SUPERCONDUCTING ALLOYS[1]

S. T. Sekula   R. W. Boom
C. J. Bergeron[2]

The critical-current behavior of cold-worked hard superconductors in a transverse magnetic field has been extensively reported,[3-5] and a marked anisotropy of critical current has been observed in these materials.[6-8] However, the dependence of critical current on magnetic field in orientations other than transverse has been studied in only a few cases;[9,10] the high-current regions have been generally neglected. The following is a report on the behavior of several cold-drawn hard superconductor wires in magnetic fields which are parallel to the superconducting transport current.

Commercially available superconducting alloys, cold drawn to 0.010-in. diameter, were tested in the Oak Ridge 100-kilogauss 2-in.-ID magnet. Joints with resistances less than 10^{-6} ohm were of the

pressed-copper type described previously.[11] All samples were cast in Emerson and Cummings Stycast type-2850FT epoxy to prevent sample motion. The current supply was controlled by carbon compression rheostats in series with a battery bank; the voltage sensitivity at initiation of a transition was about 0.1 μv. A variable shunt of approximately 10^{-3} ohm was used in the circuit to ensure that the temperature of the samples did not exceed 300°K after the resistive transition. All measurements were taken at 4.2°K.

The critical-current behavior of four cold-drawn Nb-Zr alloys from one commercial source is shown in Fig. 7.1; similar results were obtained for

---

[1]Published in *Appl. Phys. Letters* 2(5), 102 (1963).

[2]Consultant to Electronuclear Division from Louisiana State University, New Orleans.

[3]J. E. Kunzler, *Bull. Am. Phys. Soc.* 6, 298 (1961).

[4]T. G. Berlincourt, R. R. Hake, and D. H. Leslie, *Phys. Rev. Letters* 6, 671 (1961).

[5]J. E. Kunzler, *J. Appl. Phys.* 33, 1042S (1962).

[6]M. A. R. Leblanc and W. A. Little, *Proceedings of the Seventh International Conference on Low Temperature Physics*, p 362, University of Toronto Press, Toronto, 1960.

[7]R. R. Hake and D. H. Leslie, *Proceeding of the Eighth International Conference on Low Temperature Physics* (to be published).

[8]D. Freeman, Linde Corp. (private communication).

[9]J. G. Daunt et al., *Cryogenics* 1, 212 (1962).

[10]P. R. Aron and H. C. Hitchcock, *J. Appl. Phys.* 33, 2242 (1962).

[11]L. D. Roberts and R. W. Boom, *Bull. Am. Phys. Soc.* 7, 574 (1962).
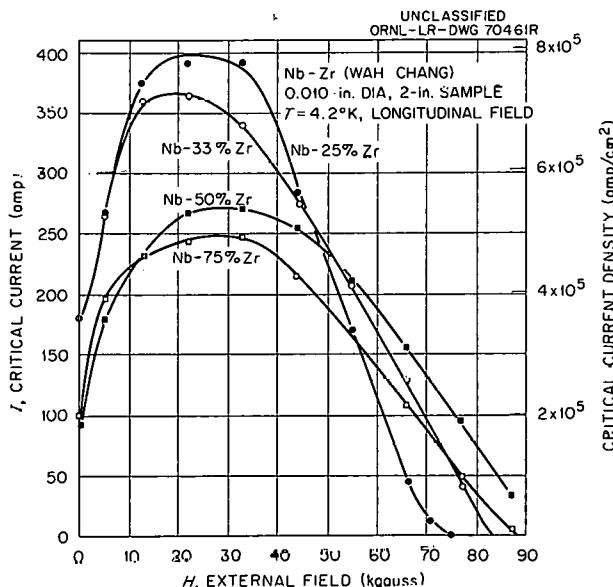
Fig. 7.1. Longitudinal Critical Current vs Applied Field for Several Cold-Drawn Nb-Zr Alloys.

samples from other suppliers. In the longitudinal configuration, maxima in critical currents for all atomic percentages of zirconium occur at 20 to 30 kilogauss. With one sample of Nb–25 at. % Zr we have measured a critical current of 480 amp at 25 kilogauss, which corresponds to a current density of 10^6 amp/cm^2. The longitudinal critical-current characteristics of a 0.012-in.-diam cold-drawn Mo–33 at. % Re sample and of two different sizes of cold-drawn Ta–25 at. % Ti are shown in Fig. 7.2. In these two alloys maximum critical currents are obtained at fields of 5 kilogauss and 20 kilogauss respectively. The maximum critical currents for these alloys in a longitudinal field represent increases over zero-field values ranging from 50% to 150%. Grassman and Rinderer[12] have previously observed a 10% peaking of the critical current in longitudinal fields for Pb–10 at. % Bi wires.

[12]P. Grassman and L. Rinderer, *Helv. Phys. Acta* **27**, 309 (1954).
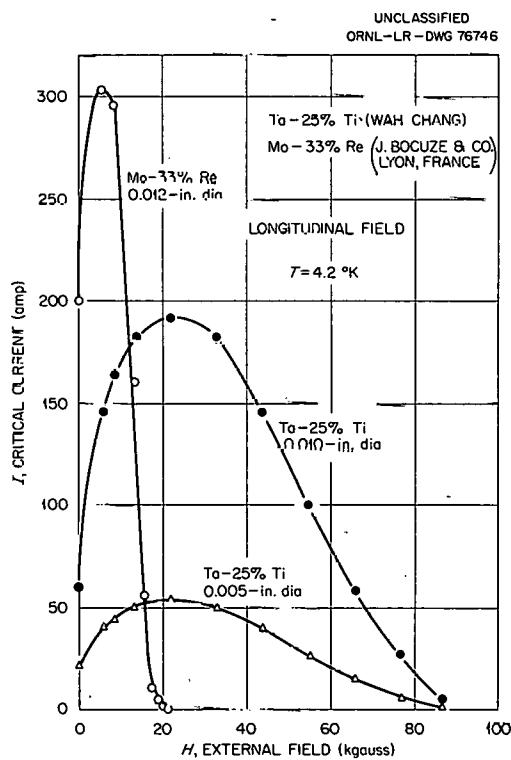
Fig. 7.2. Longitudinal Critical Current vs Applied Field for Cold-Drawn Ta–25 at. % Ti and Mo–33 at. % Re Samples.

Since the critical current is markedly enhanced in a longitudinal field, the concept of force-free magnet design[13] is made all the more tempting. Consequently, a one-layer toroid, 4 in. in mean diameter and 0.5 in. in cross-section diameter, was constructed with 0.010-in. Nb–25 at. % Zr wire in a force-free configuration, that is, current flow at 45° to the radial vector. This toroid carried 120 amp and produced a longitudinal field of approximately 4000 gauss at the winding; the critical current was only one-half of that observed for the same material in a short-wire test. Mechanical deviations from strigent force-free conditions could have caused the current loss. Since 120 amp is not unusually large for an ordinary one-layer superconducting solenoid, the above test is inconclusive and further confirming study is required.

The type of critical-current behavior as shown in the figures appears to be a common characteristic of cold-drawn superconducting alloys. An explanation of these data in the framework of extant models does not seem possible. One attractive speculation, as yet unsubstantiated, is to assume that the currents tend to flow in a force-free (helical) manner.

SMALL SUPERCONDUCTING MAGNET WITH HOMOGENEOUS FIELD

R. H. Kernohan   P. G. Huray[14]
S. T. Sekula   J. B. Sanders[14]

In order to conduct studies on the magnetic properties of superconductors, a fairly strong homogeneous magnetic field is required. The mathematics and construction of uniform-field electromagnets has been described by Garrett.[15] The method consists essentially in writing a power series involving Legendre polynomials expanded about the origin of the field. If this origin is on the axis in the center of a solenoid, there will be no odd terms in the expansion. Further, if the dimensions of the solenoid are chosen properly, the second and fourth terms in the expansion can

[13]H. P. Furth and M. A. Levine, *J. Appl. Phys.* **33**, 747 (1962).

[14]Co-op student from the University of Tennessee, Knoxville.

[15]M. W. Garrett, *J. Appl. Phys.* **22**, 9 (1951).

be made to cancel and a so-called sixth-order solenoid can be constructed with a fairly uniform field both axially and radially.

A sixth-order solenoid was constructed on a copper core with dimensions which are shown at the top of Fig. 7.3. The solenoid was designed for use in a 3-in.-ID liquid-helium Dewar with the intention of having a fairly homogeneous field about 1 in. in diameter and about 2 in. long. The windings consisted of nylon-insulated superconducting Nb–33 at. % Zr wire, which was 10 mils in diameter. There were 5635 turns of wire in 19

SUPERCONDUCTING SOLENOID CROSS SECTION

Fig. 7.3. Cross Section of Superconducting Solenoid and Typical Axial Field Profile.

layers on the main body of the solenoid and 494 turns in 19 extra layers on each of the two ends. The extra windings on the ends were connected in series with the windings on the main body of the solenoid, and two heavy copper leads were attached in order to lower the magnet into the helium Dewar.

For the purpose of calibrating and testing, the magnetoresistance of a $\frac{1}{2}$-in. length of 6-mil cp bismuth wire was employed. The bismuth wire was calibrated in liquid helium between the poles of a 10-kilogauss electromagnet, which was itself calibrated by spin resonance techniques. The bismuth-wire probe then served as a secondary calibration standard for measuring the current-field profile along the axis of the solenoid.

The current-field relationship was almost linear. in liquid helium at 4.2°K the magnet windings revert to their normal resistive condition at a maximum critical current of about 15 amp, which corresponds to a field of about 11 kilo-oersteds.

A typical profile of the field along the magnet axis for a current of 5.000 amp is shown in the lower half of Fig. 7.3. According to the calculations on sixth-order solenoids, the field should be homogeneous to within 0.1% for a distance of 1.68 in. along the axis, and the field profile of the finished magnet agrees excellently with this value.

It was found that some remanent or frozen-in flux remains in the solenoid after the current is returned to zero and the magnetic circuit is open, even though no ferromagnetic materials are nearby. The amount of frozen-in flux is dependent on the highest current used and can be somewhat minimized by increasing or decreasing the magnet current very slowly. Otherwise, this remanent field is as much as 10 to 20 oersteds in the center of the solenoid.
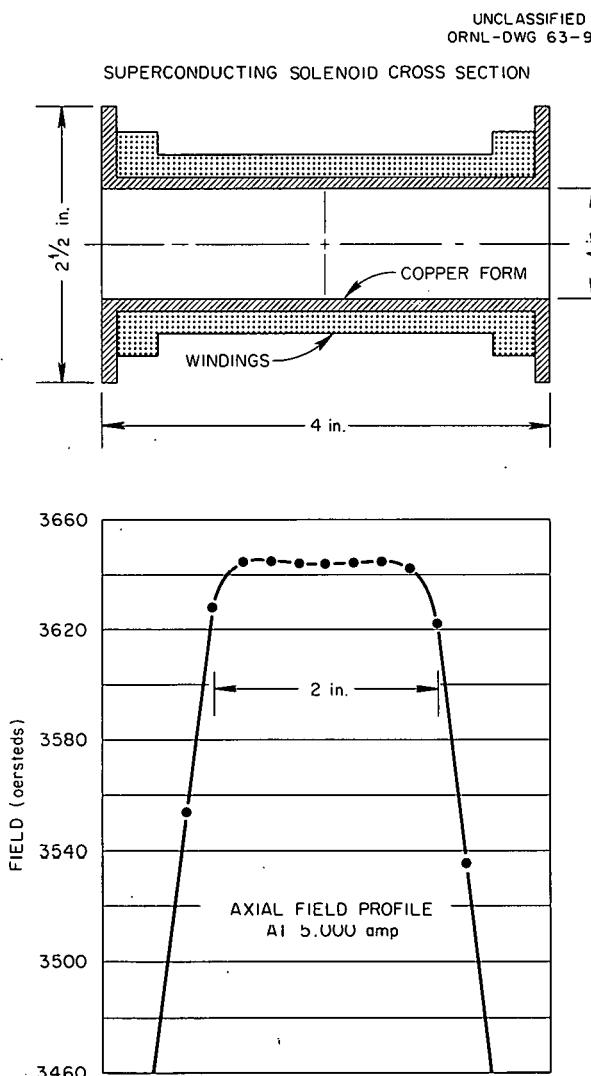
MAGNETIZATION STUDIES OF SUPERCONDUCTORS

S. T. Sekula   R. H. Kernohan
P. G. Huray[16]

The negative surface energy model of alloy (or type II) superconductors, which predicts the persistence of the superconducting state out to relatively large values of the magnetic field, has met

---

with considerable success.[17,18] On the basis of this model, one would expect the upper critical field, approximately defined as that field which destroys the superconducting state of a sample carrying a small current, to be independent to first order of the degree of cold work or heat treatment. While earlier results corroborate this viewpoint,[19] the dependence of critical current on cold work at low and intermediate values of applied field is not yet understood.

We have recently constructed a low-temperature apparatus utilizing a superconducting magnet to measure the magnetization of superconductors with the magnetic field and temperature as variables. The primary objective is to correlate critical-current measurements with the magnetic behavior in annealed type II materials in analogy to the relatively well-understood critical-current behavior of soft superconductors. The apparatus permits ballistic measurements of susceptibility and has been calibrated using samples of annealed lead and tin.

Figure 7.4 shows the magnetization curves of annealed polycrystalline lead and a cold-drawn Pb–30 wt % Tl alloy. Since the samples were in the form of bundles of fine wires, the demagnetization factor is small, so that in the case of lead, the superconducting to normal transition is quite sharp and reversible. With identical geometry, the Pb-Tl sample initially exhibits ideal flux exclusion. At larger values of field, a slow penetration of field takes place; and the last vestiges of the superconducting state disappear at a field of 3200 oersteds. The curve is not reversible and shows considerable hysteresis. Investigations are now in progress to study this effect as a function of the cold work.

Commercially available cold-drawn Nb-Zr alloys have also been examined and found to exhibit similar hysteretic effects.

CRITICAL CURRENTS IN Nb-Zr ALLOYS[20]

R. W. Boom[21]   S. T. Sekula

C. J. Bergeron[22]

Critical-current data obtained from short-wire tests in the ORNL 100-kilo-oersted magnet are given

[17]T. G. Berlincourt and R. R. Hake, *Phys. Rev. Letters* **9**, 293 (1962).

[18]J. D. Livingston, *Phys. Rev.* **129**, 1943 (1963).

[19]S. T. Sekula, R. W. Boom, and C. J. Bergeron, *Solid State Div. Ann. Progr. Rept. Aug. 31, 1962,* ORNL-3364, p 52.

[20]Abstract of paper to be submitted for publication.

[21]Now at Atomics International, Canoga Park, Calif.

[22]Consultant to Electronuclear Division from Louisiana State University, New Orleans.
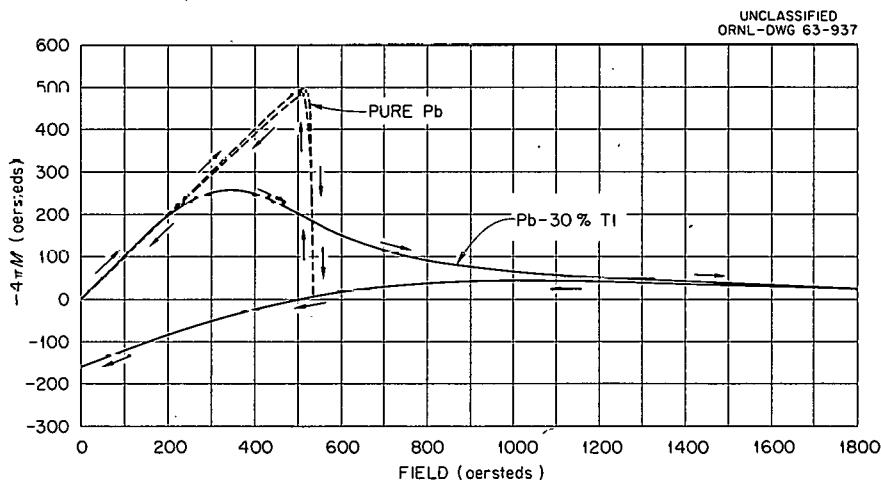
Fig. 7.4. Magnetization of Superconducting Lead and Pb–30 wt % Tl at 4.20°K.

for a series of Nb-Zr alloys, and the effect of heat treatment on the superconducting characteristics is indicated. Critical-current behavior of small test solenoids in externally applied fields is also presented. It is concluded that Nb-Zr magnets of any size, buried in 10 to 20 kilo-oersted fields, should carry current densities comparable to those observed in short-sample tests. Current degradation effects in solenoids are discussed in terms of flux-migration heating of the wire.

Part III. Metals

F. W. Young, Jr.

PAGES 47 to 48

WERE INTENTIONALLY

LEFT BLANK

8. Investigations of Metal Surfaces

F. W. Young, Jr.   Ugo Bertocci
L. D. Hulett   L. H. Jenkins
J. R. Savage

GROWTH OF COPPER CRYSTALS OF
LOW DISLOCATION DENSITY

The study of the factors controlling dislocation density in copper crystals grown from the melt has been continued. The crystals, 1 in. in diameter by 6 in., were grown in graphite crucibles by use of a Bridgman technique. For apparently identical growth conditions the orientation of the growth direction of unseeded crystals was found to be random. For unseeded crystals the dislocation density was an inverse function of the angular deviation of the growth direction from the (111) zone. Both the dislocation density and the number of small-angle (~1 min) boundaries were greater for orientations near this zone. By growing crystals in crucibles of different wall thickness, it was determined that the dislocation density for a given growth direction increased with wall thickness. Since the heat flow was probably more unidirectional in the thin-walled crucibles, this result indicated the importance of reducing thermal stresses during growth. It was also found to be necessary to heat the melt ~100°C above the melting point in order to grow low-dislocation-density crystals.

In a large number of experiments to grow seeded crystals with (111) growth direction, no low-dislocation-density crystals were obtained. Apparently, during the seeding process sufficient thermal stress was produced to greatly increase the dislocation density near the seeding interface.

The dislocation densities in the as-grown crystals were determined by etch-pit techniques. As a further check on these techniques, crystal samples have been prepared for x-ray rocking curve and transmission studies of crystal perfection.[1]

ANOMALOUS TRANSMISSION X-RAY
TOPOGRAPH OF A COPPER CRYSTAL

The copper crystal was prepared by acid sawing a 0.3-cm-thick slice with (111) faces from a 2.5-cm-diam crystal, acid polishing the sawed faces, and annealing at 1075°C for one week. The crystal was soft-soldered to a copper stem for handling and then reduced in thickness by electropolishing to its final dimensions of 2 cm in diameter by approximately 0.04 cm in thickness. In the electropolishing process the edge was thinned more than the center so that the cross section was somewhat elliptical in shape. The x-ray topograph was then obtained by Wittels and Sherrill, who utilized the Borrmann[2] diffracted beam through the crystal by use of Ag $K\alpha_1$ radiation[1] and a Lang camera (exposure time of one week, high-resolution nuclear plate). In Fig. 8.1 the x-ray image has been enlarged five times and reversed in printing for contrast purposes. (For the anomalous transmission a dislocation in the crystal serves to decrease the transmitted intensity so that the dislocations appear as light lines in a dark background on the x-ray plate.) Individual dislocations, small-angle boundaries, and slip traces can be recognized in the figure. The

---

[1]M. C. Wittels, F. A. Sherrill, and F. W. Young, Jr., "Anomalous Transmission of X Rays in Copper Crystals," this report, chap. 4.

[2]G. Borrmann, *Physik. Z.* **42**, 157 (1941).

Fig. 8.1. X-Ray Topograph of a Copper Crystal Obtained with Anomalous Transmission. 5X. Reduced 16%.

slip traces have their sources in the vicinity of that part of the crystal soldered to the stem; it has been determined that the process of soldering a low-dislocation-density copper crystal to a handle always deforms the crystal somewhat. In the black region near the stem there was very little transmission because of the high dislocation density due to this deformation. It can be seen that the small-angle boundaries served as a barrier to the gliding dislocations. The light regions around the edge indicate that the crystal was much thinner in these regions.

The fact that anomalous transmission was obtained through all the subgrains more or less in the same amount indicates that the angle between grains was ~20 sec, or less, since that was the half-width of the transmission peak. For some of the boundaries the individual dislocation can be resolved. Also, in some of the boundaries it appears that the dislocations are grouped into the boundary on one side of the crystal, while on the other side they are more widely spaced. This observation would suggest that some of the boundaries do not extend through the crystal, and such a structure can easily be understood, since the crystal as x rayed was the central part of an initially thicker section. The individual dislocations are long and do not appear to be part of a regular network. It should be remembered that only half of the dislocations are seen by this one x-ray topograph, since it is necessary that the Burgers vector have a component normal to the plane used for reflection if the dislocation is to be visible.

The (111) surfaces were etched so as to form pits at dislocation-surface intersections, and the dislocation density and arrangement were compared between the two techniques. Unfortunately, the electrothinning served to "round off" the (111) faces so that etch pits were formed on only a part of each one. However, the small-angle boundaries, the slip traces, and the average dislocation density compared very favorably between the two techniques. The subgrain near the top with the higher dislocation density had a density ~10^4/cm^2; other subgrains had appreciably lower densities.

Since the copper crystals are so soft, it has been difficult to prepare thin specimens of high perfection. It is hoped to make point-to-point comparisons of x-ray topographs with etch-pit photographs in order to make an exact correlation between these two techniques.

THE ROLE OF CRYSTAL IMPERFECTIONS IN THE CHEMICAL REACTIVITY OF COPPER SURFACES[3]

The transfer of an atom from a metal surface to its surrounding medium, be it film, solution, or vapor, probably occurs at steps, so that an understanding of the nucleation and motion of steps is central to an understanding of the mechanisms of the chemical reactions of metal surfaces. The possible role of crystal imperfections in the nucleation of steps is discussed with particular reference to dislocations, and a review is presented of previous experiments which were concerned with the role of dislocations in oxidation, thermal etching, and dissolution in solutions. The electrochemical dissolution of the (111) face of copper crystals of low dislocation density is being investigated with respect to the kinetics of etchpit formation at dislocations and step motion on the unpitted surface. The relations between step motion and the rate of growth of the pits are presented with respect to the variables: current density, orientation of the surface, dislocation density, and composition of the etching solution. The results are interpreted in terms of the kinematic theory of dissolution.

KINETICS OF LEDGE FORMATION AND MOTION

The above work is being continued with more emphasis on ledge studies. The experimental techniques and dissolution conditions are similar to those described.

Figure 8.2 illustrates the general configuration of ledges that are produced about a dislocation etch pit at the (111) pole of a copper single crystal. The angle α is an orientation parameter that is dependent on dissolution conditions. When electrolysis is carried out in solutions low in bromide concentration (0.1 to 0.25 M) and/or with high current densities (20 ma/cm^2 or higher), α approaches zero. When higher bromide concentrations and/or lower current densities are used, α increases. The angle α may be as high as 20°, but never quite reaches 30° — the point at which (111) pole symmetry would become sixfold.
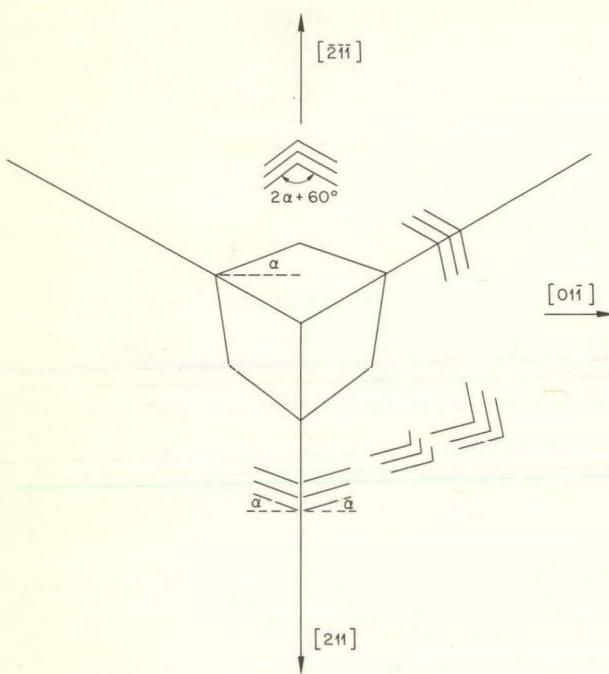
Fig. 8.2. Ledge Configuration About a Dislocation Etch Pit at the (111) Pole.

One always observes at least two types of ledges: "straight," or one-component ledges, and "pointed," or two-component ledges. The straight ledges occur on surfaces misoriented toward the [211] direction, and the pointed ledges occur on surfaces misoriented toward the [$\bar{2}\bar{1}\bar{1}$] direction. It appears that for a given dissolution condition the fronts of all ledges formed about the (111) pole tend toward the same orientation. The fronts of each of the two components of the "pointed" ledges are of about the same orientation as the fronts of the one-component ledges. As the orientation of the "straight" ledges changes, the angle between the two components of the "pointed" ledges changes accordingly. If the surface of the crystal is misoriented in the [211] direction and lies exactly on the [01$\bar{1}$] zone, and if α is appreciably greater than zero, the ledges are composed of two components.

For almost all dissolution conditions the dislocation pits have their sides broken into ledges. To a first approximation the ledges in the pits are similar to the ledges on the unpitted surface. That is, as shown in Fig. 8.2, the orientations in the (111) plane are nearly the same for ledges in both regions. This approximation must be made with reservations, however, for there are significant differences in behavior in the two types of ledges. For example, depending on the dissolution conditions and orientation of the initial surface, the pit ledges and surface ledges may or may not move with the same frontal velocities.

Ledge densities on misoriented surfaces which lie near the [01$\bar{1}$] zone in both the [211] and [$\bar{2}\bar{1}\bar{1}$] directions (see Fig. 8.1) have been measured as a function of dissolution conditions. The range of misorientation investigated was 0 to 2°. Figure 8.3 is a typical plot of ledge density as a function of misorientation in the [211] direction. For small misorientations (0 to 1° for the dissolution conditions indicated in Fig. 8.2), the ledge density was independent of dissolution time. For higher misorientations the density slowly decreased with time. For surfaces misoriented in the [$\bar{2}\bar{1}\bar{1}$] direction, the density of two-component ledges continually decreased with time for all misorientations.

In Fig. 8.3 a threshold misorientation below which the ledge density is essentially zero is indicated. This threshold misorientation varies with dissolution conditions but is always well defined. A possible explanation for its existence is: In order for ledges to form, monatomic steps must aggregate – a process which requires interaction. If initial misorientation is small enough, monatomic steps will be too widely separated to interact, and no ledges will form. For this case the limiting step spacing for the formation of ledges was of the order of 500 A.

Ledge densities as a function of orientation for different bromide concentrations have been measured. For a given orientation the ledge density goes through a minimum as bromide concentration increases. It has been observed previously that the rate of pit growth goes through a maximum as bromide increases. Further investigations may show these two effects to be related.

The effect of current density on ledge density at various misorientations is being investigated. Preliminary results indicate that ledge density is determined by the current density initially imposed on the surface. The data in Fig. 8.3 are for a 20-ma/cm^2 dissolution rate. If one etches at 10 ma/cm^2 with the same solution composition, the ledge densities at various orientations are
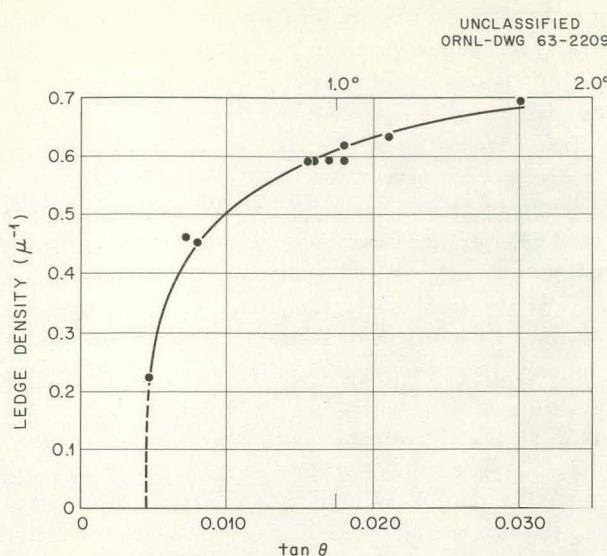
Fig. 8.3. Ledge Densities on Surfaces Misoriented in the [211] Direction Along the [00$\overline{1}$] Zone. Dissolution conditions: 6 M HCl, 0.25 M KBr; 20 ma/cm^2.

only about two-thirds as large as for 20 ma/cm^2. If one etches at 10 ma/cm^2 initially and then switches the current to 20 ma/cm^2, the ledge densities remain at the values established at 10-ma/cm^2 values for a very long time. Also, the value of α (see Fig. 8.2) of the 10-ma/cm^2 pit peripheries and ledge fronts appears to change very slowly to that normally seen at 20 ma/cm^2.

One sees a more pronounced effect of sudden changes in current density on ledge velocities and the rate of pit growth. Figure 8.4 illustrates the frontal velocities of ledges and pit peripheries before and after a current-density transition. Before the transition the velocities are about the same. There is an immediate increase in both velocities when the current density is increased, but not in the same proportion. This result and previous results indicate that at the lower current densities ledges on the pit peripheries and ledges on the surface tend to move with the same frontal velocities. Also, the values of α for the two types of ledges tend to be more nearly the same. This suggests that at lower current densities the pit ledges and surface ledges are maintained in more equal dissolution environments.

Fig. 8.4. Velocities of Ledges and Pit Edges at Different Current Densities. Direction of motion is shown schematically, and motion is measured relative to the apex of the etch pit. Dissolution conditions: 6 M HCl, 0.25 M KBr; 10 and 20 ma/cm^2.

FORMATION OF ELECTROCHEMICAL ETCH PITS ON THE (111) FACE OF COPPER[4]

In an effort to elucidate the role of defects on the anodic behavior of copper single crystals, information has been gathered about the etch pits formed at dislocations on the (111) face. The results of studies designed to determine the influence of such parameters as current density, solution composition, and orientation of the copper surface on the formation and characteristics of such pits are discussed.

SURFACES OF COPPER CRYSTALS AT CHEMICAL EQUILIBRIUM IN SOLUTIONS CONTAINING COPPER

Solutions of 0.2 M CuSO$_4$

When exposed to oxygen-free solutions of CuSO$_4$ (pH adjusted to 1 with H$_2$SO$_4$) which have been equilibrated previously with copper metal, a

spherical single crystal of copper develops facets around crystallographic poles as is illustrated in Fig. 8.5. Since there is no net transfer of material to or from the crystal, the faceting represents the rearrangement of the surface which results from exchange between atoms at the metal surface and cupric ions in solution. The lack of facet development over large areas of the sphere suggests that certain orientations are more stable than others and/or the rate of the exchange reaction varies with orientation.

To test these ideas, flat crystals $1 \times 3 \times 0.2$ cm oriented either (111), (110), (100), or (321) on the large 3×1 cm area were exposed to $CuSO_4$ solutions at constant temperature for periods up to six months. While facets did develop on (321) surfaces after about two weeks, none were observed on the other orientations even after six months in solution. Since all the crystals studied neither gained nor lost weight during the course of various equilibrations, faceting had to result from the exchange reaction. However, there are some indications that the rate of development of facets on any one orientation may be affected by the method of surface preparation. Therefore, final conclusions cannot be reached until more data are available.

Differences in the rest potentials of these crystals were also measured. The results, which are shown in Fig. 8.6, are not the absolute values of the differences between the orientations listed, since the sides of the samples constituted 10 to 20% of the total surface exposed to solution. The change of potential differences with time also indicated a contribution from edges, since no physical changes were detected on the large areas of desired orientation. It is reasonable to expect that changes in potentials as great as those observed would require a marked degree of surface reorientation. At present, measurements are being conducted on surfaces containing only the one orientation of interest.
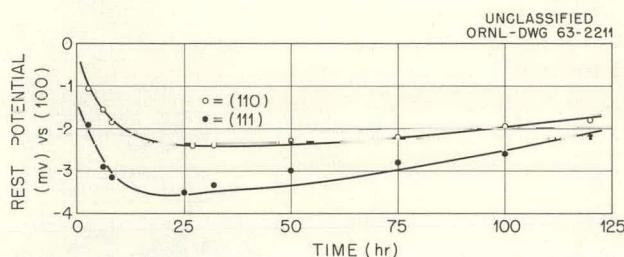
Fig. 8.6. Differences in Rest Potential of Copper Surface of Different Orientations in 0.2 M $CuSO_4$.

Fig. 8.5. Single-Crystal Sphere of Copper After Four Weeks in 0.2 M $CuSO_4$. Light areas in the photograph represent faceted crystal areas. Note the large unfaceted area around (100) poles.

Solutions of 0.03 M CuCl in 2.7 M HCl

Equilibration of single-crystal copper spheres in HCl-CuCl solutions produced only very slight surface changes after one week. Facets were developed on a triangular-shaped area surrounding the (111) pole, while a large area around the (100) pole and a smaller area surrounding the (110) remained smooth. It appears that, as in $CuSO_4$ solutions, some orientations are more stable than others and/or the exchange reaction rate varies with orientation.

Preliminary measurements of differences in rest potentials of variously oriented crystals exposed to this solution indicate the (100) is more positive than both the (111) and (110), and a polycrystal is even more negative than the (110). The differences in potential again were time dependent, but were approximately 15 to 25 mv between (100) and (110) or (111) and 10 to 15 mv between the (110) and polycrystal. Emf differences were measured vs a standard calomel electrode (S.C.E.), as well as with respect to each other.

ANODIC DISSOLUTION OF COPPER SINGLE CRYSTALS IN SOLUTIONS CONTAINING COPPER

Acidic Halide Solutions

Overvoltage measurements have been made on (111) surfaces undergoing anodic dissolution in 6 M KCl solutions containing 0.1 M HCl and either 0.1 or 0.01 M CuCl with and without addition of KBr or KI. Typical values, which are reasonably reproducible, are shown in Fig. 8.7. The data

Fig. 8.7. Effect of Addition of KBr and KI on the Open-Circuit Potential and Overvoltages on (111) Copper Surfaces in 6 M KCl Solutions Containing 0.1 M HCl.

are not yet reliable enough to determine conclusively the effect of addition of 0.4 M KBr on measured overpotentials. The open-circuit potentials measured vs the S.C.E. show that the activity of the copper ion is less in the presence of bromide, and the higher values of overvoltages measured can be attributed to decreased copper ion activity rather than to any specific effect of the bromide ion on the (111) surface.

Conversely, addition of as little as 10^{-3} M KI has a remarkable effect on the overvoltages (see Fig. 8.7), even though such small iodide concentrations cannot appreciably affect the copper ion activity. It seems only reasonable that some specific interaction occurs between the (111) surface and iodide ions.

The addition of either bromide or iodide to these solutions in the amounts indicated causes etch pits to be formed at points where dislocations intersect the (111) surface. In view of the different effects each ion produces on measured overpotentials, it seems that enhanced reactivity results from different causes in the two cases.

Similar measurements of overpotentials have been made on polycrystals, and preliminary observations have been made on (100) and (110) surfaces. Any differences from the (111) — other than the ready development of pits at dislocations — seem to be of degree only, rather than kind. It is hoped that further measurements will help explain why well-defined pits do not develop at dislocations on the (100) and (110).

Solutions of 0.2 M CuSO$_4$

To further explore the possibility that the rate of exchange between atoms of the metal and ions in solution varies with crystal orientation, the current vs overpotential characteristics were determined for the three major low-index orientations. Experimental conditions were such that only the orientation of interest was exposed to the solution. From the data shown in Fig. 8.8 and from the relation

$$i_0 = \frac{RT}{nF}\left(\frac{\partial i_a}{\partial \eta}\right)\eta \longrightarrow 0 ,$$

56

where

i_0 = exchange current density,

i_a = anodic current density,

η = anodic overpotential,

the exchange current densities for the reaction

$$Cu^{2+} \text{ (aqueous)} \rightleftharpoons Cu^0 \text{ (metal)} + 2e$$
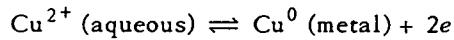
were calculated to be

$$i_{0_{(111)}} \simeq i_{0_{(110)}} \simeq 140 \, \mu a/cm^2 \,,$$

$$i_{0_{(100)}} \simeq 60 \, \mu a/cm^2 \,.$$

If the rather questionable assumption that the ratio of apparent to true surface area is constant for all orientations is made, then the previous values reflect a real variation in exchange current density with orientation. However, more data are needed before these results can be considered conclusive.

UNCLASSIFIED
ORNL-DWG 63-2213
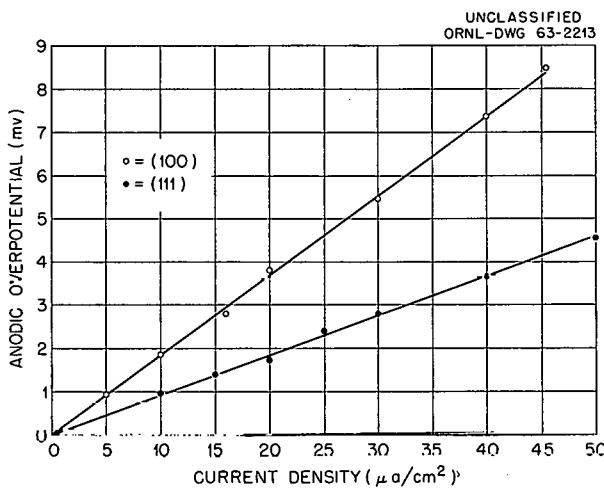
Fig. 8.8. Relation of Overpotentials and Current Density of Different Orientations in 0.2 M $CuSO_4$.

9. Low-Temperature Irradiation Studies

R. R. Coltman   D. L. McDonald[1]
C. E. Klabunde   J. K. Redman
G. F. Fielder

NEW LOW-TEMPERATURE IRRADIATION FACILITY

Construction of the new low-temperature irradiation facility located at the Bulk Shielding Reactor (BSR) is near completion. The purpose of the new facility is to provide irradiation conditions which cannot be obtained at the old facility located in the ORNL Graphite Reactor. The design of the new facility is directed toward:

1. obtaining a thermal-neutron flux of greater purity and absolute value than is possible in the Graphite Reactor,

2. obtaining a high-purity fission-neutron flux,

3. the alternate bombardment of the same specimens by thermal and fission neutrons for comparison studies,

4. the capability of greater refrigeration capacity at liquid-helium temperatures for the performance of more complex experiments.

Upon completion, this facility will be used for basic research studies of irradiation damage in pure metals.

Cryostat Housing

Figure 9.1 shows a schematic diagram of the overall arrangement of the facility. An aluminum tank $28 \times 28 \times 12$ in. filled with D_2O (286 lb) rests on the grid plate of the reactor and against the

reactor core. An aluminum cryostat housing $9\frac{1}{2} \times 12 \times 24$ in. is located with its 12×24 in. face against the D_2O tank. The sample tube of the cryostat is located at the center of the housing. A 6-in.-diam aluminum tube provides access from just above the water level to the housing box. The tank of D_2O serves as a nonabsorbing neutron thermalizer, which delivers a substantial thermal-neutron flux into the cryostat housing. The purpose of the housing, which is filled with helium at 1 atm, is to displace the light water from around the cryostat. This is done for two reasons. First, since H_2O is such a strong absorber of thermal neutrons, the void space imposed by the housing box greatly increases the solid angle over which a specimen (at the center of the box) can receive the thermal-neutron flux. Second, when a cylindrical converter is used around the cryostat to produce a fission-neutron flux, the void space serves to reduce the return of moderated flux (between fission and thermal energy) to the sample chamber.

D. K. Holmes of the Solid State Division has calculated that for the geometry used in this facility the moderated fraction of the total flux inside the proposed converter (lined inside with cadmium to eliminate thermal neutrons) will be about 0.2. Since this calculation of the moderated feedback flux includes all neutrons from thermal to fission energy, and since only neutrons above about 1 kev can cause damage, it is roughly estimated (assuming a $1/E$ spectrum for the feedback flux) that the purity of the damage obtained inside the converter will be better than 90% fission-neutron damage.
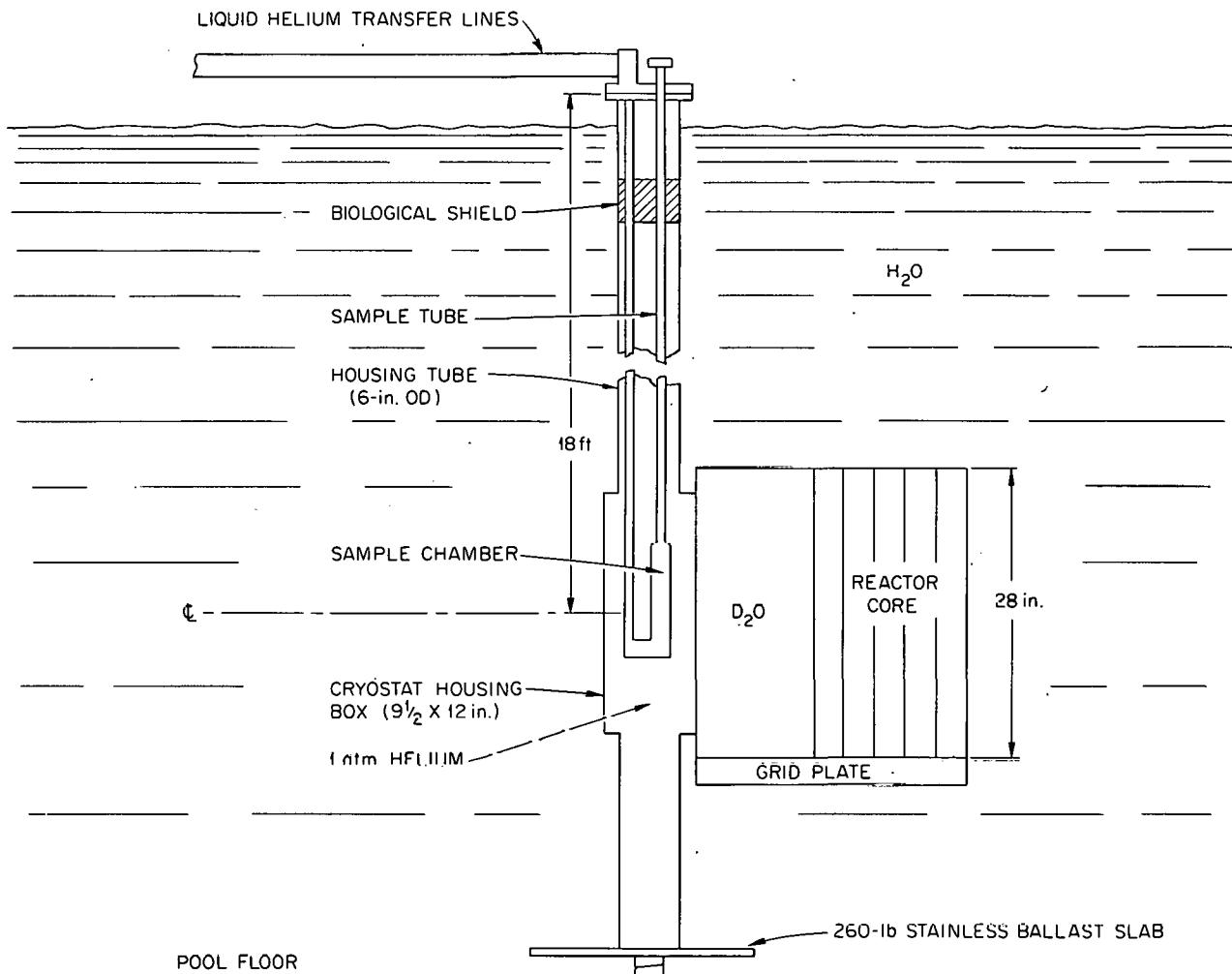
Fig. 9.1. Schematic Diagram of BSR Low-Temperature Irradiation Facility.

Proposed Converter

It is proposed that a U^{235}-in-aluminum cylindrical converter tube $2\frac{1}{2}$ in. in diameter and 12 in. long and lined with cadmium will be attached to a drawstring so that it may be raised or lowered around the sample chamber as desired. This permits alternate bombardment by thermal and fission neutrons without sample change or interruption of temperature conditions. Cooling of the converter is accomplished only by natural convection of the helium gas in the housing. To improve the convective cooling, longitudinal aluminum fins are attached to the converter, and a heavy-walled aluminum extension tube (also finned) 12 in. long is welded to the converter to further increase the cooling surface area. A mockup of this assembly with electrical power to simulate fission heating has been made. By use of eight thermocouples at various positions, the mockup was tested in the cryostat housing which was immersed in the pool water. A dummy brass tube located inside the converter mockup was used to simulate the cryostat. The highest temperatures were found at the center of the converter and were 171 and 278°C for 500- and 1000-w power dissipation respectively. Corresponding temperatures in an atmosphere of air were each about 40°C higher. It is believed that a

500-w converter of this design is a very safe device, since no external cooling system is required. It can be shown that the fission-neutron flux inside a 500-w converter of this size is 6×10^{10} neutrons cm^{-2} sec^{-1}, which produces sufficient damage for detailed study in most metals in a reasonable time (approximately 20 to 40 hr in this facility).

Flux Measurements

The thermal-neutron flux was measured under various conditions inside the cryostat housing by use of a boron thermopile. This same thermopile has been used to measure the thermal flux in the Graphite Reactor low-temperature irradiation facility, where independent measurements by experimenters with other methods gave a value of 6×10^{11} neutrons cm^{-2} sec^{-1}. Flux measurements were carried out at a reactor power of 0.4 Mw. However, full operating power of the BSR is 1.0 Mw, and all measurements reported here refer to the full power 1.0-Mw level. The measured thermal-neutron flux is 2.5×10^{12} neutrons cm^{-2} sec^{-1} at the center of the housing. Upon rotating the thermopile ($\frac{1}{2}$ in. OD and 6 in. long) on a $2\frac{1}{2}$-in.-diam circle, a total variation of 5% is observed, indicating very little horizonal flux gradient. (The cryostat sample chamber to be used in this facility is 1 in. in diameter.) A vertical traverse of the housing box showed a drop in flux of only 2% at 4 in. and 10% at 8 in. from the center line. The length of the cryostat sample chamber is 8 in. and will be centered in the vertical direction.

Following these measurements a black cadmium cylinder $2\frac{1}{2}$ in. in diameter and 12 in. long (used to simulate the presence of the cadmium-lined converter tube) is lowered down adjacent to the thermopile. The cadmium cylinder is formed with a longitudinal, semicircular groove into which the thermopile can slide, thus covering about half the solid angle over which it can receive thermal neutrons. With the exposed half of the thermopile facing the D_2O tank, a 44% drop in its output signal is observed. This indicates that the isotropy of the flux inside the housing is quite good and that the surrounding light water serves as a good reflector for the thermal neutrons. The cadmium cylinder and the thermopile are then rotated on the axis of the cylinder and readings taken at $45°$ intervals. Upon rotation of $180°$ away from the

D_2O tank the reading dropped to 50% of the value obtained when facing the tank. It is believed that this drop is due to the presence of the large absorber in the housing void space which captures neutrons that would otherwise be reflected back by the light water at the three outward walls. In this connection it is important to note that when the cadmium cylinder is lowered into the housing box no effect on the reactor operation is observed. This seems to indicate that the total number of neutrons entering the housing box through the face adjacent to the D_2O tank is independent of the conditions inside the box. This absence of a feedback effect has the very practical advantage that the experimenter may change his irradiation conditions without affecting the operation of the reactor. The thermopile data taken during rotation of the cylinder will be used to determine design details of the actual converter such as U^{235} enrichment. It is of some interest to note that when a second, slightly smaller tank of D_2O ($15 \times 15 \times 12$ in. thick) is hung behind the housing box, the thermal flux inside drops about $3\frac{1}{2}$%. This result suggests that additional D_2O surrounding the housing does not improve the thermal flux.

Gamma-Ray Heating

A small copper specimen suspended by a single copper-constantan thermocouple is mounted in an evacuated tube. With the reactor on, the tube is pushed to the center of the housing and temperature vs time data are recorded. By use of this data and the known specific heat of copper, the gamma-ray heating effect in the isolated copper specimen can be determined. The measured value is 45 mw/g. It is believed that the majority of these gamma rays originate from light-water captures near the surface of the housing. Visual evidence for this can be seen by the bright band of Cerenkov radiation which appears at the boundaries of the housing. It is presently planned to hang $1\frac{1}{2}$-in.-thick bismuth sheets on the four sides of the box. It is hoped that this shielding will reduce the gamma heating by about a factor of 4 but will not appreciably affect the thermal-neutron flux. The effect of gamma heating upon the cryostat is discussed below.

Refrigeration System

A schematic diagram of the closed-circuit helium liquefier used for this facility is shown in Fig. 9.2. Except for the cryostat, construction and testing of the system are complete. To briefly describe the operating principle of the system, it is convenient to divide the circuit into two portions, the engine circuit and the liquefier circuit. In the engine circuit, high-pressure helium gas enters the main heat exchanger at room temperature, where it is cooled by the returning low-pressure flows. It is then adiabatically expanded to a low pressure in the expansion engines, where the final cooling in this circuit takes place. It then enters the heat-sink exchanger, where it is warmed by the high-pressure liquefier flow enroute to the Joule-Thomson (J.T.) valve. This constitutes the heat load on the engine circuit. The returning flow is

further warmed to room temperature in the main heat exchanger enroute to the first-stage compressor. In the liquefier circuit a portion of the total high-pressure flow bypasses the engines and is further cooled to the engine exhaust temperature in the heat-sink exchanger. This flow is still further cooled by returning liquefier flow in the J.T. heat exchanger. It is then isenthalpically expanded at the J.T. valve, and the gas-liquid mixture proceeds through the cryostat, where most of the liquid is evaporated, but little, if any, temperature rise occurs. The returning flow is progressively warmed to room temperature in the three heat exchanger sections enroute to the liquefier compressor, where it is compressed and brought into the suction of the second-stage main compressor. It may be noted in this system that since the liquefier flow is returned to the discharge rather than the suction of the first-stage compressor, the
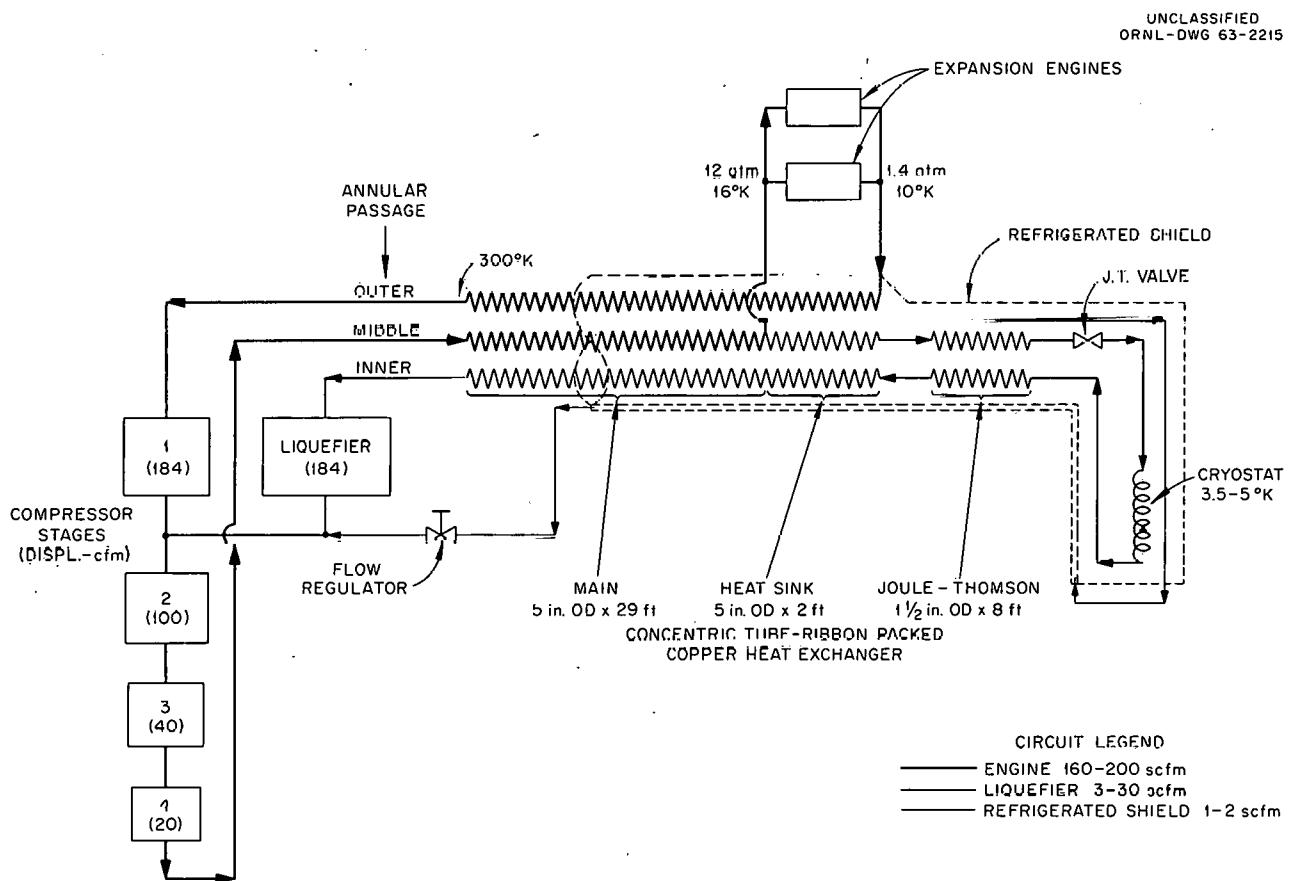
Fig. 9.2. Schematic Circuit Diagram of the Closed-Circuit Helium Liquefier. The values of pressure, temperature, and flow shown here are typical but may be changed to suit the needs of a particular experiment.

mass flow and to a great extent the refrigeration capacity of the engine circuit is fixed by the displacement of the first-stage compressor (for a fixed value of the first-stage suction pressure). It follows then that the total mass flow through the system is variable, depending upon the demand of the liquefier circuit. It is believed that this circuitry leads to a somewhat more stable behavior of the liquefier circuitry and simplifies the adjustment of the system to varied heat loads.

The complete system was tested with an electrical heat load to simulate the effect of the cryostat. With a 20-w heat load on the liquefier circuit a stable temperature of $3.6°K$ is maintained using a flow of 20 scfm. (Engine-circuit flow under these conditions is about 180 scfm.) From the general behavior of the entire system under these conditions it is clear that the liquefier flow can be increased from 50 to 100%. Such a high-flow test could not be made because of the limited range of the flowmeter, which has since been increased. Results of these tests indicate a heat capacity of about a factor of 10 greater than that of the Graphite Reactor facility. Minimum-temperature—low-flow tests are of little significance under this simulated condition, since pressure drop through the cryostat is difficult to estimate and strongly affects the results. It is believed, however, that bombardments at $3.5°K$ are possible.

Refrigerated Shield

In a low-temperature irradiation system such as described here, it can be shown that if the radiant heat load on the cryostat is about equal to or greater than the gamma-ray heat load, the use of a refrigerated shield surrounding all liquefier circuitry offers great economy. This condition prevails for the facility described here. A small flow (1 to 2 scfm) of high-pressure cold ($\sim 16°K$) helium gas taken from the engine inlet line is routed through a small tube down to the sample chamber of the cryostat, where the line is attached to a heat trap and refrigerated shield for the sample chamber (see Fig. 9.3). It is then returned along a shield which surrounds the liquid-helium transfer lines and the shield supply line, absorbing radiant heat en route. The flow rate is adjusted according to its temperature after having covered all liquefier circuitry. In test runs with an electrical heat load of 25 w to simulate the radiant heat load of the

cryostat, a flow of 1.2 scfm was required to maintain a shield return temperature of $125°K$. It is estimated that the shield reduces the liquifier radiant heat load by a factor of about 100. When operating with the cryostat it is possible to adjust the shield return temperature for optimum performance of the liquefier. The remaining heat capacity of the shield gas is used for additional shielding which surrounds the colder parts of the heat exchanger and which brings the flow up to room temperature. It then returns to the suction of the second-stage compressor via a flow regulator. High-pressure gas is used for the refrigerated shield circuit, since it can be transmitted through small-diameter low-mass tubes wherein the associated pressure drop has little effect on the remainder of the system.

Insulation

All cold portions of the system except the expansion engines are vacuum jacketed. Under operating conditions the vacuum is better than 10^{-6} torr. The engines are insulated by Santocel in a vacuum of about 20 μ. In addition to the vacuum, "super insulation" in the form of alternate layers of aluminum foil and 15-mil-thick fiber glass sheets have been wrapped on all sections. Seven foil and six glass layers are used on the heat exchangers and most transfer lines. Five foil and four glass layers are used on the refrigerated shield.

Precooling Circuit

The main heat exchanger in this system weighs about 600 lb, and considerable refrigerator running time is required to cool the system to terminal temperature in preparation for an experiment. To reduce running time and hence maintenance, a liquid-nitrogen precooling system has been installed. By use of a small compressor as a pump, liquid nitrogen is drawn through a $\frac{3}{4}$-in. tube located in the center of the main heat exchanger. After precooling overnight (~ 16 hr), one-half of the heat exchanger is at about $80°K$, and a good gradient is established in the remainder. Four hours after startup of the engine circuit the heat-sink exchanger reaches about $13°K$, and the liquefier is ready for operation.

62

SAMPLE TUBE

STAINLESS STEEL
HEAT TRAP, 8 in. LONG

THIN COPPER
REFRIGERATED HEAT
TRAP, 12 in. LONG

10°K

STAINLESS STEEL
HEAT TRAP, 2 in. LONG

THIN-COPPER
REFRIGERATED
SHIELD

LIQUID HELIUM
3.5 TO 5° K

THIN-WALLED COPPER
SAMPLE CHAMBER,
1-in. ID x 8½ in. LONG

$\frac{1}{16}$-in.-OD COPPER
TUBING

TOTAL
SYSTEM

18 ft

REFRIGERATED SHIELD

VACUUM JACKET

REFRIGERATED SHIELD SUPPLY

LIQUEFIER SUPPLY

LIQUEFIER RETURN

0   1   2
INCHES

Fig. 9.3. Liquid-Helium Irradiation Cryostat.

Irradiation Cryostat

Figure 9.3 shows a sketch of the cryostat, which is nearly completed. The U-shaped arrangement is used to reduce the diameter of the vacuum jacket around the sample chamber as much as possible, so that the smallest possible converter can be employed for fission-neutron bombardment. Thin-walled stainless steel tubes are used for all the transfer lines and most of the vacuum jacketing. The incoming refrigerated shield gas ($\sim 16°K$) is first applied to a 12-in.-long copper heat trap, which is separated from the sample chamber by 2 in. of thin-walled stainless tubing. After leaving the heat trap it cools a copper shield around the cryostat proper. The upper end of the heat trap connects to a thin-walled stainless tube, which travels 8 in. before breaking out of the vacuum jacketing and then continues to the top of the facility serving as a sample tube. In operation, helium is condensed in the thin-walled copper sample chamber, so that an experiment is immersed in nonboiling liquid helium. The mass of that portion of the cryostat located in the gamma-ray field is about 250 g. If the present gamma heating value can be reduced to 10^{-2} w/g with the proposed bismuth shielding, then the gamma heat load on the liquefier will be about 2.5 w. It is roughly estimated that the radiant heat load on the liquefier is less than 0.5 w. The mass of that portion of the refrigerated shield circuit located in the gamma-ray field is also about 250 g. The associated gamma-ray heat load, however, is small compared with the radiant heat load on the total shield circuit.

The authors wish to acknowledge the very helpful assistance given them by J. T. Howe and W. E. Busby of the Solid State Division throughout the design and development of this facility.

LOW-TEMPERATURE IRRADIATION OF BERYLLIUM OXIDE[2]

Beryllium oxide is presently of interest in reactor technology, and a considerable amount of work on the property changes of BeO caused by neutron irradiation has been carried out.[3] In order to fully understand the damage mechanism and properly interpret pile-temperature experiments, it was considered necessary to know whether the point defects produced by fast-neutron bombardment were mobile at room temperature. Since low-temperature thermal conductivity is perhaps the physical property most sensitive to defect structures in the BeO lattice, a specimen of the oxide was irradiated below 100°K, and thermal conductivity measurements were made in-pile during the irradiation and during a subsequent isochronal annealing study between 100°K and room temperature.

The cylindrical sample,[4] 0.30 in. in diameter and 1.5 in. long, was produced from Brush UOX powder by cold pressing and sintering. The resulting density was 2.96 g/cm^3, with a grain size of about 25 μ. The irradiation was performed in the ORNL Graphite Reactor nitrogen cryostat,[5] in a fast-neutron flux of 1×10^{11} neutrons cm^{-2} sec^{-1} ($E > 0.6$ Mev). The techniques employed for measurement and temperature control were similar to those of Berman,[6] except that copper-constantan thermocouples were used for measuring both absolute and differential temperatures. The cryostat operated at about 85°K with the reactor running, resulting in a sample bombardment temperature of around 91°K. For approximately 20 min during the latter part of the three-week irradiation, the sample temperature rose to 105°K.

The increase in thermal resistivity with fast-neutron dose is shown in Fig. 9.4. The damage rate curve is essentially linear up to the maximum dose of 1.8×10^{17} nvt, indicating that there are no saturation effects to this dose. The depression of the final points on the curve is probably caused by annealing during the temperature excursion described above. Following the irradiation a series of isochronal anneals up to 310°K in 20°K steps was carried out, wherein the sample was heated rapidly to the desired temperature, held there for 15 min, and cooled to the reference temperature of 93°K, at which all measurements were made.

---

[2]D. L. McDonald, *Appl. Phys. Letters* **2**, 175 (1963).

[3]B. S. Hickman, Australian Atomic Energy Commission Report AAEC/E99 (1962).

[4]Kindly supplied by Dr. A. W. Pryor of the AAEC Research Establishment.

[5]J. T. Howe, W. E. Busby, and R. R. Coltman, *Solid State Div. Ann. Progr. Rept. Aug. 31, 1959*, ORNL-2829, p 187.

[6]R. Berman, *Proc. Roy. Soc.* **A208**, 90 (1951).

The result of this annealing is depicted in Fig. 9.5. It can be seen that the damage starts to recover between 100 and 110°K and continues to anneal at a more or less constant rate up to the highest temperature. There is a hint of a recovery peak in the annealing between 160 and 190°K, but it is believed that the annealing schedule followed here is not sufficiently sensitive for positive identification. After the final anneal at 310°K, approximately 25% of the radiation-induced thermal resistance had recovered. The remaining damage could be expected to recover in the range from 400 to 1300°C, as observed in similar samples irradiated at pile temperature.[3]

X-ray diffraction and long-wavelength neutron scattering studies[3] indicate that the defects observed after a pile-temperature irradiation are present in the form of planar clusters of 15 or more defects located on basal planes, and a similar number of point defects distributed randomly throughout the lattice. It may be that the recovery observed following the present low-temperature bombardment is the result of interstitial-vacancy recombination, and the precipitation of single defects into clusters. It is not clear from the present experiment that irradiation at 90°K is sufficiently low in temperature to ensure that all the defects produced during the irradiation are immobile, but the significant amount of annealing observed following this bombardment does show that future work on BeO, and probably on other similar materials, should take into account this defect mobility far below room temperature.
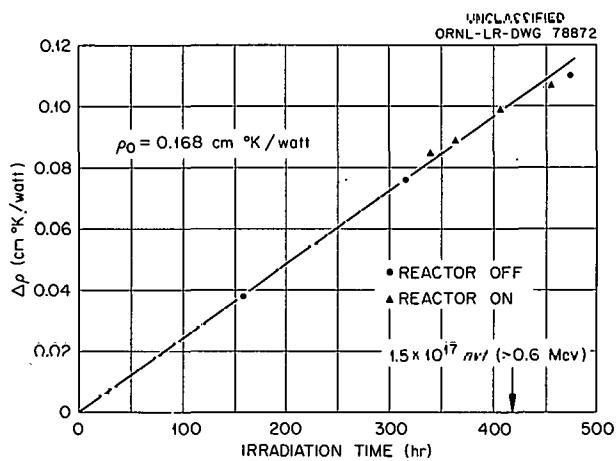
Fig. 9.4. Increase in Thermal Resistivity, $\Delta\rho$, vs Irradiation Time.
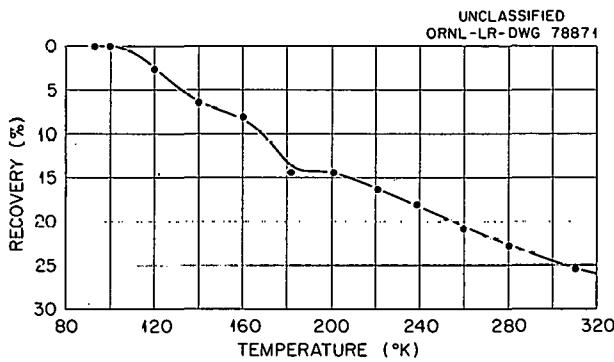
Fig. 9.5. Isochronal Annealing of Beryllium Oxide Irradiated at 91°K.

10. Elasticity and Anelasticity Studies

DOSE DEPENDENCE OF THE DISLOCATION BREAKAWAY STRESS IN NEUTRON-IRRADIATED COPPER AS MEASURED BY AMPLITUDE-DEPENDENT INTERNAL FRICTION

D. O. Thompson   V. K. Paré

A series of experiments on the amplitude dependence of internal friction in irradiated copper has been carried out in order to obtain additional information relating to the phenomenon of hardening by fast-neutron irradiation. This hardening has previously been studied quantitatively by measuring, as a function of dose, the upper or lower yield point of single crystals.[1-5] The hardening presumably occurs because radiation defects act as obstacles to dislocation motion, but there is as yet no general agreement as to the nature of the defects involved or as to whether the dominant hardening occurs by restriction of dislocation sources or by introduction of obstacles to motion of dislocations through the lattice. An additional complication is that the yield stress is observed to vary as the cube root of the dose, whereas the existing theories predict a square-root dependence.[6]

In pure copper the internal friction due to dislocation motion increases rapidly with strain amplitude, and it is generally believed that this increase results from the breakaway of dislocations from fixed pinning points. It is therefore likely that in irradiated copper the amplitude dependence of internal friction will be closely related to whatever source hardening has occurred by creation of radiation defect pinning points. Thus a close experimental relationship between amplitude-dependent internal friction and yield-point measurements would be an indication that source hardening is the dominant effect in the latter. In the present work, the amplitude dependence of internal friction is used to obtain a measure of the dislocation breakaway stress, and the dependence of this stress on radiation dose is compared with the dose dependence of the yield point. As will be seen, a remarkably close correspondence is obtained.

All internal friction and modulus measurements herein reported were performed upon a single crystal of high-purity ASR copper grown by the Bridgman technique. They were made in situ at 375°K in a shutter-equipped beam hole of the ORR in an apparatus described elsewhere.[7] A consistent set of procedures was used throughout the present experiment. Following a given neutron dose, the neutron shutter was closed, and the crystal was allowed to remain at temperature for approximately 24 hr before any large amplitude measurements were made. Previous experience has taught that this is about twice the minimum time required for the establishment of equilibrium between neutron-produced defects and the existent dislocation structure at this temperature.[8] After the measurements were made the shutter was opened and the desired additional neutron dose administered. The temperature of the sample never varied more than ±1°C during the whole set of data, nor was it handled in any way. The strain amplitude of the sample was determined from measurements of the parameters of the capacitance/frequency modulation detection system.

[1]T. H. Blewitt et al., J. Nucl. Mater. 2, 277 (1960).

[2]F. W. Young, Jr., J. Appl. Phys. 33, 3553 (1962).

[3]J. Diehl, p 129 in Proceedings of the Symposium on Radiation Damage in Solids and Reactor Materials, IAEA, Venice, 1962.

[4]J. Fischer, Z. Naturforsch. 17a, 603 (1962).

[5]T. J. Kopenaal, Bull. Am. Phys. Soc. 8, 197 (1963).

[6]A. Seeger, Proc. Intern. Conf. Peaceful Uses At. Energy, Geneva, 1958 6, 250.

[7]D. O. Thompson and F. M. Glass, Rev. Sci. Instr. 29, 1034 (1958).

[8]V. K. Paré and D. O. Thompson, Acta Met. 10, 382 (1962).

The basic data of the experiment consisted of curves of logarithmic decrement (a measure of internal friction) vs strain amplitude (taken at the center of the sample, where the strain is highest) for various values of the total fast-neutron dose, expressed in terms of neutrons per square centimeter above the Np^{237} fission threshold, about 0.6 Mev. These results are shown in Fig. 10.1. The dose levels for the various runs are given in Table 10.1.

UNCLASSIFIED
ORNL-LR-DWG 78843
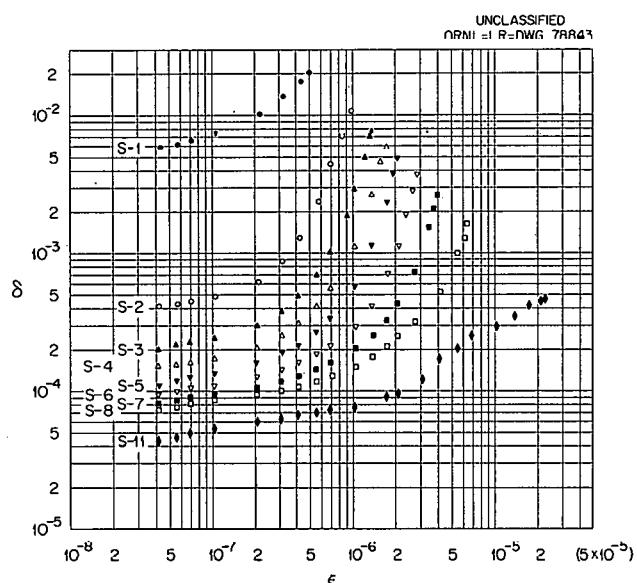
Fig. 10.1. Strain Amplitude Dependence of the Internal Friction for Several Neutron Doses.

Table 10.1. Total Integrated Dose for Each Run (Above 0.6 Mev)

Run	Dose (neutrons/cm^2)
S-1	Preirradiation
S-2	1.5×10^{11}
S-3	3.1×10^{11}
S-4	6.1×10^{11}
S-5	9.2×10^{11}
S-6	1.8×10^{12}
S-7	3.7×10^{12}
S-8	9.2×10^{12}
S-9	2.6×10^{13}
S-10	7.0×10^{13}
S-11	2.0×10^{14}

It has been hoped that it would be possible to analyze the data of Fig. 10.1 in terms of the Granato-Lücke theory[9] of amplitude-dependent internal friction, but attempts to do so were unsuccessful. The formulas of the theory did not fit the data, and for the poor fits which were obtained the dislocation parameters in the theory did not vary in a reasonable way with radiation dose. It was therefore necessary to resort to another method of analysis.

The scheme used is suggested by inspection of Fig. 10.1; it proves to be possible to superimpose the first eight curves on one another very closely by simultaneous translations along the (logarithmic) strain and internal friction axes. The resulting conversion factors on the strain axis are taken to represent the dose dependence of the dislocation breakaway stress, while those on the decrement axis give the dose dependence of the low-amplitude internal friction, which is assumed to be described by the Granato-Lücke theory of amplitude-independent internal friction due to viscous damping of dislocations.[9]

There is of course no unambiguous choice for the absolute level of the breakaway stress. In general, it would be expected that the highest attainable values in internal friction experiments would have the closest correspondence with observed yield points. The procedure which was adopted was that the highest strain attained (at maximum apparatus driving power) in run S-3 was converted to resolved shear stress and the resulting value taken as the breakaway stress for that dose; the strain-axis conversion factors mentioned above were then applied to obtain breakaway stresses for the other dose levels.

Two further pieces of information can be introduced into the analysis. The first is a temperature correction of the breakaway stress from 375°K to the temperature, 300°K, at which most yield-point measurements have been made. This correction was made using Blewitt's data and amounts to

[9]A. Granato and K. Lücke, *J. Appl. Phys.* **27**, 583 (1956).

a 12% increase. The second type of information is the dose dependence of the low-amplitude internal friction; this dependence has been found to be described by the Granato-Lücke amplitude-independent theory when one allows for diffusion of radiation defects to the dislocations and their subsequent clustering. The theory has therefore been used to derive the dose dependence of the average free dislocation length between pinning points in the present experiment. It was found that although the length decreases with increasing dose, it has at the highest dose $(7 \times 10^{13}$ neutrons/cm$^2)$ very nearly saturated at 31% of the preirradiation length. Presumably the saturation occurs when point defects, arriving at the dislocations by diffusion, cease to nucleate new pinning points and are all absorbed by existing pinning points, which then continue to grow in size and pinning strength.

Measurements of the dose dependence of the yield point have all been made at doses higher than the above value. Thus the above observations lead to a novel hypothesis concerning the hardening: if it is in fact source hardening, its dose dependence reflects not the increase in number of hardening points but the increase in their size and, therefore, in the strength of the interaction between them and the dislocations.

To be consistent with this idea, a further adjustment in the breakaway stress data was made: the value at each dose level was multiplied by the ratio of the loop length at that dose to the saturation loop length. The resulting corrected stresses should then be a measure of the pinning-point—dislocation interaction. The effect of this correction is shown in Fig. 10.2, where breakaway stresses, before and after correction, are plotted as a function of dose on logarithmic scales. It can be seen that the corrected stresses follow the cube-root law associated with the dose dependence of the yield point.

Figure 10.3 presents a summary of the experimental results of several investigations of the radiation hardening of copper. The filled points (●) in the figure are the present results (adjusted to 300°K) measured by internal friction techniques in the ORR; the filled triangular points (▲) are those of Young[2] measured in bending utilizing an etch-pit technique after bombardment in the Oak Ridge Research and Graphite Reactors; the unfilled circle points (O) are those of Diehl[3] measured by
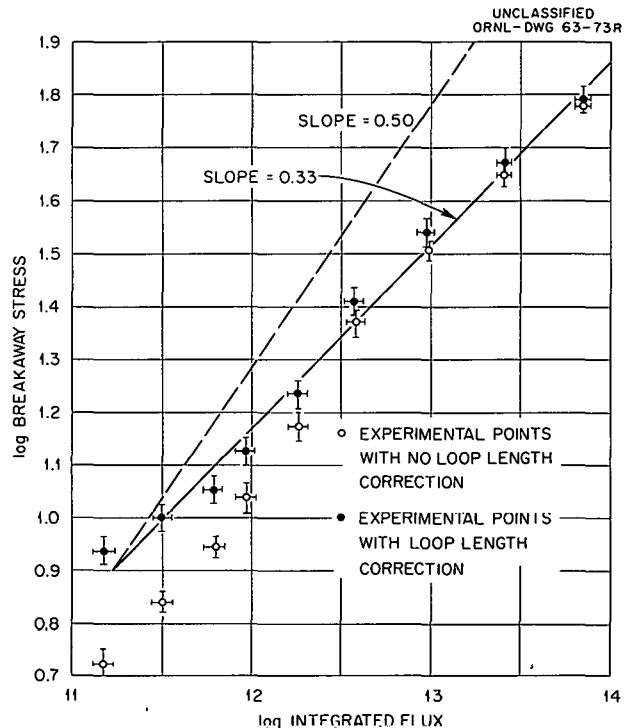
Fig. 10.2. Dose Dependence of the Dislocation Breakaway Stress in Neutron-Irradiated Copper.

tensile testing with an Instron machine after bombardment in the Munich FRM reactor; and the unfilled triangles (△) are the data of Fischer[4] using the same technique and bombardment facility as Diehl. The long dashed line represents the original work of Blewitt et al.[1] who used an Instron machine and bombardment in the Graphite and Low-Intensity Test Reactors. Not included as individual data because they fall essentially on Blewitt's line are the recent results of Kopenaal.[5] Blewitt's line has been extrapolated in this case from 10^{16} nvt to 10^{11} nvt, and replotted on a dose scale to show the total dose of neutrons above 0.6 Mev. The solid line is drawn through the present data and extrapolated to a dose of 4×10^{19} nvt. Both Diehl and Fischer originally plotted their results in terms of the neutron dose above 0.1 Mev; their points have been replotted to the present scale (dose with energies greater than 0.6 Mev) in accordance with the reactor spectrum data given by Köhler.[10] The remarkable

---

[10] W. Köhler, Z. Naturforsch. 16a, 936 (1961).
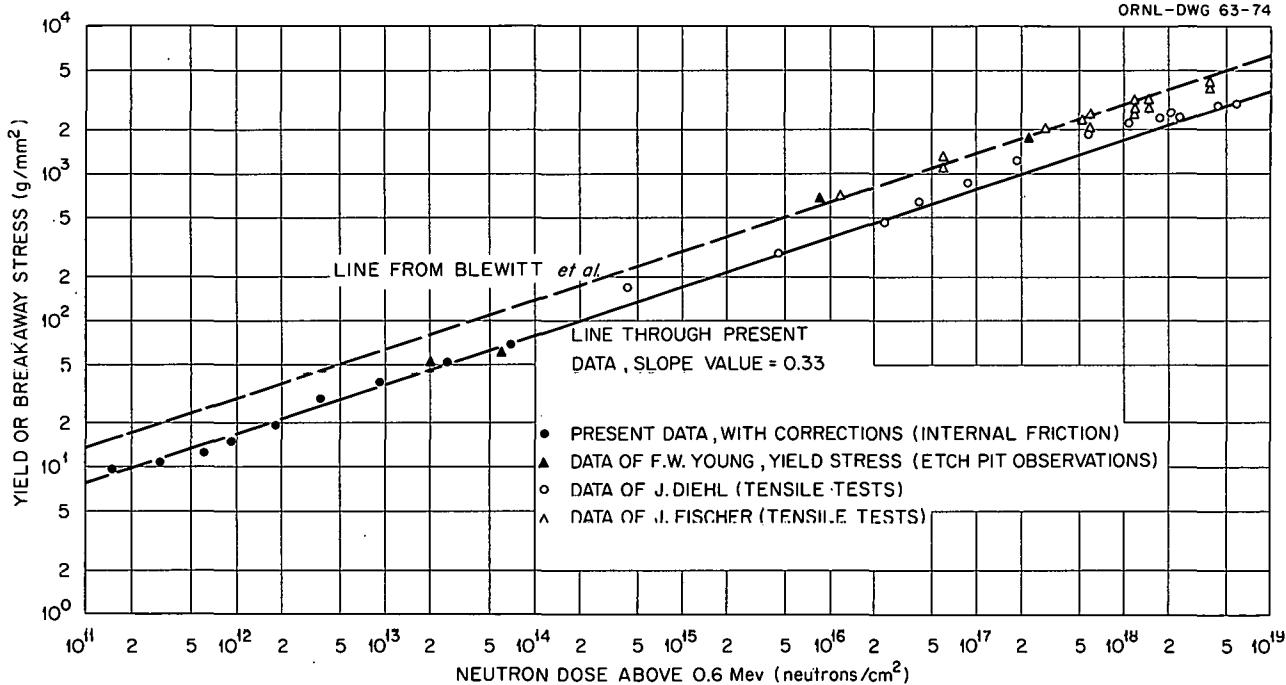
Fig. 10.3. Summary of Experimental Results for the Dose Dependence of the Breakaway Stress, Motion Stress, and Yield Stress in Neutron-Irradiated Copper.

feature of the results taken in their entirety is that a cube-root relation is obeyed with respect to the neutron dose from 10^{11} nvt to at least 4×10^{19} nvt, and that this relation, as well as the magnitude of the stresses measured, is consistent for three extremely different types of measurements and a variety of reactors.

It then appears that there is in fact a correspondence between measured yield points and the stresses necessary to break dislocations away from radiation defect pinning points formed during irradiation on dislocations at rest in their equilibrium positions. This correspondence carries the implication that radiation hardening may in fact be source hardening and that its dose dependence may reflect the growth of the hardening points during irradiation by diffusion of point defects to the dislocations. It should be noted that data exist which are apparently at variance with this hypothesis. In cases (electron and gamma irradiation) where the same sort of point defect diffusion would be expected, and where reduction of low-amplitude internal friction has been shown to occur, little or no hardening is found; and in a case (neutron irradiation at 25°K)

where little or no point defect diffusion is expected, the hardening was found to be very nearly the same (at the dose level used, about 10^{17} nvt) as for room-temperature neutron irradiation. It is hoped that additional studies will help clarify the situation.

FINITE-AMPLITUDE ULTRASONIC WAVES IN SOLIDS

D. O. Thompson   M. A. Breazeale[11]

One of the fundamental parameters of a solid which is basic to an understanding of its physical characteristics is the interatomic potential. Recent interest in theoretical radiation damage studies has emphasized again the importance of the proper description of the potential function in that area; in addition, a knowledge of the potential function is of considerable importance

in many other areas of solid-state physics. Of several properties available for the study of potentials, one is the study of the elastic constants of the material. For infinitesimally small atomic displacements Hooke's law is valid, and the materials' elastic response can be described by the ordinary elastic constants. These constants are characteristic of the atomic potential evaluated at the minimum energy position. As atomic displacements become finite, however, Hooke's law is no longer valid and the anharmonic aspects of the potential become important. In this case it is necessary to include higher-order elastic constants to describe the behavior of the material under stress. It is, therefore, clear that if the third-order elastic constants of a material can be determined in addition to the customary second-order constants, a more complete description of the potential function can be given. The additional information essentially constitutes knowledge of one additional derivative of the potential as described by a Taylor's expansion about the position of minimum energy.

In an effort to develop a technique for the measurement of third-order elasticity in metals, it was decided to make use of the distortion of a finite-amplitude ultrasonic wave. It is known that distortion of such waves is introduced as they propagate through a liquid.[12] By analogy it would be suspected that if an ultrasonic wave of sufficiently large stress amplitude is introduced into a solid so that finite atomic displacements result, then distortion of the fundamental wave should occur such that the second- and higher-order harmonics of the fundamental frequency are generated as the wave propagates in the solid. Measurement of these harmonics, then, yields information about the anharmonic behavior of the solid.

To this end, a pulsed 30-Mcps transmitter was designed which would be capable of providing drive signals up to approximately 1000 v across a 50-ohm load with pulse lengths of 1 μsec. These values represent a peak power of 5 kw, and with a repetition rate of 1000 cps, an average power of 5 w. This voltage is applied to a 30-Mcps quartz transducer crystal bonded to the sample. Detection of the second harmonic generated in the sample

is accomplished by a 20-Mcps quartz crystal bonded to the opposite face of the sample. In this way the 60-Mcps second harmonic component is accentuated in the detection system since it is the third harmonic of the receiver quartz's resonant frequency.[13] At the large intensities used, there is no difficulty in detecting the 30-Mcps signal even though it is quite far from a resonance frequency of the receiver quartz. The attenuation of the second-harmonic echo pattern can be observed at these amplitudes in many cases, and that of the fundamental in all cases considered. In addition, frequency selection of the components is greatly enhanced by the bandwidth of the i.f. amplifier, which is about 3 Mcps.

Polycrystalline aluminum was chosen as a material for the first experiments. Several reasons are involved in making such a choice. In the first place, it was desired to use an isotropic metal with relatively small values of acoustic attenuation due to dislocation damping and other sources. Second, it was thought desirable to use a material whose attenuation as a function of stress amplitude was nearly constant. If these criteria could be satisfied, then the voltage applied to the quartz transducer could be used as a proportional measure of the stress. As it turns out, aluminum satisfies this expectation very well. In addition, previous measurements have been made on this material at lower stress amplitudes in this frequency range[14] so that relative information is available.

In Fig. 10.4 are shown results for the dependence of the second-harmonic distortion signal upon the impressed quartz driver voltage for two aluminum samples. Also shown in this plot are results for the amplitude of the 30-Mc fundamental as a function of the same parameter. The ordinate values represent the ratio of the amplitude of the second harmonic at any impressed voltage to the amplitude of the harmonic at some reference value (in this case, about 140 v). A similar statement applies to the fundamental. It will be seen that the growth in amplitude of the fundamental is approximately linear with drive voltage, whereas the second harmonic grows much faster. Figure 10.5 shows the results of plotting the second-harmonic data on a log-log plot. The straight

[12]M. A. Breazeale and E. A. Hiedemann, *Naturwissenschaften* **45**, 157 (1958); *J. Acoust. Soc. Am.* **30**, 751–56 (1958).

[13]M. A. Breazeale and W. W. Lester, *J. Acoust. Soc. Am.* **33**, 1803 (1961).

[14]A. H. Hikata *et al., J. Appl. Phys.* **27**, 396 (1956).
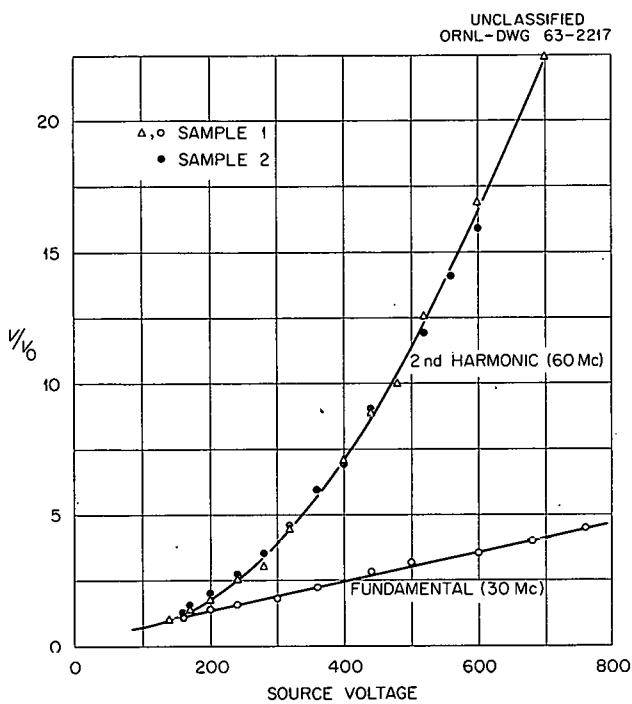
Fig. 10.4. Variation of Fundamental and Second-Harmonic Amplitude with Increasing Source Voltage (Stress Amplitude).

the acoustic attenuation in this aluminum at 30 Mc is stress dependent and levels off to approximately a constant in the present range. This suggestion implies that rather complete dislocation breakaway is achieved in the present work.

A simplified analysis of the problem of the propagation of a finite-amplitude wave in a solid has been made to determine an approximate value for the discontinuity distance in aluminum. The relation of the present results to actual measurements of the third-order elastic constants is not immediately obvious, although it seems reasonable to expect at this time that the relations may be solved for different metal crystal symmetries. A

line represents a slope of 2.00. Therefore it is concluded that whereas the amplitude of the fundamental signal is linear in applied voltage, the second harmonic which is generated in the sample in this aluminum is very nearly quadratic in applied voltage (stress).

That the applied voltage is approximately proportional to the pressure of the acoustic wave is shown in Fig. 10.6, in which the acoustic attenuation for the fundamental 30 Mc is plotted as a function of the drive voltage for two samples. It will be seen that the attenuation is approximately constant over the voltage range considered with a slight drop-off at the small amplitude. This result means that for any fixed position along a sample the stress amplitude of the acoustic wave is proportional to the applied drive voltage. It is interesting to note that the presently measured attenuation values for this aluminum are about a factor of 10 larger than those given by Truell et al. as measured at much smaller stress amplitudes. Measurement of the present samples at small amplitudes yields values which are in accord with others, so that it is concluded that

Fig. 10.5. Second-Harmonic Amplitude as a Function of Source Voltage (Stress Amplitude). Straight line has a slope of 2.00.

solution of the wave equation for solids to second order in isotropic media shows that the amplitude of the second harmonic is expected to be proportional to the square of the stress; Fig. 10.5 demonstrates that this condition is apparently fulfilled

Fig. 10.6. The Variation of Fundamental Attenuation with Source Voltage (Stress Amplitude).

in the present case. In this same solution the third-order elastic constants enter into the coefficient of the quadratic stress term, so that it is presently thought that it may be possible to separate the different constants by appropriate selection of the mode of wave propagation once a complete theoretical treatment of the problem is available.

It has been found for liquids,[15] and suggested theoretically for solids,[16] that for small distances the amplitude of the harmonic wave is proportional to the distance over which the wave passes. Attempts to verify this result in aluminum in the present work are not complete, but preliminary results on a variety of samples of different lengths indicate that there is a difference in signal amplitudes for constant impressed voltage (stress) in the direction expected.

[15]L. K. Zarembo, V. K. Krasilnikov, and. V. V. Shklovskaia-Kordi, *Soviet Phys. Doklady (English Transl.)* **1**, 434 (1956); *J. Acoust. Soc. Am.* **29**, 642 (1957).

[16]J. Melngailis, A. A. Maradudin, and A. .Seeger, *Bull. Am. Phys. Soc.* **8**, 194 (1963).

11. Ar⁺ Ion Bombardment of Metal Surfaces

A. L. Southern   D. R. Burrowbridge[1]

Emphasis in this program is on sputtering yield and atom-ejection studies. Measurements of the sputtering yield from copper crystals were extended to additional orientations, and ejection patterns were obtained from cadmium and magnesium and from ordered and disordered crystals of Cu_3Au. In order to analyze the sputtered particles from copper crystals, a dual-beam mass spectrometer has been installed and is in operation. The results obtained with this technique in conjunction with the previous work[2] on sputtering yields and atom ejection patterns of copper will be used in order to broaden our knowledge and understanding of the nature and properties of the sputtered particles.

The sputtering yields of six additional orientations of copper monocrystals were determined by use of the equipment and techniques previously described,[3,4] The results compared favorably with detailed predictions of the theoretical model previously reported.[2]

Ejection patterns for the three low-index planes of the ordered and disordered alloy Cu_3Au were studied for the sputtered ratio of copper to gold. This ratio varied from 0.8 to 6. No clear evidence for focusing chains could be determined either for the ordered or disordered samples. X-ray examination of the crystals before and after bombardment showed that the ordered crystals were slightly disordered by Ar⁺ bombardment.

The studies previously reported[5] on the hexagonal close-packed metal zinc were extended to cadmium and magnesium. While the ejection patterns of zinc showed some structure, no evidence of focusing chains or other structure was found in the ejection patterns of cadmium or magnesium.

The dual-beam mass spectrometer is described by the manufacturer.[6] Therefore, only a diagram of the bombarding ion source and the location of the solid angle for the sputtered particles is shown here (Fig. 11.1). The bombarding ion beam is variable in energy from 100 to 5000 ev, and the sputtered particles can be accelerated up to 5000 v. The target can be rotated from 0 to 90° with respect to the bombarding ion beam, and the sputtered particles are analyzed at 90° from the bombarding beam. This arrangement allows only the sputtered particles to be analyzed over the complete range, with the exception of an angle of incidence of 45°, for which both the sputtered and reflected particles are analyzed. The mass range of this instrument is 1 to 400 amu, and it has a mass scanning speed ratio of 1 to 250; the fastest speed is 5 min for 200 amu. The best background pressure obtained was 1×10^{-9} torr; according to the history of the system, pressures were generally in the range 3×10^{-9} to 1×10^{-8} torr. Typical pressures in the system during operation were 2×10^{-6} torr in the source, 3×10^{-7} torr in the target region, and 2×10^{-8} torr in the mass analyzer. The maximum bombarding argon ion beam current was 1 μa, and

[1]Co-op student from Virginia Polytechnic Institute, Blacksburg.

[2]A. L. Southern, W. R. Willis, and M. T. Robinson, J. Appl. Phys. 34, 153 (1963).

[3]A. L. Southern et al., Solid State Div. Ann. Progr. Rept. Aug. 31, 1961, ORNL-3213, p 49.

[4]A. L. Southern et al., Solid State Div. Ann. Progr. Rept. Aug. 31, 1960, ORNL-3017, p 52.

[5]A. L. Southern et al., Solid State Div. Ann. Progr. Rept. Aug. 31, 1962, ORNL-3364, p 79.

[6]A. J. Smith et al., A Mass Spectrometer for the Study of Sputtering, paper presented at the Mass Spectroscopy, Eleventh Conference, San Francisco, Calif., May 22, 1963.

GAS INLET

FILAMENT

MAGNET

BOMBARDING
ION BEAM

DEFINING
SLITS

TO MASS
ANALYZER

SPUTTERED PARTICLES 90°
FROM BOMBARDING ION BEAM

TARGET ROTATES
ABOUT CENTER LINE
FROM 0° TO 90°
WITH RESPECT TO
THE BOMBARDING BEAM
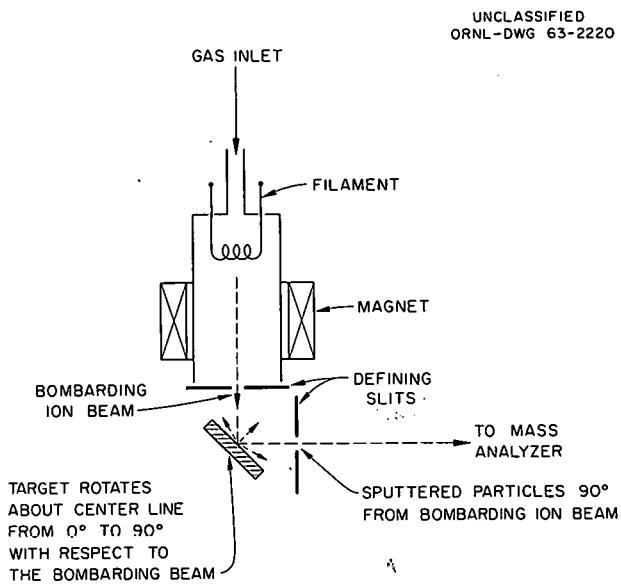
Fig. 11.1. Schematic Diagram of the Bombarding Ion Beam, Target, and Section of the Sputtered Particles Analyzed.

the corresponding analyzed beam intensity of $^{63}Cu^+$ was 10^{-14} amp. The minimum analyzer current measurable was 5×10^{-19} amp.

Table 11.1 gives a list of the positive ions ejected from a single-crystal copper surface bombarded at approximately 52° from normal. The major difference between this list and the one of Bradley's[7] is indium and the lack of CuO^+. Of the three copper target experiments to date, indium was always sputtered. A typical spectrum with only the largest peak is shown in Fig. 11.2. The high sputtering currents of Na^+, K^+, and In^+ are not completely understood. The absence of CuO^+ can be explained by the higher vacuum in this system. Figure 11.3 shows a recording of $^{63}Cu^+$ and $^{65}Cu^+$ from the same copper crystal as used for Fig. 11.2, except the bombarding angle was changed to an angle of incidence of 80°. The

---

[7]R. C. Bradley and E. Ruedl, *J. Appl. Phys.* **33**, 880 (1962).

Table 11.1. Positive Ions Ejected from a Copper Monocrystal by Bombarding with 2.5-kev, 0.2 μa Ar^+ Ions at an Angle of Incidence of 52°

Mass	Probable Identification	Current at Collector (amp)	Mass	Probable Identification	Current at Collector (amp)
		$\times 10^{-18}$			$\times 10^{-18}$
23	Na^+	290	59	Co^+	2.4
27	$C_2H_3^+$	1.5	63	Cu^+	71
28	CO	5	65	Cu^+	30
29	$C_2H_5^+$	2.5	75	As^+	1.8
39	K^+	200	89		1.5
40	Ar^+	40	113	In^+	26
41	K^+	10	115	In^+	520
52	$Cr^+, C_4H_4^+$	7.5	124	Xe^+	3
56	Fe^+	4.2	126	Xe^+, Cu_2^+	2.3
57	$Fe^+, C_4H_9^+$	3.9			
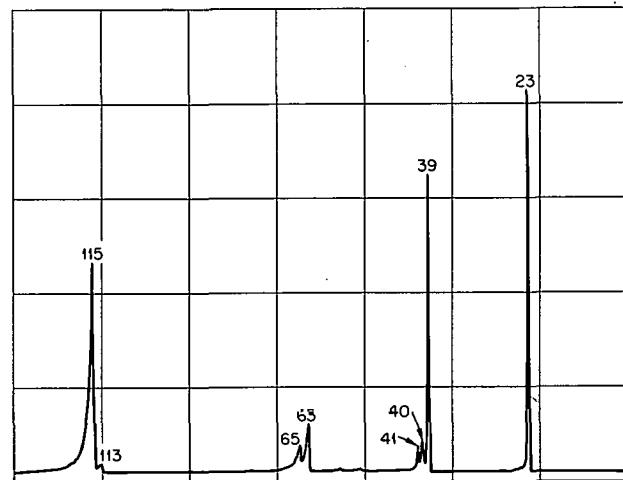
Fig. 11.2. Spectrum of Positive Ions Sputtered from Copper Monocrystals Under 2.5-kev Ar+ Ion Bombardment at an Angle of Incidence of 52°.
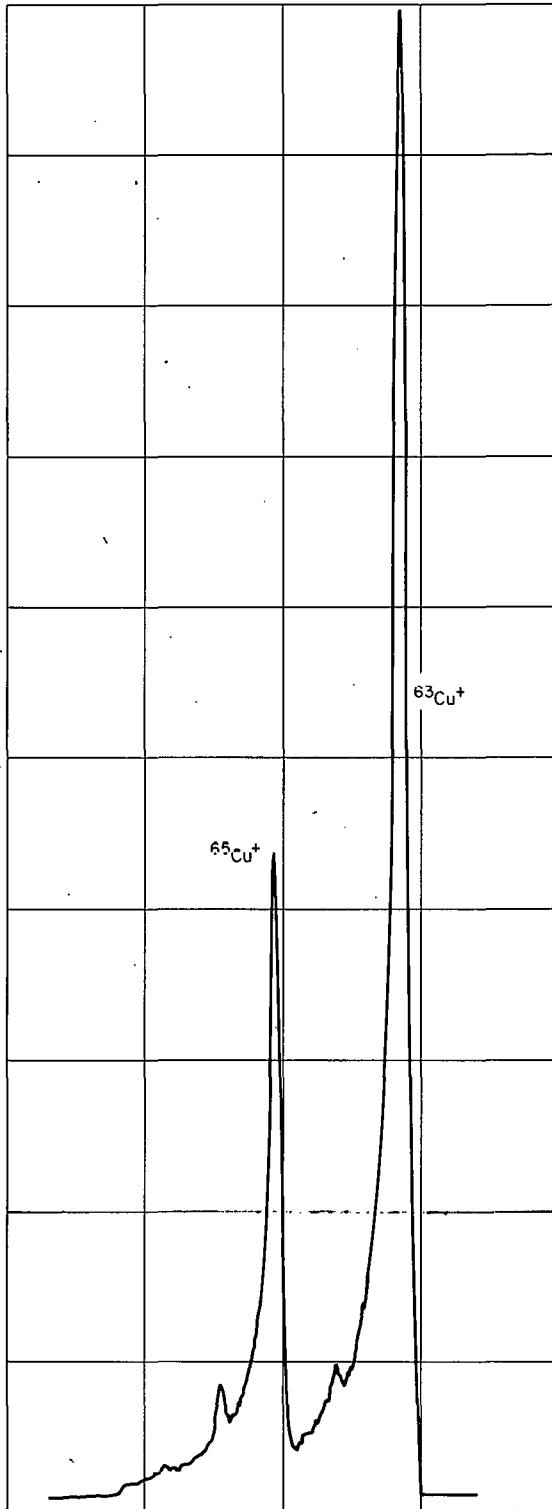
Fig. 11.3. $^{63}Cu^+$ and $^{65}Cu^+$ Sputtered from Copper Monocrystal with 2.5-kev Ar+ Ion Bombardment at an Angle of Incidence of 80°.

isotopic ratio of $^{63}Cu^+/^{65}Cu^+$ at this angle of incidence is 2.29, which compares with White's[8] value of 2.25 ± 0.02. Figure 11.4 is an energy analysis of $^{63}Cu^+$ and $^{65}Cu^+$ ejected from a (001) copper monocrystal bombarded with 2.5-kev Ar+ ions at an angle of incidence of 70°. At 50% level this energy spread is 7.5 ev for $^{63}Cu^+$ and 6.7 ev for $^{65}Cu^+$. A more detailed analysis of these peaks will be made with different angles of incidence and with different bombarding energies. Figure 11.5 is a plot of ejected $^{63}Cu^+$ and $^{65}Cu^+$ peak heights as a function of the angle of incidence from 45 to 88°. The maximum peak height at 76° compares to 78° that Molchanov[9] reported using 27-kev argon ions. The isotopic ratio and the relative peak heights compare favorably only in the range 71 to 78°.

[8]F. A. White and F. M. Rourke, *J. Appl. Phys.* **33**, 2915 (1962).

[9]V. A. Molchanov and V. G. Telkovskii, *Soviet Phys. "Doklady"* (*English Transl.*) **6**, 137 (1961).
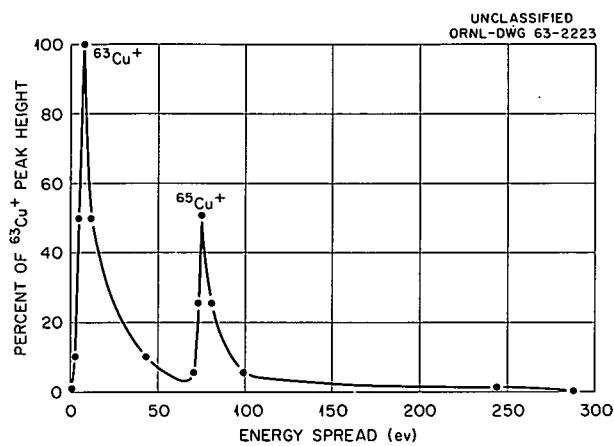
Fig. 11.4. Energy Analyses for $^{63}Cu^+$ and $^{65}Cu^+$ Sputtered from (001) Copper Monocrystal with 2.5-kev Ar$^+$ Ion Bombardment at an Angle of Incidence of 70°.
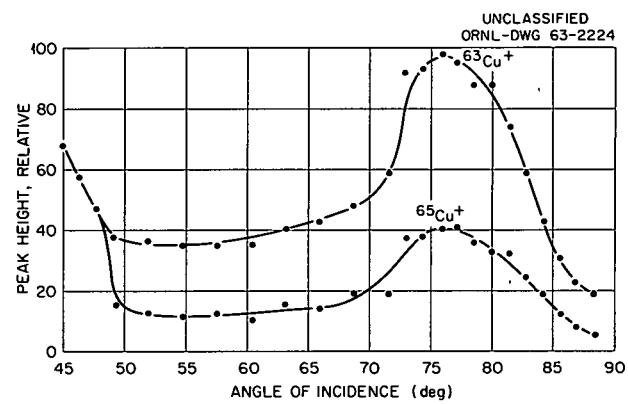
Fig. 11.5. Peak Height as a Function of Angle of Incidence of 45 to 88° for $^{63}Cu^+$ and $^{65}Cu^+$ Sputtered from (001) Copper Monocrystal with 2.5-kev Ar$^+$ Ion Bombardment.

Part IV. Nonmetals

J. H. Crawford, Jr.

PAGES 77 to 78

WERE INTENTIONALLY

LEFT BLANK

12. Semiconductor Studies

EFFECT OF DISORDERED REGIONS ON Co^{60} PHOTON-INDUCED DEFECTS IN GERMANIUM

J. W. Cleland   R. F. Bass
J. H. Crawford, Jr.

It has been observed[1] previously that the hole concentration and apparent acceptor level position of Co^{60} photon-induced defect states is markedly affected by the initial dislocation density of the germanium crystal specimens.

Crawford and Cleland[2] have discussed the introduction of a shallow acceptor state at ~0.2 ev below the conduction band and a deep acceptor state of approximately equal concentration as a consequence of Co^{60} photon irradiation of n-type germanium. Continued irradiation converts n-type germanium to p type, and an apparent defect-acceptor ionization energy of ~0.24 to 0.26 ev above the valence band is observed. A very large additional irradiation does not further alter the apparent ionization energy or apparent hole concentration; hence, no evidence of any low-lying acceptor states of the type that have been observed as a consequence of fast-neutron irradiation[3] is indicated by these experiments.

Vitovskii and co-workers[4] have also observed the 0.2-ev defect state and (in a later publication)[5] additional states at 0.26, 0.11, and 0.02 ev above

the valence band as a consequence of continued irradiation. These data are not in agreement with those obtained above. It is difficult to make any direct comparison, since the source strength, photon flux, irradiation time, and irradiation temperature were not specified; however, it is believed that any low-lying defect-acceptor states in germanium can be attributed to defects that were already present in the sample and that such defect states are not introduced in germanium by irradiation with Co^{60} photons.

Figure 12.1, which is a plot of log Hall coefficient vs inverse temperature, shows the effect of extended Co^{60} photon irradiation on two samples of n-type germanium that were cut from adjacent portions of the same ingot and that were essentially identical in carrier concentration and dislocation content at the outset. Curve II-A indicates that no evidence of any low-lying acceptor states was obtained for sample A after irradiation with 10^{18} Co^{60} photons/cm^2. Curve II-B shows the effect of an initial irradiation of sample B with 10^{13} (fission-spectrum) neutrons/cm^2 that removed 5.3×10^{13} conduction electrons/cm^3, and curve III-B shows the effect of a subsequent irradiation of sample B with 10^{18} photons/cm^2.

It is evident that fast-neutron-induced disordered regions[2,6,7] alter the apparent energy level position of Co^{60} photon-induced defect states. Sample A was reirradiated with 10^{13} (fission-spectrum) neutrons/cm^2, and the resultant data fell essentially on curve III-B, whereas the data of sample B were not further altered by a second irradiation with 10^{18} Co^{60} photons/cm^2. These results

[1]J. W. Cleland and R. F. Bass, *Solid State Div. Ann. Progr. Rept. Aug. 31, 1962*, ORNL-3364, p 103; J. W. Cleland, R. F. Bass, and J. H. Crawford, Jr., *Appl. Phys. Letters* **2**, 113 (1963).

[2]J. H. Crawford, Jr., and J. W. Cleland, *J. Appl. Phys.* **30**, 1204 (1959).

[3]J. W. Cleland, J. H. Crawford, Jr., and J. C. Pigg, *Phys. Rev.* **98**, 1742 (1955); **99**, 1170 (1955).

[4]N. A. Vitovskii, T. V. Mashovets, and S. M. Ryvkin, *Soviet Phys.-Solid State (English Transl.)* **1**, 1266 (1959).

[5]N. A. Vitovskii *et al.*, *Soviet Phys.-Solid State (English Transl.)* **3**, 727 (1961).

[6]J. W. Cleland and J. H. Crawford, Jr., "Radiation-Induced Disorder in Semiconductors," p 299 in *Proceedings of the International Conference on Semiconductor Physics, Prague, 1960*, Academic Press, New York, 1961.

[7]B. R. Gossick, *J. Appl. Phys.* **30**, 1214 (1959).
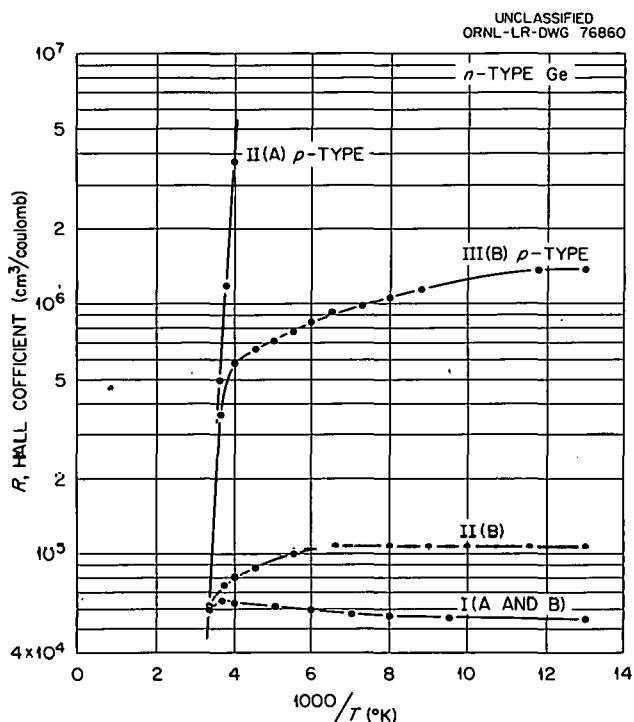
Fig. 12.1. Hall Coefficient vs Inverse Temperature of n-Type Germanium Samples A and B Before Irradiation; Sample B After Neutron Irradiation (Still n Type); and Samples A and B After Subsequent Co[60] Photon Irradiation (Now p Type).

would indicate that the order of introduction has little, if any, effect on the interaction between fast-neutron-induced disordered regions and Co[60] photon-induced lattice defects. Essentially identical behavior was observed for both arsenic- and antimony-doped material; hence, the above cannot be attributed to chemical impurity effects.

These results strongly suggest that no low-lying acceptor states are introduced in material of low dislocation density by Co[60] photons. The low-lying acceptor states reported by Vitovskii and co-workers most probably resulted from the presence of a relatively high dislocation density. The fact that disordered regions in neutron-bombarded specimens are also responsible for shallow acceptors[1] should not be taken to mean that their effect is the same as that produced by dislocations. How either of these complex imperfections affects the acceptor level structure has not yet been established.

PHOTON-INDUCED LATTICE-DEFECT INTRODUCTION RATES IN SEMICONDUCTING MATERIALS

J. W. Cleland   R. F. Bass

The apparent rate of introduction of lattice defects in semiconducting materials has been determined[8] by Hall coefficient and resistivity measurements subsequent to ambient-temperature and selected liquid-nitrogen-temperature irradiations with 0.667-Mev Cs^{137}, 1.25-Mev Co^{60}, 1.74-Mev Sb^{124}, and 2.76-Mev Na^{24} photons and with energetic cadmium capture gamma rays.

Monoenergetic-electron irradiation experiments have indicated that the minimum threshold energy for displacement of a lattice atom to a stable interstitial position is about 15 ev for germanium, 13 ev for silicon, and 6 to 10 ev for certain III-V type semiconducting intermetallic compounds. Oen and Holmes[9] have calculated the atomic displacement cross section for lattice atoms by gamma rays through the Compton process for various atomic displacement threshold energies, and Bartholomew and Higgs[10] have measured the gamma-ray spectra from thermal-neutron capture in cadmium. One can, therefore, use the data of Oen and Holmes to calculate an atomic displacement cross section for a particular material and displacement threshold energy for a known flux of monoenergetic photons directly; or one can combine their calculations with the data of Bartholomew and Higgs for a similar calculation for a flux of cadmium capture gamma rays.

Table 12.1 shows the ratio of the calculated to the observed defect introduction rates for several semiconducting materials for five different incident-photon energies. The observed values were obtained from the experimental rates of carrier removal under the assumption that two carriers are removed per Frenkel pair in germanium and one in silicon and GaAs. It is evident that the agreement between theory and experiment improves relative to the energy of the incident photon and that

[8]J. W. Cleland and R. F. Bass, Solid State Div. Ann. Progr. Rept. Aug. 31, 1962, ORNL-3364, pp 95—102.

[9]O. S. Oen and D. K. Holmes, J. Appl. Phys. 30, 1289 (1959).

[10]G. A. Bartholomew and L. A. Higgs, Compilation of Thermal Neutron Capture Gamma Rays, CRGP-784 (July 1958); quoted by E. Troubetzkoy and H. Goldstein, Nucleonics 18(11), 171 (1960).

Table 12.1. Lattice-Defect Production in Semiconductors

Type of Irradiation	Material (n-type)	N_d/ϕ (theory)	N_d/ϕ (observed)	Ratio
0.667-Mev Cs[137]	Ge	0.002	10^{-6}	2000
	GaAs	0.010	0.0004	25
1.25-Mev Co[60]	Ge	0.023	0.0006	38
	Si	0.026	0.0007	37
	GaAs	0.070	0.014	5
1.74-Mev Sb[124]	Ge	0.054	0.0027	20
2.76-Mev Na[24]	Ge	0.074	0.010	7.4
Cadmium gamma rays	Ge	0.076	0.018	4.2
	Si	0.046	0.008	5.8
	GaAs	0.450	0.320	1.4

n-type GaAs is particularly sensitive to photon-induced lattice defects.

NEUTRON-INDUCED LATTICE-DEFECT INTRODUCTION RATES IN GERMANIUM AND SILICON

J. W. Cleland   R. F. Bass

The apparent rate of introduction of lattice defects in germanium and silicon has been determined[11] by Hall coefficient and resistivity measurements subsequent to ambient-temperature and selected liquid-nitrogen-temperature irradiations with thermal, fission-spectrum, and monoenergetic neutrons.

H. C. Schweinler[12] first indicated that the average lattice atom recoil energy as a consequence of thermal-neutron absorption and capture gamma-ray emission might be as high as 180 ev for germanium and 780 ev for silicon and that multiple defect creation might be expected; however, extensive experi-

ments have indicated[13] that approximately only one electron in germanium and two electrons in silicon are removed per actual thermal-neutron capture by the lattice defects created in the (n,γ) process.

Crawford and Lark-Horovitz[14] utilized the initial slope of conductivity vs total integrated fast flux data to estimate the average net number of defect acceptors introduced as approximately −3.2 per incident fast neutron in a reactor locale. Gossick, Crawford, and Cleland[15] later introduced the concept of the disordered region and indicated that one could use the theoretical considerations of Holmes and Leibfried[16] and the experimental values of

[11]J. W. Cleland and R. F. Bass, Solid State Div. Ann. Progr. Rept. Aug. 31, 1962, ORNL-3364, pp 95—101.

[12]H. C. Schweinler, J. Appl. Phys. 30, 1125 (1959).

[13]J. H. Crawford, Jr., and J. W. Cleland, Intern. J. Appl. Radiation Isotopes 9, 189 (1960); "Transmutation Doping and Recoil Effects in Semiconductors Exposed to Thermal Neutrons," p 270 in Radioisotopes in the Physical Sciences and Industry, International Atomic Energy Agency, Vienna, 1962 (to be published in Nuovo Cimento).

[14]J. H. Crawford, Jr., and K. Lark-Horovitz, Phys. Rev. 78, 815 (1950).

[15]J. H. Crawford, Jr., and J. W. Cleland, J. Appl. Phys. 30, 1204 (1959); B. R. Gossick, J. Appl. Phys. 30, 1214 (1959); J. W. Cleland and J. H. Crawford, Jr., "Radiation-Induced Disorder in Semiconductors," p 299 in Proceedings of the International Conference on Semiconductor Physics. Prague. 1960, Academic Press, New York, 1961.

[16]D. K. Holmes and G. Leibfried, J. Appl. Phys. 31, 1046 (1960).

Binder[17] to obtain a reasonable agreement with the space charge model. The apparent rate of removal of conduction electrons was found to be about −8 per incident fission-energy neutron. The disordered region model was also applied to the monoenergetic-neutron defect-introduction rates obtained by Ruby et al.[18] for 1.7-, 3.2-, and 4.8-Mev neutrons.

The purpose of the following is to indicate that one can use a thermal-neutron locale as a convenient source of fission-spectrum neutrons and obtain a very reasonable agreement between the calculated and experimental values of the fission flux. The slant animal tunnel of the ORNL Graphite Reactor has a thermal-neutron flux of 1.5×10^9 cm^{-2} sec^{-1}, a cadmium ratio in excess of 10^3, and a background gamma-ray flux from the reactor of less than 800 r/hr. The background fast (damaging) flux from the reactor is only about 10^5 cm^{-2} sec^{-1}. The calculated number of thermal-neutron absorptions in germanium is only 0.108 per incident, and multiple defect production by recoil has not been observed.[13] Therefore one can ignore gamma-ray, background fast (damaging), and (n,γ) recoil effects in comparison with fission-spectrum-neutron effects as obtained under the following experimental conditions.

Two fission plates were made from ORR fuel-element material that contained 17.16 wt % (2.5 at. %) of 93.16% enriched U^{235}. The total weight of the two plates (1 in. $\times$ 1 in. $\times \frac{1}{8}$ in.) was 13.03 g; the total uranium weight was 2.236 g and the total U^{235} weight was 2.083 g. The samples were placed between the two plates (separation distance, 0.2 cm) for irradiation.

The concentration of U^{235} can be calculated as follows:

$$\frac{6.02 \times 10^{23}}{26.98/2.7} = 6.02 \times 10^{22} \times 2.5\%$$

$$= 1.5 \times 10^{21} \text{ atoms of } U^{235} \text{ per cm}^3 . \quad (1)$$

Also, the following equation can be used to calculate the expected number of neutron absorptions:

$$1.5 \times 10^{21} \text{ atoms/cm}^3 \times 690 \times 10^{-24} \text{ (barns)}$$

$$= 1.05 \text{ thermal neutrons cm}^{-2} \text{ sec}^{-1} . \quad (2)$$

Attenuation in the fission plates can be calculated as follows:

$$N/N_I = e^{-\lambda x} \text{ or } 1 - N/N_I = 1 - 1/e^{1.05(0.32 \text{ cm})}$$

$$= 1 - 0.72 = 28\% \text{ absorption} . \quad (3)$$

If one assumes ~ 2.5 neutrons/fission, with no flux depression or decrease due to self-absorption, then the fission-spectrum-neutron flux between the two plates can be estimated as:

1.5×10^9 thermal neutrons cm^{-2} sec^{-1}

$\times$ (0.28 absorbed) 2.5 neutrons/fission

$$= 1.05 \times 10^9 \text{ cm}^{-2} \text{ sec}^{-1} . \quad (4)$$

Table 12.2 indicates the experimental results that were obtained[19] using a wide variety of threshold detectors for total irradiation times that were as long as three weeks in certain instances. It is evident that a reasonable agreement is obtained between the calculated and experimental values of the fission-spectrum-neutron flux and that one can employ this technique to ascertain the apparent removal rate of conduction electrons in semiconductors without the possible complication of background fast (damaging) or gamma-ray effects that might be encountered in a normal reactor locale.

The Argonne National Laboratory's 3.0-Mev Van de Graaff (KN-3000) has been used[20] to obtain monoenergetic-neutron irradiations from 0.2 to 1.5 Mev with the $Li^7(p,n)Be^7$ reaction. All of the samples were irradiated on the surface of a 2-cm-diam U^{235} fission foil (294-μg mass, fission cross section of 1.2 barns at 0.7 Mev neutron energy); the foil was counted over 100 channels of a pulse-height analyzer and integrated over the two fission fragment peaks.

Ruby et al.[18] used the D-D reaction to obtain monoenergetic neutrons at 1.7, 3.2, and 4.8 Mev and observed the apparent rate of removal of conduction electrons in germanium at 78°K following irradiation at 78°K. It was necessary to use semi-intrinsic material (1.7 to 2.8 $\times 10^{12}$ electrons/cm^3) because of the low total dose (7 $\times 10^{10}$/cm^2) available in these experiments.

[17]D. Binder, Phys. Rev. 122, 1147 (1961).

[18]S. L. Ruby, F. D. Scupp, and E. D. Wolley, Phys. Rev. 111, 1493 (1958).

Table 12.2. Threshold-Detector Flux Values

Detector	Reaction	Cross Section (barns)	Threshold (Mev)	Flux (neutrons cm^{-2} sec^{-1})
Np^{237}	$Np^{237} \xrightarrow{fission} Ba^{140}$	1.90	0.60	1.10×10^9
U^{238}	$U^{238} \xrightarrow{fission} Ba^{140}$	0.578	1.00	1.00×10^9
Ni^{58}	$Ni^{58}(n,p)Co^{58}$	0.390	3.00	2.11×10^8
S^{32}	$S^{32}(n,p)P^{32}$	0.320	2.90	1.71×10^8
Al^{27}	$Al^{27}(n,\alpha)Na^{24}$	0.060	8.20	6.13×10^6

Curtis and Cleland[21] have observed an apparent electron removal rate in germanium of about −8 per incident 14.1-Mev neutron, using the ORNL Biology Division's Cockcroft-Walton generator.

The ORNL Analytical Chemistry Division's 150-kv Cockcroft-Walton generator (see ORNL TM-362), Texas Nuclear model 9501, has also been used for 14.1-Mev monoenergetic-neutron-irradiation experiments[22] on various semiconducting materials. It is believed that certain details of this apparatus and the experimental setup might be of general interest.

The 1-curie water-cooled tritium target absorbs a 600-μa beam of deuterons over an area of about 1 in.^{2}. A grid of four thin copper foils (each about $\frac{1}{2}$ in.^{2}) indicated a neutron flux of about 10^9 cm^{-2} sec^{-1} over ~ 1 in.^{2} of sample area, and all four foils agreed within a few percent as to total nvt received.

An estimated total dose of 8.5×10^{11} (14.1-Mev) neutrons/cm^2 was obtained in about 20 min of machine time. It has been estimated that each target might be expected to last for 3 hr of operation; hence, one can predict a total dose of about 10^{13} (14.1-Mev) neutrons per cm^2 per $45 target. Recent trade literature indicates that 5-curie targets are now available.

Table 12.3 shows the average lattice-defect introduction rates that have been obtained for a series of monoenergetic-neutron and fission-spectrum-neutron irradiations of n-type samples of germanium and silicon. Note that the apparent removal rate of conduction electrons in n-type germanium is a fairly sensitive function of the incident neutron energy up to about 0.7 Mev, which corresponds to a lattice atom recoil energy of about 20,000 ev; however, the apparent rate is not a sensitive function of the incident neutron energy above 0.7 Mev. It has previously been indicated[11] that one might use the apparent formation of low-lying defect-acceptor states in p-type germanium (converted from n type by irradiation) to signal the minimum energy required to produce disordered regions. Such states have been observed after a total irradiation of less than 10^{13} (14.1-Mev) fission-spectrum or 0.7-Mev neutrons/cm^2; however, they have not been observed after a total irradiation of about 10^{13} (0.2-Mev) or 10^{13} (0.5-Mev) neutrons/cm^2.

The large difference in apparent removal rates in n-type germanium for fission-spectrum neutrons, as compared with monoenergetic neutrons in the 0.7- to 1.5-Mev range, is not understood at present. The fission-neutron experiments were conducted in a thermal-neutron locale (see above); and the apparent rate of removal of conduction electrons was found to be relatively insensitive to the total neutron dose, the initial electron concentration of 10^{13} to 10^{15}/cm^3, and the reactor ambient (40°C) or liquid-nitrogen temperature irradiations.

[21]O. L. Curtis, Jr., and J. W. Cleland, J. Appl. Phys. 31, 423 (1960).

[22]We are indebted to J. E. Strain of the Analytical Chemistry Division for these irradiations.

Table 12.3. Monoenergetic-Neutron Lattice-Defect Introduction Rates

Neutron Energy (Mev)	Material (n-type)	Total Dose (neutrons/cm^2)	Removal Rate (av)
0.20	Ge	1.08×10^{12}	−6
0.50	Ge	9.20×10^{11}	−17
0.70	Ge	8.30×10^{12}	−25
1.00	Ge	1.13×10^{12}	−30
1.25	Ge	3.04×10^{11}	−25
1.50	Ge	2.81×10^{11}	−25
Fission	Ge	$0.3–1.6 \times 10^{13}$	−5 −7
Fission	Si	$0.3–1.6 \times 10^{13}$	−5
1.70[a]	Ge	6.00×10^{10}	−21
3.20[a]	Ge	6.00×10^{10}	−12
4.80[a]	Ge	6.00×10^{10}	−12
14.10	Ge	8.50×10^{11}	−12
14.10	Si	8.50×10^{11}	−12

[a]S. L. Ruby et al., Phys. Rev. 111, 1493 (1958).

DEVELOPMENT OF A COMPOSITE DEFECT IN GAMMA-IRRADIATED GERMANIUM BY ANNEALING

Jay Cee Pigg

The 0.09-ev level previously reported[23,24] in gamma-irradiated germanium has been studied in an attempt to identify the center responsible.

The level is not present after irradiation at 77°K but appears after a 70-min anneal at temperatures as low as 377°K. The level, once established, is stable to further anneal in the temperature range of 377 to 455°K.

A sample cut from the same ingot as those reported in refs 23 and 24 was heated in air for 18 hr at 600°C. The sample was then irradiated for 36 hr in liquid nitrogen, as was the case in previous experiments. The sample was then annealed for 70 min at 377°K. The change in carrier concentration when the Fermi level crossed the 0.09-ev level was 1.25×10^{13}. The change in the sample which had not been heated in air was 0.73×10^{13}.

This experiment suggests that the 0.09-ev level may be due to an oxygen-vacancy complex. Such a center has been conclusively identified in electron-irradiated silicon by electron spin resonance techniques.[25] In silicon this composite defect acts as an acceptor located 0.17 ev below the conduction band and is thermally quite stable. These similar characteristics lend further support to the model proposed here.

DEFECT PRODUCTION AND ANNEALING IN n-TYPE GERMANIUM

Jay Cee Pigg

The annealing behavior of irradiated antimony-doped germanium is strongly affected by the donor

[23]J. C. Pigg, Solid State Div. Ann. Progr. Rept. Aug. 31, 1962, ORNL-3364, p 87.

[24]J. C. Pigg, Annealing of Gamma Ray Induced Changes in Antimony-Doped Germanium, ORNL-3443 (May 14, 1963).

[25]G. D. Watkins and J. W. Corbett, Phys. Rev. 121, 1001 (1961).

concentration. For concentrations in excess of $5 \times 10^{14}/cm^3$, the thermal recovery of radiation-induced changes in both minority carrier lifetime[26] and carrier concentration[27] is dominated by recovery in the temperature range 35 to 100°C; whereas for lower donor concentrations the dominant recovery stage lies above 100°C.[28] The influence of antimony is so striking that one might suspect qualitatively different defect structures in the two concentration ranges. One possible explanation involves direct participation of the donor in the defect production process during, or immediately subsequent to, irradiation.

To further elucidate this problem, an experiment has been performed to determine whether or not the removal of carriers from n-type germanium due to Co^{60} gamma irradiation is a function of impurity concentration. Two antimony-doped samples were irradiated at liquid-nitrogen temperature. The samples were periodically removed from the irradiation source, and the carrier concentration was measured by means of Hall effect. The data are shown in Fig. 12.2.

The factor of 2 increase in electron removal rate for an order of magnitude increase in antimony con-

centration demonstrates that antimony either participates directly in the primary radiation damage process or increases the concentration of electrically active defects which are retained by the lattice at the temperature of irradiation. Since the relative concentration of donors is only 2 in 10^8, even in the heavily doped specimen, it is difficult to see how any primary effect could exist. Therefore some process subsequent to defect creation is the more probable interpretation.

The ratio of the carrier removal rates for these two specimens is the same as the ratio of the cube roots of the respective antimony concentrations. On the basis of these scanty data, the implication is that the carrier removal rate is a function of $1/r$, where r is the distance between impurity atoms. The data fit the expression

$$\Delta n = \frac{IK\phi_\gamma t}{r},$$

where Δn is the change in carrier concentration, ϕ_γ is the photon flux, t is the time, r is the distance between antimony atoms, and K is a dimensionless constant. The value of K for these samples was found to be 7.8×10^{-10}.

A more extensive examination of the dependence of removal rate on antimony concentration is necessary before the significance of this simple analysis can be evaluated. These data suggest that some species of radiation-produced defects must diffuse to the neighborhood of the impurity atom before it is effective in removing carriers. The work of MacKay and Klontz[29] shows that diffusion of some sort does take place at temperatures below 77°K. Presumably, the resulting defect structure, which is dominant in crystals containing a high antimony concentration, has a low thermal stability.

The influence of high antimony content on recovery kinetics was examined by annealing experiments. Isochronal annealing curves (a 20-min anneal at the indicated temperature and property measurement at 77°K) for specimens containing 1.3×10^{14} and 1.1×10^{15} antimony atoms/cm^3 subsequent to Co^{60} gamma irradiation are compared in Fig. 12.3. The low-temperature annealing

[26]O. L. Curtis, Jr., and J. H. Crawford, Jr., *Phys. Rev.* **126**, 1342 (1962).

[27]W. L. Brown, W. M. Augustyniak, and T. R. Waite, *J. Appl. Phys.* **30**, 1258 (1959).

[28]J. C. Pigg, *Annealing of Gamma Ray Induced Changes in Antimony-Doped Germanium,* ORNL-3343 (May 14, 1963).

[29]J. W. MacKay and E. E. Klontz, *J. Appl. Phys.* **30**, 1269 (1959); "The Role of Carriers in the Displacement Process in Germanium," paper presented at the Symposium on Radiation Damage in Solids and Reactor Materials, Venice, Italy, May 1962 (to be published).

Fig. 12.2. Carrier Removal as a Function of Antimony Concentration.
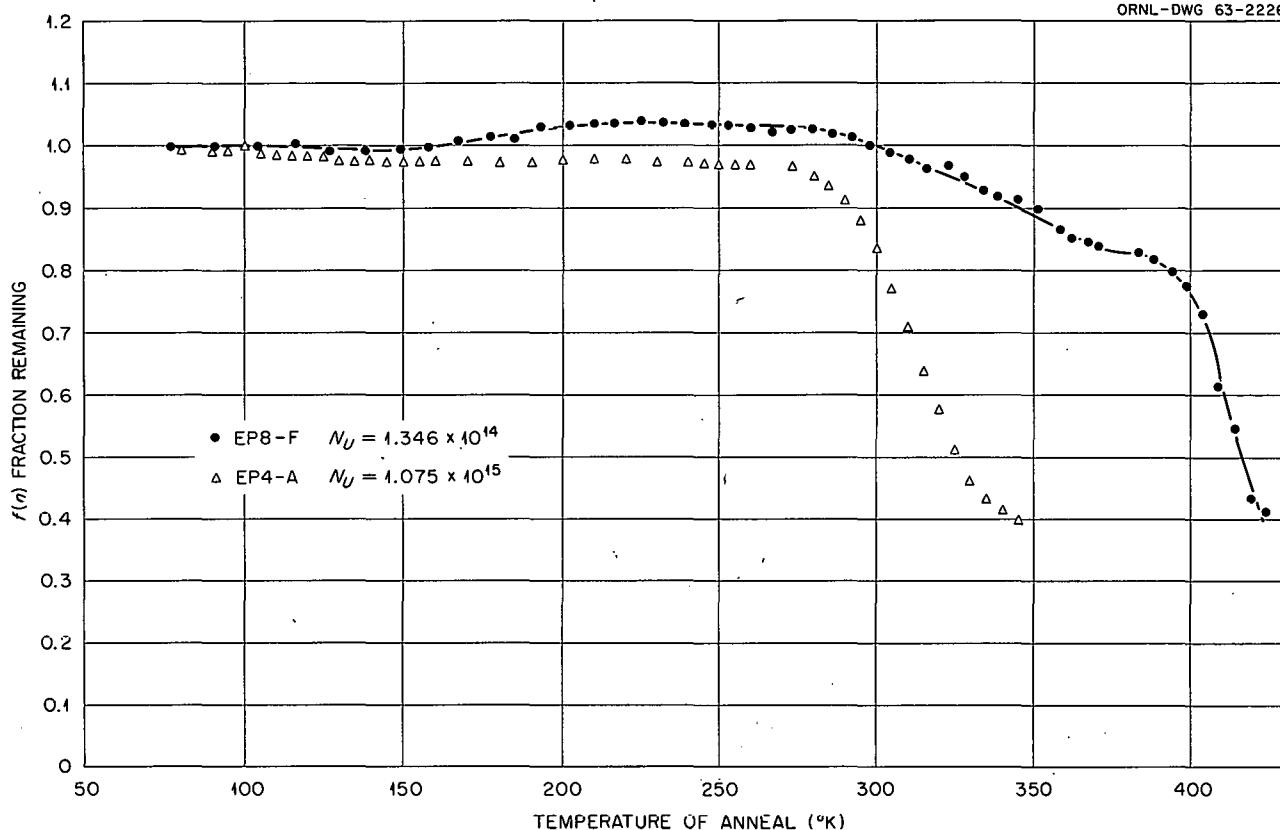
Fig. 12.3. Isochronal Anneal as a Function of Antimony Concentration.

Within the figure:

● EP8-F $N_U = 1.346 \times 10^{14}$

△ EP4-A $N_U = 1.075 \times 10^{15}$

$f(n)$ FRACTION REMAINING

TEMPERATURE OF ANNEAL (°K)

stage (270 ro 350°K) is much enhanced in the heavily doped crystal, in agreement with previous observations.[26,27] Further studies are required before a definitive model for the defect structure responsible for these observations can be formulated.

KINETICS OF ANNEALING AND COMPLEX FORMATION IN GAMMA-IRRADIATED n-TYPE GERMANIUM

Jay Cee Pigg   J. H. Crawford, Jr.

The annealing of defects introduced into antimony-doped n-type germanium irradiated with Co^{60} gamma rays at 77°K was previously shown[30] to be explicable in terms of the following solid-state reactions

involving antimony atoms and vacancies:

$$Sb + V \underset{k_2}{\overset{k_1}{\rightleftharpoons}} SbV , \qquad (a)$$

$$SbV + V \xrightarrow{k_3} SbV_2 , \qquad (b)$$

$$V + \text{dislocation sink} \xrightarrow{k_4} SbV_2 , \qquad (c)$$
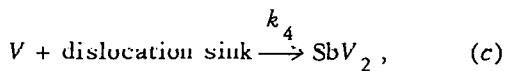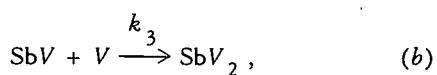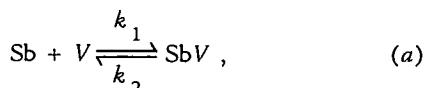
where the k's are the rate constants for the indicated reactions.

The previous simplified kinetic analysis suggested that the binding energy of the complex was ~0.4 ev. Subsequent calculations have shown that this binding energy is too small to furnish a sufficiently large concentration of SbV complexes in the appropriate temperature range for reaction (b) to occur at a reasonable rate. Therefore, to further investigate this point a more careful formulation of

[30] J. C. Pigg, *Annealing of Gamma Ray Induced Changes in Antimony-Doped Germanium,* ORNL-3443 (May 14, 1963).

kinetics has been performed under the assumption that the energy levels of the vacancy are not appreciably different in number and position from those of the SbV complex. This assumption is justified by experimental observation and has the advantage that the observable number of acceptor states of the type initially introduced can be described as

$$N_T = N_V + N_{SbV} . \tag{1}$$

Thus, the rate equations of interest are:

$$\dot{N}_V = -k_1 N_{Sb} N_V + k_2 N_{SbV}$$
$$- k_4 N_D N_V - k_3 N_{Sb} N_V ; \tag{2}$$

$$\dot{N}_{SbV} = k_1 N_{Sb} N_V - k_2 N_{SbV} - k_3 N_{SbV} N_V ; \tag{3}$$

$$\dot{N}_{SbV_2} = k_3 N_{SbV} N_V ; \tag{4}$$

and, from Eq. (1),

$$\dot{N}_T = \dot{N}_V + \dot{N}_{SbV}$$
$$= -\left(2k_3 N_{SbV} N_V + k_4 N_D N_V \right) , \tag{5}$$

where

N_V = vacancy concentration,

N_{Sb} = antimony concentration ($N_{Sb} = N_{Sb}^0$ under the conditions of interest since $N_V^0 \ll N_{Sb}^0$),

N_{SbV} = concentration of SbV complexes,

N_{SbV_2} = concentration of SbV$_2$ complexes, and

N_D = concentration of dislocations expressed as number per cm^2.

(As pointed out by Koehler et al.,[31] annihilation effectively occurs as soon as a vacancy reaches a dislocation since it should move rapidly along the stress field of the dislocation to find a jog.)

Equation (5) may be readily integrated by assuming equilibrium between vacancies and antimony atoms, that is, for $N_V^0 \ll N_{Sb}^0$ as is appropriate here:

$$N_{SbV} = K N_{Sb}^0 N_V \tag{6}$$

[31] J. S. Koehler, F. Seitz, and J. E. Bauerle, *Phys. Rev.* **107**, 1499 (1957).

and

$$N_V = N_T / (1 + K N_{Sb}^0) , \tag{7}$$

where K is the equilibrium constant,

$$K = \frac{N_{SbV}}{N_V N_{Sb}} = A e^{E_B / kT} ,$$

and E_B is the binding energy of the complex. Substitution of Eqs. (6) and (7) in Eq. (5) leads to the integral form

$$N_T = \frac{a N_T^0 e^{-t/\tau}}{a + b N_T^0 (1 - e^{-t/\tau})} , \tag{8}$$

where

$$a = k_4 N_D ,$$

$$b = \frac{2 k_3 K N_{Sb}^0}{1 + K N_{Sb}^0} ,$$

$$\tau = (1 + K N_{Sb}^0) / k_4 N_D ,$$

$$N_T^0 = N_V^0 + N_{SbV}^0 ,$$

that is, the concentrations of the species at the beginning of the anneal. At high temperatures, where $K N_{Sb}^0 \ll 1$, Eq. (8) reduces to the proper form for first-order diffusion of vacancies to dislocation annihilation sites; and at low temperatures, where vacancy migration over long distances becomes unimportant, it takes the second-order form expected for formation of SbV$_2$ complexes.

By means of Eqs. (7) and (8), Eq. (4) can be integrated directly:

$$N_{SbV_2} = \frac{\alpha}{2} N_T^0 \left[\frac{(\alpha + \beta N_T^0)(1 - e^{-t/\tau})}{\alpha + \beta N_T^0 (1 - e^{-t/\tau})} \right]$$
$$- \frac{\alpha}{2\beta} \ln \left[1 + \frac{\beta N_T^0 (1 - e^{-t/\tau})}{\alpha} \right] , \tag{9}$$

where

$$\alpha = k_4 N_D ,$$

$$\beta = \frac{2 k_3 K N_{Sb}^0}{1 + K N_{Sb}^0} ,$$

and τ takes its previous value. As expected, N_{SbV_2} approaches zero for all times at high temperatures, where $KN_{Sb}^0 \ll 1$. At lower temperatures, N_{SbV_2} increases monotonically from 0 at $t = 0$ to a saturation value determined by the relative magnitudes of k_3, KN_{Sb}^0, and $k_4 N_D$ in the relationship defined by Eq. (9). At sufficiently low temperatures, N_{SbV_2} at saturation approaches $N_T^0/2$.

Consider now the form of τ:

$$\tau = \frac{1 + KN_{Sb}^0}{k_4 N_D} . \tag{10}$$

The important consideration is its temperature dependence. Now

$$k_4 = R_D \nu_V = R_D B e^{-E_M/kT} , \tag{11}$$

where R_D is the capture radius of a dislocation ($\sim 10^{-7}$ cm), ν_V is the mean velocity of a moving vacancy, B is a constant containing the effective vibrational frequency of the vacancy ($\nu \simeq 10^{13}$/sec) and geometrical factors for vacancy jumping, and E_M is the activation energy for vacancy motion. Using the expression

$$K = A e^{E_B/kT} ,$$

one finds that

$$\tau = (1 + AN_{Sb}^0 e^{E_B/kT})/R_D BN_D e^{-E_M/kT} . \tag{12}$$

At sufficiently low temperatures ($KN_{Sb}^0 \gg 1$), Eq. (12) is approximated by

$$\tau = \frac{AN_{Sb}^0}{R_D BN_D} e^{(E_B + E_M)/kT} ; \tag{12a}$$

while for high temperatures ($KN_{Sb}^0 \ll 1$)

$$\tau = \frac{1}{R_D BN_D} e^{E_M/kT} . \tag{12b}$$

Calculations using approximate values for the constants in Eq. (12) indicate that the intermediate range over which Eq. (12) must be employed covers a temperature interval comparable to that used experimentally[30] (377 to 455°K). Hence, a plot of log $\tau_{1/2}$ vs $1/T$, where $\tau_{1/2}$ is the time required for

50% recovery and thus proportional to τ, should yield a curve whose slope changes from a value near $(E_B + E_M)/k$ at the lower temperature to a slope near E_M/k at the higher temperature.

Examination of the experimental data indicates that the values $E_M = 0.75$ ev and $E_B = 0.55$ ev are consistent with both the rates of isothermal annealing as a function of temperature and the saturation plateaus of the different isothermal annealing curves, provided the proper choice of preexponential constants is made.

The required values of A, B, and R_D are reasonable in magnitude. The actual parameter measured, however, is carrier concentration. Consequently, more extensive experimental data should be examined in order to establish the validity of the original assumption and to verify the assumed values of A, B, and R_D.

RADIATION EFFECTS IN CADMIUM SULFIDE (PART I)

J. W. Cleland   R. F. Bass

High-purity n-type single-crystal wafers of CdS were obtained from the Harshaw Chemical Company and fabricated into bridge-type Hall plates with an ultrasonic cutter; and the Hall coefficient and resistivity values were obtained in the temperature range 78 to 300°K. Typical values were an electron concentration of 3×10^{15}/cm^3 and a Hall mobility of 440 to 5000 cm^2 v^{-1} sec^{-1} as determined at 78°K. Representative samples were exposed at ambient temperature (35°C) to a total dose of 1.5×10^{17} Co^{60} photons/cm^2. The electron concentration was reduced by about 1%, which would suggest an apparent removal rate of conduction electrons of about 2×10^{-4} per incident Co^{60} photon.[32]

The kinetic energy of recoil of cadmium atoms as a consequence of thermal-neutron absorption and capture gamma-ray emission [(n,γ) process] has been estimated at about 75 ev. Subsequent transmutation of Cd^{113} (27,000-barn cross section) is to the stable isotope Cd^{114}; thus the effect of the addition of chemical impurities by transmutation

---

[32]See, however, the results of R. O. Chester, "Radiation Effects in Cadmium Sulfide (Part II)," this chapter.

would be expected to be totally negligible as compared with the introduction of cadmium interstitials and vacancies by (n,γ) recoil.

Selected samples were exposed in several thermal-neutron locales. The apparent electron concentration was reduced by 10 to 25% for different irradiations; however, the apparent rate of introduction of defect states (assuming one electron removed per Frenkel-type pair) was only 0.1 or less per thermal neutron absorbed. Approximately 60% of the apparent reduction in electron concentration was thermally annealed after 23 hr at 100°C.

One must therefore conclude that thermal-neutron-induced recoil effects [(n,γ) process] are not very effective in producing Frenkel-type lattice defects in CdS or that such defects readily anneal.

RADIATION EFFECTS IN CADMIUM SULFIDE (PART II)

R. O. Chester

Investigations of radiation effects in II-VI compounds have been continued, but emphasis has been shifted from ZnS to CdS. Two considerations which led to this change are: (1) higher-purity crystals are available for CdS than for ZnS; and (2) the smaller band gap in CdS makes the investigation possible with less elaborate and, often, already existing equipment.

Higher-purity single crystals of CdS have been obtained from the Eagle-Picher Company. Spectroscopic analysis shows silicon (10 ppm) and manganese (0.5 ppm) as the major impurities present.

Ohmic contacts to the samples are made by applying indium with an ultrasonic soldering iron. The crystals are n type with a bulk resistivity of 4.0 to 0.6 ohm-cm, as indicated in Fig. 12.4. Hall mobility is ~ 8000 cm^2 v^{-1} sec^{-1} at 52°K and decreases to 300 cm^2 v^{-1} sec^{-1} at 300°K. At temperatures greater than 77°K, Hall mobility apparently decreases as T^{-2}.

As shown in Fig. 12.4, after irradiation with 2.3×10^{18} Co^{60} gamma rays/cm^2, the room-temperature resistivity decreases by 35% and the Hall mobility decreases by $\sim 10\%$. The resultant carrier introduction rate is 0.006 carrier produced
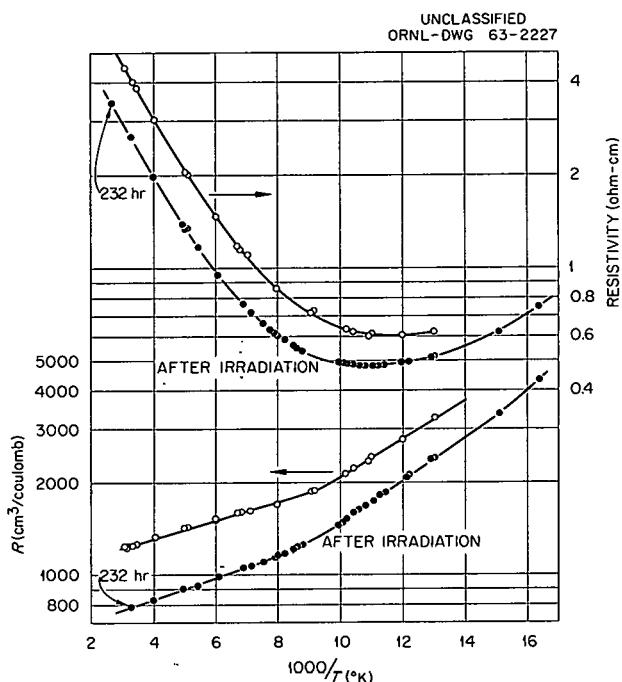
Fig. 12.4. Hall Coefficient and Resistivity Before and After 232-hr Gamma Irradiation vs $1/T$ for CdS.

per absorbed gamma photon[33] (3×10^{-4} per incident photon). The rate of introduction of carriers as indicated in Fig. 12.5 is not constant with dose.

From these Hall data there is no clear-cut evidence of a single level introduced by the Co^{60} gamma irradiation at room temperature. The large observed change in Hall coefficient is probably caused by the introduction of a number of shallow levels.

Photo Hall-effect measurements on a gamma-irradiated specimen show a decrease in mobility as well as in resistivity while light is shining on the sample. This mobility decrease precludes a predominance of the double acceptor state observed by Lorenz and Woodbury[34] upon heating CdS in a cadmium atmosphere. Such an acceptor state produced a marked increase in mobility with photo-excitation.

---

[33]Compare these results with those of J. W. Cleland and R. F. Bass, "Radiation Effects in Cadmium Sulfide (Part I)," this chapter.

[34]M. R. Lorenz and H. M. Woodbury, *Phys. Rev. Letters* **10**, 215 (1963).

Fig. 12.5. Number of Carriers Introduced vs Gamma Dose for CdS.

Fig. 12.6. Resistivity of Sample Warmed in Dark After Irradiation with Light Minus Dark Resistivity of the Sample vs Temperature.

with photoconductivity at temperatures less than 145°K. Gamma radiation introduces additional long photoconductivity decay components. These components persist up to room temperature. Figure 12.6 shows the persistence of the long decay time components vs temperature. To obtain the data[36] shown in Fig. 12.6, two samples, one irradiated with gamma rays and one unirradiated, were held in the dark until all photoconductivity had decayed. The samples were then cooled to 93°K and irradiated a few seconds with light. In the dark, the samples were then heated to room temperature at 2.5° per min. The change in sample resistivity (resistivity of the sample being warmed in the dark after irradiation with light minus the dark resistivity of the sample) vs temperature is plotted.

MINORITY CARRIER TRAPS IN GAMMA-IRRADIATED, ARSENIC-DOPED GERMANIUM

O. L. Curtis, Jr.[37]   J. H. Crawford, Jr.

Investigations of the minority carrier traps introduced into n-type germanium by Co^{60} gamma rays[38] have been continued. The isothermal annealing kinetics of both recombination centers and traps have been investigated. Figure 12.7 shows the effect of room-temperature aging and anneals for 1 hr at several elevated temperatures on the temperature dependence of minority carrier lifetime τ. The specimen in question was exposed to 10^{16} gamma rays/cm^2 at ice temperature. It is interesting to note that the fractional recovery of τ at room temperature after standing 71 hr is >0.50. Standing at room temperature, the minority carrier traps increase in concentration but decrease in apparent depth. This rapid-annealing (at room temperature) stage saturates at approximately the condition represented by the 71-hr room-temperature curve.

Optical absorption spectra[35] indicate a level at 0.55 ev which appears to grow with gamma irradiation. Irradiation with light in the 0.55-ev region does not produce a noticeable change in the bulk resistivity, indicating that this absorption band is associated with a localized optical excitation.

Gamma irradiation produces an increase in photoconductivity. Before gamma irradiation a long decay time, on the order of 30 hr, is associated

[35]We are indebted to C. T. Butler for his assistance in taking these spectra.

[36]We are indebted to O. E. Schow for his assistance in taking these data.

[37]Present address: Northrop Ventura, Newbury Park, Calif.

[38]See O. L. Curtis, Jr., and C. C. Robinson, Solid State Div. Ann. Progr. Rept. Aug. 31, 1962, ORNL-3364, p 88.
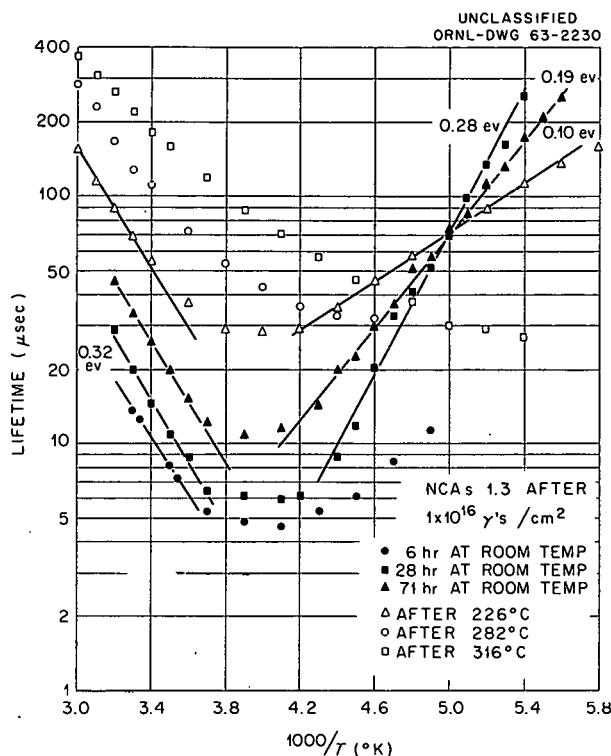
Fig. 12.7. Temperature Dependence of Minority Lifetime τ in a 1.3-ohm-cm Arsenic-Doped Germanium Specimen Exposed to 1×10^{16} Co^{60} Gamma Rays. The curves refer to measurement after room-temperature aging and 1-hr anneals at the indicated temperatures.

Fig. 12.8. The Temperature Dependence for the First-Order Rate Constants for the First-Stage Annealing of Irradiated Arsenic-Doped Germanium. The solid curve refers to 1.3-ohm-cm material. Two other points obtained for single runs on 2.5- and 5.4-ohm-cm material are shown for comparison.

Annealing at a higher temperature is necessary to accomplish further recovery, which is first accompanied by a further increase in trap concentration and a decrease in trap depth. One hour at 316°C is apparently sufficient to completely remove both traps and recombination centers.

The change in the apparent trap depth (from 0.28 ev to 0.10 ev) with annealing is rather surprising and suggests that a thermal transformation of the defects responsible for trapping is occurring during the anneal. The underlying process responsible for this behavior has not yet been established.

The rapid-annealing stage which occurs near room temperature has been investigated by isothermal measurements. After the residual change associated with the high-temperature stage has been subtracted, the process proceeds by a first-order law. The temperature dependence of the first-order rate constant k_1 is shown in Fig. 12.8 for a set of 1.3-ohm-cm arsenic-doped specimens; the

slope of the $\log k_1$ vs $1/T$ curve corresponds to an activation energy of 0.65 ev. Higher-resistivity specimens also exhibit a first-order recovery for this stage, but their smaller rate constants (see points marked NC As 5.4 and NC As 2.5, where the numbers correspond to the specimen resistivity) indicate that the recovery rate is greater the higher the arsenic content.

TRAPPING STUDIES IN GAMMA-IRRADIATED GERMANIUM

C. C. Robinson

Studies of radiation-induced trapping levels in germanium by low-temperature photoconductivity

measurements indicate that the phenomenon is a two-step process: the traps first "grow in" at low temperatures (<130°C); then they are annealed out at higher temperatures. This process is shown by Fig. 12.9, which is a composite of several samples.

These efforts are now being carried out in two parts: (1) a study of trap growth as a function of annealing, and (2) annealing out of traps at higher temperatures.

Exploratory experiments indicate that few, if any, traps are put into the crystal as a result of irradiation. Since there is not yet a sharp demarcation between the temperatures at which traps grow in and those at which they anneal out, a series of measurements at increasing temperatures is being made in which trap growth is allowed to go to saturation before the annealing temperature is raised. When a temperature at which the number of traps begins to decrease has been reached, the temperature range for trap growth will have been determined. Experiments will then be performed to determine the activation energy for trap growth in

samples of this carrier concentration and others of different purity and dopant.

Measurements on a 1-ohm-cm arsenic-doped sample indicate that this range is between 25 and 130°C. The sample was irradiated at 0°C. In order to eliminate any unobserved postirradiation annealing resulting from etching and/or other treatment at room temperature, the sample was coated with a thin film of polystyrene dissolved in toluene. This was allowed to dry thoroughly and served as surface protection during the irradiation. In addition, the sample was not allowed to come to temperatures above 0°C except for more than a few minutes during transfer to the experimental apparatus before the first measurements were made. After all changes that were going to occur at 25°C had been observed, the plastic coating was removed; and before and after measurements were compared. These indicated that the coating had no adverse effect on the experiment.

Consideration is also being given to analysis of that portion of the photoconductivity curve following the part associated with trapping for recombination lifetime studies. To do this requires assurance that there is no saturation of the photoconductivity as a function of the light intensities used in this experiment. This will be determined.

These studies will be extended to higher temperatures to determine the mechanism for the annealing-out traps.

An experimental apparatus using compressor-circulated helium in vacuum-jacketed tubes and sample chamber has been constructed. Sample temperature is set by an electrical controller which valves hot and cold gas that has previously passed through appropriate heat exchangers. The cold heat exchanger is a container filled with copper turnings submerged in a vacuum Dewar of liquid nitrogen or alcohol and dry ice. The hot exchanger is a copper-turnings-filled tube wrapped with an electrical tape heater. The current temperature range is −90°C (limited by an O-ring-sealed window soon to be replaced) to ~170°C. Temperature control is to approximately ±0.5°C.

Light is admitted through quartz windows in the inner and outer walls of the sample chamber. To suppress surface recombination effects, a thin germanium window filters out light having energy greater than the fundamental absorption edge. To avoid shifts in optical transmission when the germanium filter is heated by the light source, it is,

UNCLASSIFIED
ORNL-DWG 63-2232
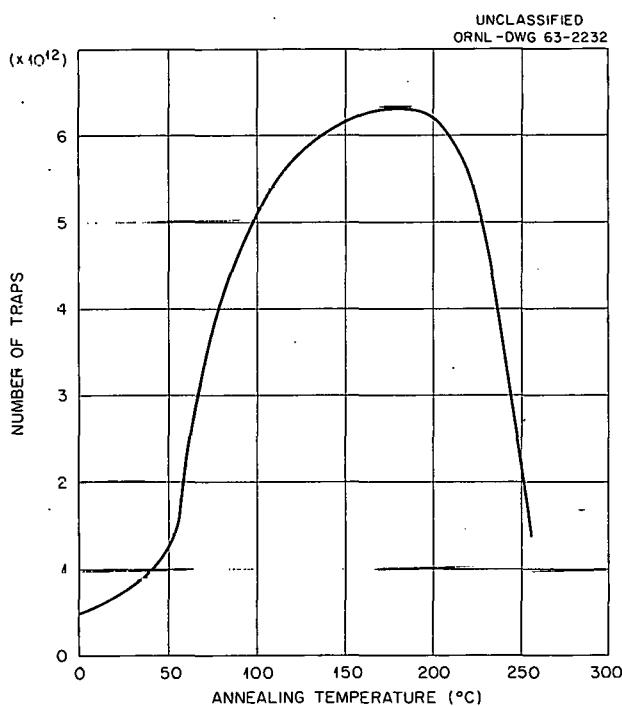
Fig. 12.9. Trapping in Low-Resistivity Arsenic-Doped Germanium as a Function of Successive 1-hr Isochronal Anneals.

and must be, on the inside of the inner chamber (that is, at the same temperature as the sample).

Of particular experimental interest is the technique used to pass electrical leads into the chamber. Experimenters have always faced the problem of running lead wires into an inner vacuum-jacketed chamber because of leaky Kovar seals, excessive heat transfer, and disassembly of soldered parts. These problems have been avoided by extending a thin-wall stainless steel tube from the inner chamber through a hole in the outer chamber (shown in Fig. 12.10). This tube is vacuum jacketed by a tubular extension of the outer chamber for a distance of 3 in. Wires from the sample pass down the length of the inner tube and through Kovar seals. The Kovar seals are always at or near room temperature; and because the air in the tube is not moving and the thermal conductivity of stainless steel is low, no difficulty has been experienced with heat losses or gains or leaky seals due to different coefficients of expansion.

These samples have no leads soldered to them; rather, pressure contacts are used. These are held in place by spring-loaded copper clamps. This arrangement has greatly reduced time lost because of contacts broken by different coefficients of expansion of the sample and rigidly held lead wires.

INNER CHAMBER

VACUUM

LEAD WIRES

KOVAR SEALS

OUTER CHAMBER
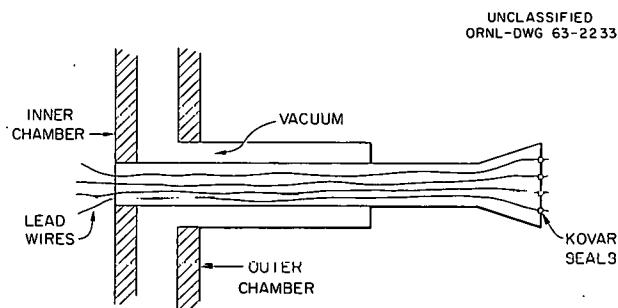
Fig. 12.10. Sample Chamber Wiring Technique.

GAMMA IRRADIATION OF SILICON

Edward Sonder   L. C. Templeton

n-Type Material

A careful study of radiation-introduced levels in the upper half of the energy gap, with particular attention to effects of concentration and species of donor atoms and oxygen content, has been completed. Results have been submitted for publication in the *Journal of Applied Physics*; an abstract[39] follows:

Measurements of the electrical properties of gamma-irradiated float-zone silicon have been used to locate a number of net acceptor levels in the upper half of the forbidden gap. In material doped with less than 10^{16} donors, a level due to a vacancy—oxygen atom pair located 0.17 ev below the conduction band is introduced at a rate comparable to its introduction in oxygen-containing material. However, in addition, there is introduced a level located 0.47 ev below the conduction band in phosphorus-doped float-zone silicon. The latter level is presumably due to vacancy-donor complexes. Annealing above 150°C removes the deep level; further irradiation and annealing causes the reappearance of a deep net acceptor level at 0.47 ev. In irradiated and annealed silicon, an additional net acceptor level at 0.21 ev below the conduction band was observed.

p-Type Material

In previous work[40] it was noted that radiation-induced changes of electrical properties appeared at different rates in oxygen-containing silicon than they did in float-zone material. These differences have been investigated further. In oxygen-containing material, a net donor level appears, located $\sim$0.35 ev above the valence band and introduced at a rate of 9×10^{-5} level/cm^3 per photon/cm^2. The center responsible for this level is stable at room temperature and shows no sign of annealing at 100°C.

In material grown by the floating-zone technique, a net donor level closer to the valence band becomes apparent. Data for one of the samples is reproduced in Fig. 12.11. The steep portion near $1/T = 6$ of the uppermost curve yields $E - E_v = 0.21$ ev for the position of the level. The center responsible for this level is not stable above room temperature. Moreover, its rate of introduction at room temperature decreases with increasing total radiation dose, suggesting that some of the centers giving rise to the 0.21-ev level disappear again during irradiation at room temperature.

[39]Edward Sonder and L. C. Templeton, abstract of a paper to be published in *Journal of Applied Physics*.

[40]Edward Sonder and L. C. Templeton, *Solid State Div. Ann. Progr. Rept. Aug. 31, 1961*, ORNL-3213, p 61.
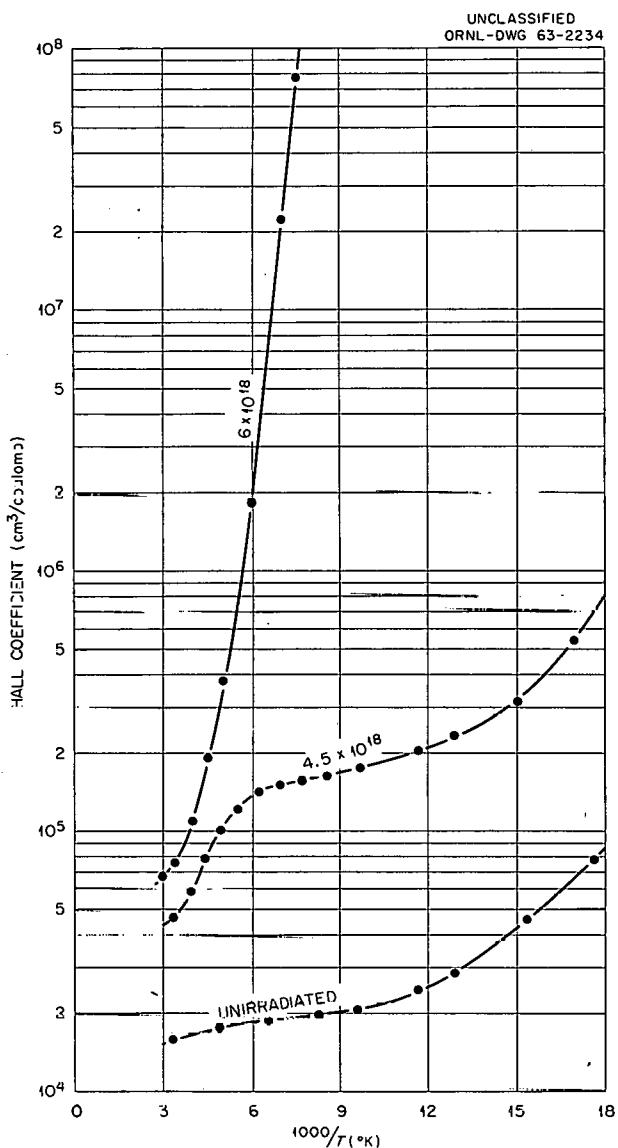
Fig. 12.11. Hall Coefficient vs Temperature for Gamma-Irradiated p-Type Float-Zone Silicon. The three curves are for the same sample, measured after irradiation to the total dose (photons/cm^2) shown on the curves.

In addition to the level at $E - E_v = 0.21$ ev, the data show the introduction of a deeper level, apparent from the room-temperature ($1/T = 3$) Hall coefficient, which increases with irradiation. The position of this level has not yet been determined, but it would not be surprising if it were the same as the level observed in oxygen-containing silicon. The introduction rate found for the deeper level in specimen 216-5A is 6×10^{-5} level/cm^3 per photon/cm^2, which is slightly less than the rate of introduction of the 0.35-ev level in oxygen-containing material.

In contrast to n-type silicon, where our results were, for the most part, consistent with other work[41,42] (specifically, the identification of defect centers by Watkins and Corbett[43]), the present results are not consistent with other work. Wertheim[41] located a level at $E - E_v = 0.27$ ev in gallium-doped, crucible-grown silicon. Klein[44] gives $E - E_v = 0.31$ ev in neutron-irradiated material. We obtain 0.35 ev in boron-doped material. Moreover, the fact that the center giving rise to the 0.35-ev level seems to be connected with oxygen is inconsistent with Watkins' scheme,[43] in which a level near $E - E_v = 0.3$ ev is attributed to the divacancy. Also, Watkins has not reported observing any center that would give rise to the level we have observed in oxygen-free material at 0.21 ev above the valence band, although a level near 0.16 ev above the valence band has been observed in neutron-irradiated silicon.[44]

It is clear that more data are necessary before some of these discrepancies can be cleared up.

[41]G. K. Wertheim, *Phys. Rev.* **110**, 1272 (1958).

[42]H. Saito, M. Hirata, and T. Horiuchi, *J. Phys. Soc. Japan* **18**, suppl 3; 246 (1963).

[43]G. D. Watkins and J. W. Corbett, *Discussions Faraday Soc.* **31**, 86 (1961).

[44]C. A. Klein, *J. Appl. Phys.* **30**, 1222 (1959).

13. Insulating Crystals

ROOM-TEMPERATURE RADIATION CHEMISTRY OF ELECTRON-EXCESS CENTERS IN KCl

Edward Sonder   W. A. Sibley

A study of radiation-induced changes in the negative-ion imperfection structure of alkali halides has been under way, using chiefly optical absorption measurements. The study of the radiation equilibrium between F- and M-centers described previously[1] has been completed and published in the *Physical Review.*[2] An abstract follows:

A study of F- and M-center coloration by electron-irradiating single crystals of KCl is made as a function of radiation intensity, electron energy, and crystal preparation. The quadratic relation between M-center and F-center concentration in any particular sample, previously observed for both x-ray and gamma irradiation, is verified for electrons if a constant current is used throughout the irradiation. However, the ratio of M-center concentration to the square of the F-center concentration is dependent upon electron current and sample preparation. Moreover, if a specimen is irradiated at one radiation intensity for a long period and then the intensity is changed for a short time, the relative M- and F-center concentrations are characteristic of the last irradiation intensity. It is concluded from this result that a dynamic equilibrium exists between F-centers and M-centers during irradiation. Interpretation of the results is proposed in terms of four simultaneous processes producing and destroying F-centers and M-centers respectively. The processes for destruction of F-centers and creation of M-centers are thought to involve a mobile imperfection created by the irradiation. Means by which small concentrations of impurities can affect some of these processes to change the F-M-equilibrium and F-center coloring curves are discussed.

In the above and previous work, the coloration efficiency in heavily colored KCl was observed to decrease continually as more F-centers were produced. It was suggested that a radiation destruction of F-centers occurred, together with the production of F-centers. The relation between this destruction process and agglomeration reactions (e.g., two F-centers forming an M-center) was unclear.

In order to obtain more information on this question, a specimen of Harshaw KCl (the apparent saturation of late-stage coloration is quite pronounced in all Harshaw KCl samples so far studied) was thinned to 127 μ by polishing, to make optical measurements possible after very heavy coloration. The sample was colored at room temperature with electrons at a relatively low current density of 0.02 $\mu a/cm^2$ until it approached an F-center saturation level near 2×10^{18} cm^{-3}. The measured absorption coefficients at the peak of the F- and M-bands plotted vs the total energy absorbed are shown in Fig. 13.1. At a total absorbed energy of 4.8×10^{16} Mev/cm^3 (see Fig. 13.1), the dose rate was increased a factor of 15, and thereafter irradiation was continued alternately at the high and low intensities.

Considering first the last section of the curves of Fig. 13.1, it seems that both the F- and M-center concentrations are decreasing with dose at the low radiation intensity. Unfortunately, the magnitude of the observed effect is barely outside experimental error. However, if this decrease is confirmed in other measurements, it would verify that in this material there is an asymptote to which the F-center concentration tends after long

[1] Edward Sonder and W. A. Sibley, *Solid State Div. Ann. Progr. Rept. Aug. 31, 1962,* ORNL-3364, p 105.

[2] Edward Sonder and W. A. Sibley, *Phys. Rev.* **129**, 1578 (1963).
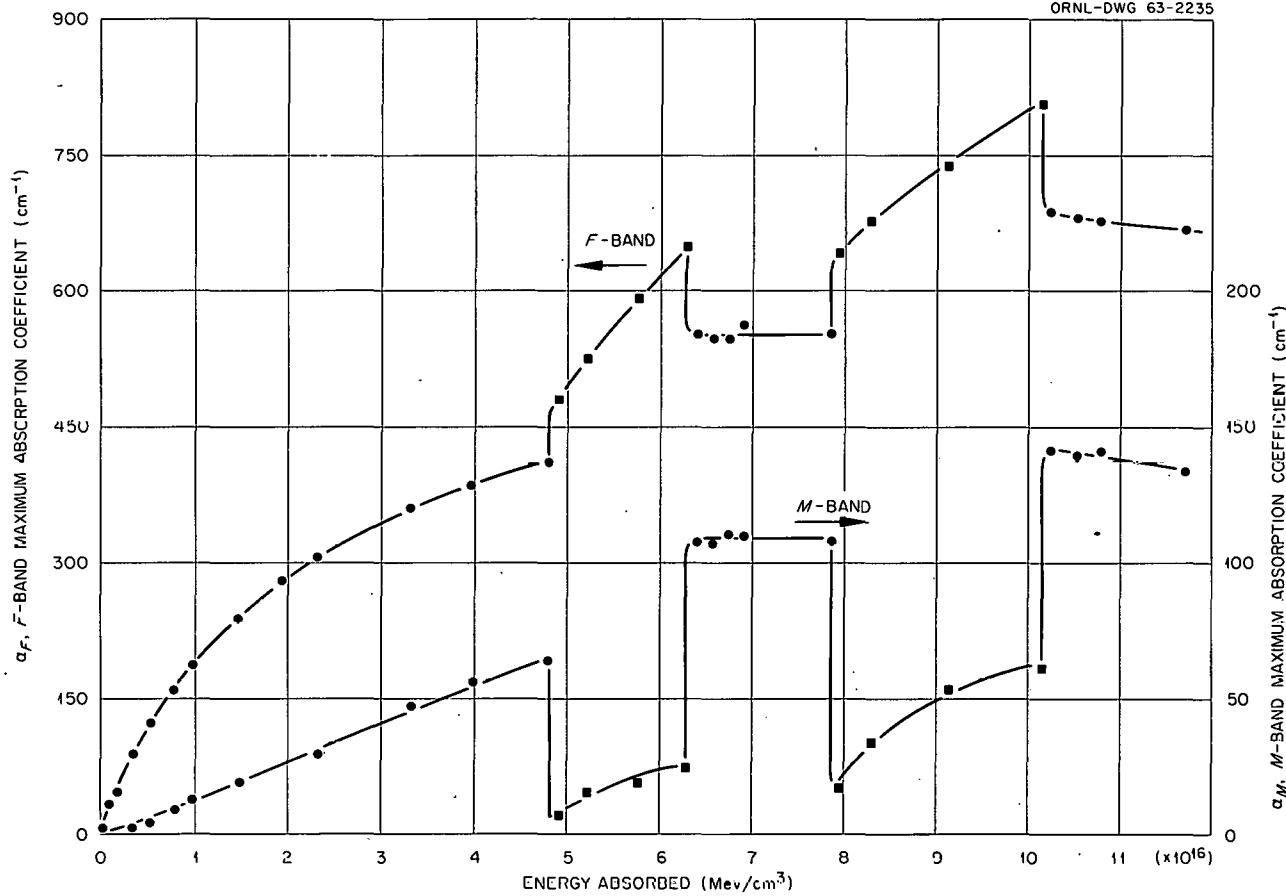
Fig. 13.1. Optical Absorption Coefficient at the Peak of the F- and M-Bands vs Absorbed Energy. The circles are for determinations immediately after 1.5-Mev electron irradiation at a current density of $0.02 \, \mu a/cm^2$; the squares are for determinations after irradiation at $0.3 \, \mu a/cm^2$.

irradiation. This asymptote is, of course, a function of radiation intensity and probably varies in different samples. However, it clearly would indicate that destruction of F-centers is proceeding at the same rate as their creation. Moreover, the long time necessary to approach saturation would indicate that these creation and destruction processes are very slow.

Considering next the F- and M-center concentration changes at the moments the radiation intensity is changed, it is evident that these changes, as has been stated before, are very rapid relative to the rate of actual production or destruction of color centers. In fact, on the scale of Fig. 13.1 they are instantaneous. This shows that the two sets of processes, one determining the F-center–M-center radiation equilibrium and the other being

responsible for the actual creation of F-centers irrespective of their state of agglomeration, can be studied independently.

It is of interest that on changing the dose rate, the decrease (or increase) of F-band height consistently equaled the increase (or decrease) of the M-band height. (It was only after the last change of irradiation intensity that the decrease of F-band height was appreciably greater than the increase of M-band height. However, a significant concentration of R-centers, which are presumably tri-F-centers,[3] was observed in this case. These would account for the difference.) The

---

[3]H. Pick, Z. Physik **159**, 69 (1960).

relative number of F- and M-centers involved in these changes (Δn) can be estimated since

$$\Delta n = 7.2 \times 10^{15}\, \Delta\alpha\,\epsilon/f \,,$$

where $\Delta\alpha$ is the change in absorption coefficient of the band in question, ϵ is the bandwidth at half maximum in electron volts, and f is the oscillator strength of the F- or M-bands. However, as shown by Okamoto,[4] higher energy bands of the M-center occur under the F-band so that

$$\Delta\alpha_F\,(\text{obs}) = \Delta\alpha_F - a\Delta\alpha_M \,,$$

where a is near unity. With the use of this information, the fact that $\Delta\alpha_F$ (obs) was approximately equal to $\Delta\alpha_M$, and the ratios[5] $\epsilon_F/\epsilon_M = 2$ and $f_M/f_F = 0.43$, it is found that $\Delta n_F/\Delta n_M = 1.7$. With uncertainty still remaining concerning the oscillator strength ratio as well as the amount of M-center absorption under the F-band, this figure may be considered as being consistent with the idea that all the F-centers disappearing *rapidly* on a decrease of dose rate appear in pairs as M-centers and, conversely, that, on increasing the radiation intensity, the rapidly disappearing M-centers simply break up to form two F-centers each.

VARIATION OF SOME OF THE PHYSICAL PROPERTIES OF COMMERCIALLY AVAILABLE KCI SINGLE CRYSTALS

C. T. Butler   W. A. Sibley
Edward Sonder

Studies at the Laboratory on F- and M-band introduction in KCl by ionizing radiation[6,7] have shown that late-stage coloring properties vary greatly among crystals obtained from various sources. As a result of this finding, the authors felt it necessary to point out in the literature just how great the variations in F-coloration rates are among crystals even from one supplier. To further emphasize the variability of physical properties of commercial KCl crystals, data on ultraviolet-excited luminescence and light scattering were added to that on F-coloration rates. The information for materials from the Harshaw Chemical Company will appear in the *Journal of Chemical Physics*,[8] and additional information will appear in a Bulletin of the Research Materials Information Center.[9] A summary of the work is presented below.

It has been known for some time that first-stage coloration rates vary considerably among samples from different sources. However, the present data show that late-stage coloration curves for material from different sources vary in slope over a range of about 15:1; those for samples purchased from the Harshaw Chemical Company over a period of a few years vary by a factor of about 3 to 4. Coloration curves for crystals taken from various places in a $1 \times 2 \times 3$ in. Harshaw crystal even vary over about a 20% range. No single impurity which would account for the observed variation was found in the crystals. Ultraviolet-excited luminescence spectra of KCl from several commercial sources show great variation in both character and intensities of luminescence bands. In general, the spectra of KCl from different sources hardly resemble one another. Samples purchased at different times from any one supplier show both qualitative differences and order-of-magnitude quantitative differences, whereas samples purchased at the same time show (with a few exceptions) only quantitative differences of typically less than about 50%. The light-scattering power both of crystals obtained from various manufacturers and of those from any single manufacturer vary by a factor of about 10. Again, as in coloration, no obvious correlation exists between the scattering power and known impurities.

These results demonstrate that variations of some physical properties in presently available alkali halides may be very much larger than has been realized. One is forced to view with some trepidation the tendency to consider results obtained on samples from one ingot as representative of a particular alkali halide. It is fairly

[4]F. Okamoto, *Phys. Rev.* 124, 1090 (1961).

[5]C. J. Delbecq, *Z. Physik* 171, 560 (1963).

[6]W. A. Sibley and Edward Sonder, *Phys. Rev.* 128, 540 (1962).

[7]Edward Sonder and W. A. Sibley, *Phys. Rev.* 129, 1578 (1963).

[8]To be published in the *Journal of Chemical Physics* for July 1, 1963.

[9]Research Materials Information Center Publication, ORNL RMIC-1, June 1963.

obvious that, in any research involving measurements of the properties mentioned above and probably others as well, great care must be taken to ensure uniformity of samples. Intercomparison of such results with different measurements made at different laboratories should be viewed with suspicion unless a procedure has been adopted in which, for instance, pieces from the same portion of a single ingot have been shared by the laboratories making the various measurements.

HARDENING OF POTASSIUM CHLORIDE SINGLE CRYSTALS BY QUENCHING AND IRRADIATION[10]

Kazou Akimoto[11]   W. A. Sibley

The effect of heat treatment and irradiation on the mechanical properties of potassium chloride single crystals of varying impurity concentrations was investigated. Some specimens were quenched in cold acetone ($0°C$) from temperatures over the range 100 to $650°C$, and other samples were irradiated with Co^{60} photons or with 1.5-Mev electrons to doses of 10^{19} photons or about 3.8×10^{15} electrons respectively. The quenching results are most easily explained in terms of the dissociation of vacancy-impurity complexes for temperatures to $375°C$. It was not possible at the quenching rate utilized to quench thermal vacancies in the lattice. Also, even for quench temperatures below $375°C$, there is evidence that some annealing of the defects occurred. Another interesting observation is that relatively impure samples have quite different hardening properties for a given dose of irradiation, electron or gamma, than do the purer specimens.

HARDENING OF KCl BY ELECTRON AND GAMMA IRRADIATION[12]

W. A. Sibley   Edward Sonder

Measurements of the flow stress and F-band coloration have been made at room temperature on a number of different samples of KCl as a function of gamma and electron irradiation. The rate of increase of flow stress with irradiation is found to be greater in samples and for irradiation conditions for which the coloring rate is greater, and smaller when the coloring rate is smaller. Moreover, the flow stress increase in any set of samples is proportional to the square root of the F-band absorption. The implication is that hardening is caused by either F-centers or other defects whose production is related to the production of F-centers. Since bleaching of F-centers does not produce any softening and since the magnitude of the hardening is of the order of magnitude to be expected for interstitial-type defects, it is concluded that the increase of flow stress due to irradiation of KCl is caused by interstitial chlorine atoms or interstitial clusters.

LIGHT SCATTERING IN ALKALI HALIDE SINGLE CRYSTALS

W. A. Sibley

Introduction

Light scattering can be used in transparent solids to obtain estimates of the size, shape, and concentration of the scattering units within the material. Unfortunately, in some transparent solids, particularly the alkali halides, there can be several different types of scattering units present; this makes the interpretation of the scattering data more difficult. For example, the possible scatterers in KCl single crystals are precipitates, vacancy-impurity clouds around dislocation lines, grain boundaries, cavities, etc.[13-17] Therefore, the scattering data may be somewhat more difficult to evaluate for these crystals than for solids containing only one type of scattering unit. However, it is hoped that careful experiments and a comparison of all the available experimental

---

[10]Abstract of a paper which will be published in the June 1963 issue of the *Journal of Applied Physics.*

[11]Present address: Chou University, Tokyo, Japan.

[12]Abstract of a paper to be published in the August 1963 issue of the *Journal of Applied Physics.*

[13]S. P. F. Humphreys-Owen, *Proc. Phys. Soc. (London)* B68, 325 (1955).

[14]K. G. Bansigir and E. E. Schneider, *J. Appl. Phys.* 33, 383 (1962).

[15]O. Theimer, C. A. Plint, and W. A. Sibley, *Ann. Phys.* 9, 475 (1960).

[16]O. Theimer and C. A. Plint, *Ann. Phys.* 3, 408 (1958).

[17]C. A. Plint and W. A. Sibley, *J. Appl. Phys.* 33, 3167 (1962).

observations with theory will allow a determination of the types of scattering units which are dominant and also their characteristic sizes, shapes, and concentrations.

The present work has a multiple purpose. First, to determine (by measurements of the wavelength dependence, angular dependence, crystal-orientation dependence, and depolarization ratios of the light scattering) the character of the dominant scattering units within the crystals. Second, to find out what type or types of defects compose the scattering centers within each scattering unit (e.g., vacancies around an edge dislocation would form a cylindrically shaped scattering unit with vacancies as the scattering centers). Third, to investigate the extent to which the "bad regions" (which are the scattering units) contribute to the formation of defects under ionizing radiation.

Experimental Procedure

The crystal ingots used in this research were purchased from the Harshaw Chemical Company, the Isomet Corporation, and the Optovac Corporation. In the case of the angular-dependence investigations, it was found best to use cylindrically shaped single crystals 2.5 cm high and about 5 cm in diameter with the cylinder axis a [100] crystallographic direction. The [010] and [100] directions in the cylindrical samples were determined by x-ray photography. Crystals of almost any shape could be used for determining the wavelength dependence of the scattering, and the minimum usable size was about 5 cm^3. Table 13.1 shows the crystal designation, purchase date, and Rayleigh ratio,

$$R_u = R^2 i / I_o V,$$

where

R = the distance of the observer from the scattering units,

i = the intensity of the scattered light,

V = the scattering volume,

I_o = the intensity of the incident light,

for incident light of wavelength $\lambda = 546$ mμ and for a scattering angle $2\theta = 90°$, for each of the samples investigated.

The intensity of the scattering light was measured using an EMI 6256S multiplier phototube which could be rotated around a cylindrical quartz holder containing the sample and the index liquid, ben-

zene. The incident light beam originated from a 300-w concentrated arc lamp and passed through a Bausch and Lomb half-meter monochromator before entering the crystal as a parallel beam of rectangular cross section. The intensity of the incident beam as a function of wavelength was found by using the same multiplier phototube used for the scattered light and by attenuating the incident beam with Cary optical filter assemblies. The intensity of the light scattering for $2\theta = 90°$ was about 10^{-7} of the incident beam intensity. The volume of the sample "observed" by the detector was about 6 mm^3. The normal precautions were taken to avoid stray light in the systems,[15] and as an additional check the wavelength dependence, dissymmetry, and depolarization ratio of the scattered light was measured for benzene and for lead silicate glass.[18] It was found that inserting a 2.5-cm-diam glass bottle containing distilled water into the incident beam did not give the Rayleigh law wavelength dependence. The scattered intensity for the water was comparable with that for the KCl sample which gave the lowest scattering power; therefore, there is some doubt as to the accuracy of the wavelength dependence for this sample, 0:103C. In this connection it should be mentioned that the mismatch in the indices of refraction between water and benzene (or glass) was much greater than that between the crystals and benzene; thus, a much higher surface scattering can be expected for the water.

The polarization measurements were made at $\lambda = 546$ mμ with Polaroid Corporation HN32 plastic laminated polarizers. A consideration of the reproducibility of the depolarization results and all the possible errors and corrections inherent in these measurements, as enumerated by Goldstein[19] and reviewed by Stacey,[20] indicated that the observations are accurate to only about 20%.

All the angular-dependence data for the scattering power $P = i_{2\theta}/I_0 V$ which are presented were corrected with the factor sin 2θ, which accounts for the fact that the scattering volume "seen" by the detector depends on the scattering angle as $1/\sin 2\theta$. Also, the Thompson factor $(1 + \cos^2 2\theta)$

[18]This sample was kindly furnished by E. Lell of Bausch and Lomb.

[19]M. Goldstein, *J. Appl. Phys.* **30**, 493 (1959).

[20]K. A. Stacey, *Light Scattering in Physical Chemistry*, Academic Press, New York, 1956.

Table 13.1. Rayleigh's Ratios, Dissymmetries, and Depolarization
Ratios of Several KCl Single Crystals

Sample	Purchase Date	Φ	$R_u \times 10^6$ [a,b]	z	ρ_u^a	ρ_v^a	ρ_b^a
Benzene			16.5	0.98	0.420	0.265	
EDF-1-2	Oct. 1961	0	28.1	0.99	0.066	0.029	
		45	28.0	0.99	0.067	0.030	
H:40	Feb. 1961	0	7.1		0.524		
H:100	June 1961	0	6.1		0.483		
H:105C	Jan. 1962	0	13.1	2.4	0.337	0.147	0.544
		45		2.0	0.283	0.031	0.112
H:107C	June 1962	0	15.0	2.6	0.217	0.070	
		45		2.8	0.187	0.036	
I:100	Nov. 1961	0	1.8				
I:101	Apr. 1962	0	1.6				
I:102C	Oct. 1961	0	5.0	2.1	0.444		
		45		2.8	0.537	0.063	
I:103C	June 1962	0	8.6	2.9	0.578		
		45		3.5	0.461	0.068	
I:104C	June 1962	0	18.0	2.0	0.625	0.214	0.388
		45		2.4	0.630	0.114	0.178
O:100	Aug. 1962	0	4.4		0.320		
O:103C	June 1962	0	1.3	2.9			
		45		2.9			
O:104C	Oct. 1962	0	3.1	2.8	0.083		
		45		3.3	0.136		

[a] All these measurements were made for $\lambda = 546$ mμ; $2\theta = 90$.

[b] These numbers are normalized to that for pure benzene, which is taken as the average of those given in ref 24.

has been removed. The scattering power of benzene when depicted in this manner should be constant as a function of scattering angle; therefore, the dissymmetry $i_{45°}/i_{135°}$ should be unity.

.The optical absorption measurements were made on crystalline plates of thickness 0.1 cm or less which were cleaved from the samples used for the light-scattering observations. The irradiations were performed in a 4.1×10^6-r/hr Co^{60} gamma source with the crystalline plates placed in light-tight holders, which were equipped with slides to permit measurement of the absorption spectra of the specimens. Further details of the color-center aspects of this work have already been published.[21]

Results

Light Scattering. — A large variation of the wavelength dependence and magnitude of the scattering power is observed for the different alkali halides and even among the different KCl crystals. Figure 13.2 pictures the wavelength dependence when the incident light beam is along a <100> direction and $2\theta = 90°$ for two crystals of KCl and one sample each of KBr and LiF, all purchased from Harshaw. Although the KBr sample

[21] W. A. Sibley and Edward Sonder, *Phys. Rev.* **128**, 540 (1962).

has a higher scattering power than any of the other specimens, the LiF crystal has a scattering power between those for the two KCl samples shown. Figure 13.3 shows the wavelength dependence for several samples of KCl obtained from different suppliers. The purchase dates of these crystals are given in Table 13.1, and no correlation with the light-scattering intensity was found. It is clear from Figs. 13.2 and 13.3 that it is not possible at this time to find the effect of the host matrix (e.g., KCl, LiF, or KBr) on the scattering units. Also, the scattering is apparently
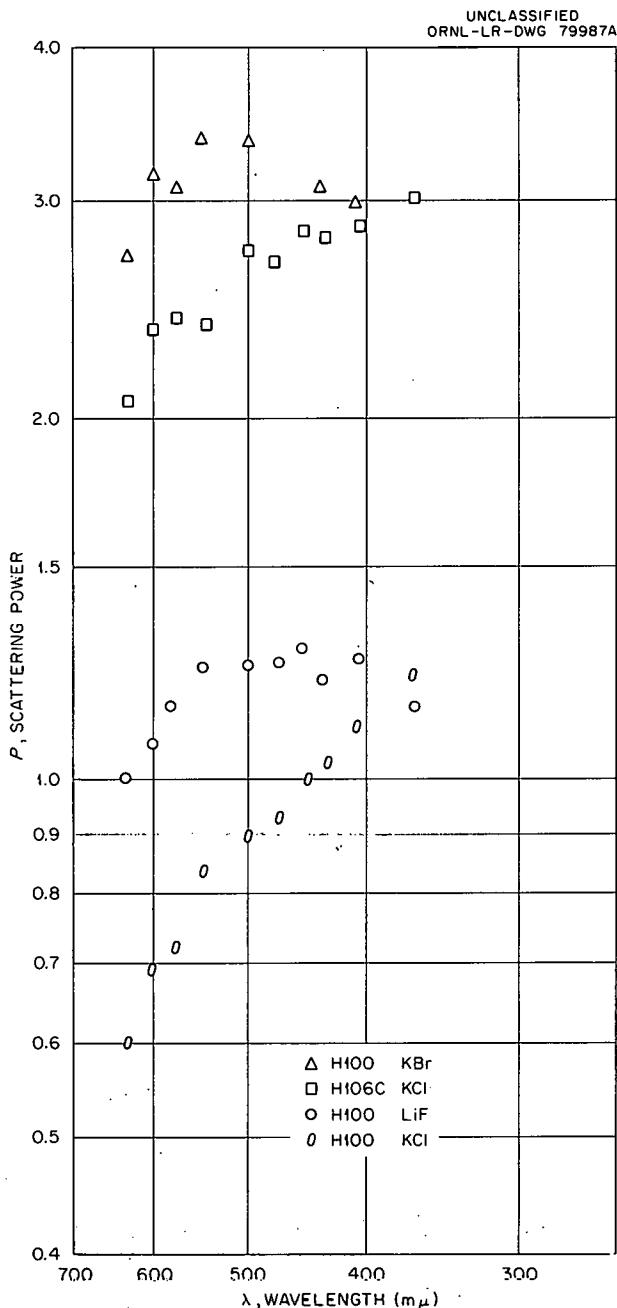
Fig. 13.2. Wavelength Dependence of the Scattering Power of LiF, KCl, and KBr Single Crystals. The wavelength λ is the wavelength of the incident beam in air.
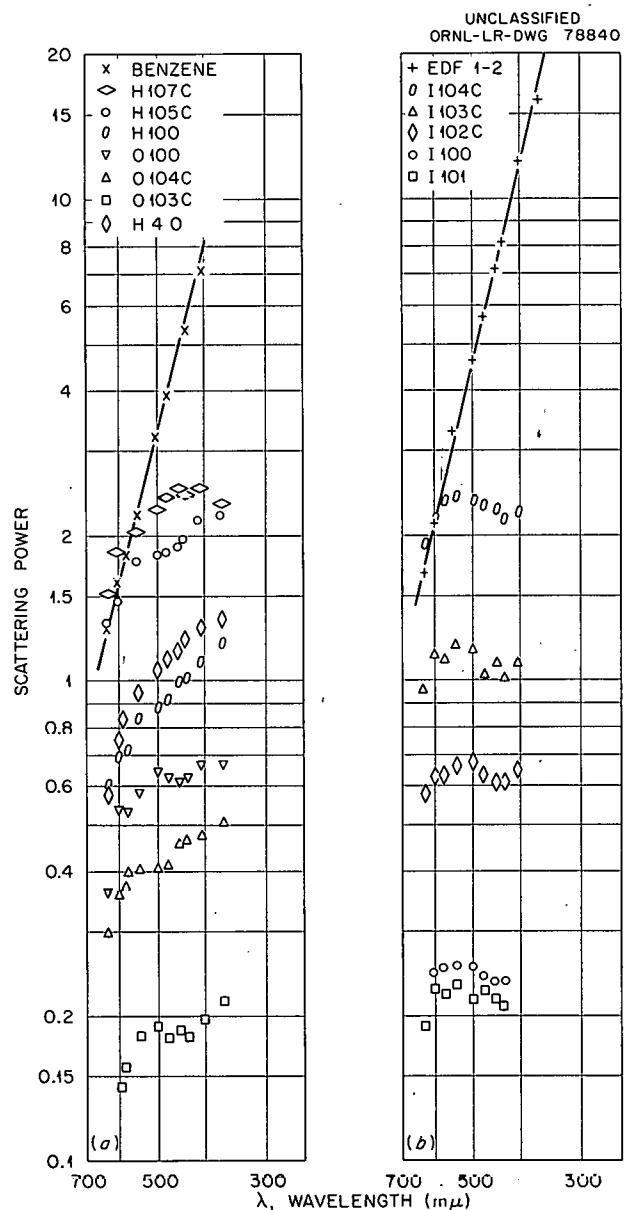
Fig. 13.3. Wavelength Dependence of the Scattering Power of Benzene, Lead Silicate Glass (EDF-1-2), and KCl Single Crystals Produced by Different Commercial Companies.

done by centers which are not intrinsic defects, such as vacancies, but extrinsic imperfections, such as impurities of various types. If this were not so, it would seem that the variations in scattering power among crystals from the same supplier and having the same approximate dislocation density should be less. An estimate of the absolute scattering power of these samples can be obtained by a comparison with the scattering from benzene (Fig. 13.3). The slope of the logarithm of the scattering power of benzene as a function of the logarithm of the wavelength is 4, as would be expected for Rayleigh scattering.

Previously, it has been observed that KCl crystals grown by Harshaw possessed an orientation dependence of the light scattering.[15] It is now possible, using an improved experimental apparatus and observing a smaller volume element within the crystals, to make a more complete study of this orientational dependence in crystals of different types and obtained from different sources. The angular dependence of the light scattering for two different orientations of the crystals is shown in Fig. 13.4 for two KCl crystals and for benzene. The open data points were taken with the crystals oriented so that the incident light beam was along a <100> crystalline direction. The full data points represent the angular dependence with the incident light beam along a <110> crystalline direction. This same procedure has been used throughout so that full data points always represent an orientation $\Phi = 45°$ with the incident beam along <110>, and the open points are for the incident light along <100>, $\Phi = 0°C$. The interesting aspects of Fig. 13.4 are the height of the peak for sample H:105C and the fact that there is no evident orientational dependence for the sample 0:104C. It should be mentioned that all the Harshaw and Isomet crystals, which could be used for investigating the angular dependence, had the orientation dependence; however, none of the Optovac specimens had a marked orientation dependence. The shape and height of this orientation peak were observed to vary from sample to sample, and Fig. 13.5 illustrates that even within one sample (I:104C) there can be a large variation, depending on which volume element of the crystal the detector observes. Sample I:104C was not a typical sample since the variations in the peak were not usually so pronounced, and it was found, when this sample was cleaved into two equal halves, that a rather large

polycrystalline grain had grown into the middle of the specimen. The well-formed peak in Fig. 13.5 was found for the good part of the crystal, and the peak shape became progressively worse as more of the polycrystalline section came into the observed volume element. The orientational dependence was also observed, as shown by Fig. 13.6, for Harshaw LiF and Harshaw KBr, although a complete investigation of these samples was not attempted.
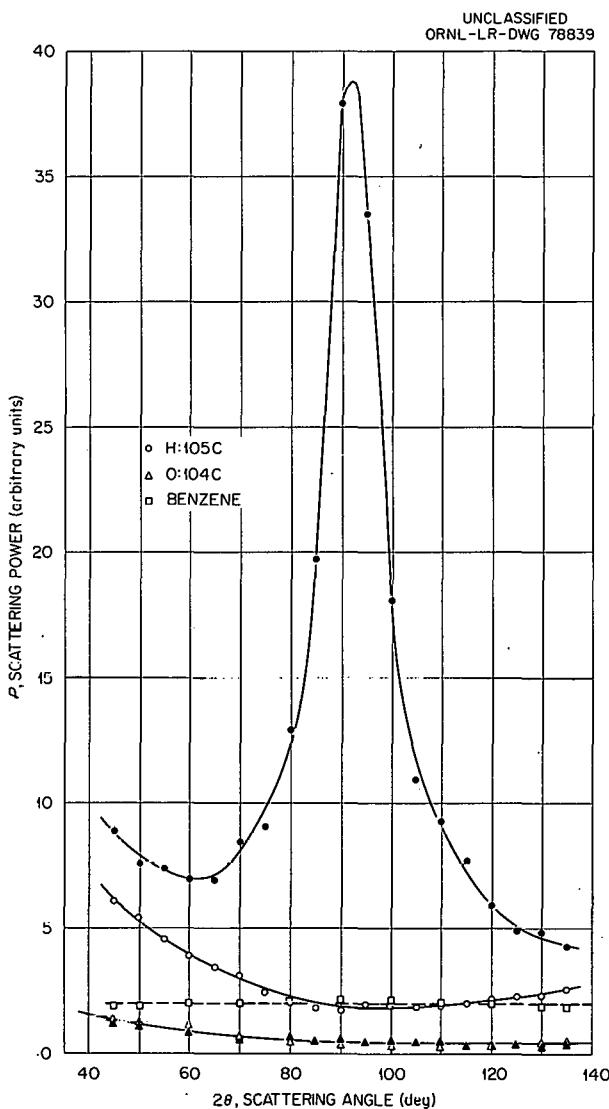
Fig. 13.4. Angular Dependence of the Scattering Power of Benzene and of KCl Crystals H:105C and O104C. The orientation $\Phi = 0°$ is shown by the open symbols, and $\Phi = 45°$ is represented by the full symbols.
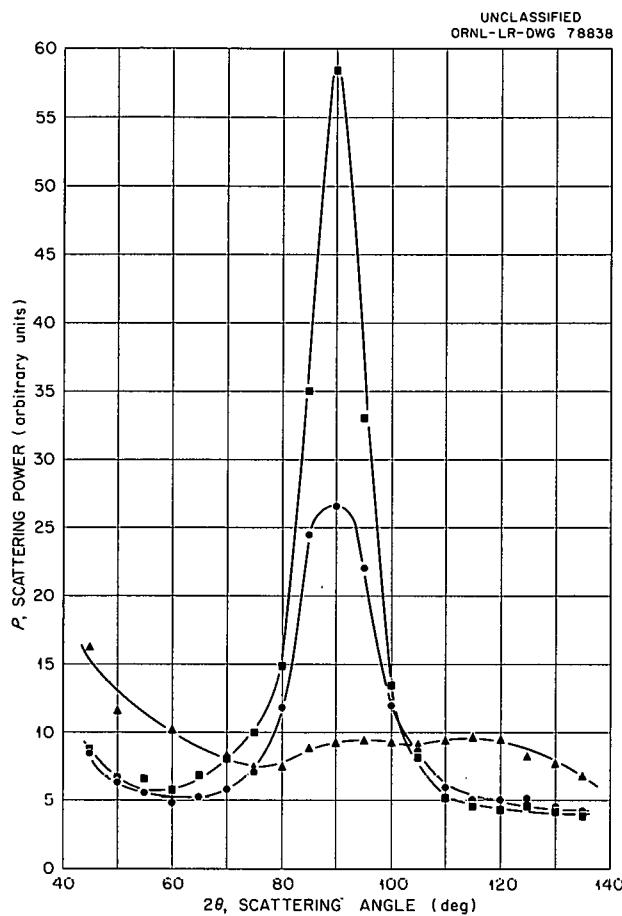
Fig. 13.5. Angular Dependence of the Scattering Power of One KCl Crystal 1104C as a Function of Position Within the Sample.

The depolarization and dissymmetry measurements are summarized in Table 13.1. As has been mentioned for the orientation $\Phi = 45°$, the pattern has the large scattering peak at $2\theta = 90°$. If Φ varies by a few degrees, then the peak shifts by twice this amount;[15] and, since the crystals could only be oriented to within $\pm 2°$ of $\Phi = 45°$, the measurements taken from a specific angle depend on the position and shape of the scattering peak. Therefore, the accuracy of the dissymmetry and depolarization measurements for the orientation $\Phi = 45°$ is not very good except where special care was taken to orient the crystal precisely, as in sample H:105C. The depolarization ratios are defined in the following manner:

$$\rho_u = H_u/V_u, \quad \rho_v = \frac{\overline{\alpha^2_{yz}}}{\overline{\alpha^2_{zz}}} = \frac{H_v}{V_v}, \quad \rho_h = \frac{V_h}{H_h},$$

where the intensities of the horizontal and vertical components of the light scattered at $2\theta = 90°$ are denoted by H and V, respectively, and the subscripts u, h, and v denote unpolarized, horizontally polarized, and vertically polarized incident light respectively. In every crystal it was observed that, within experimental error, the relation $H_v = V_h$ was obeyed. A system of optically isotropic spherical scattering units irrespective of size should give $\rho_v = 0$; it is clear from the table that, in all the crystals investigated, this case does not obtain.

Other Measurements. — In an effort to determine if a correlation could be found between the "bad regions" associated with the light scattering and other properties of the crystals, several other measurements were made. Since the scattering power of the various samples is observed to vary
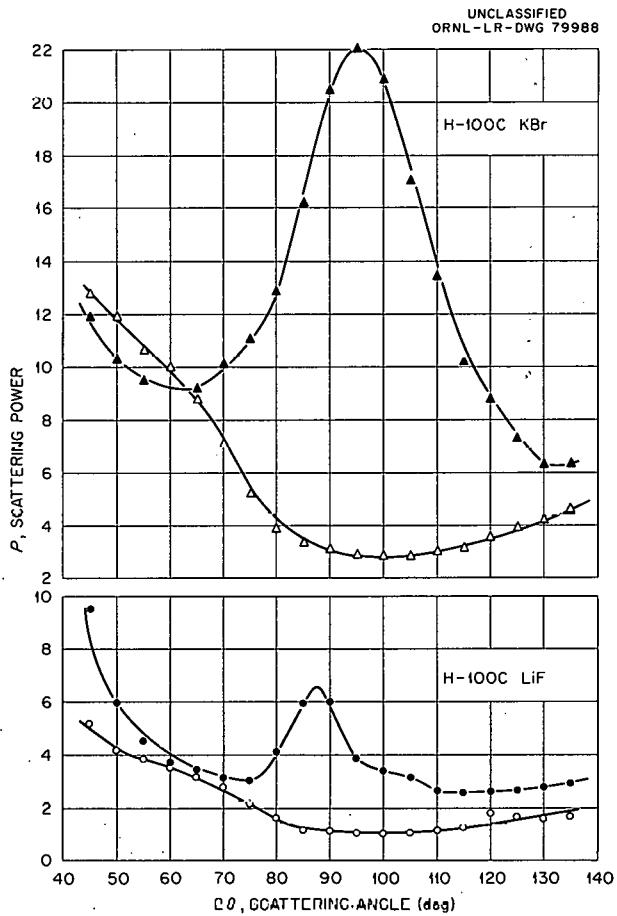
Fig. 13.6. Angular Dependence of the Scattering Power for Two Samples of Harshaw LiF and KBr.

over an order of magnitude, it should be possible to determine if the number of bad regions or their composition, which is proportional to the scattering power, influences the radiation coloration rate for such entities as the F- and M-centers.

The radiation growth curves for F- and M-centers produced by gamma rays in some of the crystals investigated are shown in Figs. 13.7 and 13.8 respectively. A comparison of these curves with the scattering power of the same specimens (see Fig. 13.3) makes it clear that the light-scattering bad regions within the crystals do not contribute to the production of F- and M-centers after first-stage coloration is completed. The first-stage coloration was not investigated in detail, and there is no evidence as to whether a correlation can be found in this case or not. It was also possible, by making optical measurements of the so-called OH^- band in KCl (204 mμ), to show that this impurity was not responsible for the light scattering in the Harshaw crystals investigated.
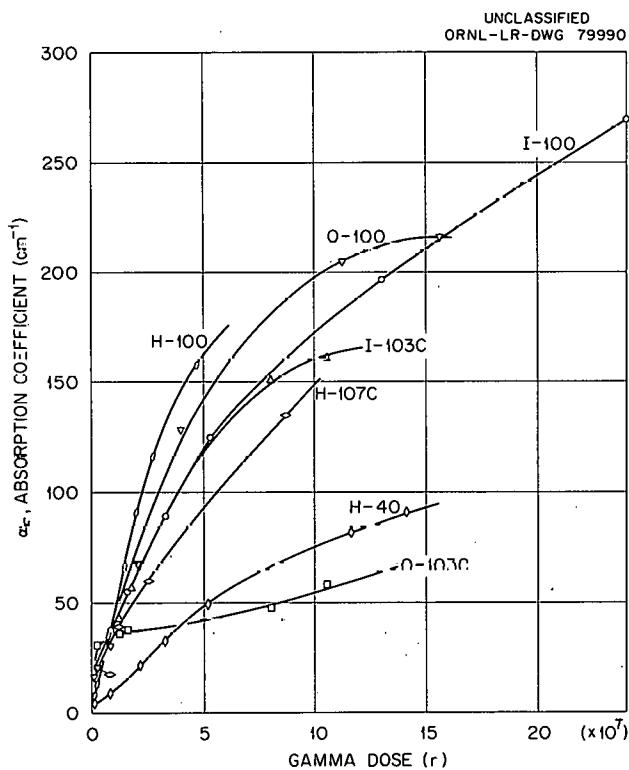
Fig. 13.7. F-Center Coloring Curves for Some of the KCl Crystals Used in This Investigation.
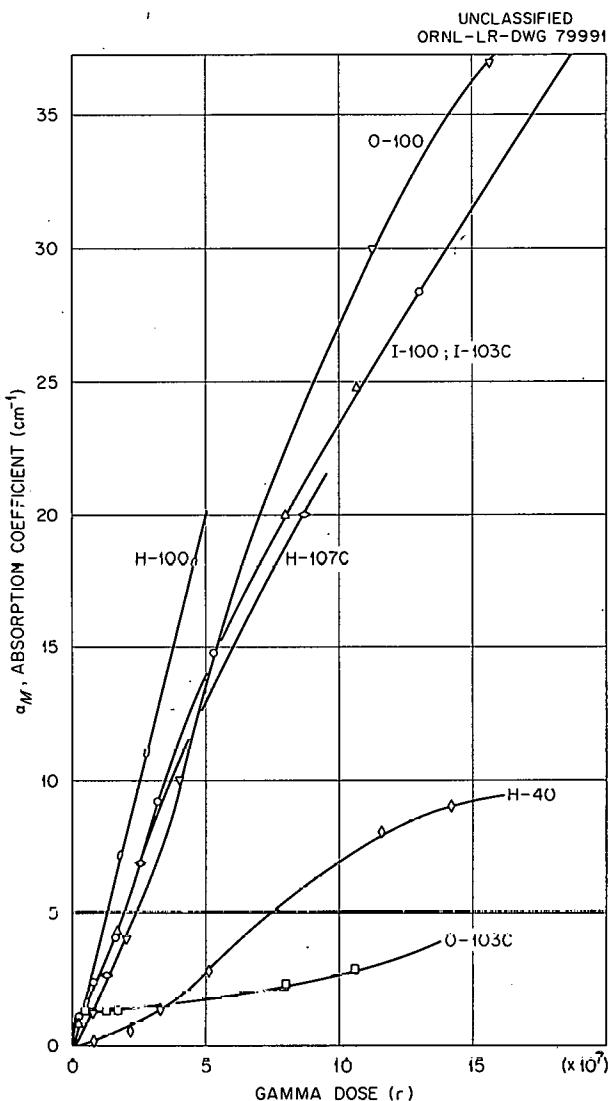
Fig. 13.8. M-Center Coloring Curves for Some of the KCl Crystals Used in This Investigation.

Theory of Light Scattering by Dislocations

The light scattering by a cylindrical bad region of length Z^* and radial distribution function $\rho(r)$ has been calculated by Lester.[22] It was found that, for

$$\rho(r) = \left(\frac{V}{2\pi r^* Z^*}\right)\frac{e^{-r/r^*}}{r},$$

[22]D. M. Lester, thesis, University of Oklahoma, 1960.

where V is the scattering volume and r^* is the effective radius of the cylinder, the scattered intensity i can be written as

$$i = I_0 \frac{2\pi^2 n^4}{R^2\lambda^4} (1 + \cos^2 2\theta)\, \overline{\alpha^2} \left(\frac{\sin CZ^*/2}{CZ^*/2}\right)^2$$
$$\times V^2 \left[\frac{1}{1 + r^{*2}(A^2 + B^2)}\right], \quad (1)$$

where

$|\mu| = \dfrac{4\pi n}{\lambda} \sin\theta$, n is the index of refraction,

$A = |\mu| \cos(\theta - \Phi)$,
$B = -|\mu| \sin(\theta - \Phi) \cos\xi$,
$C = -|\mu| \sin(\theta - \Phi) \sin\xi$,

$\overline{\alpha^2}$ = average effective square of the polarizability per unit volume for the scattering system.

The angles θ, ξ, Φ are most easily defined as follows: 2θ is the scattering angle (i.e., the angle between the direction of the incident light beam and the direction of observation); ξ is the inclination of the cylindrical bad-region axis (Z') to the vertical; and Φ is the orientation angle of the projection of this bad-region axis into the X-Y plane.

If the polarizability for the scattering system is isotropic, Eq. (1) indicates that, for a triad of mutually perpendicular cylinders oriented along X, Y, and Z, respectively, when $\Phi = 45°$, $Z^* = 3 \times 10^{-4}$ cm, and $r^* \lesssim 2.5 \times 10^{-6}$ cm, the scattering pattern of i vs 2θ should have a peak at $2\theta = 90°$ with half-width of about $15°$ and a relative height of twice the scattering power for $2\theta = 45°$. The dissymmetry, z, should be 1. The case $\Phi = 0°$ has no scattering peak and also has a dissymmetry of 1. Moreover, the scattering for $2\theta = 45°$ is the same for the cases $\Phi = 0$ and $\Phi = 45°$. The theory for this special isotropic case has also been discussed at length in refs 15 and 16, and it can be shown that Eq. (1) agrees very well with the expression found by van de Hulst[23] for scattering by cylinders.

When the scattering centers do not possess spherical symmetry and the polarizability is not isotropic, then the scattering must be pictured as a consequence of the incident light wave inducing

---

[23]H. C. van de Hulst, *Light Scattering by Small Particles*, Wiley, New York, 1957.

an oscillating electric moment in a molecule which is optically unsymmetrical. We will consider only the case where the centers possess an axis of rotational symmetry, so that their polarizability ellipsoids are spheroids ($\alpha'_{xx} = \alpha'_{yy} \neq \alpha'_{zz}$). If the principal axes of the polarizability ellipsoids are x', y', and z', and the position of the scattering center relative to the x, y, z system is fixed by the two angles ϕ and η (where η is the angle between z and z' and ϕ is the angle between the x axis and the projection of the z' axis into the x-y plane), then the relation between the polarizabilities α'_{ij} and α_{ij} can be written

$$\alpha_{zz} = \alpha'_{zz} \cos^2\eta + \alpha'_{xx} \sin^2\eta ,$$
$$\alpha_{yz} = (\alpha'_{zz} - \alpha'_{xx}) \sin\eta \cos\eta \cos\phi ,$$
$$\alpha_{xz} = (\alpha'_{zz} - \alpha'_{xx}) \sin\eta \cos\eta \sin\phi ,$$
$$\alpha_{xx} = \alpha'_{zz} \sin^2\eta \sin^2\phi + \alpha'_{xx} \qquad (2)$$
$$\times (\cos^2\phi + \cos^2\eta \sin^2\phi) ,$$
$$\alpha_{yy} = \alpha'_{zz} \sin^2\eta \cos^2\phi + \alpha'_{xx}$$
$$\times (\sin^2\phi + \cos^2\eta \cos^2\phi) .$$

In the evaluation of i vs 2θ (i.e., the effect that anistropic polarizability has on the scattering pattern), it must be remembered that any analysis of the light-scattering pattern can only determine a pair distribution function or average projection of the scattering units. Therefore, when a scattering unit has several different orientations in the lattice, the light-scattering pattern is characteristic of a superimposition of the orientations. For the special case of dislocation—defect-cloud scattering, this observation is important since for any {100} face of a crystal the line formed by the edge of the extra half planes of the edge dislocations may be in any of four directions, [100], [$\bar{1}$00], [010], and [0$\bar{1}$0]. It is therefore necessary to use an effective polarizability ellipsoid representative of the average projection of the scattering units to evaluate the scattering pattern. This can be done by averaging with the proper weighting function over ϕ. It would be expected that the scattering centers in the cloud around the edge of the extra half plane of the dislocation would be at least partially oriented because of the elastic and electric fields associated with this line. Therefore, it is necessary that the weighting function over ϕ show this effect. When a weighting function of $\cos^4 2\phi$ representing an effective defect

distribution for the case $\Phi = 0°$ is used, then Eq. (2) may be written:

$$\overline{\alpha_{zz}^2} = (\alpha_{zz}' \cos^2 \eta + \alpha_{xx}' \sin^2 \eta)^2 ,$$

$$\overline{\alpha_{zy}^2} = \frac{1}{2}(\alpha_{zz}' - \alpha_{xx}')^2 \sin^2 \eta \cos^2 \eta , \qquad (3)$$

$$\overline{\alpha_{xy}^2} = \frac{1}{24}(\alpha_{zz}' - \alpha_{xx}')^2 \sin^4 \eta .$$

If a weighting function of $\sin^4 2\Phi$ is employed, characteristic of the effective defect distribution for the case $\Phi = 45°$, then it is found that

$$\overline{\alpha_{zz}^2} = (\alpha_{zz}' \cos^2 \eta + \alpha_{xx}' \sin^2 \eta)^2 ,$$

$$\overline{\alpha_{zy}^2} = \frac{1}{2}(\alpha_{zz}' - \alpha_{xx}')^2 \sin^2 \eta \cos^2 \eta , \qquad (4)$$

$$\overline{\alpha_{xy}^2} = \frac{5}{24}(\alpha_{zz}' - \alpha_{xx}')^2 \sin^4 \eta .$$

When the scattered intensity, i, is evaluated as a function of scattering angle, it is found that the intensity peak occurring at $2\theta = 90°$ depends markedly on the orientation of the scattering center polarizability ellipsoids and on the ratio of $\alpha_{zz}'/\alpha_{xx}'$. The dissymmetry is not necessarily unity for this case, and the scattered intensity for $2\theta = 45°$ when $\Phi = 0°$ is not equal to that for $2\theta = 45°$ when $\Phi = 45°$. Also, the scattering pattern is dependent on the expression chosen for the weighting function. Therefore, the parameters that most affect the shape of the calculated scattering pattern are the weighting function, the ratio of $\alpha_{zz}'/\alpha_{xx}'$, the orientation η of the defect scattering center polarizability ellipsoid with respect to the dislocation line or bad-region cylinder axis Z', and the length of the bad region Z^*.

Discussion

If it is assumed that the dominant light-scattering units in the crystals are dislocations surrounded by impurity clouds, then it is possible through the use of Eqs. (1), (3), and (4) to calculate the scattering pattern for given values of η and $\alpha_{zz}'/\alpha_{xx}'$ and for the two different orientations $\Phi = 0°$ and $\Phi = 45°$. Also, values for η and

$\alpha_{zz}'/\alpha_{xx}'$ can be found independently from the depolarization data given in Table 13.1. Consider only crystal H:105C as a typical example; it is found that the depolarization data give $\eta = 70°$ and $\alpha_{zz}' = 6.3 \, \alpha_{xx}'$ for the orientation $\Phi = 0°$, and $\eta = 8.2°$ and $\alpha_{zz}' = 8.2 \, \alpha_{xx}'$ for $\Phi = 45°$. Figure 13.9 shows the fit of theory to experiment which
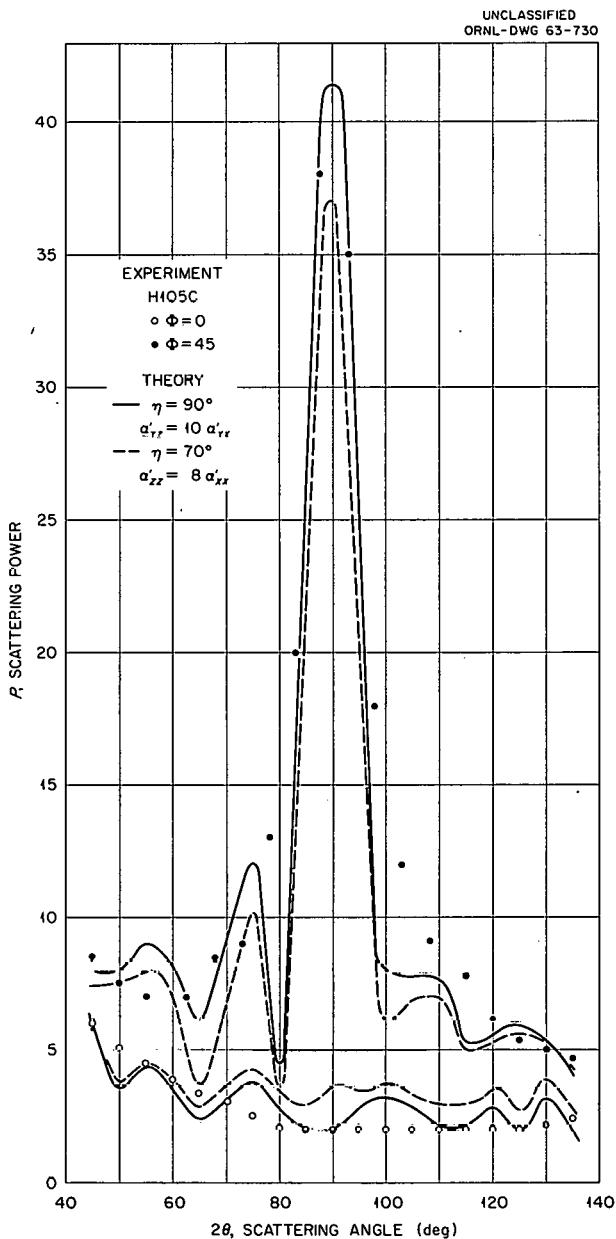
Fig. 13.9. Comparison of Light-Scattering Theory and the Experimental Data for Sample H105C. In the theory the effective dislocation length Z was taken as 3×10^{-4} cm.

can be obtained using Eqs. (1), (3), and (4) and the values shown in the figure for η and the ratio $\alpha'_{zz}/\alpha'_{xx}$ with $Z^* = 3 \times 10^{-4}$ cm. The theory has been adjusted to fit one experimental data point: that for the orientation $\Phi = 0$ and scattering angle $2\theta = 45°$. No other fitting was necessary. Of course, the experimental data points cannot give the resolution and fine structure which the theory predicts because there is a spread in the observation angle and because the dislocation networks are probably not perfectly aligned. However, the fit of theory to experiment is apparently quite good and gives credibility to the idea that the dominant scattering units within the crystals are dislocations surrounded by defect clouds.

The large variation in scattering intensity shown in Figs. 13.2 and 13.3 suggests that the individual scattering centers and their concentrations within the scattering units vary from sample to sample and are most likely impurities. Rayleigh's ratio[24] for benzene scattering at 546 mμ is 16.5×10^{-6} cm^{-1}, and a comparison of the scattering power of benzene with that of the individual samples investigated allows one to calculate a value for $NV^2 \overline{\alpha^2}$ from the formula

$$P = \frac{i}{I_o V} = NV^2 \overline{\alpha^2} \left(\frac{2\pi^4 n^4}{R^2 \lambda^4} \right) \left(\frac{\sin CZ^*/2}{CZ^*/2} \right)^2$$
$$\times (1 + \cos^2 2\theta) \left[\frac{1}{1 + r^{*2}(A^2 + B^2)} \right], (5)$$

where N is the number of scattering units per unit volume, and all other symbols are the same as those in Eq. (1). For Harshaw KCl samples the quantity $NV^2 \overline{\alpha^2}$ varies from 0.72 to 1.8×10^{-26} cm^3, and for Isomet KCl the variation is from 0.21 to 2.0×10^{-26} cm^3. The Optovac KCl crystals do not show the characteristic orientation peaks in the scattering pattern observed for the Harshaw and Isomet samples; therefore, it is perhaps not feasible to use this same analysis. However, it should be mentioned that, if the dislocation networks in these crystals are somewhat irregular and the polarizability ellipsoid is not markedly anisotropic, then the distinctive peak in the scattering pattern will not be apparent. Thus

it is not possible to eliminate dislocations as the dominant scatterers in the Optovac specimens. This point is further strengthened by Fig. 13.5, which illustrates what happens to a scattering pattern as the dislocation networks become more and more irregular.

Previously,[17] it was suggested that the relatively high forward scattering at $2\theta = 45°$ and hence the large dissymmetry could be due to a contribution to the scattering by rather large precipitates. This approach allowed the use of an isotropic polarizability in Eq. (1), and the addition of the contributions to the scattering from the two different types of scattering units did fit the data that were then available. However, the present experimental observations eliminate this possibility since the scattering at $2\theta = 90°$ for $\Phi = 45°$ is about a factor of 20 greater for some crystals than the scattering at $2\theta = 90°$ for $\Phi = 0°$. In the isotropic polarizability case this factor should be 2. Moreover, several samples were taken to high temperatures (525 to 725°C) and then air cooled. As had been noted before,[17] the scattering power of the heat-treated samples was quite different from that for the same specimens before heat treatment, but the high forward scattering and the large dissymmetry were still observed. This indicates that, unless the precipitates grew and dispersed in exactly the same manner as the defect cloud around the dislocations, only one type of scattering unit is responsible for all the scattering observed.

A comparison of the Rayleigh ratio values given in Table 13.1 with the rates of F- and M-center coloration shown in Figs. 13.7 and 13.8 indicates that the scattering centers within the bad regions do not affect the growth rates for either F- or M-centers. The differences in the Rayleigh ratios given in Table 13.1 can be due to changes (from sample to sample) of either the dislocation density N, the type of impurity (and hence $\overline{\alpha^2}$), or the effective scattering volume V. The last is relatively well known from the analysis of the scattering pattern, which gives $Z^* = 3 \times 10^{-4}$ cm and $r^* \lesssim 2.5 \times 10^{-6}$ cm. Thus it is only possible to state at this time that the coloration rates in the specimens investigated are not due to the type of impurities surrounding the dislocations and may not be affected by the number of light-scattering bad regions within the crystals.

[24]D. K. Carpenter and W. R. Krigbaum, *J. Chem. Phys.* **24**, 1041 (1950).

14. Pure Materials Program

PURE MATERIALS PROGRAM

J. W. Cleland

It is the primary purpose of this program to develop the necessary techniques required for the production of research-quality specimens (usually single crystals) of a composition, purity, and perfection not commercially available. It has been recognized that actual progress in many areas of fundamental research has been limited by the unavailability of samples with a high degree of purity and perfection. The ultimate range of certain properties in many materials can be established only by means of experiments that are conducted on pure specimens or on samples that contain a known amount of impurity. The use of single crystals is mandatory in any determination or utilization of those characteristics that depend on crystallographic orientation.

The entire program involves a number of research divisions at ORNL and the special skills of a number of other AEC installations and AEC contractors. Subcontracts have been negotiated to secure the particular skills and techniques of other research groups outside the AEC for several materials of special interest.

Many of the actual crystal growth techniques have been performed by groups in the Reactor Chemistry[1] and Metals and Ceramics[2] Divisions and have been separately reported in their annual reports. Special analytical techniques such as neutron activation analysis, mass spectral analysis, and microspectroanalysis have been developed in the Analytical Chemistry Division and have also been reported separately. It should be emphasized that close cooperation is required among those who analyze, grow, characterize, or use these materials and that this cooperation must transcend any group, division, or individual laboratory.

Included in this report are only those materials being grown or evaluated by the Solid State Division — KCl, HgS, Bi_2Se_3, Bi_2Te_3, Cu_2O.

RESEARCH MATERIALS INFORMATION CENTER

T. F. Connolly

Information concerning the availability of and need for high-purity research materials has always been difficult to obtain; hence, it is the purpose of the Research Materials Information Center (RMIC) to collect and provide information on the purification, production, characterization, and availability of research materials to both producers and users. It is felt that an accurate, up-to-date listing of the properties of available research materials will eliminate a large portion of the duplication of effort that has occurred when individual research groups have attempted to produce such materials. Equipment for automatically searching coded entries on microfilm has been purchased and installed. An experiment in coding (to establish a thesaurus and the routine of storage and retrieval) has been successfully concluded. Background information on research materials, including techniques of production and characterization, has been and is being reviewed,

---

[1] Isotopic LiF, UO_2, MgO, and CaF_2; see *Reactor Chem. Div. Ann. Progr. Rept. Jan. 31, 1963*, ORNL-3417.

[2] BeO, ThO_2, HfO_2-SiO_2, $3BeO\cdot Al_2O_3\cdot 6SiO_2$ (beryl), SnO_2, UAl_3, UAl_4, $ErMnO_3$, KCl (calcium doped), iron-substituted sodium-based micaceous materials, synthesized $Cs_2O\cdot Fe_2O_3\cdot 4SiO_2$, TiO_2, Al_2O_3; see *Metals and Ceramics Div. Ann. Progr. Rept. May 31, 1963*, ORNL-3470.

analyzed, coded, and filmed. Active participation has been expanded to include about 60 groups (outside ORNL). A bulletin containing reviews of current techniques and experimental results on alkali halides and a current listing of available and desired materials has been assembled and will be published shortly.

GROWTH OF SINGLE-CRYSTAL HgS

O. E. Schow III

Investigation of methods for the production of HgS research specimens is being continued. In the past[3] the main line of attack was vapor deposition at a temperature below the cinnabar—meta-cinnabar transformation point[4] ($\sim$335°C at 1 atm) both with and without iodine as a carrier gas. During the current period the possibility of crystal growth from the melt under pressure has been explored.

Although HgS sublimes at 580°C under atmospheric pressure, it can be melted under pressure. The melting point is $\sim$850°C at a pressure of $\sim$4 atm of helium. In exploratory experiments HgS starting material is sealed off in 6-mm-ID quartz ampoules under 1 atm of helium. The ampoules are enclosed in an Inconel vessel for protection against rupture of the ampoule, and the assembly is heated in a furnace. Polycrystalline masses of HgS have been obtained by this technique. At 600°C, HgS is in the black meta-cinnabar form; but as it cools, it converts (at an unknown temperature) to the red, hexagonal-cinnabar structure well before room temperature is reached. The helium pressure seems to elevate the transformation temperature to the extent that the difficulties with specimen fracture and crack production from the cubic to hexagonal form are reduced.

A determination of the pressure dependence of the transformation temperature is under way.

[3]O. L. Curtis, Jr., *Solid State Div. Ann. Progr. Rept. Aug. 31, 1962,* ORNL-3364, p 91.

[4]O. L. Curtis, Jr., *J. Appl. Phys.* **33,** 2461 (1962).

Co[60] GAMMA-RADIATION-INDUCED POINT DEFECTS IN Bi$_2$Te$_3$[5]

M. J. Smith

The effects of extended Co[60] gamma radiation upon the electrical resistivity, Hall coefficient, and magnetoresistance of Bi$_2$Te$_3$ have been examined. Cobalt-60 gamma radiation causes an increase in the Hall coefficient in *n*-type Bi$_2$Te$_3$ and a decrease in *p*-type. For gamma-ray exposures in the range of 10^{18} photons/cm^2, the apparent carrier removal rate is $\sim 10^{-1}$ carrier per Co[60] photon. Thermal annealing of radiation-induced damage was also investigated. The results may be most consistently analyzed in terms of a model which consists of a radiation-induced tellurium vacancy and interlaminar clusters of tellurium interstitials. The effects of the radiation-induced point defects are discussed. Evidence of an effect on impurity-band conduction at low temperatures in *n*-type Bi$_2$Te$_3$ is observed.

DETERMINATION OF THE NONSTOICHIO-METRIC DOPING MECHANISM IN Bi$_2$Se$_3$[6]

M. J. Smith

The extrinsic electrical properties of chemically pure Bi$_2$Te$_3$ and Bi$_2$Se$_3$ have been attributed to deviations from stoichiometric proportions.[7,8] Bi$_2$Te$_3$ exists as a single phase over a range of composition through the inclusion of substitutional point defects. That is, excess bismuth atoms occupy tellurium sites and are singly ionized acceptors; excess tellurium atoms occupy bismuth lattice sites and behave as singly ionized donors.[7] A similar phenomenon[8] is considered to be true in Bi$_2$Se$_3$. Excess selenium acts as an acceptor;[9]

[5]Abstract of a paper which has been submitted to the *Journal of Applied Physics.*

[6]A letter which appeared in *Appl. Phys. Letters* 1, 79 (1962).

[7]C. B. Satterthwaite and R. W. Ure, Jr., *Phys. Rev.* **108,** 1164 (1957).

[8]K. Hashimoto, *Mem. Fac. Sci., Kyushu Univ.,* Ser. B **2,** 141, 187 (1958).

[9]M. J. Smith, E. S. Kirk, and C. W. Spencer, *J. Appl. Phys.* **31,** 1504 (1960).

however, the doping mechanism has not been determined. There are only three possible doping mechanisms:[10]

(a) Substitutional: Excess selenium atoms replace bismuth atoms on lattice sites normally occupied by bismuth atoms.

(b) Subtractive: Selenium atoms occupy normal selenium sites, but some bismuth sites are vacant.

(c) Interstitial: Extra selenium atoms occupy interstitial positions.

The ability of a crystal to exist as one phase over a range of composition implies certain thermodynamic consequences which are useful in studying the material. In Bi_2Se_3 the crystal-vapor equilibrium system has two components, hence two degrees of freedom. Therefore, in principle, the composition and thus the electrical properties of the crystal can be controlled by controlling the temperature and the partial pressure of one component. The addition or removal of atoms, resulting from a disturbance of solid-vapor equilibrium conditions, is generally controlled by atomic diffusion within the crystal.[10] A description of the diffusion process will specify the particular doping mechanism (a, b, or c) involved when excess selenium is added to Bi_2Se_3.

For sufficiently long diffusion times, approach to equilibrium concentrations within a thin slab is described to a good approximation by the following relation:[11]

$$(n_{eq} - \bar{n})/(n_{eq} - n_i)$$
$$\cong (8/\pi^2) \exp (-tD\pi^2/b^2) , \quad (1)$$

where n_{eq} is the equilibrium concentration of the excess constituent in the crystal of thickness b at ambient temperature T_A, $\bar{n}$ is the average concentration in the crystal at some time t, n_i is the initial concentration at $t = 0$, and D is the diffusion coefficient of the process at the temperature of the specimen.

If the concentration of current carriers in Bi_2Se_3 is, as proposed, regulated by the vapor pressure of selenium over the crystal, one may rewrite

[10]H. C. Gatos, *Properties of Elemental and Compound Semiconductors*, vol 5, p 187, Interscience, New York, 1960.

[11]W. Jost, *Diffusion in Solids, Liquids, Gases*, 3rd ed., p 37, Academic Press, New York, 1960.

Eq. (1) for the extrinsic range in the form:

$$\frac{(1/R_{eq}) - (1/\bar{R})}{(1/R_{eq}) - (1/R_i)}$$
$$= r \cong (8/\pi^2) \exp (-tD\pi^2/b^2) , \quad (2)$$

where R is the Hall coefficient for the condition indicated by the subscript. Equation (2) may be solved numerically for r by obtaining several measurements of the Hall coefficient at varying times of exposure. A check can be made of the results by varying the vapor pressure of selenium and repeating the procedure.

It has been demonstrated that controlled selenium vapor pressures prevent loss of selenium from Bi_2Se_3 to the vapor at elevated temperatures.[9] A device similar to that described in ref 9 was used to study the vapor-crystal equilibrium system of Bi_2Se_3. The device employed the following modification: The excess selenium was not held within the specimen chamber but was contained in an additional chamber by a connecting tube. The temperatures of the selenium chamber, connecting tube, and specimen chamber were regulated separately, thereby controlling the partial pressure of selenium in the system. Resistivity and Hall measurements were taken on a number of single crystals of Bi_2Se_3 which had been cleaved to a thickness of $b \cong 10^{-2}$ cm. Measurements were made at various specimen temperatures and at selenium vapor pressures as a function of time.

The logarithm of r for specimen CBS-2 is plotted in Fig. 14.1 as a function of time for various ambient temperatures. The slope of the straight line portion of each curve gives the diffusion coefficient for the process. Diffusion coefficients obtained on all other specimens of Bi_2Se_3 were identical at higher temperatures; however, considerable scatter was encountered at lower temperatures.

Figure 14.2 gives a plot of ln D vs $1/T$. The activation energy of the diffusion process is 3×10^4 cal/mole. The dependence of the diffusion coefficient on temperature may be expressed by:

$$D = 3.4 \, e^{-(3 \times 10^4/RT)} \, cm^2/sec . \quad (3)$$

UNCLASSIFIED
ORNL-LR-DWG 73823
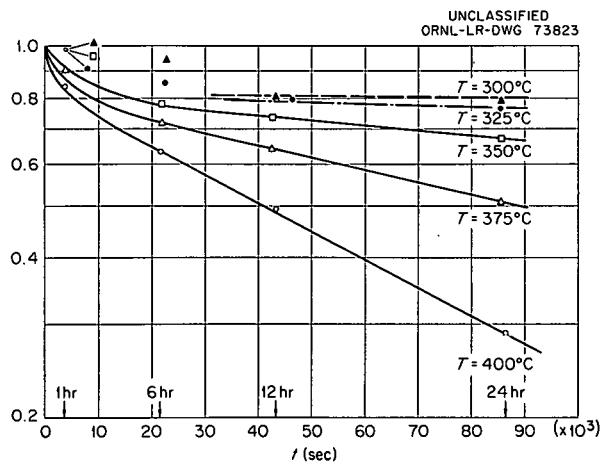
Fig. 14.1. $(n_{eq} - \bar{n})/(n_{eq} - n_i) = r$ vs t for Crystal CBS-2 at Several Ambient Temperatures.

UNCLASSIFIED
ORNL-LR-DWG 73824
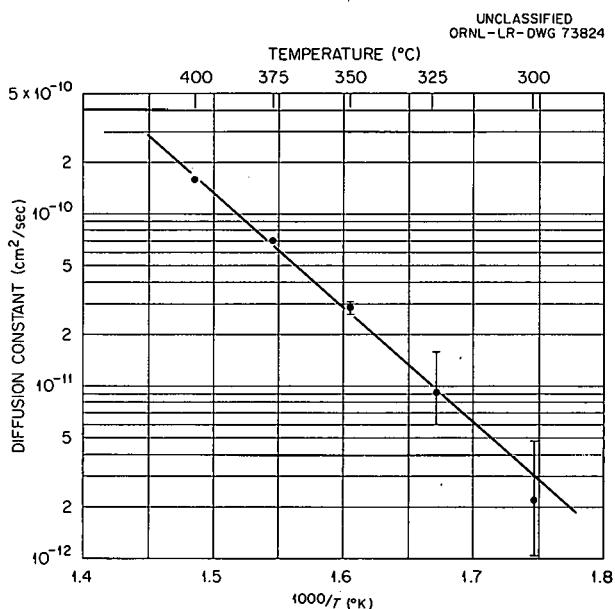
Fig. 14.2. Selenium-Vapor–Crystal Diffusion Coefficient of Bi_2Se_3 vs $1000/T$.

The self-diffusion coefficient of selenium in Bi_2Se_3 is reported to be[12]

$$D_{Se \to Be_2Se_3} = 8.5 \times 10^{-9} e^{(5.0 \times 10^4/RT)} . \qquad (4)$$

The literature does not contain information on the self-diffusion of bismuth in Bi_2Se_3; however, values for bulk diffusion in Bi_2Se_3 of antimony, which is similar to bismuth in size and electronic configuration, have been obtained:[13]

$$D_{Sb \to Bi_2Se_3} = 1.8 \times 10^{-3} e^{-(2.95 \times 10^4/RT)} . \qquad (5)$$

The activation energies of Eqs. (5) and (3) are essentially identical. It is reasonable to assume that the activation energies for motion of antimony and bismuth are similar in magnitude; hence, the results suggest that the process is controlled by diffusion of bismuth rather than selenium.

Bismuth atoms diffuse to the surface, leaving bismuth vacancies in the bulk crystal. Bismuth vacancies are acceptor type. This is to be expected for subtractive defects involving an excess of the anion.[10] Bismuth vacancies in Bi_2Te_3 also behave as acceptors.[14]

Smith and others[9] report a 0.09-ev energy level in n-type Bi_2Se_3 crystals grown from a melt containing excess selenium. It would be interesting to determine whether this level involves the release of electrons which have been trapped by bismuth vacancies.

DETERMINATION OF EXCESS OXYGEN IN Cu_2O SINGLE CRYSTALS

M. J. Smith

It is well known that Cu_2O owes its extrinsic semiconductivity to an excess of oxygen frozen into the lattice. One of the problems associated with the investigation of semiconducting behavior in this material and the evaluation of the quality of single crystals is the difficulty of analysis of deviation from stoichiometry. Since each excess oxygen ion should be accompanied by two paramagnetic cupric ions, magnetic susceptibility

[12]A. A. Kuliev and G. B. Abdullaev, Soviet Phys.-Solid State (English Transl.) 1, 545 (1959).

[13]B. I. Boltaks, Zh. Tekhn. Fiz. 25, 767 (1955).

[14]S. M. Schultz, J. P. McHugh, and W. A. Tiller, Scientific Paper No. 929-8901-P1, Westinghouse Research Laboratories.

measurements should be an effective means of assaying for excess oxygen content. The susceptibility of the host lattice should be diamagnetic and relatively insensitive to temperature, whereas the contribution from paramagnetic ions is expected to follow Curie's law:

$$\chi_{para} = \frac{N_{Cu^{2+}}\,\beta^2\,\mu^2_{Cu^{2+}}}{3\rho kT} , \qquad (1)$$

where $N_{Cu^{2+}}$ is the concentration of cupric ion per cm^3, β is the Bohr magneton, $\mu_{Cu^{2+}}$ is the moment of the Cu^{2+} ion in units of Bohr magnetons, and ρ is the density.

The experiments were performed on Cu_2O single-crystal material procured in connection with the Pure Materials Program under contract from the Virginia Institute for Scientific Research (VISR). These crystals were prepared by the carefully controlled oxidation of high-purity copper single crystals. The susceptibility was measured on one as-received crystal from room temperature to $\sim 5°K$, using the equipment designed by D. K. Stevens.[15]

Since only one crystal has been examined, the results are considered preliminary. The magnetic susceptibility, χ, of Cu_2O at room temperature was found to be -1.27×10^{-6} cgs unit in good agreement with recorded values. The diamagnetism decreases somewhat with temperature. Below $20°K$ the paramagnetic ion contribution becomes dominant, and the diamagnetism decreases rapidly. A rough analysis for the paramagnetic range according to Eq. (1), assuming $\mu_{Cu^{2+}} = 2.0\,\beta$ (ref 16) and neglecting the slight temperature dependence of the host lattice, yields an excess oxygen concentration of $\sim 4 \times 10^{17}$ cm^{-3}.

Additional specimens of more suitable shape for these measurements are under preparation at VISR. Further studies will include measurement of the effect of heat treatment in various oxygen pressures, and an attempt will be made to correlate excess oxygen concentrations with electrical properties.

[15]D. K. Stevens, *Magnetic Susceptibility of Annealed and Fast-Neutron Bombarded Germanium,* ORNL-1599.

[16]P. W. Selwood, *Magnetochemistry,* p 172, Interscience, New York, 1956.

POTASSIUM CHLORIDE SINGLE CRYSTALS

C. T. Butler   J. R. Russell

The ultimate aim of the pure KCl program is to produce very pure single crystals of KCl having also a low concentration of physical imperfections. The foremost aim of the program this past year was to further improve the growing apparatus and to learn by chemical analysis of many different crystals just which impurities are reduced (or increased) in concentration by a particular treatment.

The controlled-atmosphere Kyropoulos furnace has been somewhat improved. The vacuum system has been enlarged and redesigned to allow faster pumpdown, lower ultimate vacuum, and easier cleaning. After experimenting with several types of crucibles, one made of platinum has been adopted. It shows no visible etching or deformation after many uses in which the unused melt was often allowed to recrystallize in it. Because quartz pull rods are difficult and expensive to fabricate, rods of grade A nickel are now used. Nickel chucks have also replaced the former graphite ones. Contamination of the melt by the various materials present in the furnace chamber does not seem to be a serious problem. The zone refiner has been used to purify reagent-grade KCl powder under a dry HCl atmosphere. The zoner has performed as expected, but the yield of about 30 to 50 g per month hampers its usefulness as a means of routine purification of starting material for the Kyropoulos furnace. A glove box has been added to the available apparatus in the semi-clean room where the crystals are grown. All loading operations are performed in this box under a dry argon atmosphere.

Relatively great strides have been made in the procurement of purer starting material. "Spectroscopically pure" powder from Johnson, Matthey and Company, Ltd., has been used as an intermediate source between the relatively impure reagent-grade powder and the locally purified KCl, which, hopefully, will be purer than either of the others. The Johnson, Matthey material has been used to grow several boules, nearly all of which have been superior to commercial crystals. An arrangement has been made with members of the Analytical Chemistry Division of the Laboratory to produce very pure KCl ingots of at least the overall purity of the Johnson, Matthey

material. The program is just beginning, but already powder has been produced having less than 3, 2, and 1 $\mu g/g$ of calcium, sodium, and magnesium respectively. Additionally, KCl powder has been prepared by the two reactions

$$KOH + HCl \longrightarrow KCl + H_2O$$

and

$$KHCO_3 + HCl \longrightarrow KCl + CO_2\uparrow + H_2O \ .$$
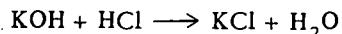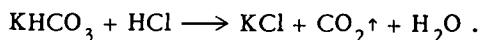
Some analyses of the various powders produced, as well as analyses of some of the finished boules, are presented in Table 14.1. Analyses of several commercial crystals are presented for comparison. In the table the powder listed as BA is reagent-grade KCl from the Allied Chemical Corporation. That listed as JM is Johnson, Matthey "Specpure"-grade KCl powder. Powder JR-1 was prepared using KOH and untreated HCl; JR-2 was made from $KHCO_3$ and untreated HCl. JR-3 used $KHCO_3$ with HCl which had been ether extracted, while JR-4 used $KHCO_3$ with

HCl which has been both extracted and distilled. AC-1 was prepared in the Analytical Chemistry Division by simply extracting reagent-grade KCl in thenoyltrifluoroacetone (TTA). A complete analysis of some of these materials is not yet available. The boule numbers may be recognized as the dates upon which they were grown, while the commercial single crystals are given numbers preceded by an H, I, or O for the Harshaw Chemical Company, the Isomet Corporation, or the Optovac Corporation respectively. Entries preceded by a "less-than" indicate that the element was sought but not found; the number is the limit of detection for the analytical method used. Where no value is listed, the element was not sought in that particular analysis. The letters indicate rough spectroscopic determinations in which F indicates a concentration somewhere in the vicinity of 1 to 10 $\mu g/g$ and E indicates 10 to 100 $\mu g/g$. Boules 021863 and 031463 were grown from JM material; the latter crystal, however, was accidentally contaminated with copper from an external source. The other boules were grown from reagent-grade material.

Table 14.1. Analyses of KCl Powders and Crystals (See Text for Explanation of Entries)

Sample Number	Element Concentration (μg/g)																							
	Al	Br	Ca	Cd	Cr	Cs	Cu	Eu	Fe	Hg	I	Li	Mg	N	Na	Ni	P	Pb	Pt	Rb	S	Sr	Tl	Zn
Powder																								
BA	0.006	133	F	0.013	<2		0.08	<0.08	0.86	0.52	<3		<1	1.5		0.17	<0.5	<0.3	<5		4	<5	<0.016	<0.31
JM	0.09	5	F	<0.004			0.33	<0.04	0.4		<2		-3.5			0.08	<0.5	0.19	<2		2		<0.02	<1.1
JR-1	<3	37	<3				F		<25		2.1	<1	<1	<3	29	<10	0.4	<120			<5	<1		
JR-2	<3	53	<3				F		<25		1.5		<1	<3	9.9	<12	<1	<120			<5	2		
JR-3		31	<3		E		E				<1		<1	4	3		<2			2.4		<2		
JR-4	<3	18	<3		<2		<1		<25		<1		<1	13	<2		<2	<120		2.1		<2		
AC-1			<3										<1		<2									
Boules																								
062062	6.9	70	<3	0.03		<4	<3	<1	2.5	<2	4	<1	<20	<3	14	0.76	<1	<0.6	<50	9	1	<4	<0.3	<8
070562	<0.3	85	<3	0.01		<4	<1	<1	<0.3	<0.2	3	<1	<20	<3	7.8	<0.1	1.7	<0.09	<17	8	1	<4	<0.04	<3
081562-T	0.026	85	<3	0.005		<4	<4	<1	<0.9	<0.5	<3	<1	<20	<3	9.1	<0.2	<1	<0.2	<10	20	<0.5	<4	<0.02	<0.3
101862	0.2	130	<3	0.03		<4	<2	<1	<0.28	<0.1	<3	<1		<3	16	<0.2	1.8	<0.03	<1	17	2	<4	<0.02	<2
021863	<8	42	<3		<4		<1		<25		<1		<1	3	<2	<12	<2			<9	<1	<2		
031463	<8	54	<3		<4		F		<25		<1		<1	6	<2	<12	<2			<9	<1	<2		
Crystal																								
H40			<2			<1		<1							<2					2.8			<1	
H102			<2			<1		<1							14					4.6			<1	
H100	<0.3	155	<3	<0.02		<4	<1.3	<3	3.1	<0.08	<3		<20	<3	29	<0.2	4.2	<0.03	<16	<5	<0.5	<4	<0.01	<5
H201	<8		<5		<2	<2	<1	<2	<25				<1		15					19			<3	
O100	<0.3	155	<3	0.38		<4	<3	<3	1.8	<0.2	6		<20	<3	94	0.29	1.5	<0.1	<20	9	<0.5	<4	<0.05	<3
I205	0.06	110	<3	<0.02		<4	<2	<2	<1	<0.5	<3		<20	<3	14	0.017	2.1	<0.2	<10	<5	5	<4	<0.09	<2

Part V. Radiation Metallurgy

M. S. Wechsler

THIS PAGE

WAS INTENTIONALLY

LEFT BLANK

15. Radiation Metallurgy

A major objective of the Radiation Metallurgy Section is the study of the radiation embrittlement of reactor materials. In the past year, continued assistance has been given the Gas-Cooled Reactor Project in the design and implementation of the pressure-vessel surveillance program for the EGCR. In this program, impact and tensile samples from the heats of EGCR steel (ASTM A212, grade B) are to be placed adjacent to the inside wall of the pressure vessel and removed at prescribed intervals for test so that the condition of the pressure vessel may be monitored. About 1500 surveillance and control samples are required. The machining of the samples of base-plate material has been completed, and the preparation of samples of weld and heat-affected-zone material is under way.

The influence of the temperature of irradiation on the radiation embrittlement of pressure-vessel steels is of interest because of the observation[1-3] that for some steels the embrittlement at first increases with increasing irradiation temperature. To further explore this aspect of the radiation-embrittlement phenomenon, instrumentation has been installed in the ORR during the past year to permit elevated-temperature irradiations. An experiment containing impact samples of simulated weld heat-affected-zone material of ASTM A212B steel is scheduled for insertion in July 1963.

These samples will be irradiated at 550°F (288°C) in order to supplement previous results[4] on samples irradiated at 120°F (49°C).

An objectionable feature of surveillance tests as a means of monitoring the condition of reactor pressure vessels is the fact that the surveillance samples do not duplicate the stress conditions under which the pressure vessel is exposed. In order to investigate the effect on pressure-vessel steels of simultaneous exposure to radiation and stress, a stress-rupture experiment containing tube-burst samples of ASTM A212B steel was inserted in the ORR in May 1963. In-pile stress-rupture tests, in which the time to rupture of pressurized tubes is observed as a function of stress and temperature, have been described previously,[5] but most of the previous work has been done on high-temperature cladding materials.

At the request of the High Flux Isotope Reactor Project, a study was made of the effect of irradiation on the tensile properties of commercial type 330 and type 270 nickel alloys. Sheet tensile samples were irradiated for about 14 weeks in a partial fuel element in the ORR at a temperature below 100°C. The postirradiation tensile tests on the type 330 material have been completed. As is described below, the irradiation was found to induce a yield point, to increase the yield strength, and to decrease the uniform elongation prior to necking.

In order to better understand flow and fracture in irradiated ferritic steels, an investigation is under way of the effect of irradiation on plastic deformation in iron and iron-base alloys. In collaboration with the Battelle Memorial Institute, Geneva, an experiment containing 45 tensile

[1]D. R. Harries, R. W. Nichols, and C. Judge, "The Effect of Neutron Irradiation on the Ductile-Brittle Transition Temperature of Steels and Its Relevance to Reactor Pressure Vessels," p 297 in *Steels for Reactor Pressure Circuits*, Special Report No. 69, Iron and Steel Institute, London, 1961.

[2]H. M. Finniston, "Metallurgical Aspects," p 545 in *Nuclear Reactor Containment Buildings and Pressure Vessels*, Butterworths, London, 1960.

[3]R. G. Berggren, "Neutron Irradiation Effects in Steels: Studies at Oak Ridge National Laboratory," p 370 in *Steels for Reactor Pressure Circuits*, Special Report No. 69, Iron and Steel Institute, London, 1961.

[4]R. G. Berggren et al., *Solid State Div. Ann. Progr. Rept. Aug. 31, 1961*, ORNL-3213, pp 39—42.

[5]W. E. Brundage et al., *Solid State Div. Ann. Progr. Rept. Aug. 31, 1962*, ORNL-3364, pp 138—47.

samples of Armco iron of various grain sizes, was inserted in the ORR. The experiment capsule also contains electron-microscope samples and neutron-dosimetry samples. Another experiment containing tensile samples of Ferrovac E iron, vacuum-melted 1020 steel, and ASTM A212B steel is planned.

The effects of radiation on the mechanical properties of alloys may be separated into two parts: those related to the introduction of defects *per se* and those associated with the enhancement of atomic rearrangements produced by the motion of the radiation-produced defects. In the latter class of effects, the possibility of radiation-enhanced precipitation is particularly important in the case of steels and other structural alloys. Low-cycle internal friction is a property widely used for the detection of precipitation of carbides and nitrides in alpha iron. The techniques for the in-pile measurement of this type of internal friction are being developed, and preliminary measurements of an iron-nitrogen alloy during irradiation are described below. Postirradiation measurements have already indicated[6] that the precipitation reaction in alpha iron is accelerated by irradiation. The ability to follow the course of the precipitation reaction during irradiation should be of great value in future work in this area.

Radiation-enhancement is observed for other types of diffusion-controlled reactions as well as for precipitation. Previous work[7-9] has indicated that the irradiation of Cu-Ni alloys stimulates the formation of solute-rich clusters. The presumption is that the clustering constitutes the elimination of a metastable atomic arrangement imposed, in the absence of irradiation, by low atomic mobilities. The clustering phenomenon in Cu-Ni alloys has also been studied in connection with quenching treatments.[10] This work indicated that interstitial migration may play a part in the diffusion process. This possibility is being further explored in the experiments described below on irradiated and cold-worked Cu-Ni alloys.

Still another type of atomic rearrangement in alloys that is accelerated by irradiation is the ordering reaction. The enhancement of short-range order on irradiation has been studied rather extensively in the past[11-13] in Cu-Al alloys, and one phase of this work has continued during the preceding year. This relates to the flux and temperature dependence of the "second-run phenomenon," in which a sample exhibits a considerably reduced reaction rate after having been irradiated and given a thermal cycling treatment to recover original properties. As the discussion given below points out, these results are being interpreted in terms of a theory of radiation-enhanced diffusion, which involves the solution of rate equations governing the concentrations of vacancies and interstitials. In order to encompass the case presented by the second-run phenomenon, numerical solutions to the rate equations are required. Therefore, a computer program is being set up.

A knowledge of the dependence of radiation-enhanced reactions on neutron flux (or dose rate) has a bearing on the mechanism of the phenomenon. In addition, the dependence on instantaneous flux may be important in connection with the use of structural materials in reactor environments. This comes about because the accelerated-irradiation tests, on which the design of reactor components is based, are performed at high fluxes for relatively short periods whereas the pressure vessel of a reactor is exposed at low fluxes for long periods of time. However, owing to the disparity in the materials and properties studied, it is recognized that the previous results on radiation-enhanced diffusion in Cu-Al alloys offer only a suggestion as to what might be expected to be important factors in the embrittlement of pressure-vessel steels.

In the coming year, increased emphasis will be placed on experiments dealing with irradiation effects in iron and iron-base alloys. A suitable

[6]H. Wagenblast and A. C. Damask, *J. Phys. Chem. Solids* 23, 221 (1962).

[7]F. M. Ryan, E. W. Pugh, and R. Smoluchowski, *Phys. Rev.* 116, 1106 (1959).

[8]A. Ascoli, "Neutron-Bombardment-Enhanced Segregation in Cu-Ni Alloys," p 105 in *Radiation Damage in Solids*, vol II, International Atomic Energy Agency, Vienna, 1962.

[9]M. S. Wechsler et al., *Solid State Div. Ann. Progr. Rept. Aug. 31, 1959*, ORNL-2829, p 120.

[10]W. Schüle and H.-P. Kehrer, *Z. Metallk.* 52, 168 (1961).

[11]M. S. Wechsler and R. H. Kernohan, *J. Phys. Chem. Solids* 7, 307 (1958).

[12]R. H. Kernohan and M. S. Wechsler, *J. Phys. Chem. Solids* 18, 175 (1961).

[13]M. S. Wechsler and R. H. Kernohan, "The Effect of Radiation on Diffusion-Controlled Reactions in Copper-Base Alloys," p 81 in *Radiation Damage in Solids*, vol II, International Atomic Energy Agency, Vienna, 1962.

system for study seems to be the iron-silicon alloys. Iron-silicon is known to undergo an order-disorder transformation[14] at compositions where brittleness develops. Also, iron-silicon exhibits a decrease in magnetic permeability after demagnetization, which has been used previously to study the diffusion of vacancies upon neutron irradiation.[15] Finally, dislocation mobility[16] and crack propagation[17] may be determined in iron-silicon by means of etch-pitting techniques.

It is also anticipated that work at the Bulk Shielding Reactor will be started in the coming year. A neutron converter facility for alloy irradiations is being designed for the BSR. This will permit irradiations to be carried out in a fission neutron spectrum. It will also be possible to irradiate in highly thermalized flux so that the separate effects of neutron collision damage and (n,γ) damage may be determined.

RADIATION EMBRITTLEMENT OF REACTOR PRESSURE VESSELS[18]

M. S. Wechsler   R. G. Berggren

The essential features of the phenomenon of low-temperature brittleness are described, including a discussion of several impact tests on the basis of which a steel's capability for low-temperature service may be evaluated. Furthermore, a review is given of the effect of neutron irradiation on the yielding and fracture properties of pressure-vessel steels. Finally, the fundamentals of radiation damage are outlined, by means of which the displacement production rate may be calculated on the basis of the neutron spectrum at a particular point in the reactor. Also, the possible importance of dose-rate effects and (n,γ) damage to pressure-vessel embrittlement is discussed.

---

[14]F. W. Glaser and W. Ivanick, *Trans.* AIME **206**, 1290 (1956).

[15]H.-D. Dietze and E. Balthesen, *Nukleonik* **3**, 8 (1961).

[16]D. F. Stein and J. R. Low, Jr., *J. Appl. Phys.* **31**, 362 (1960).

[17]A. S. Tetelman and W. D. Robertson, *Acta Met.* **11**, 415 (1963).

[18]Abstract of published paper: *Nucl. Safety* **4**(1), 42 (1962).

TENSILE PROPERTIES OF IRRADIATED TYPE 330 NICKEL ALLOY

R. G. Berggren   W. J. Stelzman   T. N. Jones

This study was initiated at the request of the High Flux Isotope Reactor Project in connection with the possible use of nickel as a control-rod material. Due to the paucity of information on the effect of radiation on the mechanical properties of nickel, it was decided to conduct an experiment in the Oak Ridge Research Reactor to obtain the necessary engineering information.

In this study, commercial type 330 and type 270 nickel sheet were used. The measurements to date refer only to the type 330 alloy. The as-received stock was from two heats (N6906A1 and N9185A1) and was in the cold-rolled condition, $\frac{1}{4}$ to $\frac{1}{2}$ hard temper. This condition approximated the anticipated condition of the HFIR control-rod material. The chemical compositions of the two heats are given in Table 15.1. The principal composition difference is in the carbon content, 0.03% for one heat and 0.15% for the other heat. Sheet tensile samples ($\frac{1}{16}$ in. thick, 0.180 in. wide at the test section) of the following types were prepared from the $\frac{1}{4}$-in.-thick sheet:

1. Base-plate samples, smooth and notched. (*a*) As received. (*b*) Cold worked to an additional 75% reduction; only heat N9185A1.
2. Weldment samples, smooth and notched. Plates of one heat were butt-welded to plates of the other heat using nickel filler metal; the samples were machined from weldments with the weld metal at the center of the gage length.
3. Heat-affected-zone samples, notched.

Metallurgical examination has been carried out on base-plate samples in the as-received and cold-worked conditions [1(*a*) and 1(*b*) above]. The as-received material from both heats exhibited an ASTM grain size of 4 with equiaxed grains. Also, it was found by sectioning that the machining of the samples apparently produced a cold-worked layer to a depth of about 0.002 in. The base-plate samples that were given an additional 75% cold reduction revealed a cold-worked structure containing bands of recrystallized material. The weldment and heat-affected-zone samples have not yet been metallographically examined.

The specimens were mounted in subassemblies as shown in Fig. 15.1. Parts *A* and *B* held the

Table 15.1. Percentage Chemical Composition of Type 330 Nickel[a]

Heat No.	C	Mn	Fe	S	Si	Cu	Ti	Mg	Co	B
N6906A1	0.03	0.20	0.03	0.002	0.01	0.01	0.003	0.078	0.064	0.001
N9185A1	0.15	0.20	0.05	0.002	0.02	0.01	0.003	0.074	0.045	0.001

[a]Sulfur, cobalt, and boron are check analyses; all others are ladle analyses.
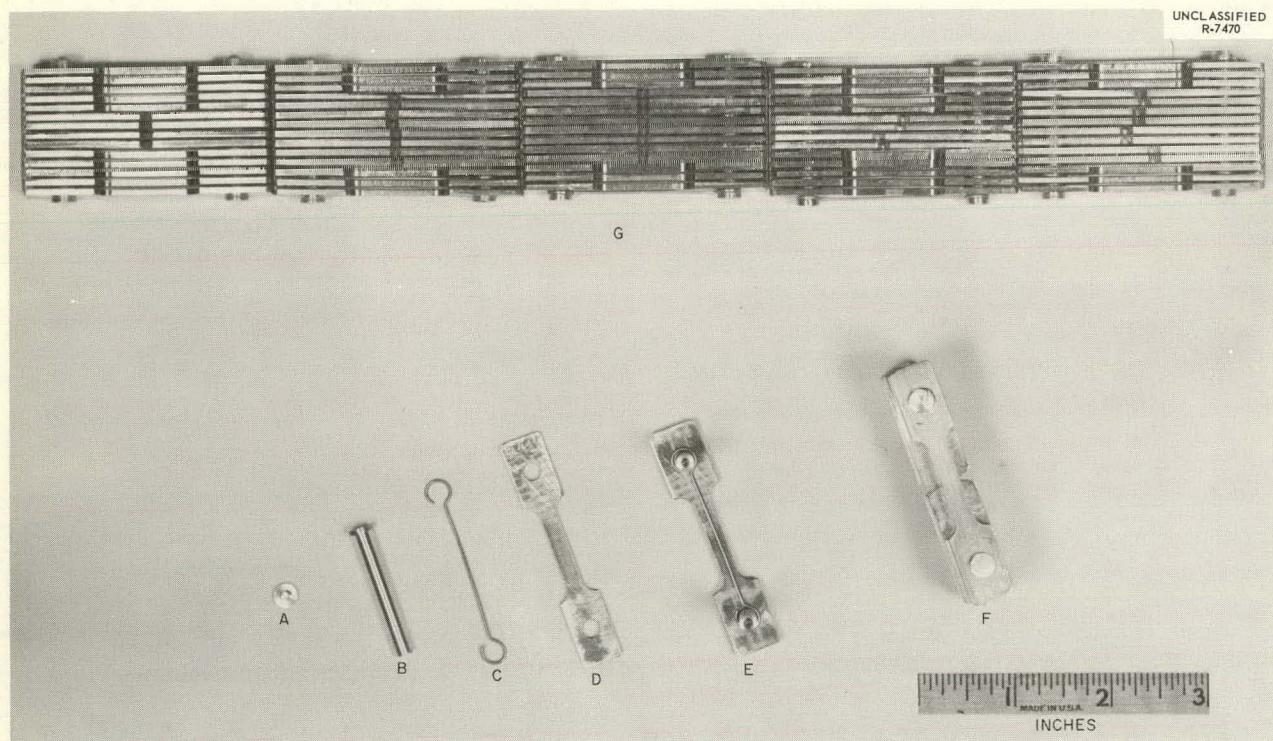
Fig. 15.1. Nickel Specimen Mounting for Irradiation in ORR, C-7 Facility.

subassemblies together, and the spacer wires C, ensured a water gap of 0.30 in. between the samples D. A partially assembled subassembly is shown in E and a completed subassembly in F. Nickel wires, spot-welded across the ends of the samples, served as neutron-flux monitors and ensured a water gap between subassemblies as shown in G. Six subassemblies were loaded in an aluminum holder that was inserted (see Fig. 15.2) in a partial fuel element in the C-7 position of the Oak Ridge Research Reactor for about 14 weeks.

The specimens were in contact with the reactor coolant water. The temperature of the samples was not measured directly, but heat-transfer calculations indicated a maximum temperature of 100°C.

The fast-neutron exposure was estimated from the activity of induced Co^{58} in the nickel wires removed from each subassembly. The calculation of fast-neutron fluxes from the Co^{58} activities requires a correction for burnup of Co^{58} due to thermal-neutron capture. The vertical distribution
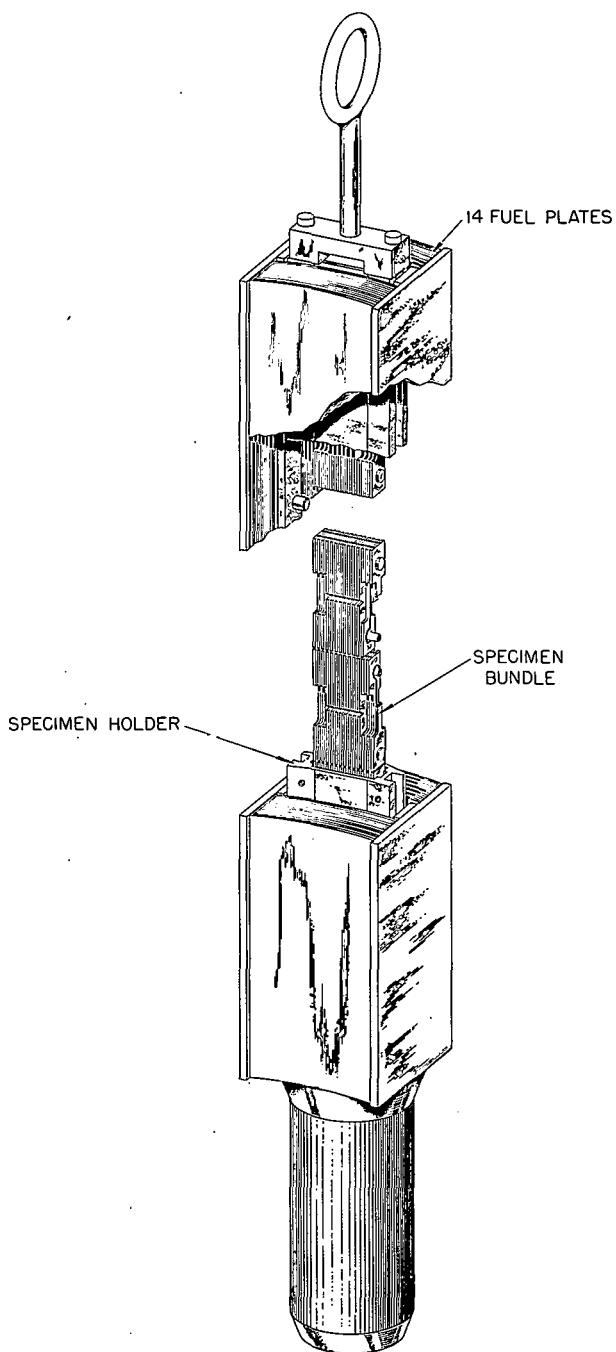
Fig. 15.2. Schematic of Arrangement for Exposure of Nickel Specimens in ORR, C-7 Facility.

Labels on figure: UNCLASSIFIED ORNL-DWG 63-703; 14 FUEL PLATES; SPECIMEN BUNDLE; SPECIMEN HOLDER

of thermal-neutron flux in this facility was obtained from measurements[19] in the "operating core with experiments" and normalized to the thermal-neutron flux determined by a $Co^{59}(n,\gamma)Co^{60}$ monitor

in this experiment. The thermal-neutron flux and the exposure time were used to obtain a correction factor R for the $Ni^{58}(n,p)Co^{58}$ monitors in this experiment. The published values[20] of R did not extend to the exposure times of this experiment; therefore, the published values were extrapolated, checked with an independent calculation, and found to be in agreement. The fast-neutron fluxes (above 2.9 Mev) were calculated using the equation

$$\phi(> 2.9 \text{ Mev}) = \frac{A_{Co^{58}} R}{N_{Ni^{58}} \sigma_{eff} (1 - e^{-\lambda t})},$$

where

$A_{Co^{58}}$ = the Co^{58} activity per g of nickel at reactor shutdown,

$N_{Ni^{58}}$ = the number of Ni^{58} atoms per g of nickel,

σ_{eff} = the effective cross section,[21] 390 mb, of the $Ni^{58}(n,p)Co^{58}$ reaction for an effective threshold energy of 2.9 Mev,

λ = the decay constant of Co^{58},

t = the exposure time,

R = the correction factor for burnup of Co^{58}, a function of thermal-neutron flux and exposure time.[20]

The fluxes of neutrons above 2.9 Mev in this experiment were 3.1 to 4.5 × 10^{13} neutrons cm^{-2} sec^{-1}. The doses of neutrons above 2.9 Mev were 2.5 to 3.6 × 10^{20} neutrons/cm^2. For a fission spectrum, the corresponding dose of neutrons above 1 Mev is 7.8 to 11.3 × 10^{20} neutrons/cm^2.

The tensile tests were conducted on the remote-control Instron tensile machine in the hot cells. All the tests were done at room temperature, and strains were measured with a specially designed extensometer, with a sensitivity of 0.01% strain. The complete extensometer system was calibrated at least once per day to an accuracy of 0.01%

[19]C. D. Cagle and R. A. Costner, Jr., *Initial Post Neutron Measurements in the ORR,* ORNL-2559, pp 35–36 (May 28, 1959).

[20]C. H. Hogg, L. D. Weber, and C. E. Yates, *Thermal Neutron Cross Sections of the Co^{58} Isomers and the Effect on Fast Neutron Flux Measurements Using Nickel,* IDO-16744 (June 18, 1962).

[21]T. O. Passell and R. L. Heath, *Nucl. Sci. Eng.* 10, 308 (1961).

strain. Strain rates in the tests on smooth speci-mens were 0.027/min.

The results of the tensile tests are summarized in Table 15.2. With but one exception (lines 11 and 13), the yield strength was at least doubled as a result of the irradiation. Table 15.2 also shows that the total elongations were decreased. However, all specimens deformed plastically before fracture. Furthermore, the as-irradiated values of yield strength were approximately the same for the samples in the as-received condition (line 8, Table 15.2) as for those given an additional 75% cold reduction (line 13). Thus it appears that at the high exposure level for this experiment, the properties of the irradiated samples were not dependent on prior cold work.

Figure 15.3 shows typical load-elongation and true-stress—true-strain curves for unirradiated and irradiated smooth samples. As is typical for face-centered cubic metals, the unirradiated samples did not exhibit a yield point. However, all irradiated samples showed a yield point. The onset of necking (localized plastic instability) was observed visually at the points on the stress-strain curve indicated in Fig. 15.3. It is interesting that, for the irradiated samples, necking did not occur at the maximum load (in this case, at the yield

point) but after some further plastic deformation had taken place.

The work-hardening characteristics may be analyzed for the smooth specimens in terms of the equation $\sigma = K\epsilon^n$, where σ is true stress, K is a constant, ϵ is true strain, and n is the work-hardening exponent. Values of n and K may be obtained from a plot of ln σ vs ln ϵ. Typical plots for the two heats are shown in Fig. 15.4. The un-irradiated specimens indicated a low, but positive, value of n (about 0.07) up to $\epsilon = 0.02$ to 0.03. This was followed by a region of higher work-hardening exponent (about 0.3). On the other hand, the irradiated samples exhibited zero or slightly negative slopes on the ln σ-ln ϵ plots up to about $\epsilon = 0.03$. This behavior is somewhat similar to "Lüders strain" in mild steel. At higher strains (up to $\epsilon = 0.08$), two specimens having yield strengths of about 100,000 psi exhibited a small, positive slope.

The notched specimens were included to determine whether a tendency exists toward an irradiation-induced notch sensitivity. The sheet specimens ($\frac{1}{2}$ in. wide) were notched on each side to one-third of the width. Also, the radius of curvature at the root was less than 0.001 in. and the included angle was 45°, thus producing a
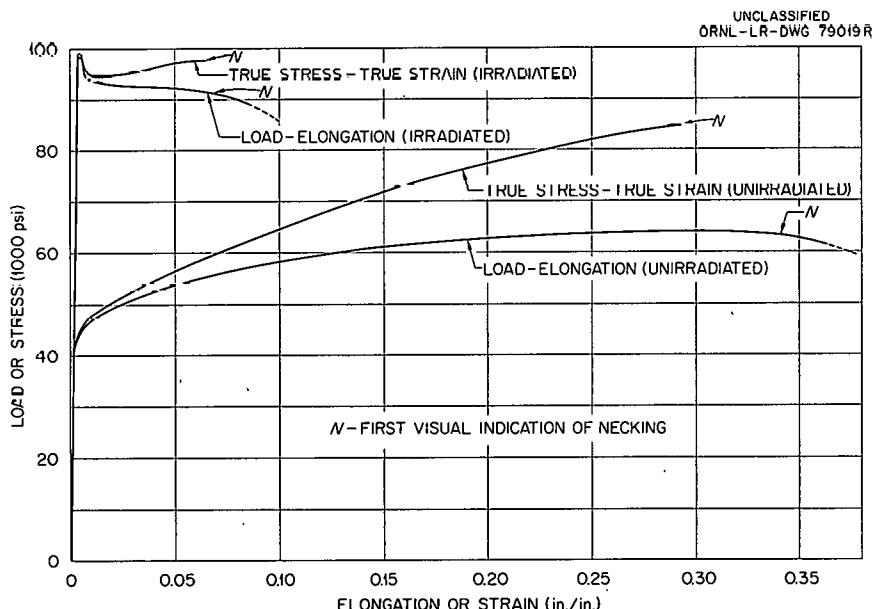

Fig. 15.3. Typical Load-Elongation and True-Stress—True-Strain Curves of Unirradiated and Irradiated Type 330 Nickel, Heat N6906A1 (Smooth Base-Plate Samples).

Table 15.2. Tensile Properties of Irradiated Type 330 Nickel

Line	Heat Number	Condition[a]	Specimen Type[b]	Irradiation Flux[c] [neutrons/cm² (>1 Mev)]	Yield Strength[d] (psi)	Ultimate Tensile Strength (psi)	Total Elongation (%)	Number of Tests
				$\times 10^{20}$				
1	N6906A1	As received	S	None	45,800	63,400	36	5
2	N6906A1	As received	S	7.8	95,600	e	10	1
3	N6906A1	As received	S	9.0	98,600	e	11	4
4	N6906A1	As received	S	11.3	101,300	e	8	1
5	N6906A1	As received	N	None	52,500	66,500		2
6	N6906A1	As received	N	7.8	108,600	e		2
7	N9185A1	As received	S	None	67,200	87,500	34	2
8	N9185A1	As received.	S	11.3	145,000	e	5	5
9	N9185A1	As received	N	None	80,000	97,400		2
10	N9185A1	As received	N	11.3	163,000	e		2
11	N9185A1	Cold worked	S	None	80,500	82,300	8	1
12	N9185A1	Cold worked	S	None	45,500	84,100	29	2
13	N9185A1	Cold worked	S	7.8	146,000	e	3	4
14	N9185A1	Cold worked	N	None	53,200	84,100		2
15	N9185A1	Cold worked	N	7.8	149,000	e		2
16	Weld-metal specimens		S	None	37,300	61,800	30	2
17	Weld-metal specimens		S	9.0	98,000	e	7	5
18	Weld-metal specimens		N[f]	None	49,600	84,700		2
19	Weld-metal specimens		N[f]	11.3	118,000	129,800		2
20	N6906A1	Heat-affected zone	N[g]	None	<40,000	63,000		1
21	N6906A1	Heat-affected zone	N[g]	9.0	104,000	e		1
22	N9185A1	Heat-affected zone	N[g]	None	43,000	82,000		1
23	N9185A1	Heat-affected zone	N[g]	9.0	118,000	e		1

[a]As-received condition is cold rolled, $\frac{1}{4}$ to $\frac{1}{2}$ hard temper; cold worked condition is cold rolled an additional 75%; heat-affected-zone condition is the heat-affected zone of a weldment; and weld-metal specimens contain base plate of both heats and weld metal.

[b]S indicates smooth sheet tensile specimens, and N indicates deep-edge-notched specimens.

[c]Based on the $Ni^{58}(n,p)Co^{58}$ reaction, assuming $\sigma_{eff} = 390$ mb, $E_{eff} = 2.9$ Mev, and fission spectrum.

[d]0.2% offset yield strength for all unirradiated samples and samples corresponding to lines 19, 21, and 23. Upper yield point for all others.

[e]Maximum load was the yield-point load.

[f]Notched in weld metal.

[g]Notched in heat-affected zone of indicated heat.

UNCLASSIFIED
ORNL-LR-DWG 79020

HEAT N-9185A1 (IRRADIATED)

HEAT N-6906A1 (IRRADIATED)

HEAT N-9185A1 (UNIRRADIATED)

HEAT N-6906A1 (UNIRRADIATED)

N—FIRST VISUAL INDICATION OF NECKING

STRESS (1000 psi)

STRAIN (in./in.)
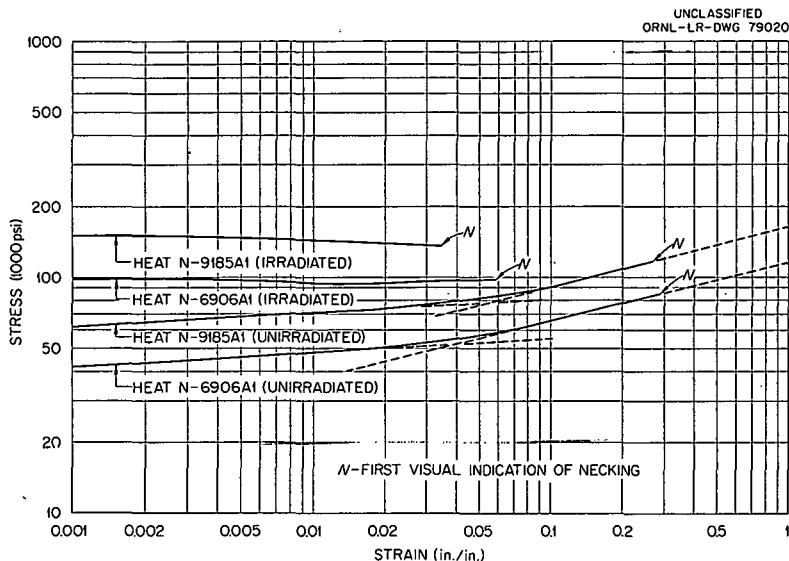
Fig. 15.4. Typical Log-True-Stress—Log-True-Plastic-Strain Curves of Unirradiated and Irradiated Type 330 Nickel (Smooth Base-Plate Samples).

large notch effect in this size specimen. As the results in Table 15.2 indicate, the notched samples exhibited slightly higher strength values than the corresponding smooth specimens, presumably due to the restraints introduced by metal on each side of the notch. Since considerable necking was observed at the notch prior to fracture·in irradiated as well as unirradiated samples, it is concluded that the irradiation did not produce an enhancement of notch sensitivity.

As regards the heat-affected-zone material, only notched samples were used, with the apex of the notch in the heat-affected zone to ensure deformation in this region. The yield and ultimate tensile strengths of the unirradiated heat-affected-zone samples were lower than those for the corresponding notched samples of the base material. This probably was the result of annealing during the welding process. Furthermore, on irradiation the increases in yield strength were approximately the same for the heat-affected-zone and the base-plate materials.

The weldment samples were of smooth and notched types. In addition to the weld metal, the gage length of the smooth weldment samples contained base-plate and heat-affected-zone material of both heats. For these samples it was found that fracture did not occur in the weld metal. No

unusual behavior was observed in the notched weld specimens.

The type 270 nickel samples have been irradiated, but the tensile tests have not yet been carried out.

EFFECT OF NEUTRON BOMBARDMENT ON THE STRESS-RUPTURE PROPERTIES OF SOME STRUCTURAL ALLOYS[22]

N. E. Hinkle

Stress-rupture experiments are being performed in the Oak Ridge Research Reactor to study the effect of neutron bombardment on the rupture strength and deformation characteristics of stressed tubular specimens at controlled elevated temperatures in oxidizing or inert-gas environments. The materials being investigated are Inconel alloy 600, type 304 stainless steel, Zircaloy-2, and a Nb—1% Zr alloy. The rupture strength of Inconel alloy 600 at 1500°F is decreased as much as 25% during irradiation. Smaller losses of rupture

---

[22] Abstract of paper presented at the *ASTM Symposium on Radiation Effects on Metals and Neutron Dosimetry, Los Angeles, Oct. 1—5, 1962,* ASTM-STP-341, p 344 (1963).

strength are observed for type 304 stainless steel at 1300 to 1500°F and for the Nb—1% Zr alloy at 1800°F. No major change is observed for Zircaloy-2 at 700 or 900°F. For the Inconel and stainless steel alloys the deformation at rupture is generally lowered; metallographic evidence indicates that these premature ruptures occur because of lowered grain-boundary cohesion.

IN-PILE STRESS-RUPTURE EXPERIMENTS

W. E. Brundage

The design of high-temperature power reactors and their components requires information on the mechanical properties of materials at elevated temperatures while under the influence of reactor environment. A series of tests of several alloys have been performed in the ORR. Tubular specimens, internally pressurized to the desired tangential stress level, were maintained at a selected temperature until rupture occurred, as indicated by a leakage of the pressurizing gas. The times to rupture were compared with those for similar control specimens tested out of pile. The results of these tests have been previously reported.[23,24]

Zircaloy-2

One additional group of Zircaloy-2 specimens was tested in the P-6 facility of the ORR in an attempt to extend to longer times the previously reported stress-rupture curves for specimens at 700 and 900°F. The ruptures occurred sooner than expected. At 700°F the specimens failed in the reactor at stresses about 15% lower than those required for rupture of the control specimens in the same times. Also, the specimens irradiated at 900°F failed at stresses over 30% lower than those for the control specimens. In contrast, the previous tests indicated little or no effect of reactor irradiation on the stress-rupture properties.

The departure from the predicted times could not be explained by variations in either specimen histories or operating procedures. Posttest examination indicated types of failures similar to those observed for previous irradiated samples. The failures all occurred in localized areas; blisters which extended about one-third the gage length and one-half the diameter were formed, as shown in Fig. 15.5.

The specimens for the Zircaloy-2 tests contained a water-cooled finger, as shown in Fig. 15.6, to remove the gamma heat from the specimen. Three furnace sections around each specimen

[23]W. E. Brundage et al., Solid State Div. Ann. Progr. Rept. Aug. 31, 1962, ORNL-3364, pp 138—47.

[24]N. E. Hinkle, "Effect of Neutron Bombardment on Stress Rupture Properties of Some Structural Alloys," p 324 in Symposium on Radiation Effects on Metals and Neutron Dosimetry, ASTM, Los Angeles, Oct. 1—5, 1962, ASTM-STP-341 (1963).
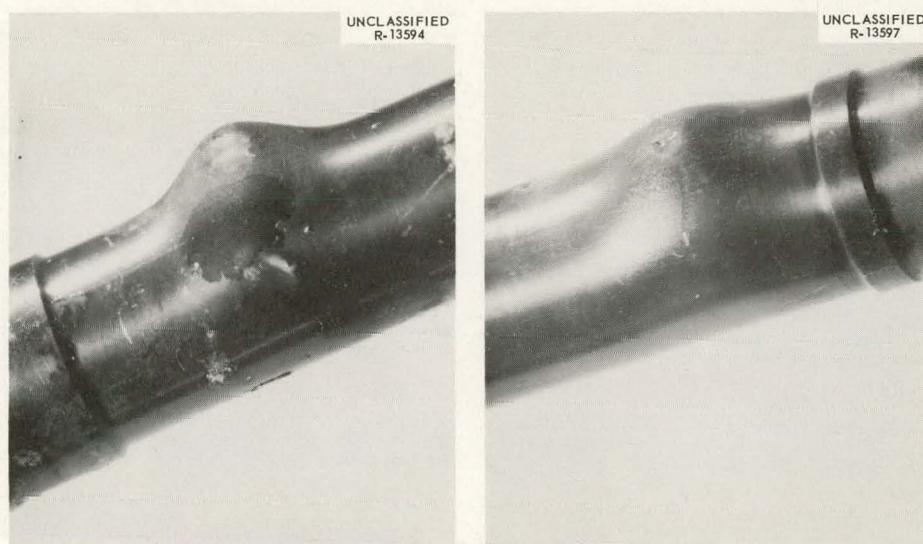
Fig. 15.5. Appearance of Typical Failures of Irradiated Zircaloy-2 Specimens.

were used, and a control thermocouple for each heater section was spot-welded to the specimen gage length. Limited access to the experiment did not permit additional thermocouples to be used to monitor the temperatures of other positions on the specimens during the initial tests.

For the last test the equipment was modified, allowing additional monitoring thermocouples to be placed on some of the specimens. These monitoring thermocouples revealed that severe axial temperature gradients existed along the length of the specimen. Low-temperature bands occurred under the junction of the heater sections. These were not found in out-of-pile mockups of the specimens. Temperatures as much as 200°F below the 900°F control temperature were noted. Although no temperatures more than 10°F above the control temperature were recorded, an analysis of the thermocouple positions, heater positions, and heat losses indicated that higher temperatures were likely at unmonitored positions. It appears that the area of highest temperature coincided with the regions at which the blisters occurred. An analysis of the situation indicates that two competing events occurred, one a strengthening effect due to the low-temperature bands, which effectively shortened the gage length, and the other a weakening effect resulting from the hot spots. In view of the unknown magnitude of these effects, the results of the in-pile Zircaloy-2 tests should be considered invalid.

ASTM A212B Steel

A stress-rupture experiment containing tube-burst samples of ASTM A212 grade B pressure-vessel steel is being conducted in the poolside facility (P-6) of the ORR. The irradiation temperature is 800°F, and a helium atmosphere is being used. A new specimen design is being used that permits operation at this temperature without auxiliary cooling. The specimens are in the form of tubes (4 in. long, $\frac{1}{2}$ in. OD, 0.020 in. wall). Hemispherical end caps are butt-welded on each end. The heaters are mounted inside the tube rather than surrounding it in order to improve the heat-transfer characteristics and to reduce the overall mass of the system. The active gage length is limited to the center 3-in. heated section.

Figure 15.7 shows the components of a specimen assembly. The heater is formed from 0.040-in.-diam metallic-sheathed heater cable. One end of the cable is welded shut, grounding the central heater wire to the sheath, and the cable is then coiled into a helix. Three sections are joined together to make one heater by spot-welding Nichrome spacer strips down its length. Figure 15.8 shows one end of an assembled heater. The heater leads and the pressurizing tubes are furnace brazed in position through one end cap, which is subsequently welded to the specimen tube.

UNCLASSIFIED
ORNL–DWG 63–1248

Fig. 15.6. Design Features of Zircaloy-2 Stress-Rupture Specimen with Cooling Finger.
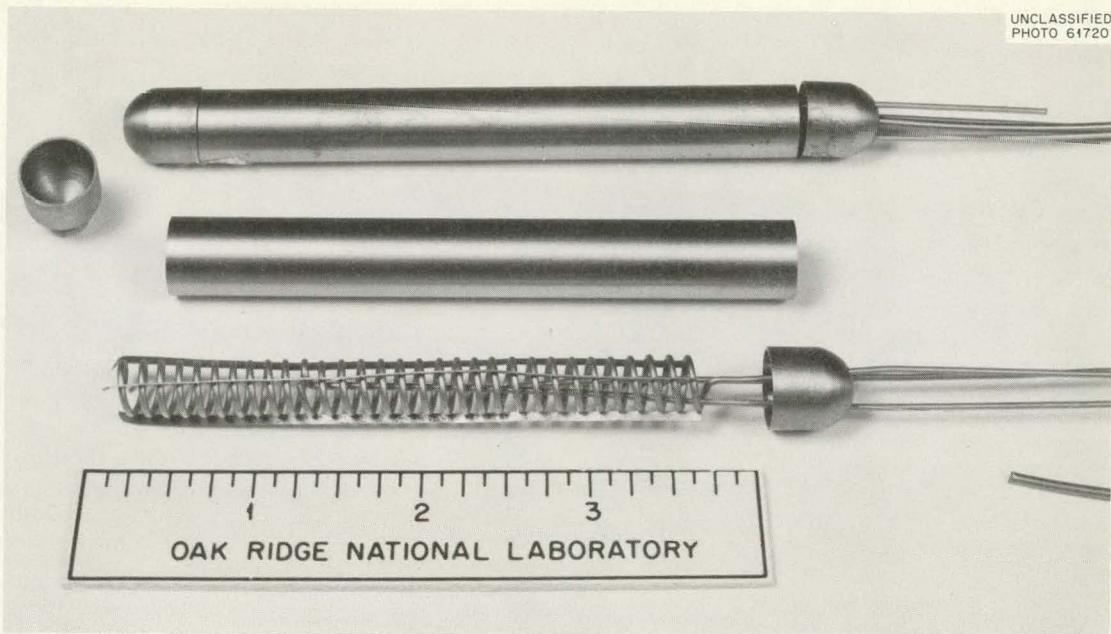
Fig. 15.7. Internally Heated Stress-Rupture Specimen of Pressure-Vessel Steel.
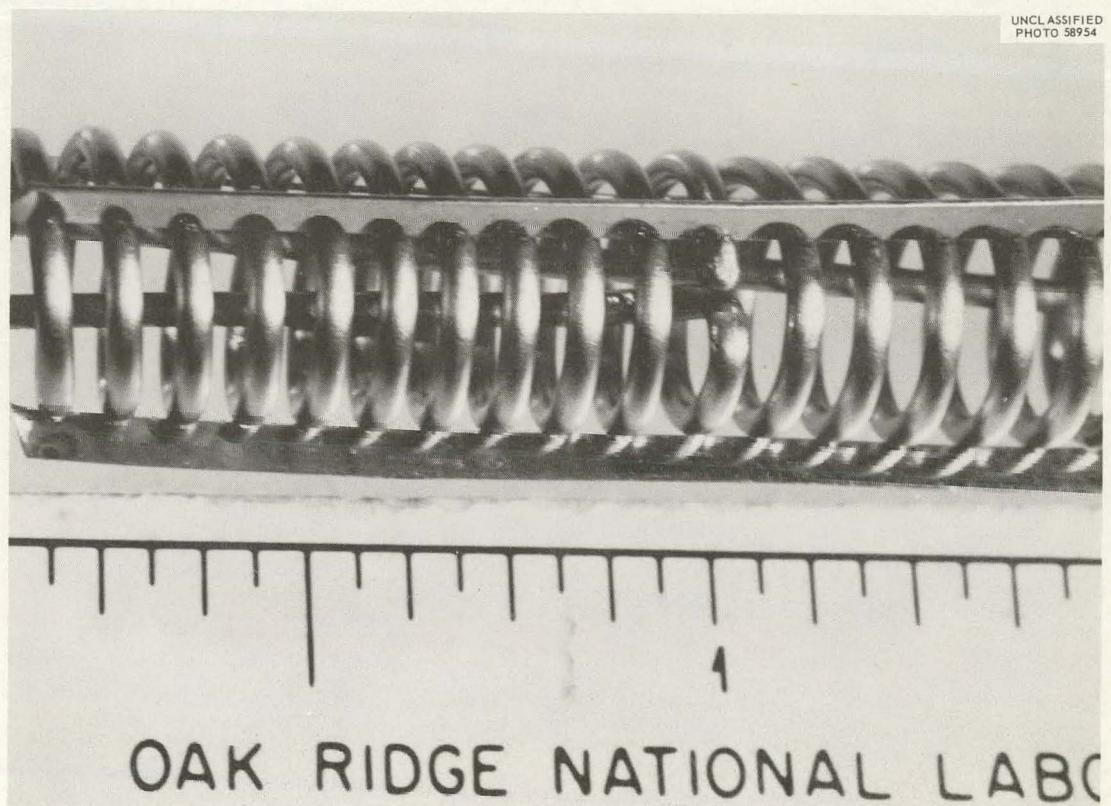
Fig. 15.8. Heater Detail.

Figure 15.9 shows a partially finished assembly of specimens prepared for insertion into the reactor. The specimens are positioned in recesses machined in an aluminum block. Control thermocouples are shown attached to the samples. Monitoring thermocouples and heater leads remain to be attached. In the final assembly the leads in the upper portion of the figure are enclosed in an aluminum box, and the unit is sealed by welding.

Operating experience to date has indicated satisfactory temperature control at 800°F. Also, no large temperature gradients appear to exist, as is shown by the fact that the maximum temperature differential monitored on the specimen gage length was 16°F with all control thermocouples maintained at 800°F.

Thermocouple access to the internally heated specimen is much easier than that for specimens previously used. In addition, this type of specimen has the advantage that it permits a more compact assembly.

IRRADIATION EFFECTS ON THE MECHANICAL PROPERTIES OF IRON AND IRON-BASE ALLOYS

N. E. Hinkle

The effect of neutron irradiation on the deformation characteristics of pressure-vessel steels has been the subject of extensive engineering studies since early in the nuclear energy program. These
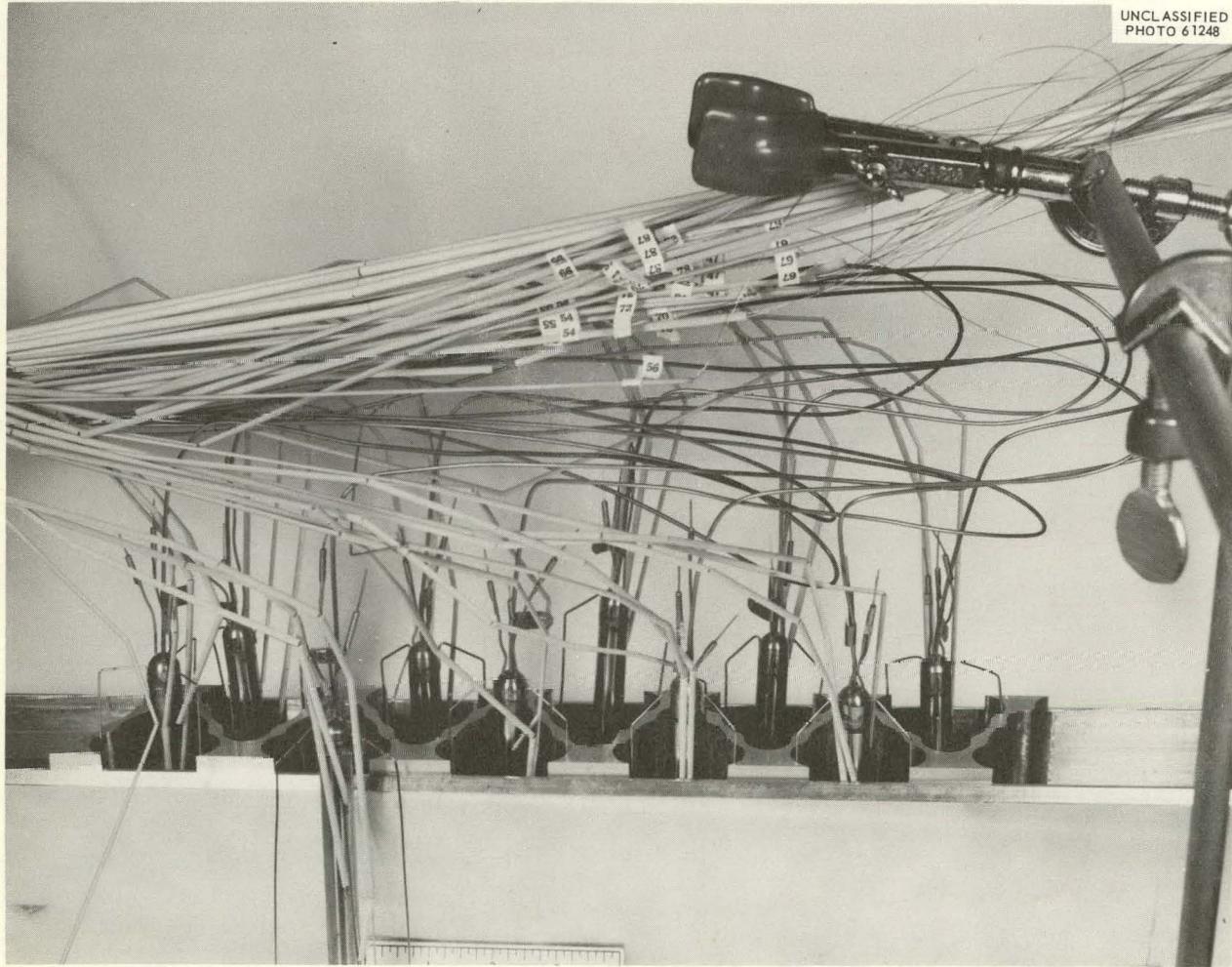
Fig. 15.9. Stress-Rupture Experiment Assembly for ORR, Pressure-Vessel Steel, Partially Assembled.

studies were necessary to determine whether the material's ability to deform on sudden loading without catastrophic failure is decreased due to the neutron bombardment. Recent reviews[25-27] have summarized the experimental results. The effect of neutron irradiation on steels is to increase the yield stress and ultimate tensile stress and to decrease the uniform elongation. Furthermore, the notch-impact brittle-ductile transition temperature is increased. Also, it has been found that, when the irradiation temperature is sufficiently high, the effects become less severe. As concerns the dependence on integrated flux or dose, earlier work[28] indicated that the increases in yield stress and the impact transition temperature vary as the cube root of the dose. However, more recently a square-root dependence has been suggested.[29] In addition, the effect of postirradiation annealing has been investigated. It is found that the original properties may be partially recovered, although in certain cases a reembrittlement is observed.[30] Also, the effectiveness of the postirradiation annealing treatment depends on the original irradiation temperature.[31]

The analysis of irradiation effects on mechanical properties in terms of basic processes has depended to a large extent on the use of the Cottrell-Petch equation[32,33]

$$\sigma_{YS} = \sigma_0 + k_Y d^{-1/2}, \tag{1}$$

where σ_0 is the lattice friction stress, k_Y is a factor proportional to the stress necessary to unpin a dislocation from its locking atmosphere, and d is one-half the grain diameter. Hull and Mogford,[34] using a British En-2 steel, found that Eq. (1) was obeyed for irradiated as well as for unirradiated samples. For doses up to 9×10^{19} (>1 Mev) neutrons/cm^2, σ_0 was found to increase, but no change in k_Y was noted.[34] For iron,[35] irradiated to 3×10^{16} neutrons/cm^2, they observed a small increase in σ_0 but, again, no change in k_Y. Campbell and Harding[36] and Chow et al.[37] also found that σ_0 for iron increases on irradiation, but they observed a decrease in k_Y at doses of 2 to 5×10^{18} neutrons/cm^2. The reason for the decrease in k_Y on irradiation is difficult to understand, since the decrease would imply less atmosphere locking. A factor that may be involved in this effect is the tendency toward subcell formation, such that the subcell size functions in the same manner as the grain size d in Eq. (1). Another point to be mentioned is the possible effect of the different heat treatments used to produce the different grain sizes. However, no firm explanation of the discrepancies among the previous results is available.

Based on the background information briefly summarized above, the following areas have been singled out as being of special interest in the present investigations:

1. The effect of irradiation on the parameters σ_0 and k_Y in Eq. (1).

[25]L. F. Porter, "Radiation Effects in Steel," p 147 in *Materials in Nuclear Applications*, ASTM-STP-276, American Society for Testing and Materials, Philadelphia, 1960.

[26]F. R. Shober, *The Effect of Nuclear Radiation on Structural Metals*, REIC-20 (Sept. 15, 1961).

[27]M. S. Wechsler and R. G. Berggren, *Nucl. Safety* 4(1), 42 (1962).

[28]A. H. Cottrell, "Theoretical Aspects of Radiation Damage and Brittle Fracture in Steel Pressure Vessels," p 281 in *Steels for Reactor Pressure Circuits*, Special Report No. 69, Iron and Steel Institute, London, 1961.

[29]R. W. Nichols and D. R. Harries, "Brittle Fracture and Irradiation Effects in Ferritic Pressure Vessel Steels," in *Symposium on Radiation Effects on Metals and Neutron Dosimetry*, ASTM, Los Angeles, Oct. 1-5, 1962, ASTM-STP-341 (1963).

[30]W. S. Pellini, L. E. Steele, and J. R. Hawthorne, *Analysis of Engineering and Basic Research Aspects of Neutron Embrittlement of Steels*, NRL-5780 (Apr. 17, 1962).

[31]J. R. Hawthorne, "Studies of Radiation Effects and Recovery of Notch Ductility of Pressure-Vessel Steels," p 343 in *Steels for Reactor Pressure Circuits*, Special Report No. 69, Iron and Steel Institute, London, 1961.

[32]N. J. Petch, *J. Iron Steel Inst.* (London) **173**, 25 (1953).

[33]A. H. Cottrell, *Trans. Met. Soc. AIME* **212**, 192 (1958).

[34]D. Hull and I. L. Mogford, *Phil. Mag.* **3**, 1213 (1958).

[35]I. L. Mogford and D. Hull, *J. Iron Steel Inst.* (London) **201**, 55 (1963).

[36]D. B. Campbell and J. Harding, "The Effect of Grain Size, Rate of Strain, and Neutron Irradiation on the Tensile Strength of α-Iron," p 51 in *Response of Metals to High-Velocity Deformation*, Interscience, New York, 1961.

[37]J. G. Y. Chow, S. B. McPickard, and D. H. Gurinsky, "The Mechanical Properties of Irradiated Iron and Iron Alloys," in *Symposium on Radiation Effects on Metals and Neutron Dosimetry*, ASTM, Los Angeles, Oct. 1-5, 1962, ASTM-STP-341, 1963.

2. The effect of varying the irradiation temperature. For some steels,[38] it has been observed that the irradiation-produced changes in mechanical properties increase at first with increasing irradiation temperature. This observation suggests that in some cases the change in properties is due to atomic rearrangements that proceed more quickly at the higher irradiation temperature.

3. The effect of dose rate. Little is known at present concerning the specific influence of dose rate. However, the factor may be important where atomic rearrangements are involved.[39] This factor takes on special significance in view of the disparity in the dose rates used in experiments on structural materials and the dose rates experienced by pressure vessels in service.

4. The effect of (n,γ) recoil events. Coltman et al.[40] have shown that measurable changes in

electrical resistivity are produced by (n,γ) damage, which results from atom recoil following thermal-neutron absorption and the emission of a capture gamma ray. The importance of this damage mechanism has not yet been investigated in connection with mechanical properties of iron and steels.

The first reactor experiment in this program was installed in the ORR in May 1963 in a piggyback position (i.e., a position attached to the back of a poolside experiment). The experiment assembly, shown in Fig. 15.10, contains 45 Armco iron tensile samples of various grain sizes. X-ray and electron-microscope samples are also included. The experiment is being conducted in collaboration with the Battelle Memorial Institute, Geneva.[41] The samples were supplied by BMI, Geneva, although a portion of them will be tested at ORNL for purposes of comparison. The samples are being irradiated in a helium atmosphere at temperatures between 40 and 60°C. Tensile tests will be conducted following irradiation in order to evaluate the effect of the irradiation on the parameters σ_0 and k_Y in Eq. (1).

A second ORR piggyback assembly is being designed and will be installed in September or October 1963. This experiment will contain tensile samples of the following materials:

[38]D. R. Harries, R. W. Nichols, and C. Judge, "The Effect of Neutron Irradiation on the Ductile-Brittle Transition Temperature of Steels and Its Relevance to Reactor Pressure Vessels," p 297 in *Steels for Reactor Pressure Circuits,* Special Report No. 69, Iron and Steel Institute, London, 1961.

[39]M. S. Wechsler, "Fundamental Aspects of Radiation Effects on Diffusion-Controlled Reactions in Alloys," p 86 in *Symposium on Radiation Effects on Metals and Neutron Dosimetry, ASTM, Los Angeles, Oct. 1–5, 1962,* ASTM-STP-341, 1963.

[40]R. R. Coltman, Jr., et al., *J. Appl. Phys.* 33, 3509 (1962).

UNCLASSIFIED
PHOTO 61247
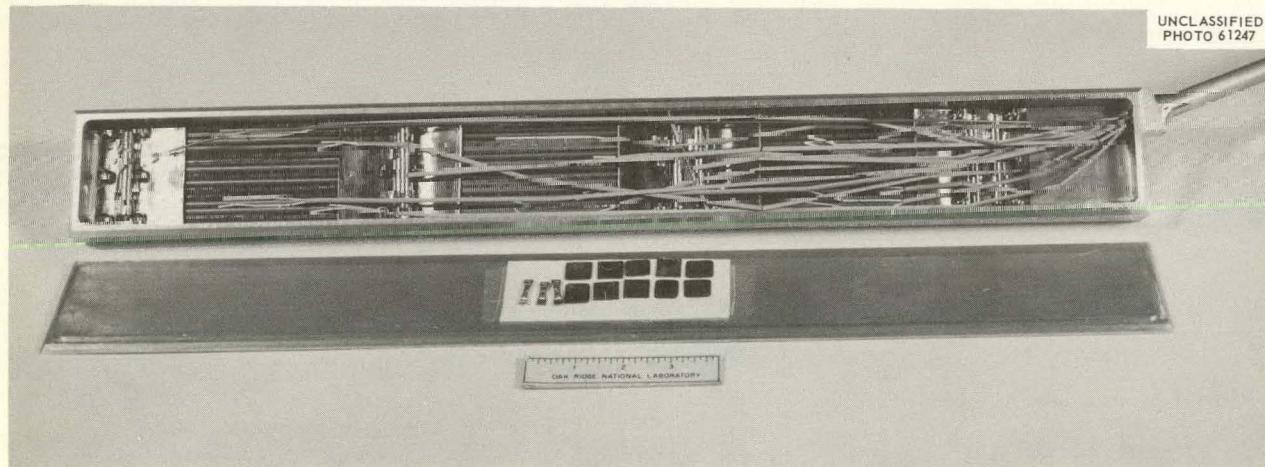
Fig. 15.10. Experiment Assembly for Armco Iron Irradiation.

1. Ferrovac E, a vacuum-melted iron. This material will be heat treated to obtain four grain sizes.
2. Ferrovac 1020 steel (0.2% C and 0.5% Mn), a vacuum-melted ternary alloy. This material will be heat treated to obtain four grain sizes.
3. Ferrovac 1020, a vacuum-melted iron-carbon binary alloy (0.2% C).
4. ASTM A212 grade B pressure-vessel steel, commercial heat. This material will be heat treated to obtain three grain sizes. The as-received material will also be included.
5. ASTM A212 grade B pressure-vessel steel, reference heat. This is a well-documented standard heat supplied to the ASTM by the United States Steel Corporation and is used to correlate the results of different laboratories doing radiation-damage studies on pressure-vessel steels.

The samples of each material and each grain size will be arranged so that the change in properties may be studied as a function of the neutron dose and dose rate. In this and future experiments, samples will be irradiated at temperatures up to 300°C.

A third experiment is being designed for insertion in the ORR at a poolside position adjacent to the core of the reactor. The same materials and temperatures will be used as in the previous experiment, but higher dose rates will be achieved.

In order to determine the possible effect of (n,γ) damage on iron and steels, two approaches will be used. In the first, certain samples will be cadmium-shielded from thermal neutrons. This will reduce the thermal-neutron exposure by two orders of magnitude. The second approach will involve the use of a D_2O tank in the Bulk Shielding Reactor to produce a highly thermalized neutron flux.

INTERNAL-FRICTION MEASUREMENTS IN IRON-NITROGEN ALLOYS

J. T. Stanley

The flexure pendulum apparatus described in an earlier report[42] was used to measure the internal friction of an iron-nitrogen alloy during reactor

[42]J. T. Stanley, *Solid State Div. Ann. Progr. Rept.* *Aug. 31, 1962*, ORNL-3364, pp 134–37.

irradiation. The results obtained in this experiment showed some features not observed in the absence of irradiation.

The specimen ($1\frac{1}{2}$ in. long and $\frac{3}{16}$ in. wide) was cut from "Ferrovac E" (0.005-in.-thick) iron foil. The specimen was loaded with 0.02 wt % nitrogen by heating to 590°C in an atmosphere of hydrogen and ammonia. One end of this specimen was clamped in the apparatus, and a small vane was attached to the other end. The vane was positioned so that it moved between two capacitance plates as the specimen vibrated. The specimen was made to vibrate by applying a voltage of the proper frequency (33 cps) between the specimen and a driving electrode. The change in capacitance was detected by a bridge circuit, and the resulting signal was displayed on an oscilloscope. Photographs of the oscilloscope screen were made and measured to determine the logarithmic decrement. The irradiation was carried out in Hole 17 of the Oak Ridge Graphite Reactor.

The data obtained in this experiment are presented in Fig. 15.11. The numbered points on the
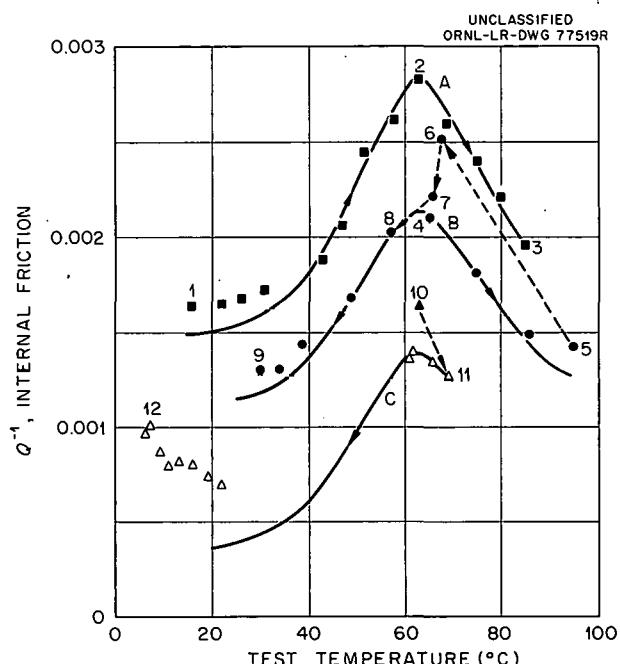
Fig. 15.11. Internal Friction vs Test Temperature for Iron-Nitrogen Alloy. In-pile flexure pendulum measurements at 33 cps. Solid symbols represent measurements with reactor on; open symbols measurements with reactor off.

curves refer to the sequence of measurements. Curve A in this figure was obtained after about three days of reactor operation. After making the measurements for curve A, Fig. 15.11, the specimen was cooled back to 65°C and held at this temperature for 17 hr. After this time, point 4 (curve B) was measured. The specimen temperature was then raised, and measurements were made along the path indicated by the arrows. After the measurement was made at 95°C (point 5), the temperature was reduced as quickly as possible to 68°C, and the measurement at point 6 was made. The measurements for points 6 and 7 were taken 38 and 71 min, respectively, after point 5. After the remaining measurements were taken, for curve B, the specimen was allowed to remain at 30°C for one day and was then heated to 63°C. The internal friction at 63°C (point 10) then remained constant at 0.00167 for 40 hr, at which time the reactor was shut down. After the reactor was shut down, the internal friction decreased rapidly, as shown by points 10 and 11 on curve C. The furnace was then allowed to cool, and the measurements in the temperature range 22 to 6°C were made.

The temperature of the internal-friction peak observed in these measurements agrees with the temperature of the nitrogen Snoek peak in iron reported by Fast and Verrijp.[43] The shape of this peak should be given by the equations

$$Q_N^{-1} = \Delta_M \frac{\omega\tau}{1 + (\omega\tau)^2} + Q_{BG}^{-1} , \qquad (1)$$

$$\tau = \tau_0 \exp(\Delta H/RT) ,$$

where Δ_M is the relaxation strength of the nitrogen Snoek peak (proportional to the amount of nitrogen in solid solution), ω is the angular frequency of vibration ($2\pi f$, $f = 33$ cps), τ is the relaxation time, Q_{BG}^{-1} is the background damping, and ΔH is the activation energy for a nitrogen-atom jump (18.6 kcal/mole).[43]

The background damping term Q_{BG}^{-1} in the above equation includes all sources of damping other than the nitrogen Snoek peak damping. Usually the background damping is quite small and constant in the temperature region of the nitrogen peak. In out-of-reactor measurements with this specimen, a background damping of 3×10^{-4} was

[43]J. D. Fast and M. B. Verrijp, *J. Iron Steel Inst.* **176,** 24 (1954).

measured. It is evident that Eq. (1) will not fit the data obtained in the reactor if one assumes that the background damping is not different from the value found in the out-of-reactor measurement. One possible solution to this problem is to assume that the background damping changes during reactor irradiation. The solid curves shown in Fig. 15.11 were derived on this assumption, but also it was assumed that the change in background was slow enough that the background damping remained constant for a given set of measurements. The results obtained by this analysis are given in Table 15.3.

Table 15.3. Internal Friction Due to Nitrogen Snoek Peak and Background[a]

	Dose (>0.6 Mev)[b] (neutrons/cm^2)	Q_N^{-1} (peak) $= \frac{1}{2}\Delta_M$	Q_{BG}^{-1}
	$\times 10^{16}$	$\times 10^{-4}$	$\times 10^{-4}$
Curve A	1.8	13.8	14.5
Curve B	2.4	10.6	10.8
Point 10		10.6	6.1
Curve C	3.9	10.6	3.3

[a]Data taken from Fig. 15.11.

[b]For curves A and B, the dose values pertain to the time of measurement at the peak; for curve C, the dose value signifies the previous irradiation exposure.

An alternative approach is to postulate the existence of other relaxation peaks at temperatures above and below the temperature of the nitrogen peak. These peaks then overlap with the nitrogen peak to give the observed behavior. Curves showing how the in-reactor measurements are analyzed using this assumption are shown in Fig. 15.12. The circles in Fig. 15.12 represent the data points of curve A, Fig. 15.11. The solid curve was obtained from Eq. (1) by assuming the same background damping (3×10^{-4}) as that for out-of-reactor measurements and by choosing the relaxation strength Δ_M so that the curve fits the data at the peak temperature (65°C) within experimental error. This curve was then subtracted from the data points (circles) to give the points shown as triangles. The dotted curves then show how the
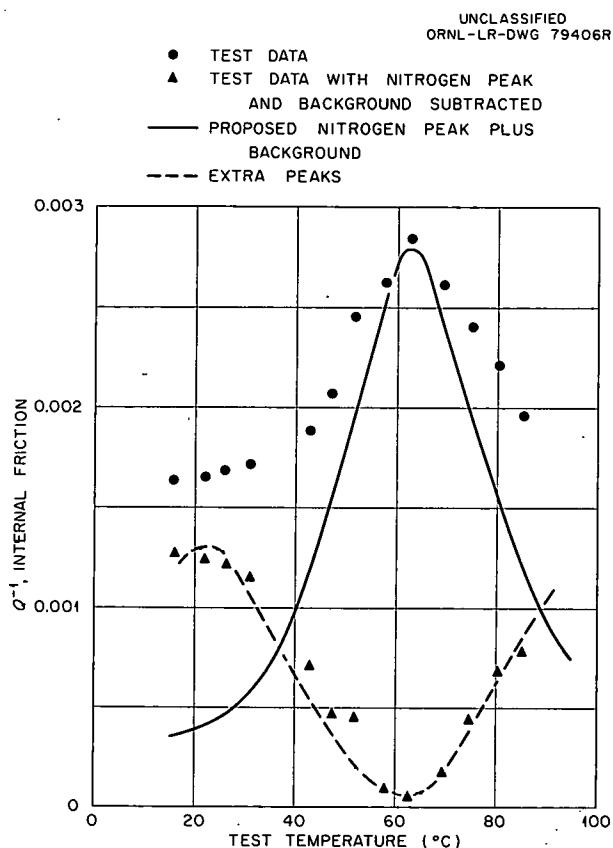
Fig. 15.12. Internal Friction vs Test Temperature for Iron-Nitrogen Alloy. In-pile flexure pendulum measurements at 33 cps.

extra peaks might look. Measurements over a wider temperature range should enable us to determine if these peaks actually exist.

An important difference between the two interpretations is found on considering the change of internal friction on reactor shutdown (points 10 and 11, Fig. 15.11). The first interpretation of the data attributes this change to a change in background damping, but the second interpretation attributes the change to a change in the amount of nitrogen in solution.

The precipitate formed on aging supersaturated iron-nitrogen alloys below 200°C is Fe_8N. The solubility of nitrogen[44] in equilibrium with Fe_8N at 65°C is about 0.0003 wt % N. Now, it was found for the sample used in the present investigation that, on aging out of the reactor at 65°C

following solution annealing and quenching, the internal friction due to nitrogen in solid solution leveled off at a value of about 3×10^{-4}. This is shown in Fig. 15.13. If we use a value of 1.0 relating the internal friction to nitrogen content in weight percent,[45] the equilibrium nitrogen content for our sample is determined to be 0.0003 wt % N at 65°C, in agreement with the previous literature. However, the measurements made during reactor bombardment (point 10, Fig. 15.11) show that the nitrogen Snoek peak levels off at a value substantially above that found in the preirradiation experiment. Thus we must conclude that during reactor irradiation more nitrogen remains in solid solution than would be found in the absence of irradiation. The exact amount of this extra nitrogen in solution depends on which of the above analyses of the data is correct. This extra nitrogen in solution might be explained in terms of a particle-size effect or a displacement-spike effect.

[45]L. J. Dijkstra, *Philips Res. Rep.* **2**, 357 (1947).
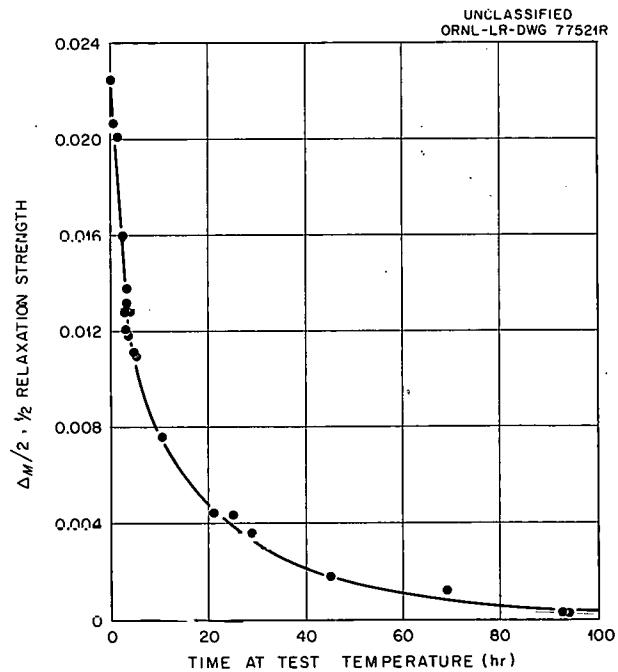
Fig. 15.13. Aging of the Nitrogen Peak in Iron-Nitrogen Alloy at 65°C. Relaxation strength vs aging time.

[44]K. Kamber, D. Keefer, and C. Wert, *Acta Met.* **9**, 403 (1961).

It has been shown for vanadium nitride precipitate particles in iron[46] that the nitrogen solubility is greater for small particles than for large particles. In the present case the effect of irradiation is to provide nucleation sites for nitride precipitates so that many more precipitates are formed than in the usual thermal aging experiments. These precipitates are very small and give rise to a higher nitrogen solubility than the precipitates formed by thermal aging. This model seems to fit the first interpretation of the shape of the internal-friction curves. The nitrogen solubility of these small particles would then be a factor of 3 greater than the nitrogen solubility of large particles.

It has also been observed that in some cases precipitated particles are broken up by displacement spikes during neutron bombardment.[47] This model appears to be more in accord with the second interpretation of the shape of the internal-friction curves. Here the displacement spikes break up precipitate particles and thus continuously furnish a fresh supply of nitrogen atoms in solution. A steady state is reached when the rate of precipitation balances the rate of dissolution of particles. When the reactor is shut down, the amount of nitrogen in solution decreases rapidly since only precipitation occurs. In this model the extra peaks might be caused by nitrogen atoms bound to defects such as interstitial iron atoms.

ATOMIC REARRANGEMENTS IN COPPER-NICKEL ALLOYS

W. Schüle[48]   B. C. Kelley

J. M. Williams   M. S. Wechsler

The copper-nickel alloy system is characterized by a continuous range of solid solutions based on the fcc lattice. Magnetic susceptibility[49] and electrical resistivity[50] measurements have indicated that the equilibrium atomic arrangement in the solid solution is not truly random but tends toward segregation of copper and nickel at lower temperatures. However, on cooling from a high temperature, atomic mobilities become so low below 350°C that the more-random configuration is frozen in. Furthermore, measurements of magnetic susceptibility,[49] electrical resistivity,[51,52] and magnetic Curie temperature[52] on neutron irradiation indicate that the reaction toward the segregated state is accelerated by irradiation. Thus, as a result of the irradiation treatment the equilibrium segregated atomic arrangement may be attained, a state that is most difficult to achieve by thermal means alone.

The mechanism of the radiation-enhanced segregation in Cu-Ni alloys has not been established, but the following may be considered: (1) diffusion enhancement due to the motion of radiation-produced vacancies, (2) diffusion enhancement due to the motion of radiation-produced interstitials (interstitialcy mechanism), and (3) enhancement due to the formation of nucleation sites for the clustering reaction. The vacancy mechanism is discussed in connection with radiation-enhanced ordering in Cu-Al alloys.[53]

In comparing the relative likelihood of the vacancy and interstitialcy mechanisms, it is interesting to make the following analysis concerning the number of jumps required for the clustering reaction. Ryan et al.[49] have found that the clustering reaction takes place during irradiation in about 40 days at 80°C, whereas only 50 hr at 350°C is required to regain the random state on postirradiation annealing. Now, Schüle and Kehrer[50] have shown as a result of quenching experiments that the activation energy for vacancy motion (E_{mv}) in Cu-Ni is 1.10 ev. The number of jumps per vacancy may be calculated from the equation

$$n_J = \nu_v t = \nu_{v0} \, t \exp\left(-\frac{E_{mv}}{kT}\right), \qquad (1)$$

[46]R. W. Fountain and John Chipman, *Trans. Met. Soc. AIME* **212**, 737 (1958).

[47]J. R. Piercy, *J. Phys. Chem. Solids* **23**, 463 (1962).

[48]Guest scientist from CCR-Euratom, Ispra (Varese), Italy.

[49]F. M. Ryan, E. W. Pugh, and R. Smoluchowski, *Phys. Rev.* **116**, 1106 (1959).

[50]W. Schüle and H.-P. Kehrer, *Z. Metallk.* **52**, 168 (1961).

[51]A. Ascoli, "Neutron-Bombardment-Enhanced Segregation in Cu-Ni Alloys," p 105 in *Radiation Damage in Solids*, vol II, International Atomic Energy Agency, Vienna, 1962.

[52]M. S. Wechsler et al., *Solid State Div. Ann. Progr. Rept. Aug. 31, 1959*, ORNL-2829, p 120.

[53]See J. M. Williams et al., "Temperature and Flux Dependence of Radiation-Enhanced Diffusion in Cu-Al," chap. 15, this report.

where ν_{v0} is about 10^{13}/sec and $E_{mv} = 1.10$ ev. For the formation of the clustered state ($t = 40$ days, $T = 80°C$), we find $n_j = 7 \times 10^3$ jumps per vacancy; whereas for the dissolution of this state ($t = 50$ hr, $T = 350°C$), $n_j = 2 \times 10^9$ jumps per vacancy. Therefore, if the number of atom jumps is the same for the two cases, we conclude that during irradiation the vacancy concentration must be greater than that during postirradiation annealing by a factor between 10^5 and 10^6. This factor appears rather high. Now let us assume that the formation of the clusters during irradiation is due to interstitial motion and that annihilation occurs mainly by vacancy-interstitial recombination. Then the concentrations of vacancies and interstitials will be nearly equal. In this case the motion energy necessary to produce 2×10^9 jumps in 40 days at 80°C [assuming $\nu_{i0} = 10^{13}$/sec in an equation similar to Eq. (1)] turns out to be between 0.7 and 0.8 ev. This appears reasonable, since if one attributes the stage III annealing after cold working to the migration of interstitials, one obtains the values 0.64 and 1.09 ev for copper[54] and nickel[55] respectively. The same energies within experimental error were determined after electron irradiation of copper[56] and nickel.[57]

Another point to be made concerning interstitialcy enhancement of diffusion relates to the sizes of the copper and nickel atoms. No interstitialcy enhancement of diffusion is expected when the atom sizes of the constituents of the alloy are greatly different. This is so because then only the smaller atom is likely to be pushed into an interstitial position, and no relative rearrangement of the two types of atoms will result. This has been pointed out to be the case for copper-gold alloys.[58] However, in copper-nickel alloys, the atomic sizes of copper and nickel are nearly equal; therefore, this factor should not prevent an interstitialcy diffusion mechanism from operating.

No information is available concerning radiation-induced nucleation in this system. However, such an effect has been observed for the precipitation of carbon in alpha iron.[59]

In order to investigate further the phenomenon of radiation-enhanced clustering in Cu-Ni, a series of foil samples (~ 0.008 in. thick) have been prepared in the composition range 35 to 75 at. % Ni at 5 at. % Ni intervals. A portion of the samples have been inserted in Hole 50 of the ORNL Graphite Reactor, where they will be irradiated for three weeks at $-185°C$. At the completion of the irradiation period, the samples will be removed from the reactor and maintained at liquid-nitrogen temperature until the electrical resistivity can be measured on isochronal and isothermal annealing. Similar measurements will be made on samples cold worked at low temperature. Also, a further experiment is planned in which resistivity measurements will be made during reactor irradiation at room temperature and above.

TEMPERATURE AND FLUX DEPENDENCE OF RADIATION-ENHANCED DIFFUSION IN Cu-Al

J. M. Williams   M. S. Wechsler
J. H. Barrett   W. Schüle[60]
B. C. Kelley

Introduction

When alpha Cu-Al alloys are bombarded with neutrons at temperatures between 0 and 210°C, a decrease in electrical resistivity is observed, which results from an increase in short-range order.[61-63] The increase in order proceeds at

[54]W. Schüle, J. Phys. Soc. Japan 18, 292 (1963).

[55]D. Schumacher, W. Schüle, and A. Seeger, Z. Naturforsch. 17a, 228 (1962).

[56]C. J. Meechan and J. A. Brinkman, Phys. Rev. 103, 1193 (1956).

[57]A. Sosin and J. A. Brinkman, Acta Met. 7, 478 (1959).

[58]J. A. Brinkman, C. E. Dixon, and C. J. Meechan, Acta Met. 2, 38 (1954).

[59]H. Wagenblast and A. C. Damask, J. Phys. Chem. Solids 23, 221 (1962).

[60]Guest scientist from CCR-Euratom, Ispra (Varese), Italy.

[61]M. S. Wechsler and R. H. Kernohan, "The Effect of Radiation on Diffusion-Controlled Reactions in Copper-Base Alloys," p 81 in Radiation Damage in Solids, vol II, International Atomic Energy Agency, Vienna, 1962.

[62]C. R. Houska and B. L. Averbach, J. Appl. Phys. 30, 1525 (1959).

[63]B. S. Borie and C. J. Sparks, Metals and Ceramics Div. Ann. Progr. Rept. May 31, 1962, ORNL-3313, pp 204–206.

an accelerated rate owing to the radiation enhancement of diffusion in this temperature region.[61,64] Furthermore, it has been shown[65] that samples which have undergone the ordering reaction can be returned to their original state of order, characterized by the higher resistivity value, by warming them to 210°C. Also, if such a sample is irradiated a second time below 210°C, the ordering reaction occurs again, but this time the rate of the reaction is smaller than it was the first time.[64] This decrease in the rate of the reaction after thermal cycling in the reactor has been called the "second-run phenomenon."[66]

The samples used in these experiments are single crystals of the Cu—15 at. % Al alloy. The initial preparation consists of a 2-hr anneal at 750°C, followed by a slow cool at 15°C/hr to room temperature. The behavior of the resistivity is illustrated schematically in Fig. 15.14. Curve AC represents the equilibrium resistivity-vs-temperature curve, unobservable in feasible aging times below T_2 (210°C). Curve AB represents the observed resistivity-vs-temperature curve below T_2. Thus, the nonequilibrium order, indicated by the resistivity difference between curves AB and AC, is frozen in on cooling below T_2. On isothermal irradiation at T_0, the decrease BC is observed.

The procedure for observing the second-run phenomenon is as follows. After the initial decrease in resistivity [BC (Fig. 15.14)] takes place, the sample is warmed to T_2 (210°C) with the reactor on and allowed to recover its initial value at A. Then, with the reactor off, the sample is cooled back down along AB to B at T_0. When the reactor is turned on again, the decrease BC is observed a second time. The magnitude of the decrease is the same as for the first run, but the rate of decrease is considerably reduced.

A series of runs following such cycling treatments is shown in Fig. 15.15 for an irradiation temperature (T_0) of 100°C. The normalized change in resistivity is plotted vs the logarithm of the irradiation time. The time for half completion ($\tau_{1/2}$) for the second run is greater than that for

the first run by a factor of 2.5. The third and fourth runs coincide with the second run, indicating that the effect saturates.

A point to be noted in Fig. 15.15 is that the shapes of the curves in the log-time plot are roughly the same (i.e., the curve for the first run may be superimposed on the curves for the repeated runs by a translation along the abscissa). This suggests that the factor responsible for the reduced reaction rate for the second run is not
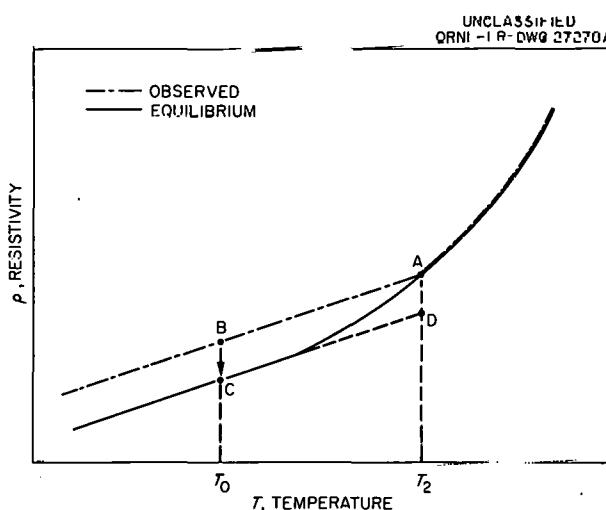
Fig. 15.14. Schematic Plot of Resistivity vs Temperature.
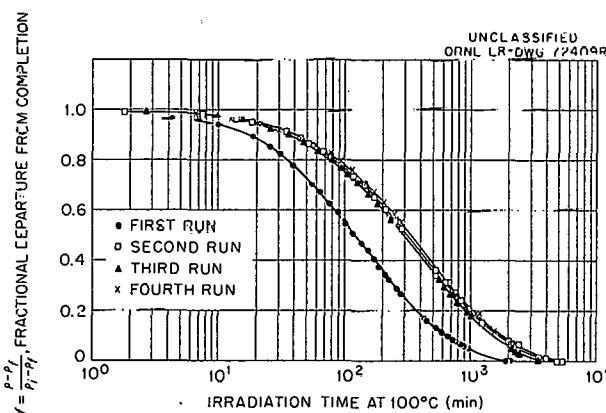
Fig. 15.15. Fractional Departure from Completion of the Decrease in Resistivity of Cu-Al (15 at. % Al) vs Time of Irradiation for Repeated Runs at Position 4, Hole C, ORNL Graphite Reactor.

[64]M. S. Wechsler et al., Solid State Div. Ann. Progr. Rept. Aug. 31, 1962, ORNL-3364, pp 127—34.

[65]R. H. Kernohan and M. S. Wechsler, J. Phys. Chem. Solids 10, 175 (1961).

[66]J. M. Williams, M. S. Wechsler, and J. H. Barrett, Bull. Am. Phys. Soc. 8(II), 197 (1963).

produced gradually during the first run. Instead, it would appear that it sets in during the cycling treatment. To test this idea, a sample was irradiated for 88 hr at 210°C (at a position in Hole C of higher flux than for the curves in Fig. 15.15) before the first run was made at 100°C. Figure 15.16 shows that this sample (curve B, Fig. 15.16) exhibited a smaller reaction rate than a fresh sample (curve A, Fig. 15.16). Now, previous experiments have indicated[65] that an irradiation at 210°C produces negligible ordering. Nevertheless, this experiment shows that the irradiation at 210°C is partly effective in bringing about the reduced reaction rate. This lends support to the idea mentioned above that the factor responsible for the longer second run is introduced during the cycling treatment in which the temperature is raised from 100°C to 210°C with the reactor on. Furthermore, the curves C and D in Fig. 15.16 show that the second runs for these samples displayed approximately the same reaction rate, which again suggests a saturation in the effect.

One further experiment should be mentioned at this point. It was stated earlier that the standard prior heat treatment for all samples consisted in an anneal at 750°C, followed by cooling to room temperature at 15°C/hr. The question arises as to whether this heat treatment is sufficient to erase the state giving rise to the second-run phenomenon. Therefore, a sample which had been cycled several times in the reactor was removed, and the standard heat treatment was reapplied. On reirradiation at 100°C, this sample exhibited a rate of decrease in resistivity characteristic of a fresh sample.

The theory of radiation-enhanced diffusion presented by Dienes and Damask[67] and Lomer[68] and extended in a previous report[64] shows that a study of the temperature and flux dependence of the radiation-accelerated reaction yields information concerning the mechanism of annihilation of the diffusion-enhancing defect. The temperature and flux dependence of the first runs has been reported previously.[64,65] During the past year, further insight into the mechanism of defect annihilation was gained as a result of experiments performed to determine the temperature and flux dependence of the second runs.

Temperature Dependence

For the work on the temperature dependence of the radiation-enhanced ordering, the samples were located at the center of Hole C of the ORNL

[67]G. J. Dienes and A. C. Damask, J. Appl. Phys. 29, 1713 (1958).

[68]W. M. Lomer, Diffusion Coefficients in Copper Under Fast Neutron Irradiation, AERE-T/R-1540 (December 1954).
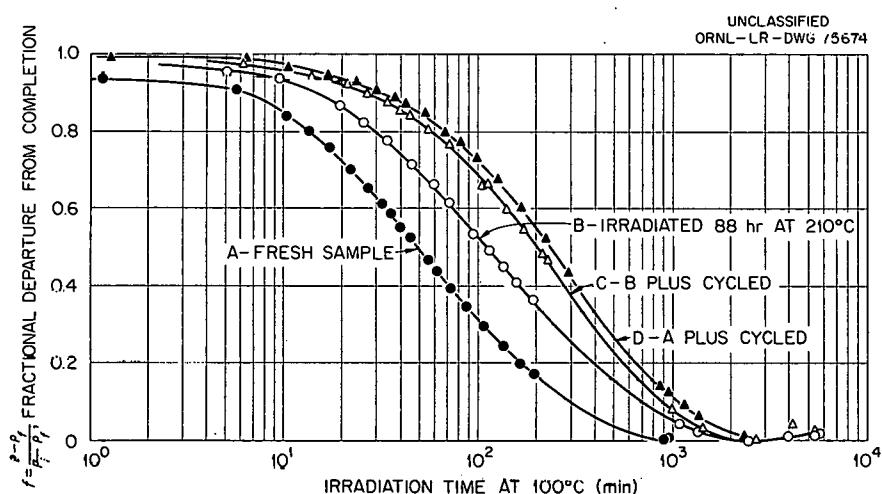
Fig. 15.16. Fractional Departure from Completion of Resistivity Decrease in Cu-Al (15 at. % Al) vs Irradiation Time for Two Samples with Different Treatments.

Graphite Reactor. Previous measurements have shown[64] that at this position the flux of neutrons with energies greater than 0.6 Mev is about 1.2×10^{11} neutrons $cm^{-2} sec^{-1}$, and the thermal flux is about 9×10^{11} neutrons $cm^{-2} sec^{-1}$. The time for half completion is plotted as a function of reciprocal irradiation temperature in Fig. 15.17. For the fresh samples (no prior irradiation), the activation energy is seen to be about 0.4 ev.

The temperature dependence of the cycled samples is also shown in Fig. 15.17. The Roman numerals I to V indicate the chronological order of successive runs on the same sample (i.e., run I was carried out on a fresh sample; the sample was cycled to regain the original resistivity, then run II was performed; then the sample was cycled again; and so on). Each run required one week of irradiation time, except run IV (at 50°C), which required two weeks. The use of repeated runs on the same sample was predicated on the results shown in Fig. 15.15, which indicate that the half-completion time does not depend on the irradiation history of the sample after the first run. Nevertheless, the half-completion time for run V in Fig. 15.17 is somewhat greater than that for run II. This difference is small, however, compared to the difference (on the logarithmic scale) in half-completion times for runs I and II. Therefore, it appears that the essential features of the phenomenon are not appreciably affected by the use of successive runs on the same cycled sample. One unnumbered point for cycled samples is shown on Fig. 15.17; this point refers to a different sample whose first and second runs were conducted at 100 and 30°C respectively.

The chief result shown in Fig. 15.17 is the marked decrease in the dependence on irradiation temperature for cycled samples as compared to fresh samples. Furthermore, we note that the curves for the fresh and cycled samples appear to merge at the lower temperatures. A further discussion of the significance of these observations is given below.

Flux Dependence

The flux dependence of the decrease in resistivity is studied by irradiating samples at various positions in Hole C. The integral flux above various threshold energies has been measured as a function of position in the hole by means of the threshold detectors.[64] Also, the thermal flux has been measured using cobalt monitors.[64] By the use of these flux measurements and the results of Coltman et al.[69] concerning the relative damage due to fast neutrons and thermal neutrons at the center of the reactor, we are able to estimate the displacement production rate K as a function of position in the hole.[64] The flux dependence of the reaction is then described in terms of the dependence of the half-completion time $(\tau_{1/2})$ on the displacement production rate K for a constant irradiation temperature. In our experiments on the flux dependence, the irradiation temperature was 100°C.

In the previous report,[64] it was shown that $\tau_{1/2}$ is proportional to $K^{-1/2}$ for the first runs (fresh samples, series I, Fig. 15.18). In addition, the flux dependence of the second runs has been investigated in two distinct ways, designated series II and series III. For series II, each second run


Fig. 15.17. Time for Half-Completion of the Resistivity Decrease in Cu-Al (15 at. % Al) vs Reciprocal Irradiation Temperature for Fresh and Cycled Samples. All irradiations at center of hole C.

[69]R. R. Coltman et al., J. Appl. Phys. 33, 3509 (1962).
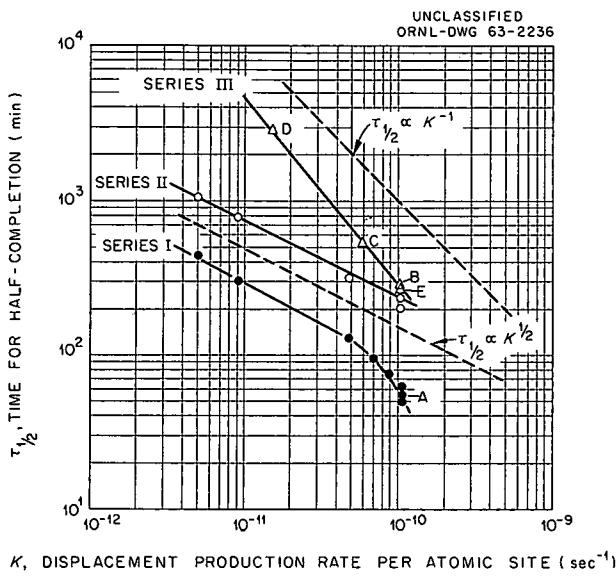
Fig. 15.18. Time for Half-Completion of the Resistivity Decrease in Cu-Al (15 at. % Al) as a Function of the Defect Production Rate for Fresh (Series I) and Cycled (Series II and III) Samples. In series II, the first runs were conducted at the same flux levels as the second runs. In series III, the same first run was used for each of the second runs. Irradiation temperature was 100°C.

is done at the same position in the reactor as the corresponding first run. Thus, each second run had a different irradiation history as regards the flux level. The curve labeled "series II" in Fig. 15.18 shows that for this case the flux dependence is described approximately by $\tau_{1/2} \propto K^{-1/2}$ as for the first runs (series I), although the $\tau_{1/2}$ values are greater than those for the first runs. After several of the runs in series II the sample was recycled, and a third run was made at 100°C. The third runs in each case indicated no further increase in $\tau_{1/2}$ after the second run, in agreement with the observations shown in Fig. 15.15.

For the second runs performed in series III, a succession of runs was performed on a single sample. The order of the runs is indicated by the symbols A—E in Fig. 15.18. We see that for the series III runs, $\tau_{1/2}$ is approximately proportional to K^{-1}. Also, the point for run III-E lies quite close to that for run III-B, which justifies the use of successive "second runs" on the same sample.

Discussion

Previous analyses[67,68] of radiation-enhanced diffusion have considered the radiation-produced defects to be at their steady-state concentrations. Estimates of the buildup time were made to set limits on the range of conditions under which the steady-state concentration could be used. The present discussion will show that many sets of experimental conditions lie in the transient region of defect concentration. This discussion will consider three simple annihilation mechanisms for the defects: (1) diffusion to fixed sinks, (2) pair recombination, and (3) diffusion to fixed sinks together with pair recombination. The concentrations of defects in thermal equilibrium will be neglected since it is believed that such concentrations are much less than those produced by the irradiation.

Fixed-Sink Mechanism. — For this mechanism radiation-produced vacancies and interstitials will anneal independently of each other. For either defect the time-dependent concentration will be[67]

$$c = \frac{K}{\beta \nu}(1 - e^{-\beta \nu t}), \qquad (1)$$

where c is the defect concentration per lattice site, K is the defect production rate per lattice site, $\nu = \nu_0 \exp(-E_M/kT)$ is the defect jump frequency, $\beta = a\lambda^2$, a is the concentration of fixed sinks, and λ is the defect jump distance. The number of defect jumps per lattice site which will have taken place by a time t is

$$J(t) = \int_0^t \nu c(t') \, dt' = \frac{K}{\beta^2 \nu} (\beta \nu t - 1 + e^{-\beta \nu t}). \qquad (2)$$

This equation can be solved numerically to give the time $t(J)$ to produce a certain number J of defect jumps per lattice site. The two solid curves in Fig. 15.19 illustrate how $\tau_{1/2}$ varies with $1/T$ for this annihilation mechanism. These two curves were selected to correspond approximately to the behavior of first and second runs, and the experimental points from Fig. 15.17 are shown for comparison. In Fig. 15.19, $J_{1/2}$ was chosen equal to unity, where $J_{1/2}$ is the number of jumps per lattice site necessary to complete half of the ordering process. If desired, the value of $J_{1/2}$ may be used as a parameter to aid in fitting the experimental results. In the calculations for Fig. 15.19 and in all other calculations
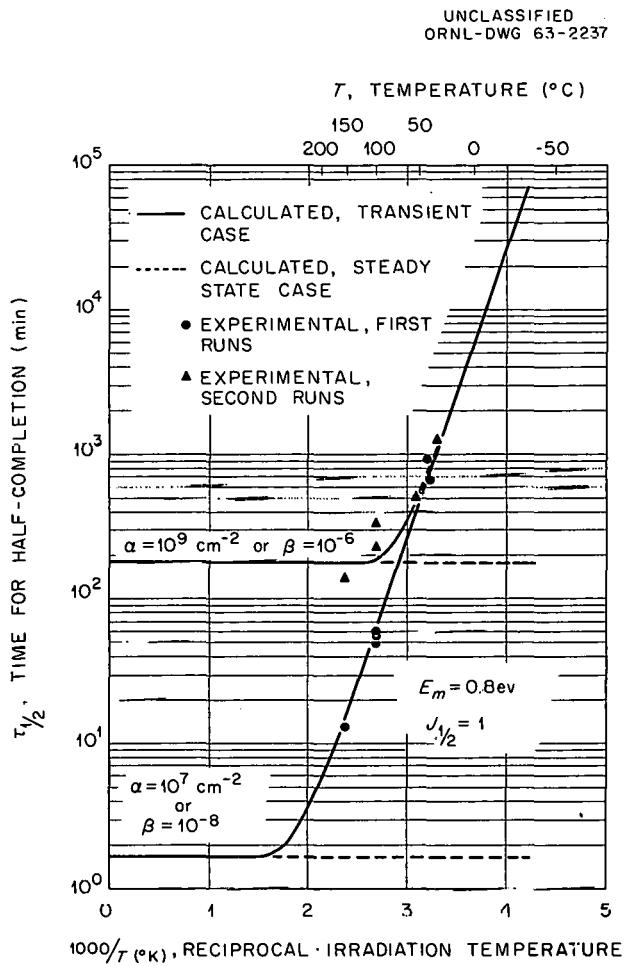
Fig. 15.19. Time for Half-Completion of the Ordering Process as a Function of the Reciprocal Irradiation Temperature in the Case of the Fixed-Sink Annihilation Mechanism.

for use in this discussion, values of $K = 10^{-10}$/sec, $\lambda^2 = 10^{-15}$ cm^2, and $\nu_{0v} = \nu_{0i} = 10^{14}$/sec have been used.

The dotted curves in Fig. 15.19 indicate the values of $\tau_{1/2}$ that are obtained if one uses the steady-state concentration in place of Eq. (1). They merge with the correct curves at high temperatures. The flux dependence of $\tau_{1/2}$ varies from K^{-1} at the high-temperature ends of the solid curves to $K^{-1/2}$ at the low-temperature ends.

If one calculates c at $t = \tau_{1/2}$ for a first run at $T = 100°C$, the result is $c \sim K\tau_{1/2} = (10^{-10}$/sec) $\times$ $(3 \times 10^3$ sec$) = 3 \times 10^{-7}$. The maximum value of β appropriate for the first runs is about 10^{-7}.

Use of these two numbers indicates that the rate of annihilation by pair recombination, which would be $\nu_i c^2$, would be greater than the rate of annihilation of interstitials by the fixed-sink mechanism, which would be $\nu_i \beta c$. Hence, it is inappropriate to neglect the effects of pair recombination.

Pair-Recombination Mechanism. — It is generally thought that the motion energy for interstitials is at least a few tenths of an electron volt less than that for vacancies. Therefore, it will be assumed that the interstitials have much the higher jump frequency and that pair recombination will take place predominantly by their migration to vacancies. The two defects will have the same concentration,

$$c = \sqrt{K/\nu_i}\ \tanh\ (\sqrt{K\nu_i}\ t)\ , \qquad (3)$$

and the numbers of defect jumps per lattice site are given by

$$J_v(t) = (\nu_v/\nu_i)\ \ln\ \cosh\ (\sqrt{K\nu_i}\ t)\ , \qquad (4a)$$

$$J_i(t) = \ln\ \cosh\ (\sqrt{K\nu_i}\ t)\ . \qquad (4b)$$

One might consider either type of defect to be the diffusion-enhancing defect. If the vacancies are the diffusion-enhancing defect, we find that, when $J_v = (J_v)_{1/2} \cong 1$, the process has already reached close to the steady state. In this case a plot of $\ln \tau_{1/2}$ vs $1/T$ gives a straight line[64] with a slope corresponding to $E_{mv} - \tfrac{1}{2}E_{mi}$. Thus, from the "fresh-samples" line of Fig. 15.17 we see that $E_{mv} - \tfrac{1}{2}E_{mi} = 0.41$ ev. On the other hand, if the interstitials are the diffusion-enhancing defect (by an interstitialcy mechanism), the steady state is not reached by a time for which $J_i = (J_i)_{1/2} \cong 1$. Nevertheless, from Eq. (4b) we see that

$$\tau_{1/2} = \frac{1}{\sqrt{K\nu_i}}\ \cosh^{-1}\ \exp\ (J_{1/2})\ ,$$

and $\ln \tau_{1/2}$ is proportional to $E_{mi}/2kT$. It may be seen from the above equation that this conclusion is valid regardless of the value chosen for $(J_i)_{1/2}$. Therefore, the measured activation energy of 0.41 for the fresh samples in Fig. 15.17 implies a value of 0.82 ev for E_{mi}. In regard to the curve for the cycled samples in Fig. 15.17, it is significant that neither type of pair-recombination mechanism appears capable of explaining the second-run

phenomenon. Instead, it seems necessary to propose that fixed sinks are introduced as a result of the cycling treatment, which alters the kinetics for the second and succeeding runs compared with the first run.

As regards the K dependence (Fig. 15.18), both pair-recombination mechanisms imply that $\tau_{1/2} \propto K^{-1/2}$. This follows from the forms in which K and t appear in the argument of the cosh function in Eqs. (4). Hence, these mechanisms will not explain the series III curve of Fig. 15.18, and we are again led to the suggestion that fixed sinks are introduced during the cycling treatment.

Fixed-Sink and Pair-Recombination Mechanisms Together. — The discussion in this case will be based on an approximate analysis[64] of the time-dependent behavior. For the approximations to be valid, $\nu_i \gg \nu_v$; for the temperature range of interest, this requires $E_{mi} < (E_{mv} - 0.3 \text{ ev})$. The equations for the defect concentrations only define these concentrations implicitly. Hence, no analytic form of $J(t)$ is available. However, it is possible to find two limiting cases for which approximate analytical solutions exist. If it is specified that $t(J)$ have better than 1% accuracy, we find for vacancy enhancement of diffusion that

$$t(J_v) = \left(\frac{3}{2\sqrt{2}}\right)^{2/3} \left(\frac{J_v}{\nu_v}\right)^{2/3} (\beta K)^{-1/3}$$

$$\text{for } \frac{\beta^2 \nu_v}{K} \lesssim \frac{64}{9 J_v^2} \times 10^{-6}, \quad (5a)$$

$$t(J_v) = \frac{\beta J_v}{K} \text{ for } \frac{\beta^2 \nu_v}{K} \gtrsim \frac{10^2}{J_v}. \quad (5b)$$

These two approximations have been used to plot the two full-line portions of each solid curve in Fig. 15.20. The dashed section connecting the two full-line sections of each curve has been interpolated by eye. This interpolation procedure is not exact but does indicate the general behavior of the curves. Unfortunately, the experimental points lie in the interpolated portions of the curves. Computer calculations are being planned in order to get the exact behavior of these curves. Once again the experimental points from Fig. 15.17 are shown, and the dotted curves show the results obtained if the steady-state concentration of defects

is assumed. From Eqs. (5), we see that the K dependence of $\tau_{1/2}$ varies from K^{-1} at the high-temperature ends of the curves to $K^{-1/3}$ at the low-temperature ends.

The comparison in Fig. 15.20 of the theoretical curves and the experimental points shows that the mechanism incorporating simultaneous fixed-sink and pair-recombination annihilation is capable of explaining the reduced temperature dependence of the second runs and the fact that the points for the two types of runs tend to merge at the lower temperatures. The curves in Fig. 15.20 are based on the choice of $E_{mv} = 0.8$ ev and $(J_v)_{1/2} = 1$. It is possible to fit the experimental points equally well with other choices of E_{mv} and $(J_v)_{1/2}$, but
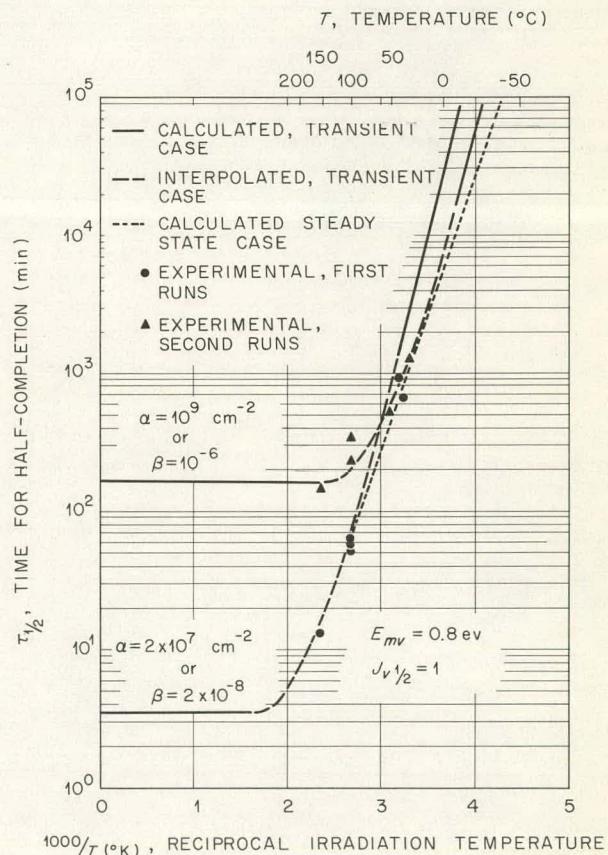
Fig. 15.20. Time for Half-Completion of the Ordering Process as a Function of the Reciprocal Irradiation Temperature in the Case of the Fixed-Sink and Pair Recombination Annihilation Mechanisms Together.

the two quantities must be varied in a coordinated way. For example, the sets of values $E_{mv} = 0.7$ ev, $(J_v)_{1/2} = 5$ and $E_{mv} = 0.85$ ev, $(J_v)_{1/2} = 0.2$ were found to satisfy the experimental results. Recent Monte Carlo calculations on the ordering process[70] indicate that $(J_v)_{1/2} \cong 5$. This result suggests a value of 0.7 ev for E_{mv}.

The curves in Fig. 15.20 suggest that the irradiation and cycling treatment of the first run must raise the dislocation density to about 10^9 dislocations per cm^2. Electron-transmission-microscope studies[71] have been initiated on unirradiated and irradiated thin foils. A photomicrograph of a sample irradiated at 100°C so as to produce minimum resistivity is shown in Fig. 15.21. The preliminary observations on samples given low radiation exposures have not identified any changes in dislocation arrangement or density related to the irradiation. The electron-microscope work is being continued. In particular, a cycled sample has been prepared; this sample will be examined to test the suggestion that the fixed sinks are introduced during the cycling treatment following the first run.

The proportionality of $\tau_{1/2}$ to K^{-1} for the series III second runs in Fig. 15.18 indicates that the annihilation mechanism is primarily diffusion to fixed sinks. Such a result is in accord with the temperature dependence found for the second runs.

We have seen in Fig. 15.18 that $\tau_{1/2} \propto K^{-1/2}$ for the series II second runs, in which the first runs were conducted at different K values. The close agreement of runs B and E (series III) in Fig. 15.18 indicates that neither the two intervening runs nor run B itself alters the number of fixed sinks introduced during the first run (run A, Fig. 15.18). From this it may be concluded that the important part of the irradiation history is the first run. Therefore, it is not unreasonable to suppose that the fixed-sink concentration, β, introduced by these first runs is a function of K. Now the second runs tend to fall in range of validity of Eq. (5b) in which $\tau_{1/2}$ is proportional to β/K. As a result, we find that the observed $\tau_{1/2} \propto K^{-1/2}$ is consistent with the assumption that $\beta \propto K^{1/2}$, that is, the fixed-sink concentration introduced by the first run depends on the square root of the K value at which the first run was carried out. This assumption can be rationalized in terms of the collapse of vacancy clusters into dislocation loops; however, this explanation is by no means unique and it warrants no further discussion at this time.

---

[70]P. A. Finn and G. M. McManus, *Phys. Rev.* **124**, 54 (1961).

[71]T. S. Noggle, chap. 5, this report.

UNCLASSIFIED PHOTO G2021

Fig. 15.21. Electron Transmission Photomicrograph of a Cu—15 at. % Al Foil Irradiated at 100°C to 10^{16} Neutrons/cm^2 (>0.6 Mev). The dislocation structures to be noted here are believed to have been introduced primarily during preparation of the foil.

FUNDAMENTAL ASPECTS OF RADIATION EFFECTS ON DIFFUSION-CONTROLLED REACTIONS IN ALLOYS[72]

M. S. Wechsler

A review is given of the present concept of the vacancy mechanism of diffusion in metals and alloys and of the experimental evidence that supports it. The freezing-in problem and radiation-enhanced diffusion are discussed from the point of view of the vacancy mechanism. The displacement production rate and the mechanism of vacancy annihilation are outlined in the light of current theories. Finally, the results of the theory are compared with experimental observations, particularly in regard to the temperature and the flux dependence of radiation-enhanced diffusion.

Publications, Papers, and Seminars

THIS PAGE

WAS INTENTIONALLY

LEFT BLANK

Publications and Papers

JOURNAL ARTICLES

K. F. Berggren and R. F. Wood
  "Effect of Correlation on the Hyperfine Interaction in Lithium," *Phys. Rev.* **130**, 198 (1963).

R. M. Carroll
  "Fission-Product Release From UO_2," *Nucl. Safety* **4**(1), 35 (1962).

J. G. Castle, D. W. Feldman, P. G. Kelmens, and R. A. Weeks
  "Electron Spin Lattice Relaxation at Defect Sites: E′ Centers in Synthetic Quartz at Kilo-Oersteds," *Phys. Rev.* **130**, 577 (1963).

J. W. Cleland, R. F. Bass, and J. H. Crawford, Jr.
  "Lattice Defect Production in Thermal Neutron Shielded Materials," *J. Appl. Phys.* **33**, 2906 (1962).

  "The Effect of Dislocations and Disordered Regions on Co^{60} Photon Induced Defects in Ge," *Appl. Phys. Letters* **2**, 113 (1963).

R. R. Coltman, C. E. Klabunde, D. L. McDonald, and J. K. Redman
  "Reactor Damage in Pure Metals," *J. Appl. Phys.* **33**, 3509 (1962).

C. Lehmann and G. Leibfried
  "Higher Order Momentum Approximations in Classical Collision Theory," *Z. Physik* **172**, 465 (1963).

G. Leibfried
  "Higher Order Averages of Primary Recoil Distributions," *Z. Physik* **171**, 1 (1962).

W. C. Mallard, A. B. Gardner, R. F. Bass, and L. M. Slifkin
  "Self-Diffusion in Silver-Gold Solid Solutions," *Phys. Rev.* **129**, 617 (1963).

D. L. McDonald
  "Low Temperature Irradiation of Beryllium Oxide," *Appl. Phys. Letters* **2**, 175 (1963).

Axel Meyer and R. B. Murray
  "Effect of Energetic Secondary Electrons on the Scintillation Process in Alkali Halide Crystals," *Phys. Rev.* **128**, 98 (1962).

J. G. Morgan, M. F. Osborne, and Oscar Sisman
  "Irradiation Effects in the EGCR Fuel," *Nucl. Sci. Eng.* **14**, 83 (1962).

R. B. Murray
  "Specific Heat of Single-Crystal $MnCl_2$ in Applied Magnetic Fields," *Phys. Rev.* **128**, 1570 (1962).

O. S. Oen and M. T. Robinson
  "The Effect of Channeling on Displacement Cascade Theory," *Appl. Phys. Letters* **2**, 83 (1963).

O. S. Oen, D. K. Holmes, and M. T. Robinson
  "Ranges of Energetic Atoms in Solids," *J. Appl. Phys.* **34**, 302 (1963).

M. L. Picklesimer and S. T. Sekula
  "Superconducting Transition Temperature of Purified Technetium," *Phys. Rev. Letters* **9**, 254 (1962).

M. T. Robinson

"Deduction of Ion Ranges in Solids from Collection Experiments," *Appl. Phys. Letters* **1**, 49 (1962).

M. T. Robinson and O. S. Oen

"The Channeling of Energetic Atoms in Crystal Lattices," *Appl. Phys. Letters* **2**, 30 (1963).

S. T. Sekula, R. W. Boom, and C. J. Bergeron

"Longitudinal Critical Currents in Cold Drawn Superconducting Alloys," *Appl. Phys. Letters* **2**, 102 (1963).

W. A. Sibley and Edward Sonder

"F- and M-Absorption in Heavily Gamma Irradiated KCl," *Phys. Rev.* **128**, 540 (1962).

M. J. Smith

"Determination of the Nonstoichiometric Doping Mechanism in Bi_2Se_3," *Appl. Phys. Letters* **1**, 79 (1962).

Edward Sonder and W. A. Sibley

"Radiation Equilibrium of F- and M-Centers in KCl," *Phys. Rev.* **129**, 1578 (1963).

A. L. Southern, W. R. Willis, and M. T. Robinson

"Sputtering Experiments with 1- to 5-kev Ar^+ Ions," *J. Appl. Phys.* **34**, 153 (1963).

M. S. Wechsler and R. G. Berggren

"Radiation Embrittlement of Reactor Pressure Vessels," *Nucl. Safety* **4**(1), 42 (1962).

R. A. Weeks

"The Paramagnetic Spectra of E_2' Centers in Crystalline Quartz," *Phys. Rev.* **130**, 570 (1963).

M. C. Wittels, F. A. Sherrill, and F. W. Young, Jr.

"X-Ray Observations of Nearly Perfect Copper Single Crystals," *Appl. Phys. Letters* **1**, 22 (1962).

"Anomalous Transmission of X-Rays in Copper," *Appl. Phys. Letters* **2**, 127 (1963).

F. W. Young, Jr.

"Etch Pit Studies of Dislocations in Copper Crystals Deformed by Bending: I. Annealed Crystals; II. Irradiated Crystals," *J. Appl. Phys.* **33**, 3553 (1962).

BOOKS AND PROCEEDINGS

R. G. Berggren

"Critical Factors in the Interpretation of Radiation Effects on the Mechanical Properties of Structural Metals," Bulletin No. 87, p 1, Welding Research Council, New York, 1963.

D. S. Billington

"Introduction," p 1 in *Rendiconti della Scuola Internazionale di Fisica "E. Fermi," XVIII Corso*, Academic Press, London, 1963.

D. S. Billington and D. O. Thompson

"Radiation Damage Research in Low-Power Nuclear Reactors," p 223 in *Programming and Utilization of Research Reactors*, vol I, Academic Press, London, 1962.

T. H. Blewitt

"Low-Temperature Irradiation Studies," p 630 in *Rendiconti della Scuola Internazionale di Fisica "E. Fermi," XVIII Corso*, Academic Press, London, 1963.

C. D. Bopp, W. W. Parkinson, and Oscar Sisman
"Plastics," p 183 in *Radiation Effects on Organic Materials,* chap. 5 (ed. by R. O. Bolt and J. G. Carroll), Academic Press, New York, 1963.

R. O. Chester, R. W. Peelle, and F. C. Maienschein
"Nonlinear Least-Squares Fitting Applied to Gamma-Ray Scintillation Detector Response Functions," p 201 in *Applications of Computers to Nuclear and Radiochemistry,* NAS-NS 3107 (March 1963).

J. W. Cleland
"Transmutation Doping and Recoil Effects in Semiconductors Exposed to Thermal Neutrons," p 84 in *Rendiconti della Scuola Internazionale di Fisica "E. Fermi," XVIII Corso,* Academic Press, London, 1963.

R. R. Coltman
"Reactor Irradiation Studies at 4°K," p 205 in *Radiation Damage in Solids,* vol II, International Atomic Energy Agency, Vienna, 1962.

J. H. Crawford, Jr.
"Radiation Effects in Semiconductors," p 333 in *Rendiconti della Scuola Internazionale di Fisica "E. Fermi," XVIII Corso,* Academic Press, London, 1963.

D. K. Holmes
"The Ranges of Energetic Atoms in Solids," p 3 in *Radiation Damage in Solids,* vol I, International Atomic Energy Agency, Vienna, 1962.

"Terms and Concepts in Radiation Damage Theory," p 182 in *Rendiconti della Scuola Internazionale di Fisica "E. Fermi," XVIII Corso,* Academic Press, London, 1963.

"Radiation-Damage Studies Using Dislocation Properties," p 777 in *Rendiconti della Scuola Internazionale di Fisica "E. Fermi," XVIII Corso,* Academic Press, London, 1963.

M. J. Kelly, W. W. Johnston, and C. D. Baumann
"The Effects of Nuclear Radiation on Thermocouples," p 265 in *Temperature: Its Measurement and Control in Science and Industry,* vol III, pt 2 (ed. by A. I. Dahl), Reinhold, New York, 1962.

G. Leibfried
"Radiation Damage Theory," p 227 in *Rendiconti della Scuola Internazionale di Fisica "E. Fermi," XVIII Corso,* Academic Press, London, 1963.

R. B. Murray
"Scintillation Counters," p 82 in *Nuclear Instruments and Their Uses,* vol I (ed. by A. H. Snell), Wiley, New York, 1962.

T. S. Noggle
"Dislocations in UO_2," p B-5 in *Proceedings Fifth International Conference on Electron Microscopy,* vol I, Academic Press, New York, 1962.

"Critical Shear Stress for Slip," p 508 in *Encyclopaedic Dictionary of Physics,* vol 6 (ed. by J. Thewlis), Pergamon, London, 1962.

M. T. Robinson, D. K. Holmes, and O. S. Oen
"Monte Carlo Calculations of the Ranges of Energetic Atoms in Solids," p 105 in *Le Bombardement Ionique,* Centre National de la Recherche Scientifique, Paris, 1962.

Oscar Sisman, W. W. Parkinson, and C. D. Bopp
"Polymers," p 127 in *Radiation Effects on Organic Materials,* chap. 5 (ed. by R. O. Bolt and J. G. Carroll), Academic Press, New York, 1963.

M. S. Wechsler and R. H. Kernohan
"The Effect of Radiation on Diffusion-Controlled Reactions in Copper-Base Alloys," p 81 in *Radiation Damage in Solids,* vol II, International Atomic Energy Agency, Vienna, 1962.

THESES

J. C. Pigg
"Annealing of Gamma Ray Induced Changes in Antimony-Doped Germanium," thesis, submitted to the Graduate Council of the University of Tennessee in partial fulfillment of the requirements for the Ph.D. degree, 1963.

PAPERS PRESENTED AT TECHNICAL MEETINGS

C. J. Bergeron, R. W. Boom, and S. T. Sekula
"Longitudinal and Transverse Critical *I-H* Characteristics for Nb-Zr," presented at American Physical Society Annual Meeting, New York, Jan. 23–26, 1963.

R. G. Berggren
"Radiation Effects on Metal Materials," presented at ASME Symposium on Advanced Technology, Albuquerque, N. M., Nov. 3, 1962.

Ugo Bertocci, L. D. Hulett, L. H. Jenkins, and F. W. Young, Jr.
"On the Formation of Electrochemical Etch Pits on the (111) Face of Copper," presented at Electrochemical Society Phenomena at Interfaces Symposium, Boston, Sept. 16–20, 1962.

R. O. Chester, R. W. Peelle, and F. C. Maienschein
"Nonlinear Least-Squares Fitting Applied to Gamma-Ray Scintillation Detector Response Functions," presented at Applications of Computers to Nuclear and Radiochemistry Symposium, Gatlinburg, Tenn., Oct. 17–19, 1962.

J. W. Cleland and R. F. Bass
"Lattice Defect Production in Ge by Photons and by Neutrons," presented at American Physical Society March Meeting, St. Louis, Mar. 25–28, 1963.

"Lattice Defect Production in GaAs by Photons and by Neutrons," presented at American Physical Society Southeastern Meeting, Knoxville, Tenn., Apr. 4–6, 1963.

J. H. Crawford, Jr.
"Investigations of Color Centers in Alkali Halides at Oak Ridge National Laboratory," presented at International Conference on Crystal Lattice Defects, Kyoto, Japan, Sept. 7–12, 1962.

O. L. Curtis, Jr., and C. C. Robinson
"Trapping Centers in As-Doped Ge," presented at American Physical Society March Meeting, St. Louis, Mar. 25–28, 1963.

R. Gwin and R. B. Murray
"Emission Spectra of CsI(Tl) Crystals and the Possible Role of Self-Trapped Holes," presented at American Physical Society Thanksgiving Meeting, Cleveland, Nov. 23–24, 1962.

N. E. Hinkle
"The Effect of Neutron Bombardment of the Stress Rupture Properties of Some Structural Alloys," presented at ASTM Symposium on Radiation Effects on Metals and Neutron Dosimetry, Los Angeles, Oct. 1–5, 1962.

L. D. Hulett and F. W. Young, Jr.
"The Rate of Growth of Electrochemical Etch Pits at Dislocations on (111) Copper Surfaces," presented at Electrochemical Society Phenomena at Interfaces Symposium, Boston, Sept. 16–20, 1962.

E. Lell and R. A. Weeks
"Effects of Irradiation on Polarization Currents in a Lead Silicate Glass," presented at American Physical Society Spring Meeting, Washington, D.C., Apr. 22–25, 1963.

A. Meyer and R. F. Wood
"Electron Structure and the M Center," presented at American Physical Society Spring Meeting, Washington, D.C., Apr. 22–25, 1963.

T. S. Noggle
"Dislocations in UO_2," presented at Fifth Annual Congress of Electron Microscopy, Philadelphia, Aug. 29–Sept. 5, 1962.

O. S. Oen and M. T. Robinson
"Ranges of Energetic Atoms in Solids for a Thomas-Fermi Potential," presented at American Physical Society March Meeting, St. Louis, Mar. 25–28, 1963.

M. T. Robinson
"Slowing Down of Energetic Atoms in Crystals," presented at American Physical Society Southeastern Meeting, Knoxville, Tenn., Apr. 4–6, 1963.

M. T. Robinson and O. S. Oen
"Orientation Dependence of the Ranges of Atoms in Crystals," presented at American Physical Society March Meeting, St. Louis, Mar. 25–28, 1963

A. I. Schindler and R. H. Kernohan
"The Interaction Between Irradiation-Induced Defects and Magnetic Structure," presented at International Conference on Crystal Lattice Defects, Kyoto, Japan, Sept. 7–12, 1962.

Edward Sonder and W. A. Sibley
"Radiation Hardening in KCl Single Crystals," presented at American Physical Society March Meeting, St. Louis, Mar. 25–28, 1963.

D. O. Thompson
"Evidence for Vacancy Clustering in Dislocations in Copper as Measured by Internal Friction Techniques," presented at International Conference on Mechanical Aspects of Lattice Defects on Crystals, Tokyo, Japan, Sept. 3–4, 1962.

M. S. Wechsler
"Fundamental Aspects of Radiation Effects on Diffusion-Controlled Reactions in Alloys," presented at ASTM Symposium on Radiation Effects on Metals and Neutron Dosimetry, Los Angeles, Oct. 1–5, 1962.

M. S. Wechsler, J. M. Williams, and H. M. Otte
"Atomic Rearrangements in Deformed Cu-Si and Cu-Si-Mn Alloys," presented at International Conference on Crystal Lattice Defects, Kyoto, Japan, Sept. 7–12, 1962.

R. A. Weeks
"Direct Field Effects in the Hyperfine Spectra of a Paramagnetic Defect in Quartz: The $\bar{E}_2'$ Center," presented at American Physical Society Southeastern Meeting, Knoxville, Tenn., Apr. 4–6, 1963.

M. K. Wilkinson
"Magnetic Structure of Rare-Earth Metals and Intermetallic Compounds," presented at American Physical Society Southwestern Meeting, Houston, Feb. 28–Mar. 2, 1963.

J. M. Williams, M. S. Wechsler, and J. H. Barrett
"2nd-Run Phenomenon in Irradiated Cu–15 at. % Al," presented at American Physical Society March Meeting, St. Louis, Mar. 25–28, 1963.

R. F. Wood
"Calculations of Some Ground-State Properties of F Centers," presented at American Physical Society Spring Meeting, Washington, D.C., Apr. 22–25, 1963.

F. W. Young, Jr.
"Etch Pit Studies of Dislocations in Copper Crystals Deformed by Bending: I. Annealed Crystals; II. Irradiated Crystals," presented at International Conference on Mechanical Aspects of Lattice Defects on Crystals, Tokyo, Japan, Sept. 3–4, 1962.

F. W. Young, Jr., and L. D. Hulett
"On the Role of Crystal Imperfections in the Chemical Reactivity of Copper Surfaces," presented at ASM-AIME Surfaces Symposium, New York, Oct. 27–28, 1962.

REPORTS ISSUED

J. C. Pigg
Annealing of Gamma Ray Induced Changes in Antimony-Doped Germanium, ORNL-3443 (May 14, 1963).

Seminars

SOLID STATE SEMINARS AT ORNL

The following visitors to the Solid State Division gave seminars during the period covered by this report:

1962

September 14   J. Spreadborough, Battelle Institute, Geneva
     "Lüders Bands in Iron"

September 19   H. R. Hahn, Institut für Reaktorwerkstoffe, Jülich, West Germany
     "Anharmonicity Effects on Neutron Scattering in Solids"

October 1   J. C. Pfister, Ecole Normale Superieure, Paris
     "Radiation-Enhanced Diffusion in Silicon"

October 4   J. B. Birks, University of Manchester, England
     "Organic Fluorescence"

November 23   J. W. Christian, Case Institute of Technology, Cleveland
     "Flow Stress Measurements in Body-Centered Cubic Metals"

1963

February 14   Martin Goldstein, Ford Motor Company Research Laboratory, Dearborn, Mich.
     "Some Light Scattering Problems Soluble by a Fourier Transform Method, with
     Applications to Radiation Damage"

February 21   Cavid Erginsoy, Brookhaven National Laboratory
     "Crystal Symmetries in Atomic Displacement Processes"

March 29   H. J. Queisser, Shockley Laboratories, Clevite Corp., Palo Alto, Calif.
     "Dislocations and Diffusion in Silicon"

April 4   Nicolaas Bloembergen, Harvard University, Cambridge, Mass.
     "Electric Shifts in Magnetic Resonance"

April 15[a]	Brebis Bleany, Clarendon Laboratory, Oxford, England "Nuclear Moments of the Lanthanons"
April 16[a]	Brebis Bleany, Clarendon Laboratory, Oxford, England "Crystal Field Effects in Pr, Ce, Nd Metals"
April 17[a]	Brebis Bleany, Clarendon Laboratory, Oxford, England "Crystal Field Effects in $LnNi_2$, $LnNi_5$ Compounds"
April 17	Walter Bollman, Argonne National Laboratory "Analysis of Dislocation Networks"
April 18	Robert Nathans, Brookhaven National Laboratory "Polarized Neutron Studies on Antiferromagnetic Materials"
April 26	Ian Firth, University of British Columbia, Vancouver, British Columbia "Microwave Studies of Phonon Entrapment"
May 2	H. A. Gersch, Georgia Institute of Technology, Atlanta "Quantum Cell Model for Bosons"
May 7	J. A. Morrison, National Research Council, Ottawa "Thermodynamics of Molecular Crystals"
May 27	Richard W. Davies, Carnegie Institute of Technology, Pittsburgh, Pa. "Some Studies of Electronic Spectral Distributions in Randomly Disordered Lattices"
May 31	J. K. Mackenzie, RIAS, Inc., Baltimore "Atomic Configurations at Flat Crystal Surfaces"

EDUCATIONAL LECTURES AND SEMINARS

Four members of the Solid State Division participated in the University Traveling Lecture Program sponsored by ORINS. They presented the following lectures under the auspices of this program:

J. H. Crawford, Jr.	North Texas State University, Denton, Apr. 24, 1963 "Processes in Alkali Halides" Austin College, Sherman, Tex., Apr. 25, 1963 "Ionization in Solids"
D. K. Holmes	Auburn University, Auburn, Ala., Jan. 25, 1963 "Radiation Damage Theory"
T. S. Noggle	Georgia Institute of Technology, Atlanta, Mar. 6, 1963 "Electron Microscope Studies of Fission Fragment Tracks in Thin Films"
R. A. Weeks	Emory University, Atlanta, Ga., May 3, 1963 "Paramagnetic Defects in Insulators" Arizona State University, Tempe, May 22, 1963 "Effects of Irradiation on Polarization Currents in Glass"

[a]Joint Physics and Solid State Divisions seminar.

A number of other seminars and lectures were presented during the year by members of the Division, both in this country and abroad:

R. G. Berggren	Knoxville Technical Society, Knoxville, Tenn., Jan. 28, 1963 "Radiation Effects in Structural Steels"
R. O. Chester	Instrumentation and Controls Division, ORNL, Oct. 8, 15, and 22, 1962 "Semiconductor Basics"
J. W. Cleland	Instrumentation and Controls Division, ORNL, Nov. 19, 1962 "Radiation Damage in Semiconductors" Illinois Institute of Technology, Chicago, May 15, 1963 "Radiation Effects in Semiconductors"
L. H. Jenkins	University of Alberta, Edmonton, Canada, Sept. 19, 1962 "Electrochemical Properties of Copper Single Crystals"
C. Lehmann	Brookhaven National Laboratory, Mar. 19, 1963 Atomic Energy of Canada Limited, Chalk River, Ontario, Mar. 22, 1963 North American Aviation Science Center, Los Angeles, May 28, 1963 "Long Range Channeling in Irradiated Crystals"
G. Leibfried	University of Illinois, Urbana, Mar. 15, 1963 "Channeling Effects in Crystals"
M. T. Robinson	Atomic Energy of Canada Limited, Chalk River, Ontario, May 7, 1963 "Computer Studies of the Slowing Down of Atoms in Crystals"
W. Schüle[b]	Atomics International, Los Angeles, Apr. 18, 1963 Brookhaven National Laboratory, May 24, 1963 "Enhancement of Diffusion in Alloys" U.S. Naval Research Laboratory, Washington, D.C., May 21, 1963 Thomas J. Watson Research Center, IBM, Yorktown Heights, N.Y., May 23, 1963 "Enhancement of Diffusion by Interstitials in Alloys" University of Illinois, Urbana, May 28, 1963 "Point Defects in Noble Metals" Northwestern University, Evanston, Ill., May 31, 1963 "Interstitial and Vacancy Migration in fcc Metals"

[b]Guest scientist from C.C.R.-EURATOM, Ispra, Italy.

M. J. Smith	Cornell University, Ithaca, N.Y., May 13, 1963 "Co^{60} Gamma-Radiation-Induced Point Defects in Bi_2Te_3"
D. O. Thompson	University of Illinois, Urbana, Dec. 5, 1962 "Behavior of Lattice Defects in Dislocations"
M. S. Wechsler	Stanford Research Institute, Menlo Park, Calif., Oct. 4, 1962 "Radiation-Enhanced Ordering in Copper-Aluminum Alloys"
R. A. Weeks	Johns Hopkins University, Baltimore, Dec. 12, 1962 "Paramagnetic Characteristics of the E' Centers in Quartz Single Crystals" Parma Research Center, Cleveland, May 14, 1963 "Electron Spin Resonance Research at Oak Ridge National Laboratory" Sandia Corporation, Albuquerque, N.M., May 20, 1963 "Paramagnetic Spectra of E_2' Centers" Hughes Aircraft Corporation, Los Angeles, May 23, 1963 "Effects of Irradiation on Polarization Currents in Glass"
M. K. Wilkinson	Research and Development Unit, U.S. Navy Reserve, Oak Ridge, Tenn., Nov. 28, 1962 "The Use of Nuclear Reactors in Solid State Investigations" North Carolina State College, Raleigh, Jan. 21, 1963 "Techniques and Applications of Neutron Diffraction" Atomic Energy of Canada Limited, Chalk River, Ontario, Feb. 7, 1963 "Magnetic Ordering in Rare-Earth Metals and Compounds" IBM Research Center, Yorktown Heights, N.Y., May 9, 1963 "Magnetic Structures of Rare-Earth Metals and Intermetallic Compounds"
M. C. Wittels	Lehrstuhl f. Reaktorwerkstoffe, KFA, Jülich, Germany, Sept. 20, 1962 "X-Ray and Thermal Studies of Radiation Damage" University of Paris, Orsay, France, Oct. 9, 1962 "Phase Transitions Due to Fast Neutrons, Fission Fragments and Thermal Neutron Capture" C.E.N.S., Saclay, France, Oct. 10, 1962 "Transmutation Effects in Gold" Institut f. Technische Physik, ETH, Zurich, Switzerland, Oct. 17, 1962 "The Growth of Small Single Crystal Spheres" C.E.N., Grenoble, France, Oct. 22, 1962 "X-Ray Diffraction Studies of Irradiated Single Crystals"

F. W. Young, Jr. Harvard University, Cambridge, Mass., Apr. 11, 1963
"The Role of Dislocations in the Dissolution of
Copper Crystals"

During March, April, and May 1963, G. Leibfried gave a series of six lectures on "Lattice Dynamics," and H. C. Schweinler gave six lectures on "Brillouin Zone Theory." These lectures were given in the Solid State Division and were open to interested Laboratory personnel.

CONFERENCES

A three-day conference was held on Oct. 17–19, 1962, on the general subject of "Ranges of Atoms in Solids." This was principally organized and guided by the theorists of the Solid State Division who are interested in range problems. The conference was informal in character and brought together about 40 scientists from all over the United States and Canada with a great variety of interests: interatomic potentials, range measurements, atomic scattering, sputtering, and radiation damage. The conferees agreed that this type of conference was very productive, and many suggested that other meetings of a similar character would be more fruitful than large, formal meetings.

INTERNAL DISTRIBUTION

1. J. H. Barrett
2. R. F. Bass
3. S. E. Beall
4. P. R. Bell
5. W. T. Berg
6. R. G. Berggren
7. U. Bertocci
8. J. O. Betterton, Jr.
9. D. S. Billington
10. E. P. Blizard
11. A. L. Boch
12. E. G. Bohlmann
13. C. J. Borkowski
14. G. E. Boyd
15. M. A. Breazeale (consultant)
16. M. A. Bredig
17. R. B. Briggs
18. H. Brooks (consultant)
19. F. R. Bruce
20. W. E. Brundage
21. C. T. Butler
22. N. Cabrera (consultant)
23. R. O. Chester
24. J. W. Cleland
25. T. F. Connolly
26. R. R. Coltman
27. J. A. Cox
28. J. H. Crawford, Jr.
29. F. L. Culler
30. J. F. Cunningham
31. P. B. DeNee
32. H. D. Dietze
33. J. L. Fowler
34. J. H Frye, Jr.
35. J. L. Gabbard
36. B. R. Gossick (consultant)
37. R. J. Gray
38. W. R. Grimes
39. D. E. Harrison (consultant)
40. N. E. Hinkle
41. A. Hollaender
42. D. K. Holmes
43. A. S. Householder
44. J. P. Howe (consultant)
45. J. T. Howe
46. L. D. Hulett
47. H. B. Huntington (consultant)
48. L. H. Jenkins
49. R. W. Johnson
50. R. J. Jones
51. W. H. Jordan
52. C. E. Klabunde
53. G. W. Keilholtz
54. M. T. Kelley
55. R. H. Kernohan
56. E. M. King
57. J. S. Koehler (consultant)
58. J. A. Krumhansl (consultant)
59. E. J. Lee
60. C. Lehmann
61. G. Leibfried
62. H. Leidheiser, Jr. (consultant)
63. A. B. Lewis (consultant)
64. T. A. Lincoln
65. S. C. Lind
66. R. S. Livingston
67. H. G. MacPherson
68. C. J. McHargue
69. W. D. Manly
70. A. Meyer
71. A. J. Miller
72. E. C. Miller
73. J. W. Mitchell (consultant)
74. K. Z. Morgan
75. R. B. Murray
76. C. M. Nelson (consultant)
77. M. L. Nelson
78. T. S. Noggle
79. O. S. Oen
80. V. Paré
81. R. B. Parker
82. J. C. Pigg
83. H. Pomerance
84. M. E. Ramsey
85. T. A. Read (consultant)
86. J. K. Redman
87. C. C. Robinson
88. M. T. Robinson
89. A. F. Rupp
90. O. E. Schow
91. H. C. Schweinler
92. H. E. Seagren
93. F. Seitz (consultant)
94. S. T. Sekula

95. F. A. Sherrill
96. E. D. Shipley
97. W. A. Sibley
98. R. H. Silsbee (consultant)
99. O. Sisman
100. M. J. Skinner
101. L. Slifkin (consultant)
102. G. P. Smith
103. H. G. Smith
104. M. J. Smith
105. A. H. Snell
106. E. Sonder
107. A. L. Southern
108. R. L. Sproull (consultant)
109. J. T. Stanley
110. E. E. Stansbury
111. W. J. Stelzman
112. C. D. Susano
113. J. A. Swartout
114. E. H. Taylor
115. L. C. Templeton
116. D. O. Thompson
117. G. T. Trammell (consultant)
118. David Turnbull (consultant)

119. D. Walton
120. C. C. Webster
121. M. S. Wechsler
122. R. A. Weeks
123. A. M. Weinberg
124. E. P. Wigner (consultant)
125. M. K. Wilkinson
126. G. C. Williams
127. J. M. Williams
128. W. R. Willis (consultant)
129. M. C. Wittels
130. E. O. Wollan
131. R. F. Wood
132. F. W. Young
133. Gale Young
134. Biology Library
135–137. Central Research Library
138–187. Laboratory Records Department
188. Laboratory Records, ORNL R.C.
189. Laboratory Shift Supervisor
190–191. ORNL – Y-12 Technical Library,
Document Reference Section
192. Reactor Division Library

EXTERNAL DISTRIBUTION

193. W. W. Shaver, Corning Glass Works, Corning, New York
194. R. W. McNamee, Union Carbide Corporation, New York
195. Boeing Airplane Company
196. Research and Development Division, AEC, ORO
197. J. R. Johnson, Minnesota Mining and Manufacturing Co., St. Paul
198. A. E. Ruark, AEC, Washington
199. G. L. Stiehl, Convair Division of General Dynamics Corp., San Diego
200. R. O. Bolt, California Research Corp., Richmond
201. Benjamin Lax, Lincoln Laboratory, Lexington, Massachusetts
202. George H. Wagner, Linde Air Products Company, Tonawanda Laboratory, East Park Drive
and Woodward Avenue, Tonawanda, New York
203. D. K. Stevens, Materials and Metallurgy Branch, Division of Research, U.S. Atomic Energy
Commission, Washington, D.C.
204. R. I. Leininger, Battelle Memorial Institute, 505 King Avenue, Columbus, Ohio
205. Westinghouse Electric Corp., Research Laboratories, Pittsburgh, Pennsylvania
206. J. G. Castle, Jr., Physics Dept., Westinghouse Electric Corp., Research Laboratories,
Pittsburgh, Pennsylvania
207. C. Kikuchi, University of Michigan, Willow Run Laboratory, Ann Arbor, Michigan
208. N. R. Beaudry, Office of Ordnance Research, Duke Station, Durham, North Carolina
209. J. Hitch, Office of Isotope Development, AEC, Washington, D.C.
210. P. W. McDaniel, Division of Research, USAEC, Washington, D.C.
211. H. Y. Fan, Solid State Physics Dept., Purdue University, Lafayette, Indiana
212. T. J. Turner, Department of Physics, Wake Forest College, Winston-Salem, North Carolina
213. J. B. Trice, Military Space Vehicle Department, General Electric Co., Philadelphia, Pennsylvania
214. T. H. Blewitt, Argonne National Laboratory, Chicago, Illinois

215. R. A. Charpie, Union Carbide Corporation, New York, New York
216. L. B. Emlet, Union Carbide Corporation, New York, New York
217. C. D. Yost, ARPA, Pentagon, Washington, D.C.
218. D. F. Cope, Reactor Division, Oak Ridge Operations Office
219. J. M. Simmons, Division of Reactor Development, AEC, Washington, D.C.
220. H. Shulman, Diamond Ordnance Fuse Laboratory, Washington, D.C.
221. G. D. Watkins, General Electric Research Laboratories, Schenectady, New York
222. R. Street, Department of Physics, Monash University, P.O. Box 92, Clayton, Victoria, Australia
223. R. A. Young, Georgia Institute of Technology, Atlanta, Ga.
224. H. A. Gersch, Georgia Institute of Technology, Atlanta, Ga.
225. A. Merlini, Solid State Physics Department, C.C.R.-EURATOM, Ispra (Varese), Italy
226. S. Amelinckx, Solid State Physics Department, C.E.N., Mol-Donk, Belgium
227. A. Seeger, Max Planck Institut für Metallforschung, Seestrasse 75, Stuttgart N, Germany
228. J. Diehl, Max Planck Institut für Metallforschung, Seestrasse 75, Stuttgart N, Germany
229. P. Baruch, Laboratoire de Physique, Ecole Normale Superieure, Paris V, France
230. V. B. Bhanot, Physics Department, Panjab University, Chandigarh-3, India
231–868. Given distribution as shown in TID-4500 (21st ed.) under Physics category (75 copies – OTS)

Reports previously issued in this series are:

ORNL-1025*	Period Ending January 31, 1951
ORNL-1095	Period Ending April 30, 1951
ORNL-1128*	Period Ending July 31, 1951
ORNL-1214*	Period Ending October 31, 1951
ORNL-1261*	Period Ending January 31, 1952
ORNL-1301*	Period Ending May 10, 1952
ORNL-1359*	Period Ending August 10, 1952
ORNL-1429*	Period Ending November 10, 1952
ORNL-1506*	Period Ending February 10, 1953
ORNL-1606	Period Ending August 31, 1953
ORNL-1677	Period Ending February 28, 1954
ORNL-1762*	Period Ending August 30, 1954
ORNL-1851*	Period Ending February 28, 1955
ORNL-1852	Period Ending February 28, 1955
ORNL-1944	Period Ending August 30, 1955
ORNL-1945	Period Ending August 30, 1955
ORNL-2051	Period Ending February 29, 1956
ORNL-2052*	Period Ending February 29, 1956
ORNL-2188	Period Ending August 30, 1956
ORNL-2189*	Period Ending August 30, 1956
ORNL-2413	Period Ending August 31, 1957
ORNL-2614	Period Ending August 31, 1958
ORNL-2829	Period Ending August 31, 1959
ORNL-3017	Period Ending August 31, 1960
ORNL-3213	Period Ending August 31, 1961
ORNL-3364	Period Ending August 31, 1962

*Classified